ASSESSMENT OF INDIRECT ESTIMATION METHODS TO EXTEND OBSERVED STAGE-DISCHARGE RELATIONSHIPS FOR ABOVE-STRUCTURE-LIMIT CONDITIONS AT FLOW-GAUGING WEIRS

by

VERNON HENRY WILLIAMS

A dissertation submitted in fulfilment of the requirements for the degree
Master of Engineering in Civil Engineering
in the
Department of Civil Engineering
of the
Faculty of Engineering, Built Environment, and Information Technology
of the
Central University of Technology, Free State, South Africa

Supervisor: Prof. OJ Gericke Pr Eng. IntPE (SA)

Co-supervisor: Mr. D van der Spuy Pr Eng.

January 2023

Central University of
Technology, Free State

DECLARATION

I, the undersigned, declare that the dissertation hereby submitted by me for the degree Master of Engineering in Civil Engineering at the Central University of Technology, Free State, is my own independent work and has not been submitted by me to another university and/or faculty in order to obtain a degree. I further cede copyright of this dissertation in favour of the Central University of Technology, Free State.

Vernon Henry Williams

Signature: ………………

Date: 02 January 2023

Bloemfontein, South Africa

ABSTRACT

Streamflow is seldom directly measured; instead, the stage (flow depth) is continuously measured and converted into a discharge using a stage-discharge (SD) rating curve (RC) at a flow-gauging weir or specific river section. During flood events, flow-gauging weirs might be flooded with the water level beyond the gauging weir's designed measuring capacity, also referred to as the structural limit of the weir. Subsequently, the standard calibration of the flow-gauging weir will no longer be a true reflection of the actual discharges that occurred during the flood events, and the standard SD RC must then be extended beyond the highest stage reading to reflect these high discharges at above-structure-limit flow conditions. Direct measurements, e.g., conventional current gaugings, are also not always possible owing to various practical constraints associated with these high discharge events. As a result, various indirect methods for extending SD RCs are available; however, the impact of using these different methods varies significantly and highlights the need for a robust and reliable extension method.

The overall aim of this research is to assess and compare a selection of indirect extension methods (e.g., hydraulic and one-dimensional modelling methods) with direct extension (benchmark) methods (e.g., at-site conventional current gaugings, hydrograph analyses and level pool routing techniques), in order to establish the best-fit and most appropriate SD extension method to be used in South Africa. As pilot case study, 10 flow-gauging sites in the Free State, Gauteng, KwaZulu-Natal, Limpopo, Mpumalanga, and the Western Cape provinces were selected based on the range of possible site conditions present, e.g., type of flow-gauging weir, at-site and river geometry, flow conditions, type of hydraulics controls, and data availability. The following hydraulic methods were considered and applied at each site: (i) Simple extension (SE), (ii) Logarithmic extension (LE), (iii) Velocity extension simple approach (VE-SA), (iv) Velocity extension hydraulic radius approach (VE-HRA), (v) Velocity extension Manning's approach (VE-MA), (vi) Slope area method (SAM), and (vii) Stepped backwater analysis (SBA). In addition, one-dimensional modelling (1-D) was conducted using the Hydrologic Engineering Centre River Analysis System (HEC-RAS).

Data were collected based on the hydrometric and geometric requirements for the extension of SD relationships. The processing of the geometric data, e.g., wetted perimeter, wetted area, and hydraulic radius, was done using the Windows Cross-Section Professional (WinXSPRO), which is essentially a channel cross-section analyser. All the SD extensions were executed in the Microsoft Excel environment using semi-automated tools. The indirect extension methods' results were compared and independently assessed against the direct SD measurements or estimates at each site by using a ranking-based selection procedure based on a selection of goodness-of-fit (GOF) criteria.

In considering the overall GOF-based rankings, the SBA, SAM, and 1-D HEC-RAS steady flow modelling were identified as the most appropriate indirect estimation methods to reflect the hydraulic conditions during high discharges at a flow-gauging site. The other indirect extension methods were characterised by larger statistical differences between the at-site benchmark values and the modelled values. The VE-MA and SE methods are regarded as the least appropriate methods. In general, any extension method must be hydraulically correct if it is to be used as a robust approach to extend SD RCs beyond the structural limit. The extension of a RC is significantly more affected by the site (and river reach) geometry, initial hydraulic conditions, flow regimes and level of submergence at high discharges than the actual extension method used. Hence, there is no one-size-fits-all approach available for the extension of SD RCs in South Africa.

By improving the quality of all input data and assigning more appropriate roughness coefficients, in conjunction with the implementation of new or alternative SD extension methods, the improved extension of SD RCs is warranted to result in consistent and acceptable results. Consequently, the improved and extended RCs will result in improved hydrological data sets, all of which, will contribute towards enhanced operational water resource planning, management, and allocation in South Africa. The recommendations for future research are towards the review of the current procedures used to estimate roughness coefficients for flash floods, and the consideration of alternative methods to extend SD relationships, e.g., hydrodynamic models, support vector machines (SVMs) and artificial neural network (ANN) methods.

ACKNOWLEDGEMENTS

A number of special acknowledgements deserve specific mention:

(a) The Rectorate and relevant functionaries from the Central University of Technology, Free State, for the opportunity of completing this research.

(b) The various agencies for funding and in particular the Central University of Technology, Free State and the Water Research Commission.

(c) Prof. OJ Gericke, my supervisor, for guidance, the support given, and patience during my studies.

(d) Mr. D Van der Spuy, my co-supervisor, from the Department of Water and Sanitation (Directorate Hydrological Services: Flood Studies) for expert and technical advice pertaining to the extension of stage-discharge relationships.

(e) Mr. C Allnutt, my colleague, for support and documentation to assist in the completion of this dissertation.

(f) Mr. JPJ Pietersen, for guidance and documentation to assist in the completion of this dissertation.

(g) The Department of Water and Sanitation for providing the hydrometric information, current gaugings, calibration reports, discharge-rating tables, and survey data required.

(h) The anonymous external examiners for their constructive review comments, which have helped to improve the dissertation significantly.

(i) My family and colleagues, for their patience and understanding throughout this research.

(j) Everyone that showed love and support throughout this journey.

Acknowledgement above all to my Heavenly Father for setting my feet on a rock and making my steps secure (Ps. 40).

TABLE OF CONTENTS

APPENDIX A

APPENDIX B

LIST OF TABLES

LIST OF FIGURES

LIST OF ABBREVIATIONS

ArcGIS	Aeronautical Reconnaissance Coverage Geographic Information System
ANN	Artificial neural network
ANON	Anonymous
BSI	British Standards Institution
BSI ISO	British Standards Institution International Organisation for Standardisation
CAD	Computer-aided design
CHZ	Chézy’s approach
DCM	Divided channel method
DS	Downstream
DSS	Data storage system
DT	Discharge table
DWAF	Department of Water Affairs and Forestry
DWS	Department of Water and Sanitation
EA UK	Environmental Agency United Kingdom
FS	Free State
FS	Flood section
GOF	Goodness-of-fit
GP	Gauteng Province
GP	Gauge plate
GRG	Generalised reduced gradient
GVF	Gradually varied flow
HEC-RAS	Hydrologic Engineering Centre River Analysis System
HRA	Hydraulic radius approach
HSD	Hydrologic Services Division
KZN	KwaZulu-Natal
LE	Logarithmic extension
LP	Limpopo Province
MA	Manning’s approach
MARE	Mean absolute relative error
MP	Mpumalanga Province

NSE	Nash-Sutcliffe coefficient
NWS-HSD	National Weather Service, Hydrologic Services Division
RC	Rating curve
RMSE	Root mean square error
RMF	Regional Maximum Flood
SA	Simple approach
SAM	Slope area method
SAM-CHZ	Slope area method Chézy's approach
SAM-MA	Slope area method Manning's approach
SANRAL	South African National Roads Agency Limited
SBA	Stepped backwater analysis
SBA-CHZ	Stepped backwater analysis Chézy's approach
SBA-MA	Stepped backwater analysis Manning's approach
SD	Stage-discharge
SE	Simple extension
SE_E	Standard error of estimate
SRM	Structural risk minimisation
SVMs	Support vector machines
VBA	Visual Basic for Applications
VE	Velocity extension
VE-HRA	Velocity extension hydraulic radius approach
VE-MA	Velocity extension Manning's approach
VE-SA	Velocity extension simple approach
US	Upstream
USACE	United States Army Corps of Engineers
USGS	United States Geological Survey
WC	Western Cape
WinXSPRO	Windows Cross-Section Professional
WMO	World Meteorological Organisation
WRC	Water Research Commission
WSE	Water surface elevation
WSW	Water surface width

CHAPTER 1 : INTRODUCTION

This chapter provides some background on the extension of stage-discharge rating curves at flow-gauging weirs and river sections. The problem statement, purpose and limitations of the research are subsequently discussed. The outline of the dissertation structure is provided at the end of the chapter.

1.1 Introduction

The first flow-gauging weirs were constructed in 1904 in the Transvaal Province to measure streamflow continuously in South Africa (Menné, 1960). By the year 2007, streamflow data had already been recorded continuously at 782 different flow-gauging sites, comprising of sharp-crested weirs (55%), Crump weirs (35%) and the remaining 10% consisting of broad-crested weirs, dam spillways and velocity-area gauging sites (Wessels and Rooseboom, 2009a). However, streamflow is seldom directly measured; instead, the stage (flow depth) is continuously measured and converted into a discharge using a stage-discharge (SD) rating curve (RC) at a flow-gauging weir or specific river section. During flood events, flow-gauging weirs might be flooded with the water level beyond the structural limit. Subsequently, the standard calibration of the flow-gauging weir will no longer be a true reflection of the actual discharges that occurred during the flood events. The standard SD RC must then be extended beyond the highest stage reading to reflect these high discharges (Petersen-Øverleir and Reitan, 2009).

1.2 Problem Statement

According to the World Meteorological Organisation (WMO) (WMO, 2008), accurate streamflow data are required in practice from a robust SD relationship, which is the continuous measurement of a water level or flow depth that is accurately converted into discharge. Direct measurements, e.g., conventional current gaugings, are not always possible owing to various practical constraints associated with high discharge events, e.g., high velocities and water depths, danger to staff and equipment entering a required river reach, and operational difficulties (Lang *et al.*, 2010). Therefore, developing reliable SD relationships at high discharges using direct measuring techniques becomes problematic (Lindner and Miller, 2012). As a result, different indirect methods for extending SD RCs are available; however, the impact of using these different methods varies significantly and highlights the need for a robust and reliable extension method, since significant errors could be introduced (Lang *et al.*, 2010).

According to Shao *et al.* (2018), *"Streamflow discharge is a fundamental data set required by hydrological, ecological, agricultural and engineering studies."* Hence, in the absence of accurate SD relationships at high flood discharges above the structural limit of a flow-gauging weir, the standard RC representative of the SD relationship up to the structural limit needs to be extended. However, such an extension could introduce uncertainty and variable systematic bias when discharge values are estimated (Shao *et al.*, 2018). For example, in flood hydrology, where probabilistic flood frequency analyses are conducted to estimate design peak discharges, the exclusion of above-structure-limit discharges typically would result in the underestimation of flood events, while the inappropriate extension thereof could introduce uncertainty and ordered bias when design peak discharges are estimated (Gericke and Smithers, 2017).

Various studies were undertaken in an attempt to develop robust and reliable extension methods. For example, the Environmental Agency in the United Kingdom (EA UK), undertook a study entitled *Extension of Rating Curves at Flow-gauging Stations* to compile a best practices manual using hydraulic and computational modelling techniques (Ramsbottom and Whitlow, 2003). Dymond and Christian (1982) evaluated the accuracy of SD RCs by considering both the individual and average discharge measurement errors during a specific period. Petersen-Øverleir and Reitan (2009) examined the joint impact of sample variability and RC inaccuracy on at-site flood frequency analysis. Lang *et al.* (2010) extended SD RCs using hydraulic modelling to ultimately improve flood frequency analyses. Shao *et al.* (2018) extended SD RCs using hydrodynamic models and, as a result, quantified the uncertainty associated with the overall process.

However, despite of all the above studies, there is currently no user manual or standard practices available to extend SD relationships in South Africa (Van der Spuy, 2022). The absence of standard practices to extend SD RCs is ascribed to the different and unique hydraulic characteristics, topography and discharge conditions present at South African flow-gauging sites; hence, site visits and a fundamental understanding of the at-site hydraulics are crucial to ensure the accurate extension of SD RCs. Therefore, the use of appropriate SD extension methods is warranted not only to enhance the estimation of design flood events, i.e., peak discharges, but also to impact on water resources management. Even if high flood events for above-structure-limit conditions at flow-gauging weirs might occur only 5% of the time, it could still constitute 80% or more of the total runoff volume, which is essential in effective water resources management.

1.3 Research Aims

The overall aim of this research is to evaluate and compare a selection of indirect extension methods (e.g., hydraulic and one-dimensional modelling methods) with direct extension (benchmark) methods (e.g., at-site conventional current gaugings, hydrograph analyses and level pool routing techniques), in order to establish the best-fit and most appropriate SD extension method to be used in South Africa.

The following hydraulic methods were considered and applied at each site: (i) Simple extension (SE), (ii) Logarithmic extension (LE), (iii) Velocity extension simple approach (VE-SA), (iv) Velocity extension hydraulic radius approach (VE-HRA), (v) Velocity extension Manning's approach (VE-MA), (vi) Slope area method (SAM), and (vii) Stepped backwater analysis (SBA). In addition, one-dimensional modelling (1-D) was conducted using the Hydrologic Engineering Centre River Analysis System (HEC-RAS) (USACE, 2016).

1.3.1 Research assumptions

The research is based on the following assumptions:

(a) **Assumption 1:** The SAM and by extension, the Divided channel method (DCM), are more appropriate and hydraulically correct than the other SD extension methods available.

(b) **Assumption 2:** The SBA is more accurate than the SAM.

(c) **Assumption 3:** One-dimensional hydraulic models (e.g., HEC-RAS) better illustrate the actual hydraulic conditions in a river reach than simple hydraulic methods.

1.3.2 Specific research objectives

To achieve the overall research aim, and to investigate the research assumptions, the specific objectives are to:

(a) Conduct a comprehensive literature review on the extension of SD relationships.
(b) Identify appropriate flow-gauging weirs operated and maintained by the Department of Water and Sanitation (DWS), where direct measurement data applicable to the extension of SD RCs above the structural limit are available for benchmarking and comparison purposes.
(c) Develop a semi-automated extension tool in the Microsoft Excel environment to enable the consistent application of the various hydraulic methods with limited manual user input.
(d) Conduct 1-D HEC-RAS steady flow modelling at the identified flow-gauging sites.
(e) Compare and independently assess the indirect extension method results with the direct SD measurements at each site to ultimately identify the most appropriate indirect extension method to be used for above-structure-limit discharge conditions in South Africa.

1.4 Limitations of Research

The research is limited to the application of hydraulic SD extension methods as defined in the literature, and 1-D hydraulic modelling using HEC-RAS.

The following methods were not considered in this research owing to limited or no information being available on the methodological approach followed and software used:

Leonard *et al.* (2009) proposed the use of a modified Manning's equation, where discharge is expressed as a function of the hydraulic radius and longitudinal surface slope instead of water levels only. Sivapragasam and Muttil (2004) used support vector machines (SVMs) and artificial neural networks (ANNs) to extend SD RCs using linear regressions in a higher dimensional feature space.

As highlighted above, 1-D hydraulic modelling using HEC-RAS was exclusively used for modelling purposes in this research. The EA UK (2002b) highlighted that in using 2-D hydraulic modelling, the primary improvement is achieved by the better representation of outflanking flow at flow-gauging weirs; however, with limited data available, it is doubtful whether an increased accuracy would be achieved when the standard weir formulae and/or available control sections are used. Any accuracy improvement associated with 3-D modelling, is associated with the explicit representation of complex or non-standard structures and the interaction between the main channel and floodplain discharges. However, if the latter data are not available, no significant improvement in the accuracy would be achieved in comparison to when either 1-D or quasi-2D modelling is used (EA UK, 2002b).

1.5 Outline of Dissertation

The remainder of this dissertation is organised as follows:

Chapter 2 represents a comprehensive literature review on the fundamentals applicable to open-channel flow, flow-gauging weirs in South Africa, hydraulic methods for the extension of SD relationships, and HEC-RAS modelling. Chapter 3 focusses on the selection criteria used to identify the 10 chosen case study flow-gauging sites scattered throughout South Africa. Typically, details on the locality, data availability, and hydraulic conditions are discussed. Chapter 4 contains the detailed methodology adopted in meeting the specific objectives of this research. Chapter 5 presents the results based on the methodology described in Chapter 4, with some discussion and interpretation of the results. Chapter 6 provides the conclusions and recommendations for future research. A comprehensive reference list is included in Chapter 7. All the additional and/or supporting data sets are included in Appendices A and B, respectively.

CHAPTER 2 : LITERATURE REVIEW

Firstly, the literature review focuses on the fundamental principles applicable to open-channel flow. Thereafter, flow-gauging structures and SD extension methods are discussed. Lastly, HEC-RAS modelling is briefly discussed and explored as a SD extension method.

2.1 Basic Principles of Open-channel Flow

Open-channel flow is regarded as “free surface flow,” which is subjected to atmospheric pressure. Discharge conditions in open channels are complicated by the fact that the position of the free surface could vary in time and space. The flow depth (y), discharge (Q), the slope of the channel bottom (S_0), and the free surface are interdependent as shown in Figure 2.1 (Chow, 1959):

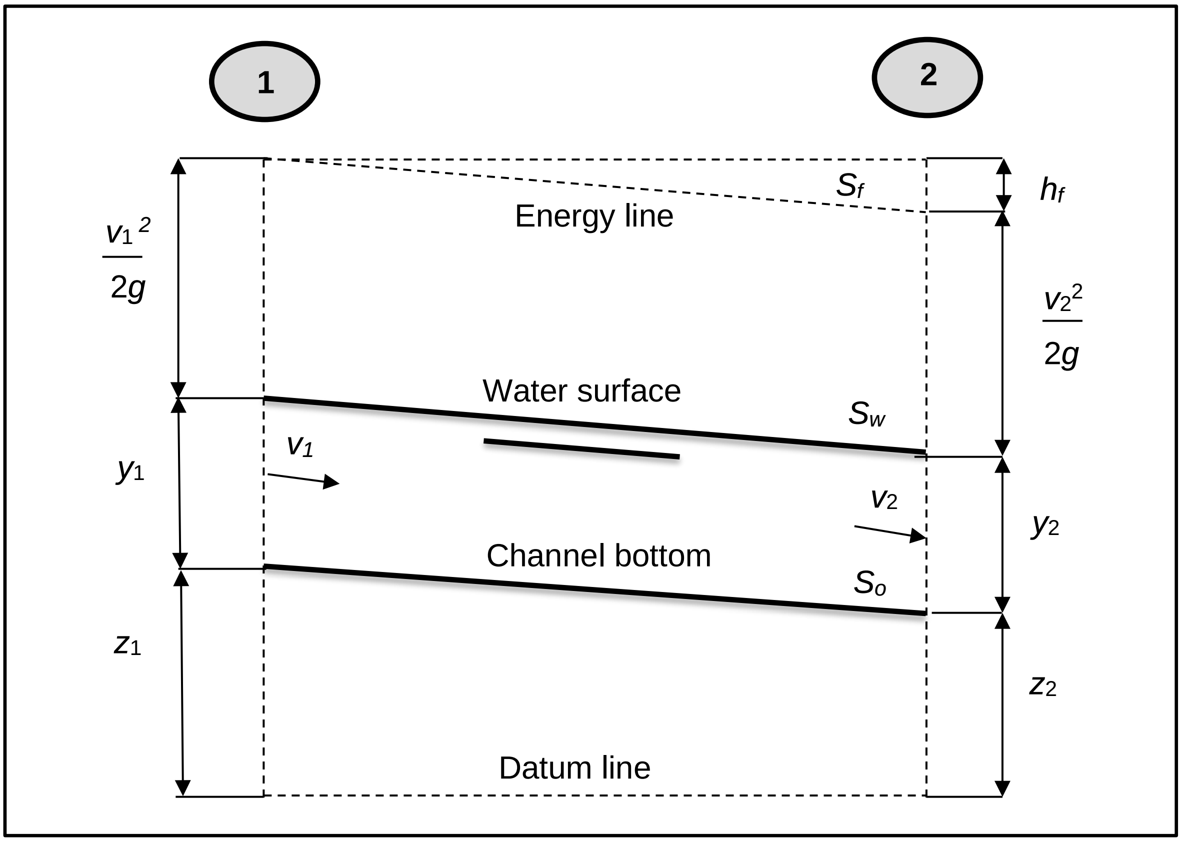

Figure 2.1: Variables applicable to open-channel flow (after Chow, 1959)

2.1.1 Open-channel flow theory

Open-channel flow can be classified in a variety of ways; these classifications are explained below (Chow, 1959):

(a) **Steady (S) flow:** The flow depth at a point does not change during the time interval under consideration.

(b) **Unsteady (US) flow:** The depth of flow changes with time at a point. A flood surge is a typical example of US flow.

(c) **Uniform flow:** The flow depth is the same at every channel cross-section.

(d) **Varied flow:** The depth of flow changes along the length of the channel.

(e) **Rapidly varied flow:** The depth of flow in a channel changes abruptly over a relatively short distance. A hydraulic jump is a typical example.

(f) **Gradually varied flow (GVF):** The flow depth changes gradually in a channel. A river flood wave is a typical example.

Based on the definitions listed above, the theory applicable to uniform and GVF flow is detailed in the subsequent paragraphs.

The corresponding flow depth associated with uniform flow is referred to as the normal flow depth. Water is subjected to flow resistance in a channel. The velocity of the water is higher closer to the water surface and towards the middle than at the channel boundaries, i.e., bottom and sides (Chaudhry, 2008).

The Chézy equations, Eqs. (2.1) and (2.2) were introduced by Antoine Chézy in 1768 and determine the uniform flow velocity [Eq. (2.1)] in a prismatic channel by considering the channel bed slope (S_o) and flow resistance [Eq. (2.2)] as a function of the absolute roughness (k_s) and the hydraulic radius (R), which in turn, changes as the flow depth changes. In the case of non-uniform steady flow in non-prismatic channels, Eq. (2.3) could be used, and the slope of the energy grade line (S_f) is used to determine the flow velocity (Chow, 1959; Henderson, 1966). If S_f is not known, then S_0 may be used as a first approximation; however, this is not always accurate given that adverse (negative) bed slopes in the direction of flow can typically be present in a river reach (Van der Spuy, 2022).

$$v = C\sqrt{RS_o} \tag{2.1}$$

$$C = 18LOG\left(\frac{12R}{k_s}\right) \tag{2.2}$$

$$v = C\sqrt{RS_f} \tag{2.3}$$

where v is the flow velocity (m/s), C is the Chézy's roughness coefficient ($m^{0.5}/s$), R is the hydraulic radius (m), S_f is the friction slope, i.e., energy grade line (m/m), S_o is the channel bed slope (m/m), and k_s is the absolute roughness parameter, representing the sizes for irregularities on the channel beds and sides (m).

The estimation of Chézy's roughness coefficients in the field is normally based on different field condition descriptions associated with the average k_s-values found in literature. When attempting to estimate realistic k_s-values for natural conditions, it is worth bearing in mind that the k_s-values represent the effective average size of the eddies formed to fit the irregularities on the bed. In this way, realistic k_s-values can be estimated for extreme conditions (SANRAL, 2013).

Manning's equation [Eq. (2.4)] was a further attempt to define the uniform flow theory. The Manning's roughness coefficient (n) depends mainly on the flow depth, channel alignment, surface roughness, vegetation in the channel, channel irregularities, and scour and deposition (Chaudhry, 2008).

$$v = \frac{1}{n}R^{\frac{2}{3}}S_f^{\frac{1}{2}} \tag{2.4}$$

where v is the flow velocity (m/s), n is the Manning's roughness coefficient ($s/m^{1/3}$), R is the hydraulic radius (m), and S_f is the friction slope (m/m).

It should be noted that Manning's equation [Eq. (2.4)] is fundamentally incorrect and does not account for roughness variations associated with flow depth, and subsequently, hydraulic radius changes (SANRAL, 2013). In estimating Manning's n-values, three methods are generally used (Hardy *et al.*, 2005): (i) direct solution, if the hydraulic radius for different flow depths, channel slopes, and velocities are known, (ii) standard n-value tables, and (iii) empirical equations based on hydraulic predictor variables.

Non-uniform flow, i.e., GVF, is derived from the difference between the channel bed slope (S_o) and the friction slope (S_f). GVF, as expressed in Eq. (2.5), is the result of variable channel cross-sections, bed slopes, and surface roughness along a river reach (distance *x*), while friction losses due to boundary shear, must be accounted for:

$$dE/dx = S_o - S_f \tag{2.5}$$

where S_o is the channel bed slope (m/m), and S_f is the friction slope (m/m).

Two types of flow conditions occur in open-channel flow, i.e., laminar, and turbulent flow. Laminar flow is characterised by low flow velocities or high water viscosity. This flow condition seldom occurs in practice and is often ignored (Van Heerden *et al.*, 1986). Turbulent flow commonly occurs in engineering practice. Essentially, the particles, which make up the fluid, move in erratic paths causing rapid fluctuations in the velocity components. These turbulent vacillations cause momentum exchange and setting up extra shear stresses to a large extent (Marriot, 2016).

The Reynolds number [Eq. (2.6)] is normally used to distinguish between laminar and turbulent flow (Marriot, 2016):

$$R_{echannel} = \frac{\rho v R}{\mu} \tag{2.6}$$

where $R_{echannel}$ is the Reynolds for open-channel flow, ρ is the fluid density (kg/m^3), R is the hydraulic radius (m), μ is the kinematic viscosity of the fluid (m^2/s), and v is the flow velocity (m/s).

In the case of pipe flow, R_e < 2 000 represents laminar flow, while turbulent flow occurs when R_e > 4 000, with transitional turbulent flow for 2 000 ≤ R_e ≤ 4 000 (Marriot, 2016). In practice, laminar and turbulent flow for open-channel flow is not that well defined. Typically, in open-channel flow, R_e < 500 implies laminar flow, while R_e > 2 000 implies turbulent flow. A transition zone also applies to 500 ≤ R_e ≤ 2 000 (Goodwill and Sleigh, 2009).

Critical flow is a special type of open-channel flow and occurs under specific conditions. It is a cross-sectional flow type. In other words, critical flow is not maintained along a length of a river reach. It may occur at the entrance of a steep channel, at the exit of a mild channel, and at sections where channel characteristics change. Critical flow conditions are characterised by: (i) Froude numbers equal to unity, (ii) specific energy being at a minimum for a given discharge, (iii) the discharge being a maximum for a given specific energy, (iv) the specific momentum being a minimum for a given discharge, and (v) the discharge being a maximum for a given specific momentum (Akan, 2006).

It is possible for water to flow at two different depths associated with two different velocities. The latter relates to sub-critical and supercritical flow conditions, which is defined by the Froude number [Eq. (2.7)] (Van Heerden *et al.*, 1986). The definition sketch for the Froude number is shown in Figure 2.2:

$$F_R = \sqrt{\frac{Q^2 B}{g A^3}} = \frac{v}{\sqrt{gD}} = \frac{v}{\sqrt{g(A/B)}} = \frac{Q}{\sqrt{g(A^3/B)}} = 1 \qquad (2.7)$$

where F_R is the Froude number, A is the cross-sectional area of the water body in the channel (m^2), B is the top width of water in the channel (m), D is the hydraulic depth (m), g is the gravitational acceleration (9.81 m/s^2), and Q is the discharge (m^3/s). The denominator $\sqrt{gD}$ represents the speed at which gravity waves propagate in open channels (Akan, 2006).

The flow is considered sub-critical when the Froude number is less than unity ($F_R < 1$) and conversely supercritical if the Froude number exceeds unity. Critical flow occurs when $F_R = 1$ (Van Heerden *et al.*, 1986).

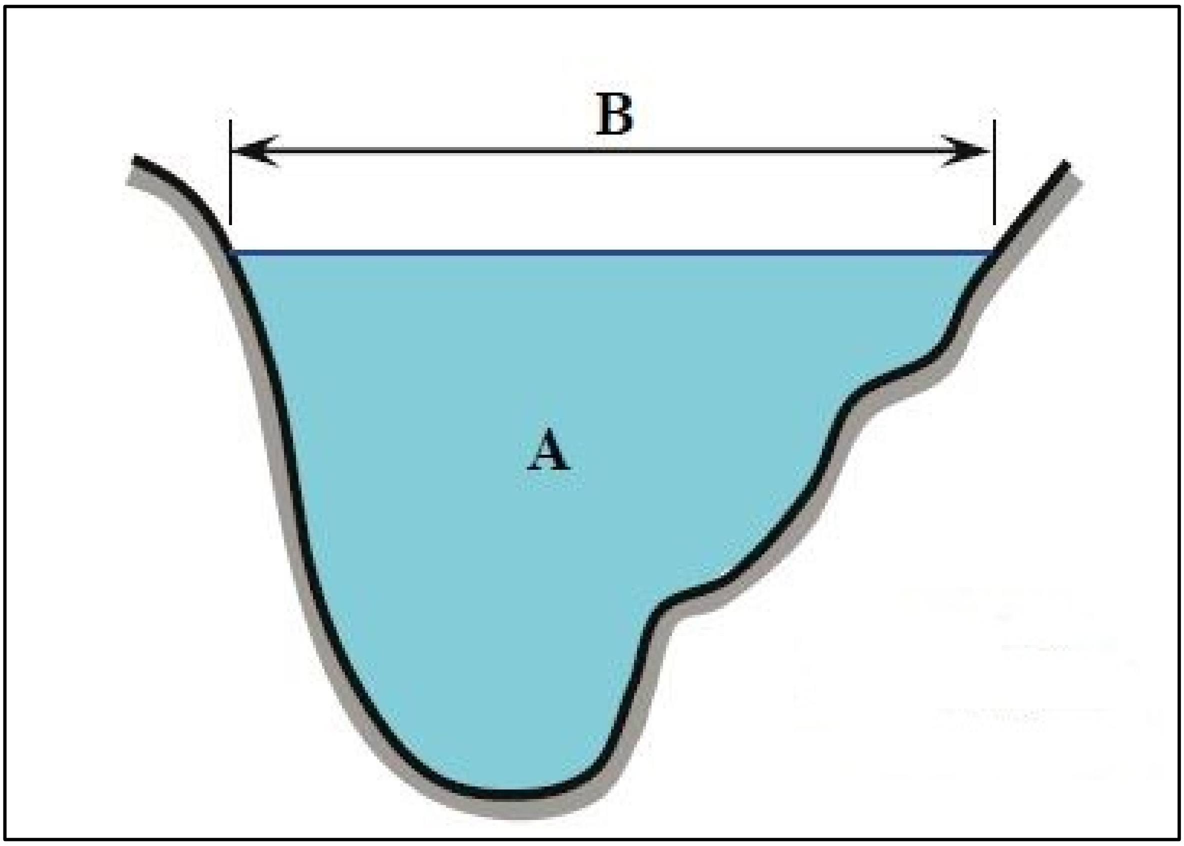

Figure 2.2: Definition sketch for the Froude number (Wessels and Rooseboom, 2009a)

2.1.2 Fundamental flow principles

Water flows along the path of least resistance by obeying fundamental laws, i.e., the conservation of mass, energy, and momentum. Typically, these laws are used in mathematical analysis to explain the behaviour of water (Van Heerden *et al.*, 1986). The fundamental laws are detailed below (*cf.* Figure 2.1):

(a) **Conservation of mass:** Matter can neither be created nor be destroyed. Mass flow entering = Mass flow leaving (Van Heerden *et al.*, 1986).

(b) **Conservation of energy:** Energy, similar to matter, cannot be destroyed, but it can only be converted to other forms of energy, i.e., Bernoulli's equation [Eq. (2.8)] for ideal flow conditions (Van Heerden *et al.*, 1986).

$$H = y_1 + \frac{\partial v_1^{2z}}{2g} + z_1 \qquad (2.8)$$

(c) **Conservation of momentum:** Based on Newton's second law, i.e., the change in momentum of a body per unit time is equal to the resultant of all external forces acting on the body (Chadwick and Morfett, 2004):

$$F = \rho Q(v_2 - v_1) \quad (2.9)$$

where F is the external force (N), H is the energy (or stage) (m), A is the cross-sectional area (m²), B is the top width of channel or river section (m), g is the gravitational acceleration (9.81 m/s^2), Q is the discharge (m^3/s), ρ is the fluid density (kg/m^3), v is the average velocity (m/s), v_1 is the average velocity at the upstream point, Point 1 (m/s), v_2 is the average velocity at the downstream point, Point 2 (m/s), y_1 is the flow depth at Point 1 (m), and z is the height above the datum line (m).

2.1.3 Hydraulic controls

Chadwick and Morfett (2004) define a control point as any section or point where the depth of flow is known for a given discharge or any section at which the discharge is known for a given depth of flow. In other words, the flow conditions at a control point are critical (F_R = 1); hence, there is only one possible solution for the flow depth, while the maximum possible discharge is associated with the lowest energy requirement. The following type of controls can occur in open channels (Wessels, 1999; Chadwick and Morfett, 2004):

(a) **Section control:** This flow condition occurs when the flow changes from sub-critical to supercritical. Hence, critical flow (F_R = 1) exists in the channel section when the F_R changes from sub-critical (< 1) to supercritical flow (> 1).

(b) **Channel control:** This flow condition occurs in long straight channels with a constant cross-section and slope. The geometry, slope and channel roughness dictate the SD relationship of the channel. Flow conditions are uniform if the flow velocity does not change with distance. Both the velocity and direction must be constant.

(c) **Complete control:** This flow condition occurs only when a single control dictates the SD relationship for the entire range of flows that may occur. A section can be considered a complete control if it is a high weir, dam, cascade, or waterfall.

(d) **Compound control:** This flow condition occurs when the SD relationship in a section is determined by more than one control as per the following example: The section acts as a control during low discharges, and channel control is present during high discharges. A control can combine with another control to determine the SD relationship, known as partial control. An example of partial control is a low weir structure (section control) submerged by tailwater. Before being completely submerged (channel control), the upstream stage and associated discharge at the weir, depend on the weir crest elevation and tailwater elevation.

The water surface level of stationary water corresponds to its energy level. If this is not affected by inflows from lakes, oceans and other sources of inflows, a condition of minimum energy exists, and the water surface level becomes the control level. When the energy level of a given section is determined, several possible control sections occasionally become available. Determining effective control means energy levels must be calculated at the given section, starting from the various control sections. The maximum energy level computed for a specific discharge will represent the effect of the dominant control (Wessels, 1999).

2.2 Flow-gauging Structures in South Africa

Water is an essential resource for all forms of life. In order to plan, control and management water effectively for optimal utilisation, the availability thereof should be accurately measured. Regardless of careful planning, the successful development of regions' water resources is likely to fail without adequate and reliable historical hydrological data (Wessels, 2001).

A flow-gauging station forms an essential component in the hydrological monitoring network of any region, while it enables the accurate measurement of water on a continuous basis. According to Lambie (1978), "*A gauging station is a site on a river which has been selected, equipped and operated to provide the basic data from which systematic records of water level and discharge may be derived. Essentially, it consists of a natural or artificial river cross-section where a continuous record of* *the stage can be obtained and where a relation between stage and discharge can be determined."*

The first flow-gauging weirs to measure discharge on a continuous basis in South African rivers were completed in 1904 in the former Transvaal Province (Menné, 1960). By 2007, the discharge was recorded at 782 different geographical locations; 55% of these stations consist of sharp-crested weirs and 35% Crump weirs. The remaining 10% of these gauging stations are dam structures, broad-crested weirs, and velocity-area gauging sites. From 1855 to 2007, the total number of gauging stations opened, was ± 1 600, with 800 to 900 stations in operation at the beginning of 1975 (Wessels, 2001). In 1990, 90 odd stations were closed-down owing to not meeting DWS standards (Wessels and Rooseboom, 2009a). According to Wessels and Rooseboom (2009b), "*Flow conditions in South African rivers vary considerably with time and therefore, it has been the policy in the South African Directorate of Hydrological Services in the Department of Water Affairs and Forestry (DWAF) to build flow-gauging structures in streams."* Figure 2.3 shows how the flow-gauging stations increased from 1880 to 2000:

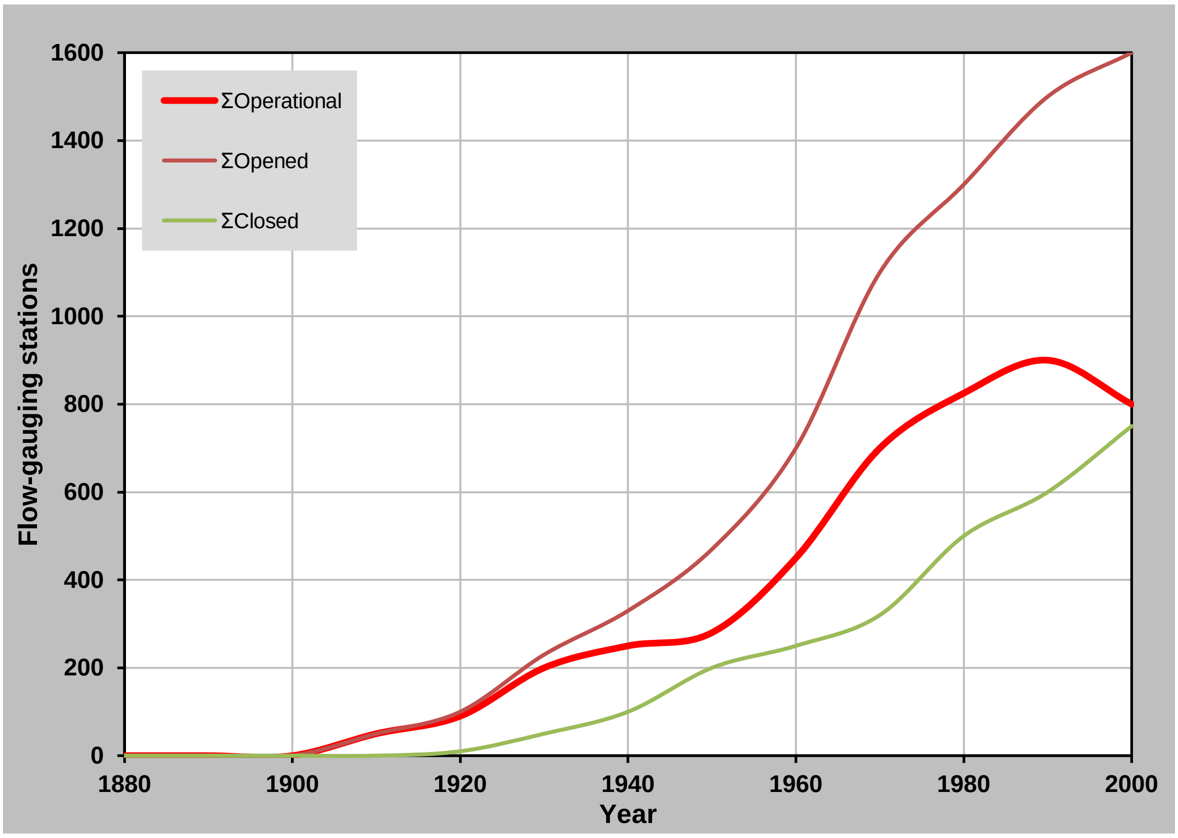

Figure 2.3: Status quo of the flow-gauging network in South Africa since 1880 (after Wessels, 2001)

2.2.1 Classification of flow-gauging weirs

The following flow-gauging weirs are commonly encountered in South Africa:

<u>Rectangular sharp-crested weirs:</u>

A thin-plate weir, as shown in Figure 2.4, has a crest profile with a narrow horizontal top surface at a right angle to the upstream face of a steel plate and a chamber of a minimum of 45 degrees on the downstream edge (Ackers *et al.*, 1978). Thin-plate weirs are only used on a small scale and are limited to small, natural streams, given that their crests are fragile and easily damaged by debris.

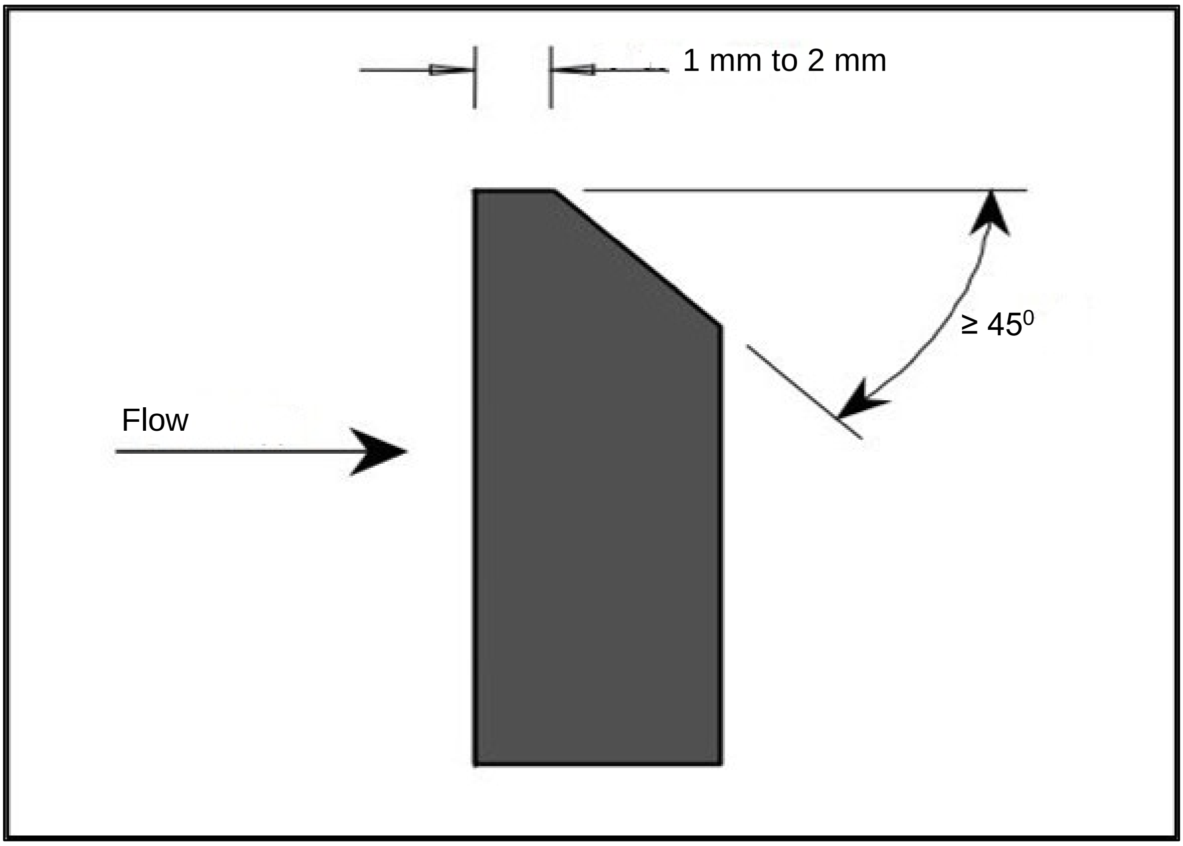

Figure 2.4: Thin-plate weir crest (Wessels, 2001)

In South Africa, the shape of the thin-plate weir crest was modified by using angle iron (*cf.* Figure 2.5), making the structure more robust for use in natural streams and rivers (Kriel, 1963). Subsequently, the thin-plate weir is referred to as a sharp-crested weir.

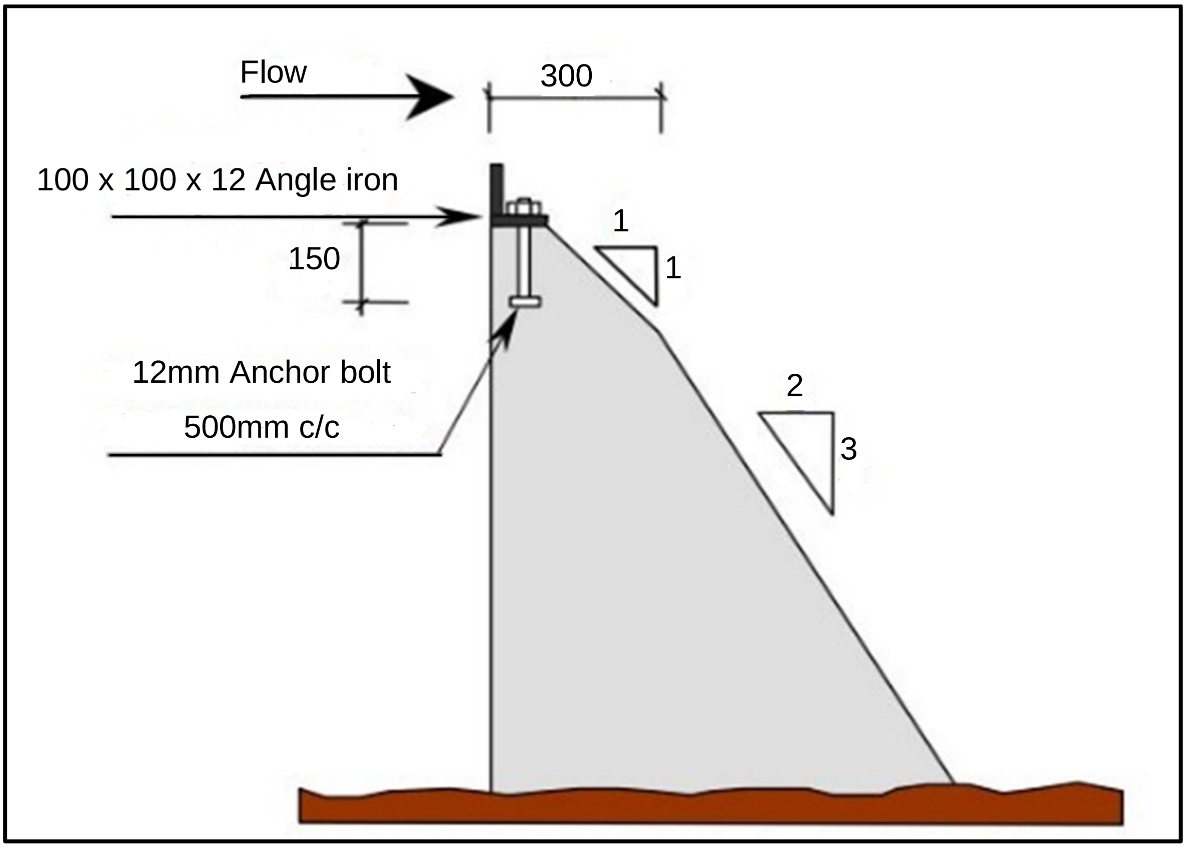

Figure 2.5: Modified thin-plate (sharp-crested) weir used in South Africa (Wessels, 2001)

Modular flow conditions occur when the downstream water level does not influence the discharge over a weir. For a sharp-crested weir to measure discharge accurately, it is essential to ensure that the pressure on the lower surface of the nappe over the weir crest, is atmospheric. The sharp-crested weir is sensitive to submerged (non-modular) flow conditions; and this is also regarded as its most significant disadvantage (Wessels, 2001). The definition sketch for a sharp-crested (thin plate) weir under modular flow conditions is shown in Figure 2.6 and applies to Eqs. (2.10) – (2.16).

DWS equation to rate thin-plate weirs:

$$Q = 1.77 C_p (H + 0.001)^{3/2} \tag{2.10}$$

$$C_p = 1.000 + 0.11 \left(\frac{P}{H+P}\right) 1.24 \text{ if } H/P \leq 3.4 \tag{2.11}$$

$$C_p = 1.145 \left(\frac{P}{H+P}\right)^{0.04} \text{ if } 3.4 < H/P \leq 200 \tag{2.12}$$

$$C_p = 0.0926 \text{ if } H/P > 200 \tag{2.13}$$

DWS equation to rate sharp-crested weirs:

$$Q = 1.61LC_p(H + 0.001)^{1.416} \text{ only if } H \leq 0.31 \text{ and with } H/P \leq 3.4 \tag{2.14}$$

$$C_p = 1.000 + H\left(\frac{0.35H}{H+P}\right)^{1.34} \text{ in this range} \tag{2.15}$$

$$Q = 1.777LC_p(H + 0.001)^{3/2} \text{ if } H > 0.310 \text{ m} \tag{2.16}$$

where Q is the discharge (m^3/s), C_p is the discharge coefficient, H is the total energy head relative to the weir crest (m), L is the length of the weir crest (m), and P is the upstream depth of the pool (water depth below crest level in upstream pool) (m).

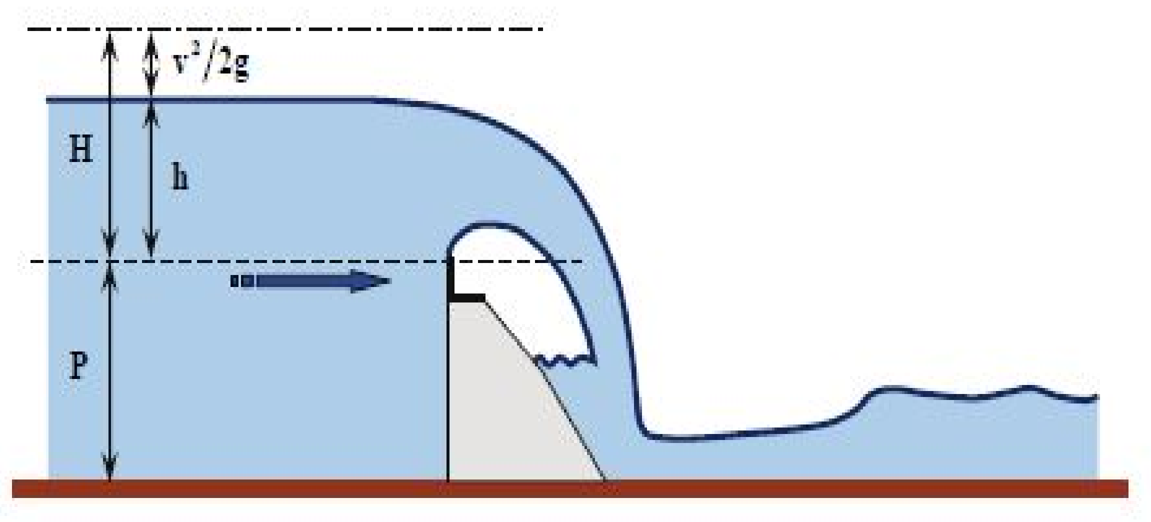

Figure 2.6: Sharp-crested (thin-plate) weir during modular flow conditions (Wessels and Rooseboom, 2009b)

In South Africa, sharp-crested weirs are widely used to measure flow in natural streams. The weir operates under submerged flow conditions when downstream water levels are higher than the crest elevations. These situations are fairly standard, and adjustments need to be made for submerged flow in the form of an equivalent modular upstream head (Wessels, 2001). The definition sketch for a sharp-crested (thin plate) weir under submerged flow conditions is shown in Figure 2.7 and applies to Eq. (2.17).

DWS equation for submerged flow conditions:

$$h_e = \frac{h\sqrt{1-\left(h_2/h\right)^2}}{\alpha} \tag{2.17}$$

$$a = \frac{-b+\sqrt{b^2-4c}}{2} \tag{2.17a}$$

$$b = -0.3407 - 0.3062\left(\frac{h_2}{h}\right) \tag{2.17b}$$

$$c = 0.6288\left(h_2/h\right)^2 + 0.01016\left(h_2/h\right)^2 - 0.6096 \tag{2.17c}$$

where h is the gauged upstream head for submerged flow conditions (m), h_e is the equivalent modular upstream head (m), h_2 is the downstream gauged head relative to the crest, and h_2/h is the submergence ratio.

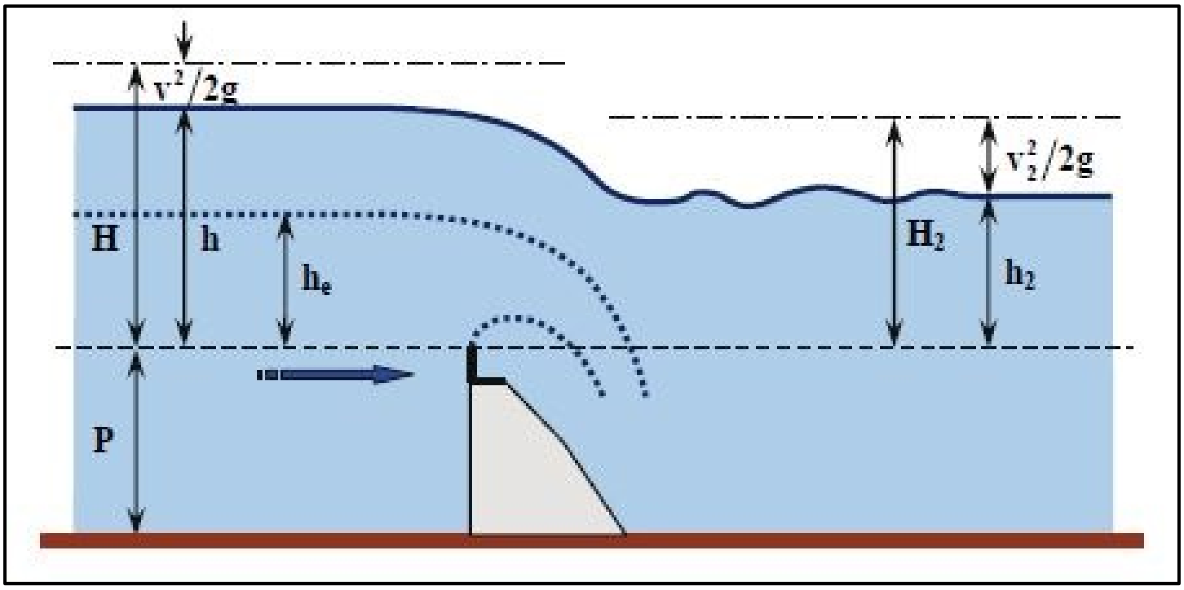

Figure 2.7: Sharp-crested (thin-plate) weir during submerged flow conditions (Wessels and Rooseboom, 2009b)

<u>Triangular profile (Crump) weirs:</u>

The Crump weir is the most popular triangular weir globally. In South Africa, the side slopes of the V-Crump are at present standardised at 1 vertical to 10 horizontals. This weir is easy to construct, robust, and immune to minor damage on the triangular profile of the crest. It has a constant discharge coefficient under modular flow conditions. The biggest advantage of a Crump weir is its insensitivity to submerged flow conditions (Wessels, 2001).

Horizontal Crump weir modular flow conditions:

$$Q = C_{de} \frac{2}{3} \sqrt{\frac{2}{3} g} L H^{3/2} \tag{2.18}$$

$$C_{de} = 1.163 \left(1 - \frac{0.0003}{h}\right)^{3/2} \tag{2.18a}$$

where Q is the discharge (m^3/s), C_{de} is the discharge coefficient, g is the gravitational acceleration (9.81 m^2/s), h is the gauged head (stage) relative to the weir crest (m), H is the total energy head relative to the weir crest (m), L is the length of the weir crest (m), and P is the pool depth below the crest level (m). The following limitations apply: (i) $h \geq 0.06$ m for a crest section of fine concrete or equivalent, (ii) $P \geq 0.06$ m, (iii) $l \geq 0.30$ m, (iv) , and (v) $l/h \geq 2.0$.

The definition sketch for a horizontal Crump weir under modular conditions is shown in Figure 2.8 and applies to Eq. (2.18).

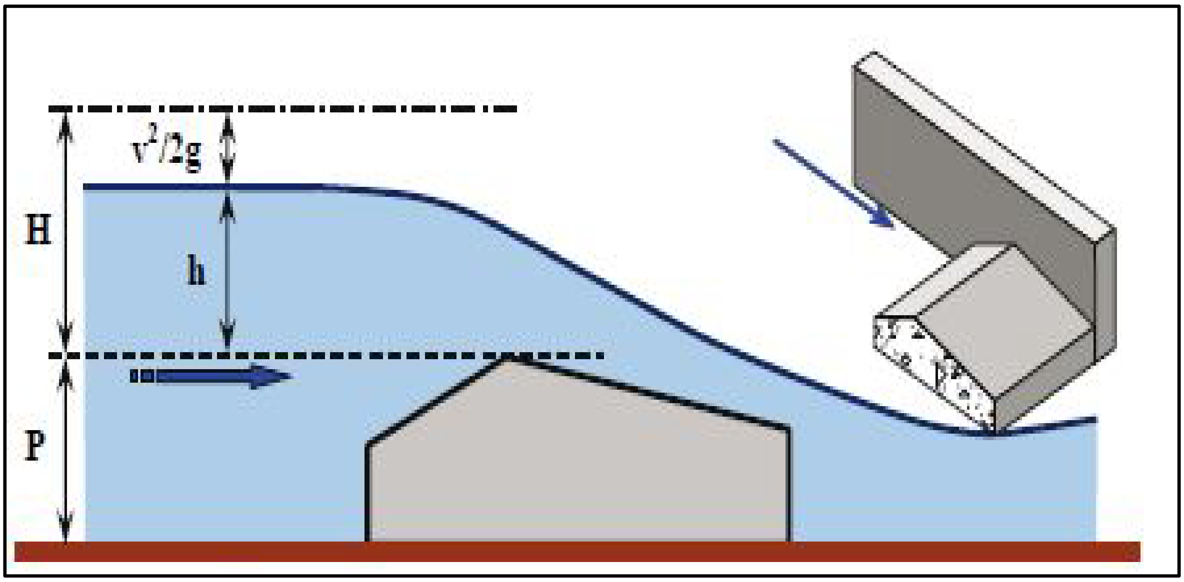

Figure 2.8: Horizontal Crump weir under modular flow conditions (Wessels and Rooseboom, 2009b)

Horizontal Crump weir submerged flow conditions:

Under submerged flow conditions, the SD relationship is dependent on both the upstream and downstream water levels. Provision is made to gauge tailwater levels through crest tappings in the downstream face of the weir, close to the crest of the weir. In South Africa, these openings are blocked by sediment; hence, water levels downstream of the hydraulic jump are used to apply corrections during submerged flow conditions (Wessels and Rooseboom, 2009b).

$$Q = C_{de} f \frac{2}{3}\sqrt{\frac{2}{3}g}\, bH^{3/2} \tag{2.19}$$

$$C_{de} = 1.163\left(1 - \frac{0.0003}{h}\right)^{3/2} \tag{2.20}$$

where Q is the discharge (m^3/s), b is the is the length of the weir crest (m), C_{de} is the discharge coefficient, f is the submerged flow reduction factor, g is the gravitational acceleration (9.81 m^2/s), H is the upstream energy head relative to the weir crest (m), and h is the gauged head (stage) relative to the weir crest (m).

The drowned flow-factor is a function of the H_2/H submergence ratio. f is determined as follows:

$$f = 1.00 \quad if \quad 0.75 \geq H_2/H \tag{2.21}$$

$$f = 1.035[0.817 - (H_2/H)^4]^{0.0647} \quad if \quad 0.75 < H_2/H \leq 0.93 \tag{2.22}$$

$$f = 8.686 - 8.403(H_2/H) \quad if \quad 0.93 < H_2/H \leq 0.985 \tag{2.23}$$

where H_2/H is the submergence ratio.

The definition sketch for a horizontal Crump weir under submerged flow conditions is shown in Figure 2.9 and applies to Eqs. (2.19) – (2.23).

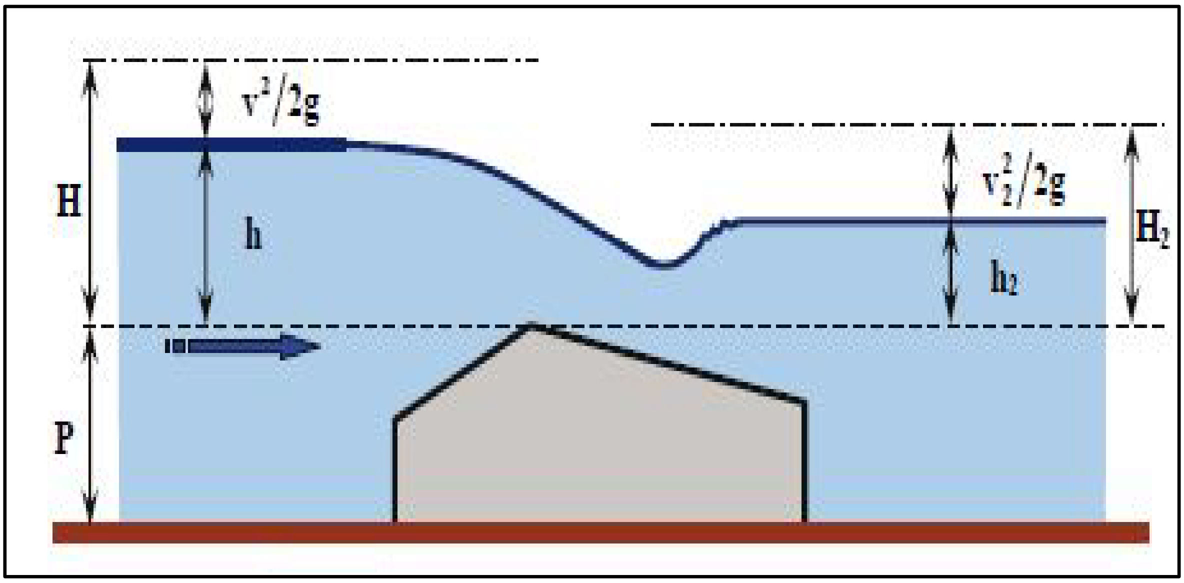

Figure 2.9: Horizontal Crump weir under submerged flow conditions (Wessels and Rooseboom, 2009b)

V-Crump weir modular flow conditions:

The standard V-Crump weir used in South Africa is shown in Figure 2.10.

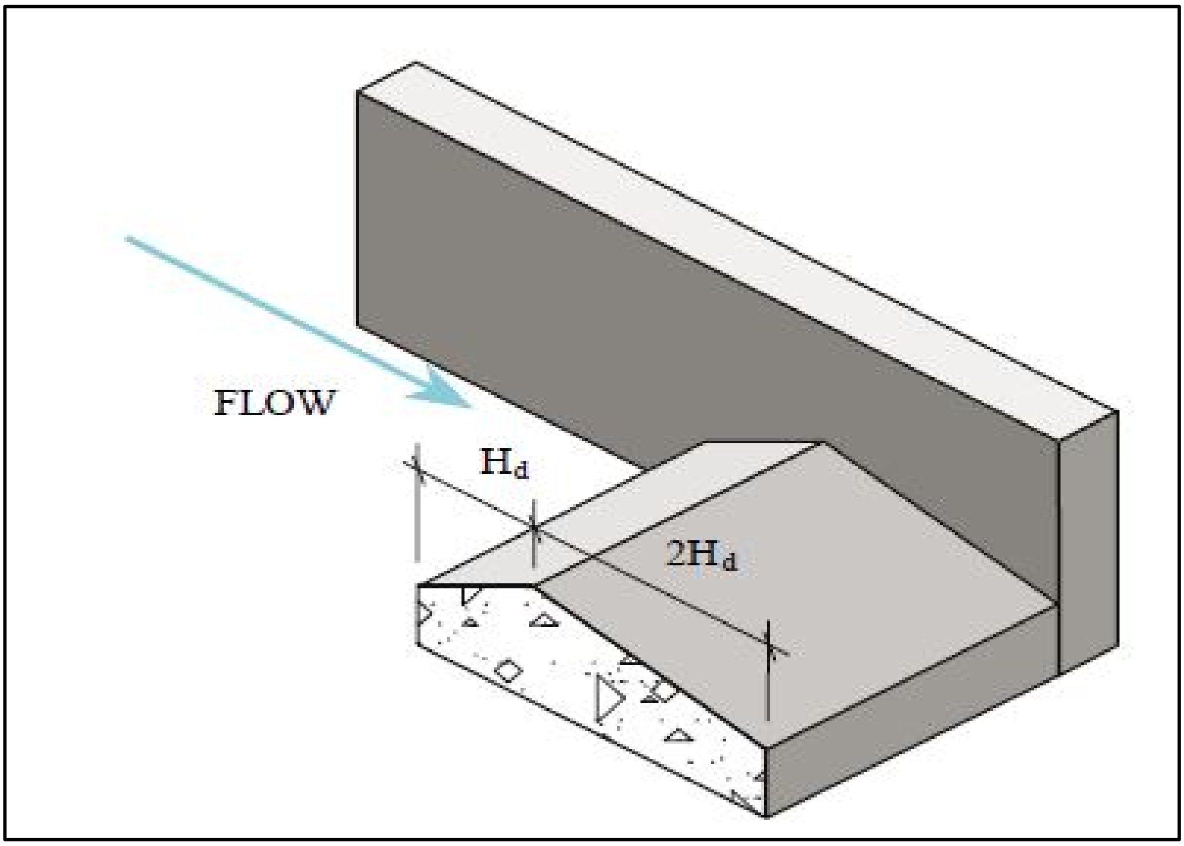

Figure 2.10: Standard V-Crump weir (Wessels and Rooseboom, 2009a)

Equation (2.24) applies when *H* is within a depth of D_v and Eq. (2.25) applies when *H* is above the V-crest, i.e., greater than D_v.

$$Q \quad = C_D \frac{4}{5}\sqrt{g}nH^{5/2} \tag{2.24}$$

$$Q \quad = C_D \frac{4}{5}\sqrt{g}nH^{5/2}[(1-{D_v}/{H})^{5/2}] \tag{2.25}$$

where *Q* is the discharge (m^3/s), C_D is the discharge coefficient (equal to 0.633 for a V-Crump with a 1:2/1:5 profile), D_v is the vertical depth of the *V*-crest (m), *g* is the gravitational acceleration (m^2/s), *H* is the total energy head (m), and *n* is the crest cross slope, normally 1:10 (*n* = 10).

The following limitations apply: (i) $h \leq 0.06\,\text{m}$, (ii) ${D_v}/{p} \leq 2.5$, and (iii) ${H}/{P_2} \leq 2.5$, with *P* the pool depth below the crest level (m), P_2 representing the difference in height between the V-crest and the downstream channel bed.

The definition sketch for a V-Crump weir under modular flow conditions is shown in Figure 2.11 and applies to Eqs. (2.24) – (2.25).

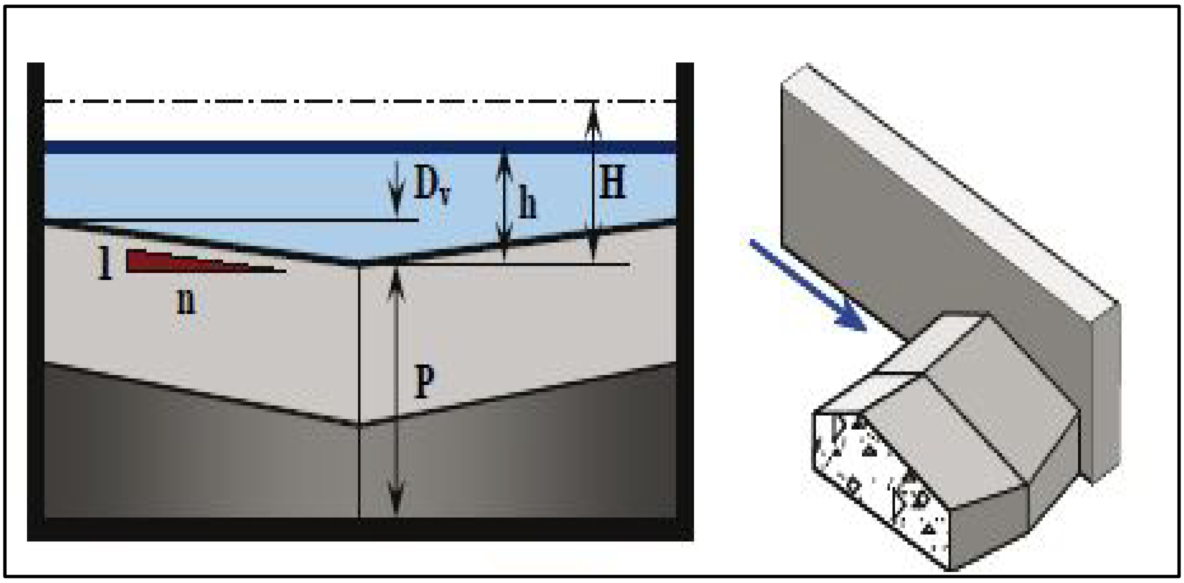

Figure 2.11: Definition sketch for V-Crump weirs (Wessels and Rooseboom, 2009b)

V-Crump weir submerged flow conditions:

Under submerged flow conditions, the SD relationship is dependent on both the upstream and downstream water levels. Provision is made to gauge tailwater levels through crest tappings in the downstream face of the weir, close to the crest of the weir. In South Africa, these openings are blocked by sediment; hence, water levels downstream of the hydraulic jump are used to apply corrections during submerged flow conditions (Wessels, 2001).

Equation (2.26) applies when H is within a depth of D_v and Eq. (2.27) applies when H is above the V-crest, i.e., greater than D_v.

$$Q = C_D f \frac{4}{5}\sqrt{g} n H^{5/2} \tag{2.26}$$

$$Q = C_D f \frac{4}{5}\sqrt{g} n H^{5/2}[1-(1-D_v/H)^{5/2}] \tag{2.27}$$

$$f = 1.00 \text{ if } 0.78 \geq H_2/H \tag{2.28}$$

where Q is the discharge (m^3/s), C_D is the discharge coefficient (equal to 0.633 for a V-Crump with a 1:2/1:5 profile), D_v is the vertical depth of the *V*-crest (m), f is the submerged flow reduction factor, g is the gravitational acceleration (m^2/s), H is the total energy head (m), and n is the crest cross slope, normally 1:10 (n = 10).

If the submergence ratio H_2/H is greater than 0.78, then f is determined by:

$$H_d = H/D_v \tag{2.29}$$

$$F_1 = 1.2[1-(H_2/H)^4]^{0.40147} \tag{2.30}$$

$$F_2 = 1.1019[0.914-(H_2/H)^4]^{0.17353} \tag{2.31}$$

$$F = F_1 \text{ if } 0.5 > H_d \tag{2.32}$$

$$F = F_2 + (F_1 - F_2)(1.5 - H_d) \quad \text{if } 0.5 \leq \mathrm{H_d} \leq 1.5 \tag{2.33}$$

$$F = F_2 \quad \text{if } 1.5 < H_d \tag{2.34}$$

where *F, F_1 and F_2* are factors to determine the submerged flow reduction factors, H_2 the total downstream energy head (m), and H_d is the total energy head divided by the vertical depth of the *V*-crest (m).

Compound flow-gauging structures:

South African rivers experience sudden and significant variations in discharge; hence, the use of compound flow-gauging structures is an attempt to ensure accurate gaugings and sensitivity over a wide range of discharge rates. According to Wessels (2001), "*Almost without exception, all the gauging structures built in South African rivers till the beginning of the 1980s were compound sharp-crested weirs."* A compound weir consists of many contrasting, but similar types of weirs with their crests at different levels, across the width of a stream. Low discharges flow only over the lowest crest of the compound weir; this is generally referred to as the low notch. With an increase in discharge, the higher notches in the compound weir start to function, ensuring that the discharge can be accurately measured for an extensive range of discharges without an excessive increase in the water levels upstream of the weir (Wessels, 2001).

Each crest of a compound weir should function as a simple weir. Dividing walls should be constructed between the different weir sections or notches to help minimise the effect of three-dimensional flow conditions. These dividing walls should extend upstream beyond the section where the stage (flow depth) is recorded. The height of the dividing walls should be high enough to separate flow throughout the design range of the compound weir. The minimum thickness of the dividing walls should be 0.3 m to avoid sharp curvatures at entrances, which may be semi-circular or semi-elliptical. According to the British Standards Institution (BSI, 1981), the maximum difference of adjacent crest levels should be limited to 0.5 m.

The BSI (1981) highlighted that in situ or model calibrations are necessary for compound weirs without dividing walls. Practically, all compound weirs in South Africa have been constructed without dividing walls. The reasons are both economical and practical; branches, trees and other debris are trapped on the dividing walls and therefore negatively affect the accuracy of the measured flows (Wessels, 2001).

<u>Natural rated sections:</u>

A gauging site is not always suitable for the construction of a weir. In such a case, the streamflow can be measured using conventional current gaugings, Acoustic Doppler's, or pre-defined sub-sections (USGS, 2020).

The simplest method to determine the discharge in a river is to position a current meter at predetermined sub-sections along a marked line in a stream or across a bridge to determine the flow velocity. The depth of the water is also measured in these sub-sections. The velocity and depth measurements are then used to compute the cross-sectional area and total volume of water flowing past the marked line (USGS, 2020).

2.3 Stage-discharge Relationships

Based on the details contained in Section 2.2, it was evident that streamflow is seldom directly measured; instead, the stage (flow depth) is continuously measured and converted into a discharge using a SD RC at a flow-gauging weir or specific river section. Hence, the subsequent sections focus on the calibration of flow-gauging weirs, natural sections, and the development of RCs.

2.3.1 Calibration of flow-gauging weirs

According to Wessels and Rooseboom (2009b), "*The most significant advantage of a permanent structure is that it can be pre-calibrated."* Flow-gauging weirs can only be preliminarily calibrated for submergence by introducing a flow reduction factor, while accurate calibrations can only be done after construction. The final calibration of a flow-gauging weir requires two control surveys, i.e., upstream, and downstream of the gauging site. Therefore, the construction plan is used to determine the final accurate calibration (Van Heerden *et al.*, 1986). In terms of hydraulic controls, the construction of a gauging weir in a river section allows the channel to be stabilised and it also creates an artificial control with a relatively stable and known theoretical relationship between the stage and the discharge at that section (Wessels and Rooseboom, 2009b).

As highlighted before, weirs are most commonly used at flow-gauging sites to measure the stage continuously. Weirs have standard RCs based on the general weir equation (WE), with different weir coefficients for different weir types (EA UK, 2002a). Equations (2.35) and (2.36) display the general WE for modular and submerged flow conditions, respectively.

$$Q = CbH^{1.5} \tag{2.35}$$

$$Q = CbfH^{1.5} \tag{2.36}$$

$$C = C_d \left(\tfrac{2}{3}\right)^{1.5} \sqrt{g} \tag{2.36a}$$

where Q is the discharge (m^3/s), b is the crest width of the weir (m), C is the weir coefficient, C_d is the discharge coefficient based on the weir geometry and head, f is the submerged flow reduction factor, g is the gravitational acceleration (m^2/s), and H is the total head relative to the zero-discharge stage (m).

Weirs operate under modular and submerged flow conditions; compound weirs have separate calculations for each crest, and the results are combined (EA UK, 2002a). The different weir equations and theories applicable to the different weirs were discussed in Section 2.2. Ramsbottom and Whitlow (2003) advised that the downstream rating should be plotted on the existing weir SD RC to determine when submerged flow conditions are likely to occur; and this will enhance the calibration of the submerged structure when only upstream data are available.

2.3.2 Calibration of natural sections

As highlighted above, streamflow is rarely measured directly; instead, the continuously measured stage is transformed into discharge by making use of RCs (Petersen-Øverleir and Reitan, 2009). The RC or SD relationship can also be used to transform forecasted flow hydrographs into stage hydrographs. Empirical approaches are commonly used to develop SD relationships as obtained from continuous measurements of stage at natural calibrated river sections. According to the National Weather Service, Hydrologic Services Division (NWS-HSD, 2018), at-site current gaugings must be conducted periodically to validate the underlying SD relationship and to track changes in the SD relationship for a natural river section. At least ten measurements a year are required unless no changes in the SD relationship are evident over time. If discharge measurements lack definition in the upper range of the RC, indirect extension methods should be applied to approximate the discharge at these high stages (NWS-HSD, 2018).

2.3.3 Development of RCs

In order to develop a RC manually, SD measurements are drawn on either arithmetic or logarithmic plotting paper. Discharge is plotted on the *x*-axis, and the stage or gauge readings are plotted on the *y*-axis. The discharge measurements are also dated to identify temporal trends (NWS-HSD, 2018).

Hand-drawn curves are used to fit a SD relationship curve. Judgement is used to decide on the best SD relationship. Factors considered during this judgment are extensive knowledge of the river and the quality and magnitude of each measurement. The simplest case would be the presence of a single control in a river, where the SD relationship is presented by a straight line drawn on a logarithmic scale (NWS-HSD, 2018).

Once the RC has been established, points that lie precisely on the curve are extracted; these points define the SD relationship. Once these defining points have been selected, one or more logarithmic equations are used to fit the points mathematically. The number of points extracted can be two for a simple control to more than 20 points for flow-gauging stations with compound control. Subsequently, actual rating tables are derived (NWS-HSD, 2018).

A logarithmic scale is usually used to plot RCs since it produces a linear fit to the observed data. With compound control, changes in the slope of the logarithmic RC can be used to identify the range in the stage to which the particular control applies. A linearised rating also makes the extension of SD relationships comparatively easy in comparison to arithmetic scale graphs. The benefit of using rectangularcoordinate paper is that trend changes in the lower portion of the curve are better defined, and zero flows are also more evident. Logarithmic scale graphs cannot describe zero flow. However, a logarithmic scale is preferred for flood forecasting owing to its ability to identify control changes. The logarithmic scale is also functional when real-time flood monitoring is done (NWS-HSD, 2018).

An example of a typical SD RC is shown in Figure 2.12. In this case, the structural limit defines the upper limit at which the flow-gauging weir is regarded as being accurate in presenting the SD relationship.

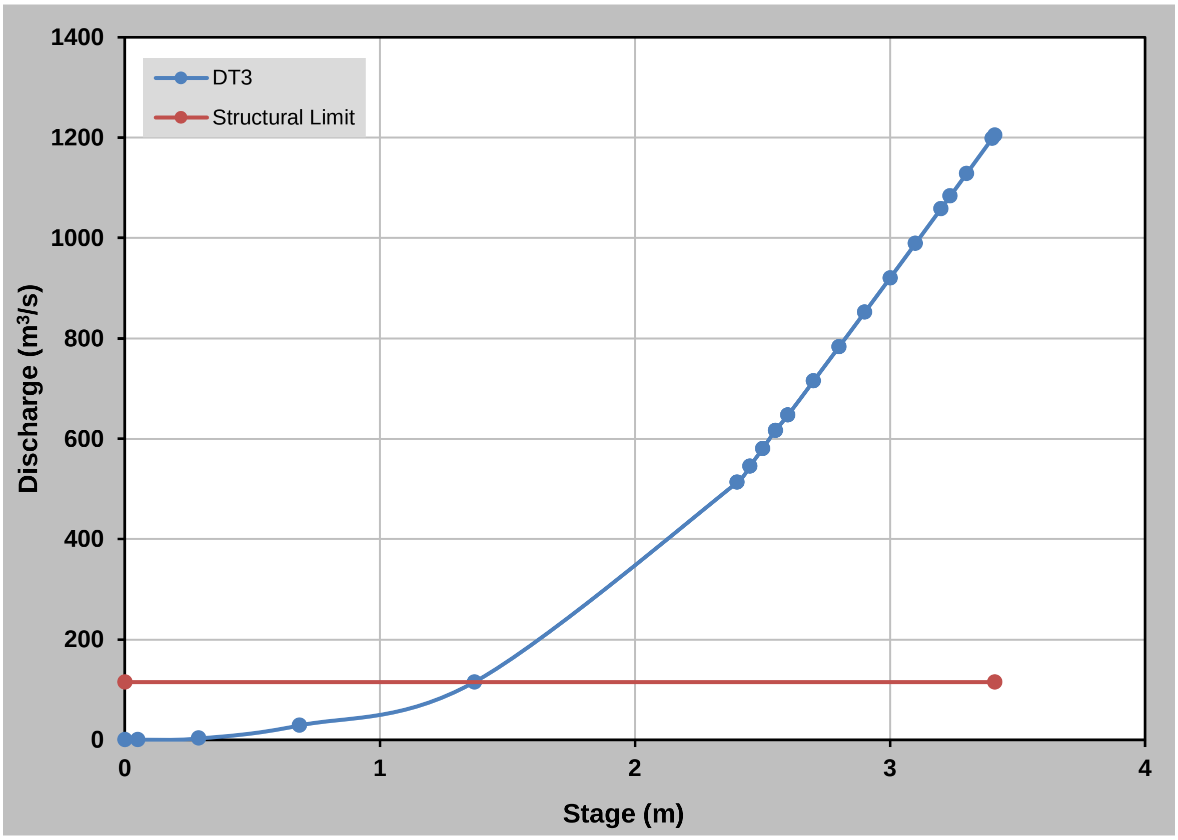

Figure 2.12: Example of a typical SD RC at flow-gauging site A4H035

All the above methods focussed on the manual compilation of RCs. Nowadays, technological advancements have enabled SD relationships to be developed in the Microsoft Excel environment or by using other relevant software. For example, the United States Geological Survey (USGS, 2021) developed customised RC Builder software which allows field measurement inputs, while the output can be plotted on either a linear or logarithmic scale. In addition, RC correction tables, with mathematical adjustment factors, are available on their website. However, it is also declared on the website that the developed RCs are only provisional and subject to change, given that ratings change over time owing to changes in the hydraulic controls present. Hence, ratings may change weekly, monthly, or not for several years. Therefore, users should exercise alertness before using the RCs, which concerns public safety and operational consequences (USGS, 2021).

Muzzammil *et al.* (2018) conducted a study which focussed on using Microsoft Excel Solver functions to develop SD RC parameters. The generalised reduced gradient (GRG) solver function was used to solve non-linear RC equations, while regression analysis and an array of goodness-of-fit (GOF) criteria were used to assess the performance. The GRG solver outperformed the conventional methods used, with Nash-Sutcliffe (*NSE*) coefficients of 0.95 as opposed to 0.86 in the case of the conventional methods. The GRG solver also eliminates the tedious trial-and-error computation that needs to be done manually (Muzzammil *et al.*, 2018).

2.4 Collection and Interpretation of Hydrometric Data and Site Geometry

Before any SD RC can be extended to present the above-structure-limit flow conditions, an assessment of the physical site characteristics and hydraulics is necessary to establish the type of rating extension method(s) to be considered.

2.4.1 Hydrometric data and site geometry

In order to develop an enhanced understanding of the site hydraulics, the following steps need to be considered in terms of hydrometric data and site geometry (EA UK, 2002a):

(a) Inspect any photographs and videos of the site, especially at high flows.
(b) Discuss the site with the relevant authorities, especially members who have visited the site over many years, particularly at high flows.
(c) Inspect the data of the site which are held by the relevant authorities.
(d) Establish the existing range of SD relationships and stages where cross-sections change.
(e) Determine the range of flows for which the SD relationship extension is required.

(f) If possible, establish the modular limit for the flow-gauging weir and the stage or discharge when channel control occurs.
(g) If any site modelling has been done in the past, the relevant authorities who undertook the modelling should be contacted.
(h) A cross-sectional survey of the flow-gauging weir is required. The flow range covered by each cross-section segment should also be shown. The cross-sections are also required to determine which hydraulic extension method would be applicable.

A report or case study should be prepared, which includes a base plan of the site and a statement of the following (EA UK, 2002a):

(a) The type of section/flow-gauging weir and its dimensions.
(b) Information on changes of the cross-section with stage that will affect the choice of the extension method.
(c) The in-bank and out-of-bank flow paths where extensions will be required to be shown on the site plan.
(d) The maximum flow is generally regarded as equal to the 1: 200-year return period (T) flood event. In South Africa, the maximum flow is based on the Regional Maximum Flood (RMF) method; however, in comparison to probabilistic flood frequency analyses conducted at various sites, the RMF method is associated with T = 10 000 years (Van der Spuy, 2022).
(e) The site, channel and floodplain geometry and their associated roughness properties.
(f) The likelihood and impact of sediment transport present, if any.
(g) Structures and natural controls which could affect the SD relationship, e.g., weirs, flumes, gates, bridges, sluices, culverts, and features of the channels.
(h) The submergence of structures.
(i) Any variable backwater effects experienced, such as tides or vegetative growth. Variable backwater effects can also be caused by tributaries that enters the river downstream of the section/weir that needs to be rated. In addition, variable water levels in downstream dams due to variable operation rules, could also result in variable backwater effects.
(j) Flood banks and other floodplain features, e.g., roads and railway embankments which could affect the flow.

(k) A determination of whether US flow conditions will potentially affect the rating.
(l) Any relevant fabricated or natural storage areas that will affect the flow.

2.4.2 Identification and selection of flood sections

Typically, flood sites can be identified after a flood event, or they are formally rated and included in the National Flood Network. Flood sections (FSs) are extensively used in hydraulic modelling and hydraulic extension methods, e.g., SAM and SBA. If FSs are incorrectly chosen, calculations will become complex, while systematic errors will be evident. The following primary aspects should be considered: (i) identification of the flood reach, and (ii) selection of suitable cross-sections (Van der Spuy, 1999).

<u>Identification of the flood reach:</u>

As highlighted in the preceding paragraphs, the flood reach and cross-sections are interdependent; the two cannot be separated when geometric data need to be prepared. Possible flood reaches can be identified before a field visit by reviewing detailed contour plans and aerial photographs. The most important factors to consider when a flood reach is to be identified, include the following (Van der Spuy, 1999):

(a) **Uniform flood reach:** The friction equations (*cf.* Section 2.1) only apply to uniform flow conditions; hence, sections should be chosen so that the enclosed river reaches are regarded as uniform to assist in estimating the friction losses.
(b) **Large weirs or dams:** These are to be avoided, given that when sections are chosen across sharply curved streamlines (e.g., above a spillway crest), the average flow velocity is no longer a function of continuity (*cf.* Section 2.1), while the pressure distribution is no longer hydrostatic, and ($y + z$; *cf.* Figure 2.1) does not represent the potential energy. Hence, energy and momentum terms become challenging to quantify.
(c) **Bends, tributaries, structures (bridges) and irregular cross-section areas:** These are to be avoided; this will ensure a more uniform flow pattern and transition losses will also be limited. If included, calculations should make provision for flow obstructions (e.g., bridges and approach embankments),

given that these obstructions can cause flow contractions with subsequent higher water levels.

(d) **Uniform bed slope:** The bed slope must be as uniform as possible over the selected reach. This will enable the use of fewer cross-sections.

<u>Selection of cross-sections:</u>

After choosing the flood reach, a series of cross-sections must be selected for computation purposes. Defining the geometric properties of a prismatic channel is straightforward; however, more effort is required when determining these properties for natural non-prismatic channels (Van der Spuy, 1999). The first geometric consideration is the centreline of the cross-section (Van der Spuy, 1999):

(a) Cross-sections perpendicular or nearly perpendicular to the direction of flow must be chosen. The position of these flow streamlines will also depend on the stage. The chainages of the sections are based on the spacing along the streamline. If the cross-sections are not at right angles to the flow direction, computations will become unnecessarily complicated. As shown in Figure 2.13, it is recommended to take several adjoining straight sections, each of these sections being perpendicular or approximately perpendicular to the flow direction.

(b) The chosen cross-sections must then be further subjected to selection to ensure that these cross-sections are characterised by having parallel or nearly parallel flow lines.

As shown in Figure 2.14, the sub-division of cross-sections is necessary to generate similar absolute roughness and flow depth categories to result in constant velocities across the sub-cross-section under consideration. The flow depth and absolute roughness factor (k_s) should preferably not differ above a factor of two from each sub-section, excluding end sections (Van der Spuy, 1999).

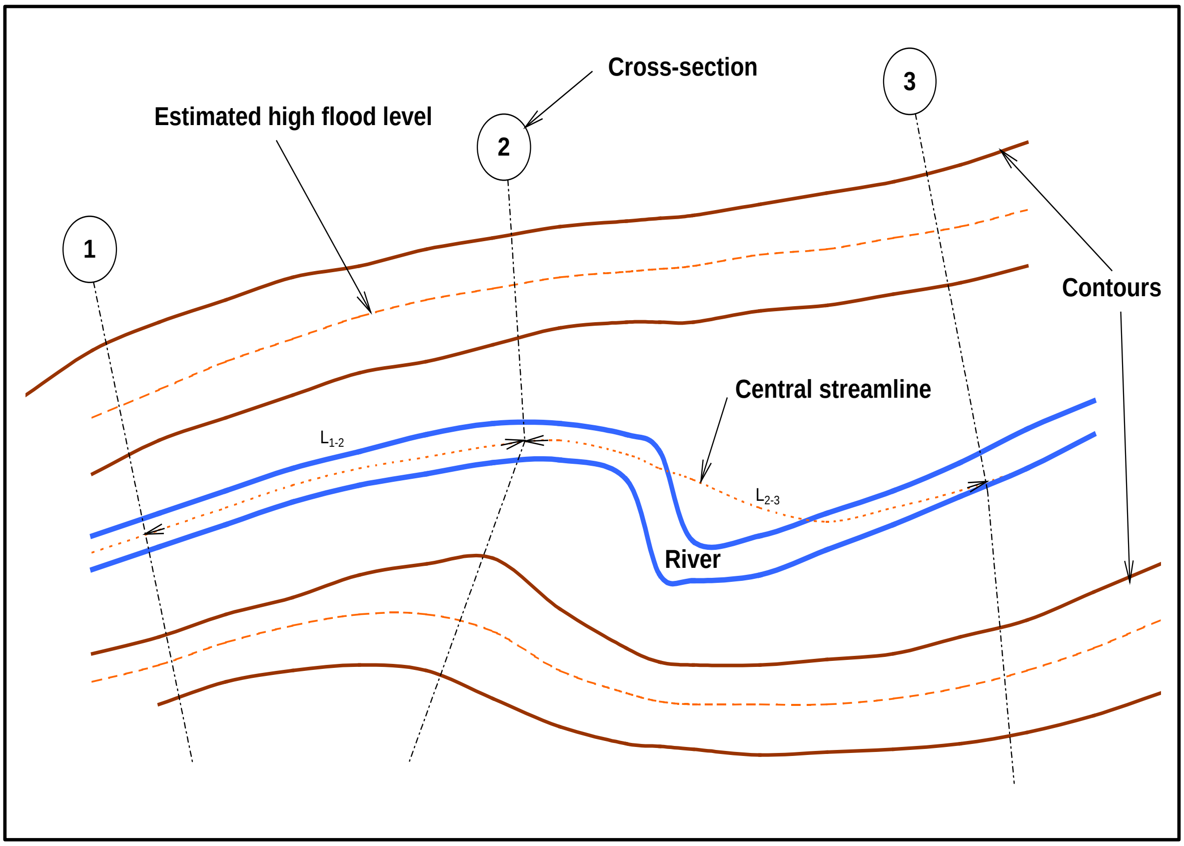

Figure 2.13: Selection of perpendicular cross-sections (Van der Spuy, 1999)

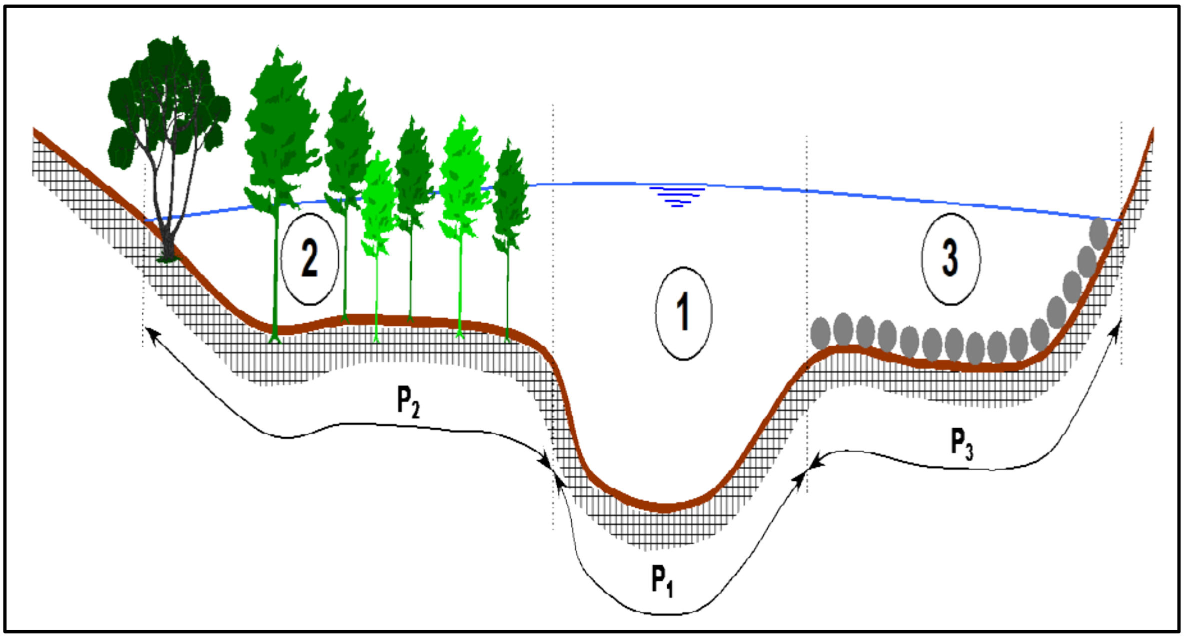

Figure 2.14: Sub-division of cross-sections (Van der Spuy, 1999)

The effective cross-sectional flow area in terms of dead water, must also be considered. Cross-sections with dead water, e.g., sudden inlets, should be avoided (Van der Spuy, 1999). In Figure 2.15, effective cross-sections and ineffective flow areas are illustrated.

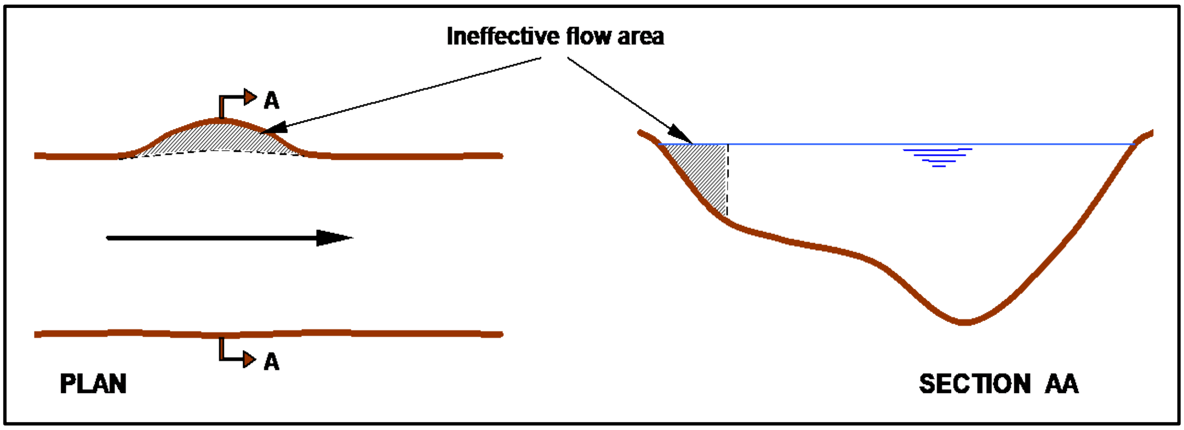

Figure 2.15: Dead water and ineffective flow areas in cross-sections (Van der Spuy, 1999)

Bends in a river decrease the velocity and increase the water level from the inner to the outer bank; hence, flood levels will be higher on the outer bank. Therefore, gathering adequate information at bends is essential when conducting a flood survey (Van der Spuy, 1999). The guidelines listed below are based on experience when dealing with river bends (Van der Spuy, 1999):

(a) **Gradual Bends > 30º and < 45º:** Cross-sections must be taken at the start of the bend, at the end of the bend, and a minimum of one cross-section in-between.

(b) **Gradual bends > 45º:** The same directives apply as in (a), but at least five cross-sections in total.

(c) **Gradual bends < 30º:** No special requirements necessary. If the bend has a small radius, then at least three cross-sections should represent the bend.

Figure 2.16 displays the effect of river bends on cross-sections.

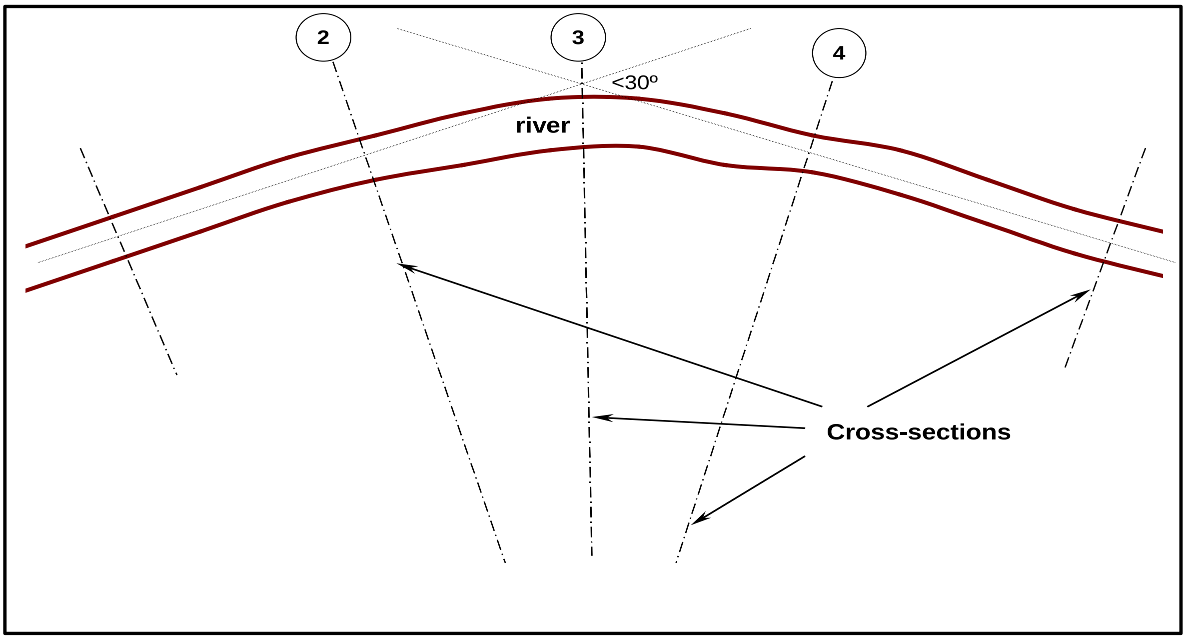

Figure 2.16: Cross-sections with bends (Van der Spuy, 1999)

In terms of the estimation of roughness coefficients, a field inspection, and detailed photographs (in up- and downstream directions) on both the left and right bank at each cross-section, would be required to allocate more representative roughness coefficients (Van der Spuy, 1999).

2.4.3 Processing of geometric data for extension

All the hydrometric and geometric data as discussed in Sections 2.4.1 and 2.4.2, need to be processed prior to application in the various hydraulic extension methods, e.g., VE, SAM and SBA, and modelling systems, e.g., HEC-RAS. Typically, geometric properties such as the wetted area (*A*), wetted perimeter (*P*), and hydraulic radius (*R*) need to be derived from survey data using appropriate software. Typically, Windows Cross-Section Professional (WinXSPRO), which is an interactive software program used for cross-section analyses, could be used (Hardy *et al.*, 2005).

2.5 Extension of Stage-Discharge Relationships

It is essential that a hydrometric data, gauging, and rating review be conducted prior to extending any SD relationship (Ramsbottom and Whitlow, 2003). Therefore, the theory applicable to the hydraulic methods used for the extension of SD relationships, is discussed in the subsequent sections. In each section, special attention is given to the: (i) background and theory, (ii) application and limitations under variable hydraulic conditions, (iii) data requirements, and (iv) methodological approach of each method.

2.5.1 Simple extension method

The SE uses the rating equation for the highest limb to extend the SD RC to stages exceeding the above-structure-limit or conversely, for the lowest segment in the case of lower stages (EA UK, 2002a).

The SE method can be used under the following hydraulic conditions (EA UK, 2003):

(a) Uniform channel cross-sections throughout the entire RC range.
(b) No transitions between modular and submerged (non-modular) flow conditions. If submergence is evident in the RC, it should have already happened before the above-structure-limit of the RC.
(c) Standard RC is inclusive of floodplain flows and the width of the flooded section does not increase significantly. In practice, this is rare because of the difficulty of floodplain flow-gauging.

The following hydraulic conditions are not suitable for using the SE (EA UK, 2003):

(a) Above bankfull conditions; except for the in-floodplain flow conditions listed above.
(b) A transition from in-channel flow to overbank full flow conditions during the RC extension.
(c) Transitions from modular to submerged flow conditions and vice versa during the RC extension.
(d) A transition from submerged flow to complete channel control flow during the RC extension.
(e) Any changes in vegetation and cross-sections.

The data requirements associated with the SE are as follows (EA UK, 2002a):

(a) Rating parameters, e.g., stage, discharge, structural limit, and rating limit of the existing RC.

(b) A cross-section showing the range of stage readings covered by the current/standard rating. Typically, such data are used to identify transitions such as the bank limit, where the method should not be applied.

(c) Information on the stages where submergence and channel control occurred.

According to Brezinski and Zaglia (1991), a more mathematical approach applicable to the SE should be followed by using both linear and polynomial extensions. In using a linear extension [Eq. (2.37)], a tangent line at the end of the existing RC is evident and it extends beyond the known limit as shown in Figure 2.17. A polynomial curve can be generated using first to sixth order functions [Eqs. (2.38) – (2.42)] fitted to either the higher stages or the entire data set.

$$Q = aH + b \tag{2.37}$$

$$Q = aH^2 + bH + c \tag{2.38}$$

$$Q = aH^3 + bH^2 + cH + d \tag{2.39}$$

$$Q = aH^4 + bH^3 + cH^2 + dH + e \tag{2.40}$$

$$Q = aH^5 + bH^4 + cH^3 + dH^2 + eH + f \tag{2.41}$$

$$Q = aH^6 + bH^5 + cH^4 + dH^3 + eH_2 + fH + g \tag{2.42}$$

where *Q* is the discharge (m^3/s), *H* is the stage (m), and *a* to *g* are algebraic constants.

The SE (as done in this research) can be applied systematically by following the steps listed below (Brezinski and Zaglia, 1991; Ramsbottom and Whitlow, 2003):

(a) Plot the existing SD relationship up to the structural limit in Microsoft Excel on a scatter plot graph.

(b) Determine a best-fit trend line equation that best fits the existing SD relationship using the coefficient of determination (r^2) closest to unity; the equation can be a first to sixth order polynomial function as well.

(c) Conduct a trend line review as multiple polynomials may all provide acceptable r^2 values; however, the discharges can vary significantly. Both visual and numerical inspections of the data are required to determine the best-fit trend line for extension purposes.

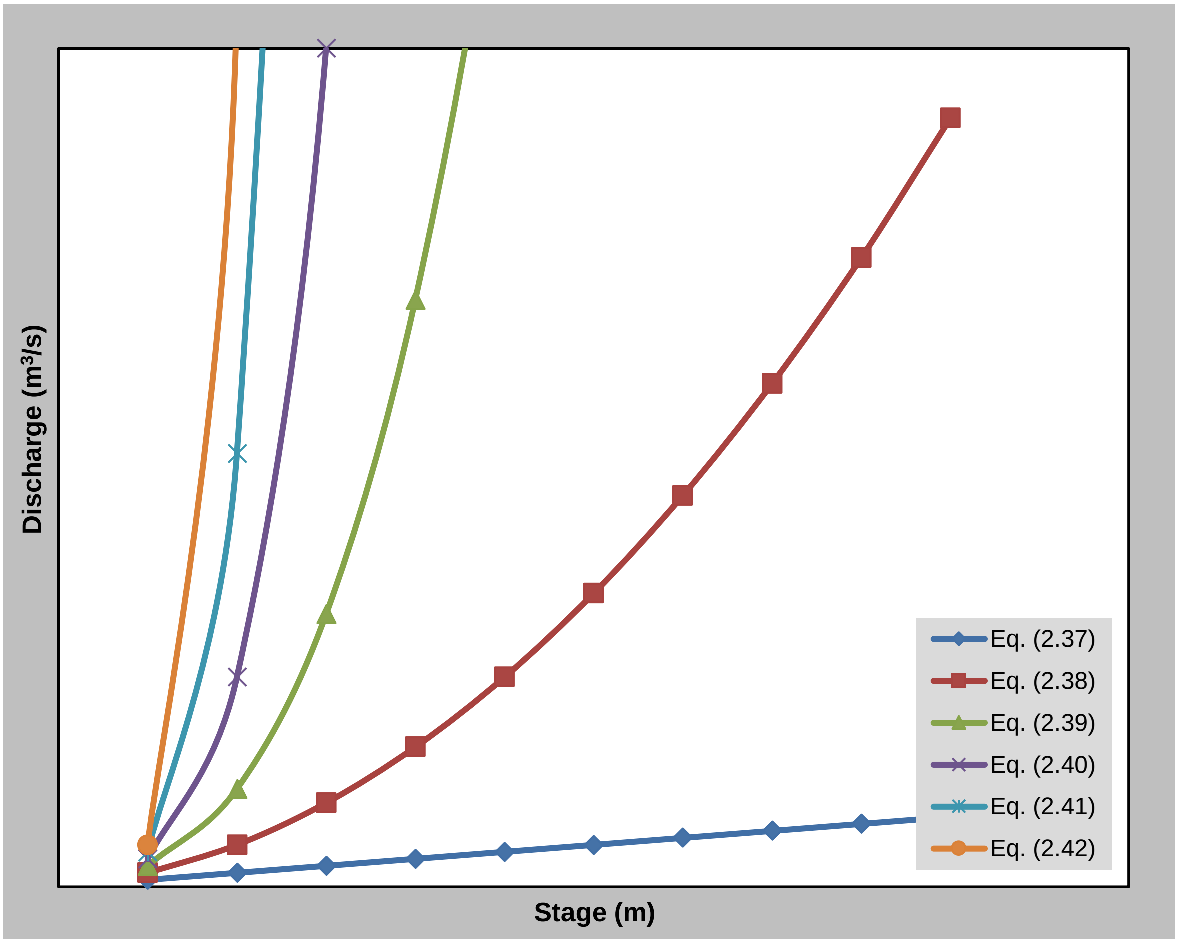

Figure 2.17: SE definition diagram

2.5.2 Logarithmic extension method

The LE method has similarities to the SE method; however, the stage and discharge are plotted on a logarithmic scale. The advantage of the LE is that it could accommodate changes in the slope of the rising limb of a RC (EA UK, 2002a; Ramsbottom and Whitlow, 2003). According to the British Standards Institution International Organization for Standardization (BSI ISO) (BSI ISO, 1998), the LE method is not recommended given that it can generate substantial errors and is regarded as inferior to the SE method in many ways. Essentially, the LE is a modified version of the SE method limited to a first-order polynomial; the values are converted to logarithmic values and plotted as shown in Figure 2.18:

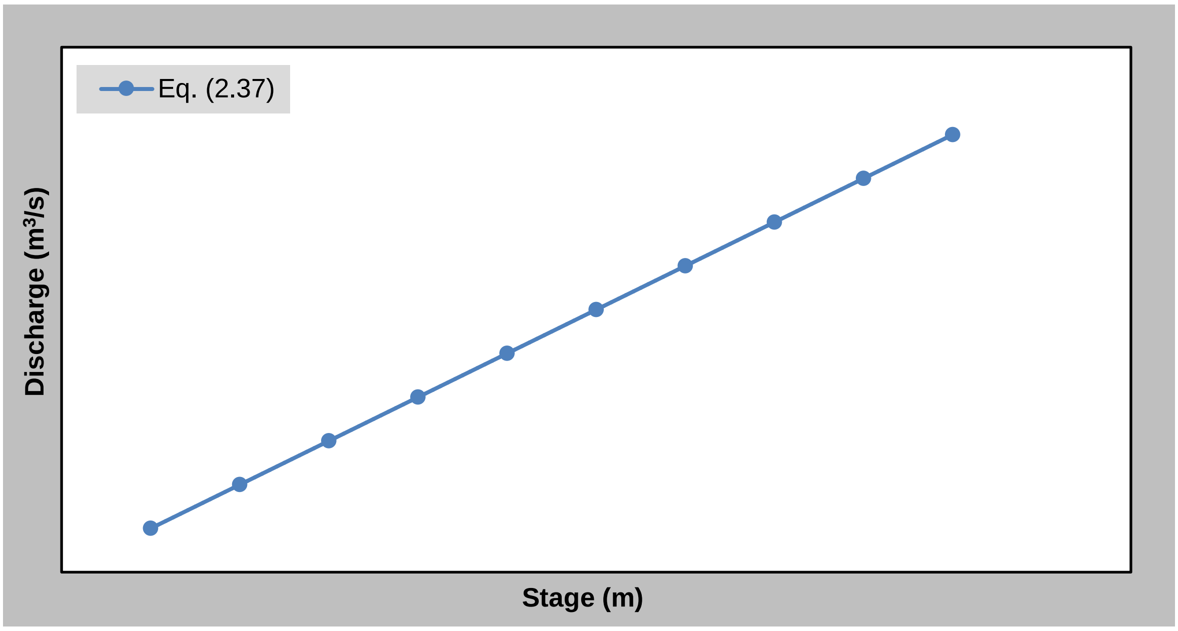

Figure 2.18: LE definition diagram

The same hydraulic conditions, limitations, and data requirements as applicable to the SE method apply to the LE method. The LE can be applied systematically as follows (Brezinski and Zaglia, 1991; Ramsbottom and Whitlow, 2003):

(a) Convert the stage and discharge of the SD relationship to logarithmic values up to the structural limit. By using a scatter plot, plot discharge on the *y*-axis and stage on the *x*-axis.

(b) Determine the first-order polynomial (linear trend line) that fits the trend line of the plotted values in step (a) the best.

(c) Extend the current logarithmic rating values using a first-order polynomial (linear equation) to the new SD relationship limit.

(d) Convert these extended logarithmic values to arithmetic values.

(e) If the limit of the current rating is below bankfull conditions, the bankfull stage must be shown on the plot, and the rating should not be extended beyond this point. Once over-bank flow occurs, the rating slope will change, thereby rendering the method invalid. Do not apply this method in regions where channel shape changes occur.

The BSI ISO (1998) recommends the following methodology to negate significant errors:

(a) If the shape of the control does not change drastically and channel roughness remains constant, then a straight-line extension on a logarithmic plot is acceptable.
(b) The LE method is well suited to channel control with medium to high flows.
(c) The LE method should not be used to extend the highest measured stages more than more than 1.5 times.
(d) For extensions in the lower flow ranges subjected to section control, the gauged height of the zero-flow reading must be known. In such cases, it is better to plot the rating on linear scales to determine the zero-flow gauge height.

2.5.3 Weir equation

The calibration of flow-gauging weirs was discussed in Section 2.3. If the control at a flow-gauging station consists of a weir, the rating can be extended using the general weir equation (WE) applicable to the specific type of weir under consideration (EA UK, 2002a).

The following hydraulic conditions are suitable for the WE to extend SD relationships (Ramsbottom and Whitlow, 2003):

(a) Modular and submerged flow conditions.
(b) SD relationships subjected to channel control.

The following hydraulic conditions are not suitable for using the WE to extend SD relationships (EA UK, 2003):

(a) Above-structure-limit conditions or significant changes in the cross-section shape. However, the DCM approach can be used in the latter case; WE applied in the main channel up to structural limit and the SAM applied in the floodplains.
(b) In applying the WE equation under submerged flow conditions, care must be taken given that controls changes can occur, i.e., sectional to channel control.

The data requirements associated with the WE are as follows (EA UK, 2003):

(a) The weir level(s) and the gauge height representative of zero flow.
(b) Structure geometry, e.g., weir width(s) and layout.
(c) Cross-section at the head measurement section (upstream) to determine the total upstream head.
(d) Gauged calibration data and the established C_d values.
(e) Modular flow limit.
(f) Equation or curve representative of the submerged flow reduction factor.

Standard SD RCs are available for standard structures based on the general weir equation. Each weir type (e.g., sharp-crested, broad-crested, Crump, etc.) has its own weir coefficient (C). It is advisable to establish the range of possible discharge coefficient (C_d) values to be expected, since many standard structures do not conform to the standards, while C (and C_d) varies with stage and discharge. The calibration of C_d values is necessary in the case of non-standard structures. The calibration is done using gauged data for the modular limit and submerged flow reduction factors (Ramsbottom and Whitlow, 2003).

The WE can be applied systematically as follows (Ramsbottom and Whitlow, 2003):

<u>Modular flow RC extension:</u>

(a) Identify the appropriate WE for the structure under consideration.
(b) Determine the crest width (b) of the structure.
(c) Plot a graph of C or C_d against stage (h) for the entire SD range.
(d) Compare the estimated discharge values with current gaugings and theoretical equations. The following process can be followed in Microsoft Excel: Identify the upper limit of the extension required to avoid: (i) structure full conditions, (ii) the start of the by-passing of flows, unless it is dealt with separately, and (iii) the start of submerged flow conditions in the rating. It is recommended that sound judgement be practised to identify an appropriate limit for the RC extension. Data availability must be considered; the revised extension limit may be lower than those limits suggested by the data.

(e) Extend the curve of C or C_d against h to the identified limit by taking account of the data and conclusions drawn in Steps (a) to (d).

(f) Use the WE with the extended values of C or C_d to calculate discharge pairs and fit a standard SD curve equation to the points. The total head must be calculated, and an iterative approach should be followed to calculate the total discharge. The iteration can be simplified by using the Microsoft Excel *Goal Seek* function.

<u>Submerged flow RC extension:</u>

The method assumes constant backwater, and that no current crest tappings, or downstream water level measurements are available. The application for submerged flow conditions is a two-stage process whereby the modular limit must first be identified; after that, the SD relationship can be generated:

(a) Identify the modular limit by using one of three methods.

  i. The preferred method is to plot suitable current gaugings on the same graph as the WE SD relationship. The expected pattern should agree with the rating below a certain threshold; however, the gauged flow should progressively reduce to the rated flows above this threshold. This threshold is the modular limit of the structure.

  ii. If previous downstream or crest tapping levels are available and agree with the current control and downstream conditions, then a graph of the submergence ratio against observed stage levels can be plotted. The modular limit for each type of weir can be found in the relevant standards, while the stage of the modular limit is obtained from the graph.

  iii. If no current gaugings or appropriate downstream water levels or crest tapping levels are available, the downstream water levels need to be estimated by using the uniform flow theory. In addition, a backwater profile could be generated using a 1-D modelling system. The choice of method should be based on the hydraulics of the downstream reach. Once this is done, the modular limit can be determined as in Point (ii).

(b) Generate the RC in the same manner as for modular flow conditions, except for the inclusion of the submerged flow reduction factor (f), which requires the submergence ratio to be estimated for the range. In order to determine the submergence ratio:

i. Generate an RC for the downstream levels using the uniform flow theory (normal flow depth calculations), a backwater profile, or 1-D hydraulic models.

ii. For a range of discharges under submerged flow conditions, use the downstream RC generated in Point (i) to estimate the total downstream head, H_2.

iii. Calculate H_1 using an iterative technique by substituting pairs of Q and H_2 into the appropriate WE.

(c) Identify the upper limit to which the rating can be extended to avoid:

i. The following change in cross-section, for example, at structure full conditions.

ii. The start of by-passing flows, unless it is dealt with separately.

iii. The transition to full channel control, when the drop in water level of the weir becomes very small.

(d) Determine a curve of C against H_1 (upstream gauged head), calculate the velocity at the location where water levels are being gauged and apply it to the WE. Extend the curve of C against H_1 to the identified limit in Step (c).

(e) Use the WE with the extended values of C to calculate pair values of stage and discharge and fit a standard RC equation to the points. The total head must be calculated, and an iterative approach must be followed to calculate the total flow.

The WE definition diagram is illustrated in Figure 2.19, while Eqs. (2.43) to (2.48) apply to the extension of the C and/or C_d values.

$$C \text{ or } C_d = ah + b \tag{2.43}$$

$$C \text{ or } C_d = ah^2 + bh + c \tag{2.44}$$

$$C \text{ or } C_d = ah^3 + bh^2 + ch + d \quad (2.45)$$

$$C \text{ or } C_d = ah^4 + bh^3 + ch^2 + dh + e \quad (2.46)$$

$$C \text{ or } C_d = ah^5 + bh^4 + ch^3 + dh^2 + eh + f \quad (2.47)$$

$$C \text{ or } C_d = ah^6 + bh^5 + ch^4 + dh^3 + eh^2 + fh + g \quad (2.48)$$

where C is the weir coefficient, C_d is the discharge coefficient, h is the gauged head (m), and a to g are algebraic constants.

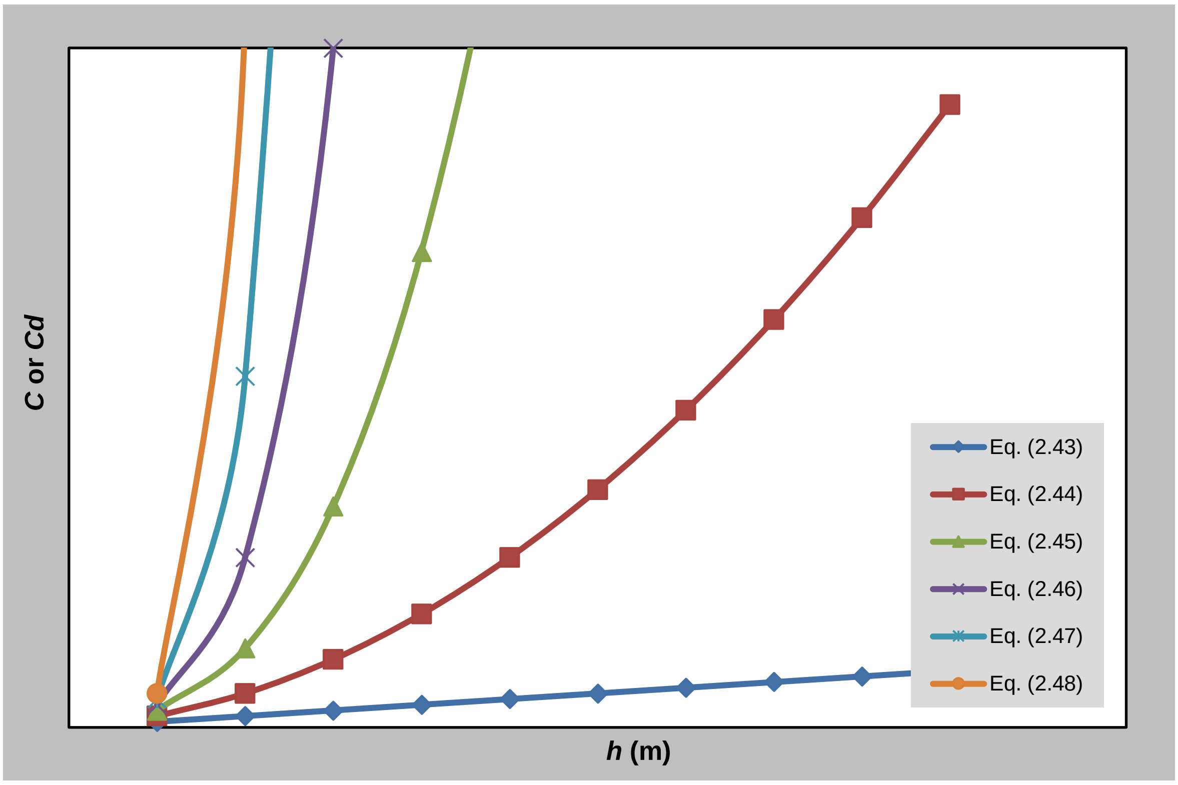

Figure 2.19: WE definition diagram

<u>DWS WE methodology:</u>

Firstly, as shown in Figure 2.20 (Schematic 4), the WE can be used to extend a RC vertically between the red dotted lines up to the structural limit. The left and right banks above the structural limit are regarded as natural sections which can be calibrated vertically using either Manning’s or Chézy’s roughness coefficients. Secondly, the blue dotted lines in Schematic 4 can be considered as sloped broad-crest notches, i.e., part of the weir, and modelled accordingly, on condition that modular flow conditions exist, or submergence effects have been quantified (Van der Spuy, 2022).

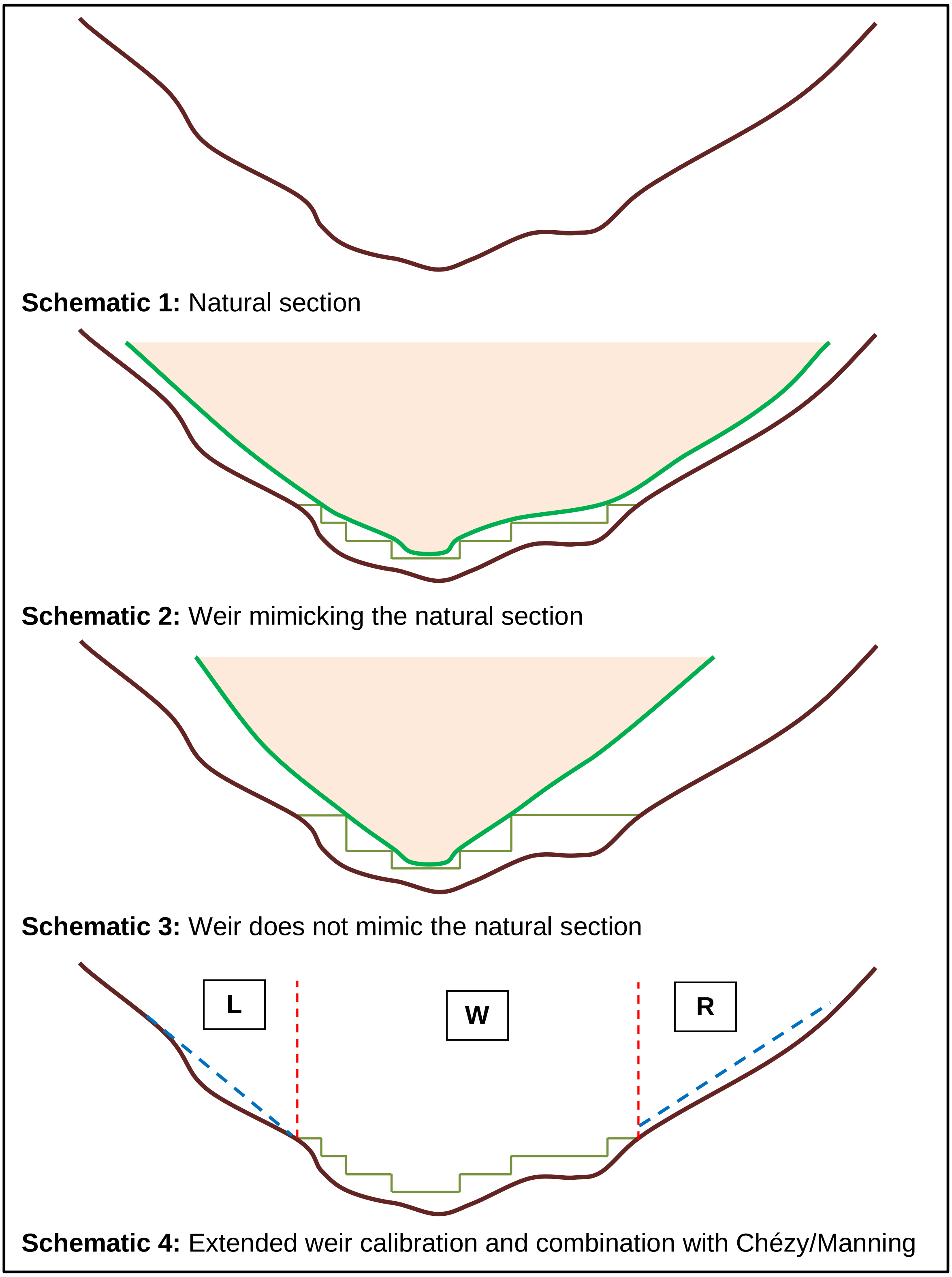

Figure 2.20: DWS WE extensions (Van der Spuy, 2022)

2.5.4 Velocity extension methods

The VE methods constitute three approaches using various channel and hydraulic parameters to extend SD relationships to high flow regions and include the (EA UK, 2002b):

(a) **Simple approach (SA):** Velocity is extended against the stage.

(b) **Hydraulic radius approach (HRA):** Velocity is extended against the hydraulic radius, i.e., channel dimensions are assumed to remain constant in the higher flow region of the SD relationship.

(c) **Manning's approach (MA):** Discharge is extended against the geometric properties of the Manning equation, i.e., $AR^{2/3}$.

The VE-SA requires the computation of the cross-sectional area and velocity at incremental river stages similar to the stages used to derive the existing SD relationship. The RC extension is based on an extension of velocity against the stage. One cross-section is required at the flow-gauging site to calculate the change in cross-sectional area with stage. The method assumes there is slight curvature in the velocity-stage graph. Once the cross-sectional area and velocity are known in the extended range, the discharge is calculated using the conservation of mass as discussed in Chapter 2, Section 2.1 (Ramsbottom and Whitlow, 2003).

In using the VE-HRA, a plot of velocity against hydraulic radius frequently shows a linear relationship; this can also be used to provide values of velocity in the extended range of the RC. Once the velocity and cross-sectional area have been derived, the flow can be calculated using the conservation of mass as discussed in Chapter 2, Section 2.1 (Ramsbottom and Whitlow, 2003).

In using the VE-MA, Eq. (2.49) is used by assuming that the square root of channel slope ($S_o^{1/2}$) and Manning's roughness coefficient (n) are constant across the full range of flows when compared to $AR^{2/3}$. The relationship of Q versus $AR^{2/3}$ is then extended to provide the SD relationships for above-structure-limit conditions (Ramsbottom and Whitlow, 2003).

$$Q \quad = AV = \frac{AR^{2/3} S_o^{1/2}}{n} \tag{2.49}$$

where Q is the discharge (m^3/s), A is the cross-sectional area (m^2), n is the Manning's roughness coefficient ($s/m^{1/3}$), R is the hydraulic radius (m), S_o is the channel bed slope (m/m), and v is the mean velocity (m/s).

The following hydraulic conditions are suitable for the use of the VE methods to extend SD relationships (EA UK, 2003):

(a) No or limited changes in the channel section geometry for above-structure-limit conditions.
(b) No transition of modular to submerged flow conditions.

The hydraulic conditions, which are regarded as unsuitable for the SE method, also apply to the VE methods. The data requirements of the VE methods include (EA UK, 2002b):

(a) A single cross-section at the flow-gauging site which covers the full range of required flows.
(b) The parameters and limits applicable to the current/standard SD RC.

The VE-SA method is limited to a first-order polynomial function [Eq. (2.50)], while the VE-SA definition diagram is shown in Figure 2.21.

$$v \quad = aH + b \tag{2.50}$$

where v the velocity (m/s), H is the stage (m), and a to b are algebraic constants.

The VE-SA can be applied systematically as follows (Ramsbottom and Whitlow, 2003):

(a) A complete, up-to-date cross-sectional survey is required, and it must cover the full range of stage values up to the envisaged extension levels.
(b) Calculate the cross-sectional area (A) at incremental stage levels (0.1 m intervals) for the current rating up to the maximum stage and discharge for the rating. The cross-sectional area (A) must also be calculated

(corresponding to the stage intervals) from the structural limit to the envisaged maximum rating level.

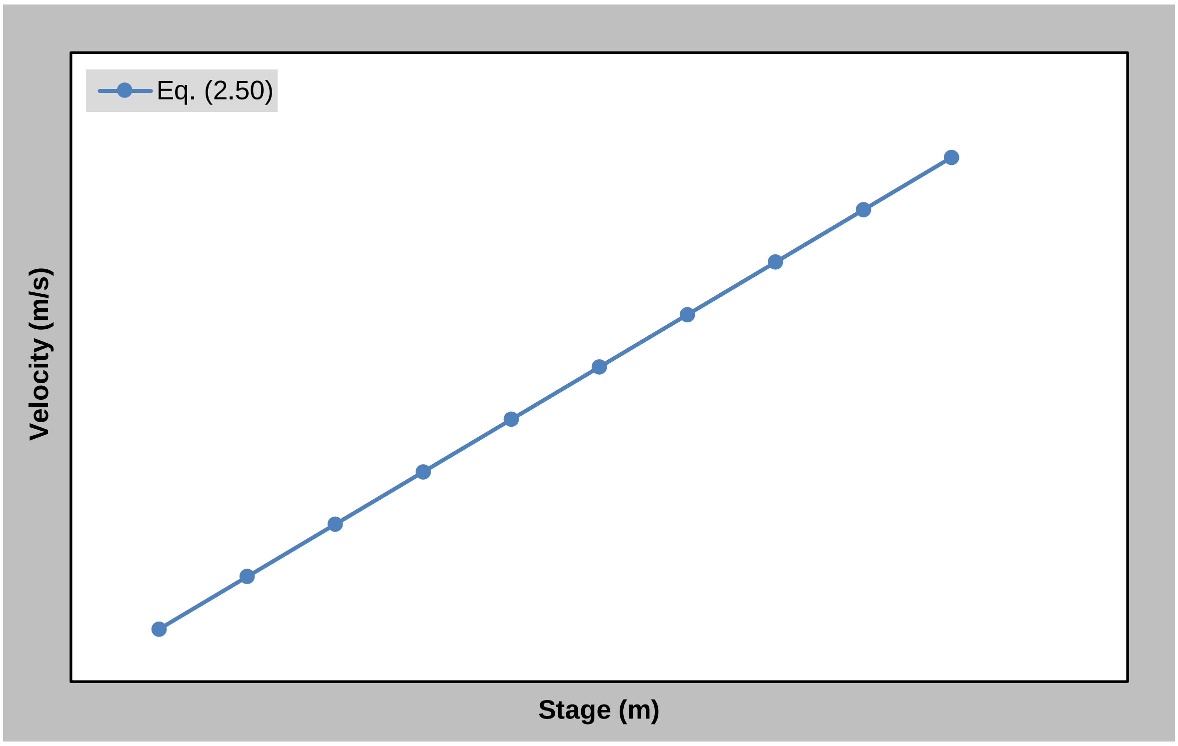

Figure 2.21: Definition diagram VE-SA computation

(c) Calculate the discharge (Q) for corresponding stage levels on the standard SD relationship up to the maximum rating level.

(d) Compute the velocity (v) from discharge (Q) and cross-sectional area (A) using the conservation of mass. Tabulate the stage, cross-sectional area, and discharge for the existing rating to the maximum rating.

(e) Plot the velocity-stage relationship for the current rating and best-fit a linear trend line through the data points.

(f) Use the accompanying best-fit linear trend line equation to calculate the velocity for stage values at above-structure-limit conditions.

(g) Use the derived velocity (v) and surveyed cross-sectional area (A) to calculate the discharge (Q), using the conservation of mass for stages above the structural limit.

(h) Identify the revised upper (or lower) limit to which the SD relationship could apply. When extending the rating to higher flows, this should not go beyond: (i) the following change in cross-section, (ii) the start of outflanking flow, (iii) a change from modular to submerged flow conditions if the current rating is below the modular limit, and (iv) the following change in submergence if submerged conditions already exist. Sound judgement must be exercised to determine these thresholds.

(i) Fit a standard power-law equation to the pairs of *Q* and *H* values for the above-structure-limit conditions.

The VE-HRA method is limited to a first-order polynomial function [Eq. (2.51)], while the VE-HRA definition diagram is shown in Figure 2.22.

$$v = aR + b \qquad (2.51)$$

where *v* the velocity (m/s), *R* is the hydraulic (m), and *a* to *b* are algebraic constants.

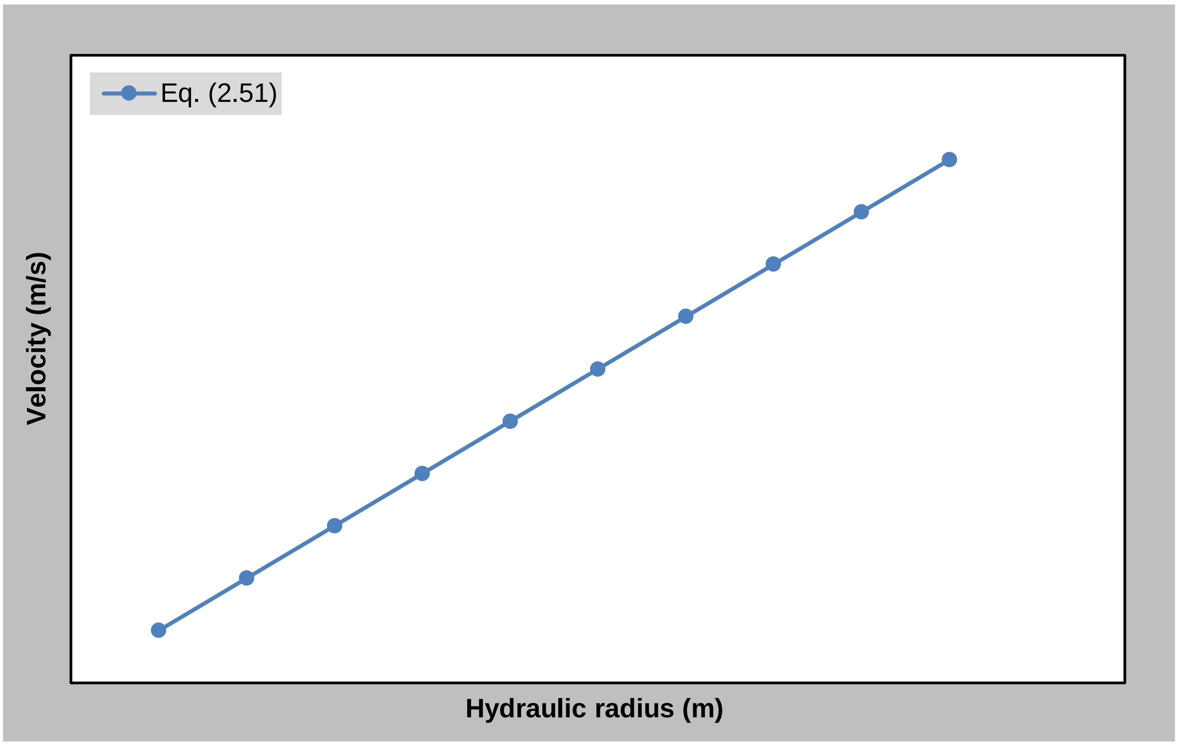

Figure 2.22: Definition diagram VE-HRA computation.

The VE-HRA can be applied systematically as follows (Ramsbottom and Whitlow, 2003):

(a) A complete, up-to-date cross-sectional survey is required; it must cover the full range of stage values up to the envisaged extension levels.

(b) Calculate the cross-sectional area (A), wetted perimeter (P), and hydraulic radius ($R = A/P$) at incremental stage values (0.1 m intervals) at the cross-section for the current rating up to the maximum stage. The hydraulic radius (R) must also be calculated (corresponding to the stage intervals) from the structural limit to the envisaged maximum rating level.

(c) Calculate the flow (Q) at the same stage values using the current rating to the current maximum SD relationship.

(d) Determine the velocity (v) from discharge (Q) and cross-sectional area (A) using the conservation of mass. Tabulate the stage, cross-sectional area, wetted perimeter, discharge, and hydraulic radius for the existing rating to the maximum rating.

(e) Plot the hydraulic radius-velocity relationship for the current rating and best-fit a linear trend line through the data points.

(f) Use the accompanying best-fit linear trend line equation to calculate the velocity for hydraulic radius values at above-structure-limit conditions.

(g) Use the derived velocity (v) and surveyed cross-sectional area (A) to calculate the discharge (Q) using the conservation of mass for stages above the structural limit.

(h) Identify the revised upper (or lower) limit to which the SD relationship could apply. When extending the rating to higher flows, this should not go beyond: (i) the following change in cross-section, (ii) the start of outflanking flow, (iii) a change from modular to submerged flow conditions, if the current rating is below the modular limit, and (iv) the following change in submergence if submerged conditions already exist. Sound judgement must be exercised to determine these thresholds.

(i) Fit a standard power-law equation to the pairs of Q and H values for the above-structure-limit conditions.

The VE-MA method is limited to a first-order polynomial function [Eq. (2.52)], while the VE-MA definition diagram is shown in Figure 2.23. In applying the VE-MA, it is assumed that n and $S_f^{1/2}$ are constant for corresponding Q values, while $AR^{2/3}$ plot as straight line, given that A and R are reliant on stage.

$$Q \quad = aAR^{2/3} + b \qquad (2.52)$$

where Q is the discharge (m^3/s), A the cross-sectional area (m^2), R is the hydraulic (m), and a to b are algebraic constants.

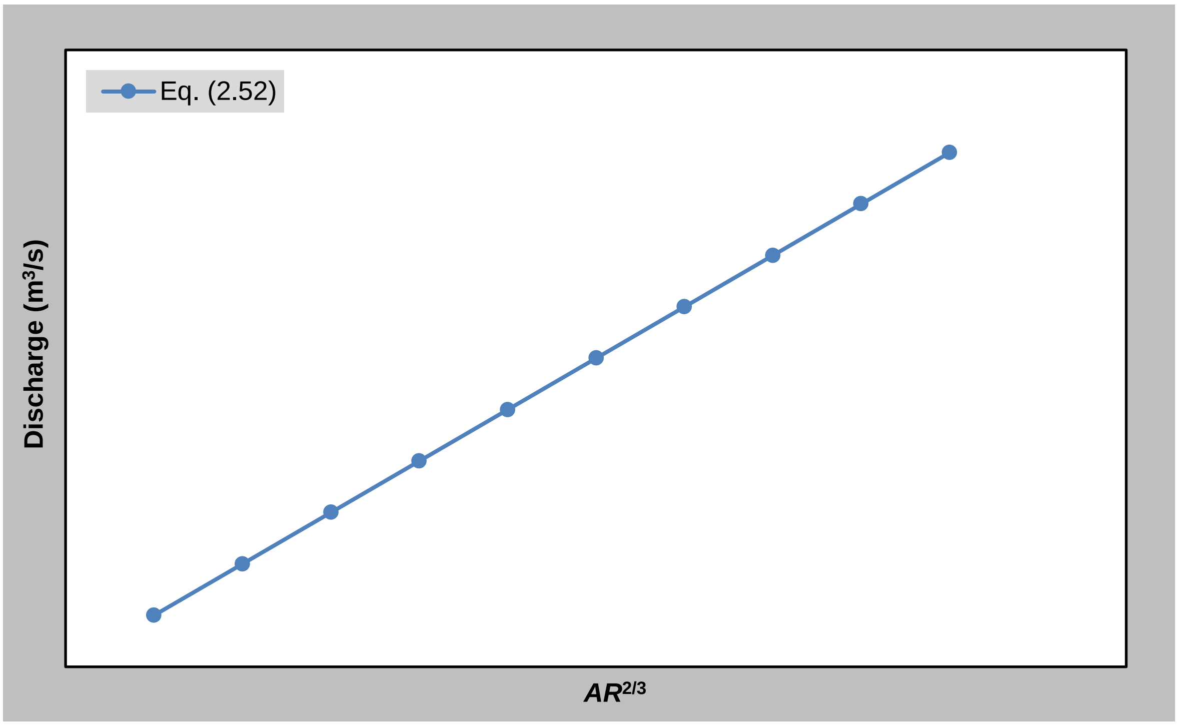

Figure 2.23: Definition diagram VE-MA computation.

The VE-MA can be applied systematically as follows (Ramsbottom and Whitlow, 2003):

(a) A complete, up-to-date cross-sectional survey is required, and it must cover the full range of stage values up to the envisaged extension levels.

(b) Calculate the cross-sectional area (A), wetted perimeter (P), and hydraulic radius (R = A/P) at incremental stage values (0.1 m intervals) at the cross-section for the current rating up to the maximum stage. The hydraulic radius (R) must also be calculated (corresponding to the stage intervals) from the structural limit to the envisaged maximum rating level.

(c) Calculate the flow (Q) at the same stage values using the current rating to the current maximum SD relationship. Tabulate the stage, cross-sectional area, wetted perimeter, discharge, hydraulic radius, $AR^{2/3}$ for the existing rating to the maximum rating.

(d) Plot the discharge-$AR^{2/3}$ relationship for the current rating and best-fit a linear trend line through the data points.

(e) Use the accompanying best-fit linear trend line equation to calculate the discharge for $AR^{2/3}$ values for above-structure-limit conditions.

(f) Identify the revised upper (or lower) limit to which the SD relationship could apply. When extending the rating to higher flows, this should not go beyond: (i) the following change in cross-section, (ii) the start of outflanking flow, (iii) a change from modular to submerged flow conditions, if the current rating is below the modular limit, and (iv) the following change in submergence if submerged conditions already exist. Sound judgement must be exercised to determine these thresholds.

(g) Fit a standard power-law equation to the pairs of Q and H values for the above-structure-limit conditions.

2.5.5 Slope area method

The SAM considers the hydraulic radius, cross-sectional area, channel bed (water surface) slope and roughness coefficients (e.g., Manning's n-values or Chézy's k_s-values) to determine the SD relationship at a given site. Two approaches are associated with SAM, i.e., the simple approach (SA) and divided channel method (DCM) (EA UK, 2002a).

In using the SAM-SA, the cross-sectional areas and water surface slopes are determined for a range of discharges, while the mean velocity and discharge in the channel are calculated using Manning's or Chézy's open-channel flow equation (EA UK, 2002a).

The cross-sectional area and hydraulic radius are calculated for different stage values based on a cross-sectional survey. At least three cross-sections should be used to obtain an average reach. Both Manning's n-values and the water surface slope differ with stage; therefore, these parameters must be estimated for different stage values. Subsequently, the corresponding discharges will be calculated, and a rating equation can be fitted to the set of calculated discharge and stage values (EA UK, 2002a).

Accurate measurements of the water surface slope, which is assumed to be parallel to the channel bed slope (S_o), are often challenging to obtain since the friction slope (S_f) is often used to approximate S_o. The latter approximation is considered to be accurate in uniform river reaches unaffected by backwater and drawdown effects (Ramsbottom and Whitlow, 2003).

The SAM-SA does not permit the accurate extension of SD relationships for overbank flow conditions where the wetted perimeter and the hydraulic radius change rapidly. The overbank conditions will affect the calculated ratings above bankfull conditions. In addition, variable roughness coefficients present in these ranges will render the SAM unsuitable (Ramsbottom and Whitlow, 2003).

The SAM-DCM requires surveyed cross-sections that include the main channel and floodplains. The surveyed cross-sections are divided into three panels using vertical division lines, i.e., the left bank floodplain, main channel, and the right bank floodplain. The channel rating is extended above bankfull, assuming no friction on the vertical boundaries for above bankfull flow conditions. Separate ratings are calculated for each component using different roughness coefficient values and summed to obtain a rating for the section. The roughness coefficients are split among the right bank, left bank and weir (main channel) (Ramsbottom and Whitlow, 2003). Vertical lines will form between the weir (main channel) and the left and right banks, respectively. These vertical lines will be evident during the computations, i.e., the weir computation will continue vertically past the structural limit, assuming there is no friction on the vertical lines for the above bankfull conditions.

The following hydraulic conditions are suitable for the use of the SAM to extend SD relationships (EA UK, 2003):

(a) Uniform reaches without longitudinal changes along the river reach, channel shape and backwater effects.
(b) Straight or gradually curved channels with parallel floodplains.
(c) The SAM can be used in combination with other methods to provide an overbank SD rating, such as the VE methods.

The following hydraulic conditions are not suitable for using the SAM (EA UK, 2003):

(a) Meandering channels, channels which cross the floodplain on a skew angle or bend. The SAM can only be used in short straight river reaches.

(b) The SAM method does not consider the interference between the fast-moving channel flow and slow-moving floodplain flow, and this can be significant during shallow depths of floodplain flow.

The following data requirements are essential in the application of the SAM (EA UK, 2002b):

(a) At least one, but preferably three cross-sections of the main channel, and floodplains if the DCM is used.

(b) The current SD RC, while conventional current gaugings at higher flows are required to enable the calibration of the channel roughness parameters.

(c) Estimates of water surface slope, and if not available, the water surface slope can be assumed to be parallel to the riverbed. The assumption of the riverbed being parallel can be obtained from survey data.

In applying the SAM, the cross-sectional area, hydraulic radius, and water surface slope are estimated first. Thereafter, the mean velocity is estimated using either Manning's or Chézy equations for uniform flow in open channels. The SAM can be applied systematically as follows (Ramsbottom and Whitlow, 2003):

(a) At each cross-section, determine the cross-sectional area (A), wetted perimeter (P) and subsequently the hydraulic radius (R) at incremental levels of stage (0.1 m intervals) up to the proposed new rating limit.

(b) Determine the water surface slope (S_o) either directly or using the riverbed slope. A single value of S_o is generally used for all stages.

(c) Estimate the roughness coefficients using the current rating to the maximum rating. Ideally, the roughness coefficients should be estimated from or calibrated against actual current gaugings. When extending the SD RC to higher stages, either the roughness coefficients at the maximum rating should be used, or a plot of the roughness coefficients against stage could be used to extend these to higher stages.

(d) The corresponding discharges are calculated by applying the equation to the stages for above-structure-limit conditions. A best-fit trend line is then fitted to the plot to establish the rating equation.

The SAM-DCM applies to compound channels where over-bank flow conditions exist. The method assumes that the river channel and flood plain cross-sections are constant upstream and downstream from the flow-gauging site under consideration and can be applied systematically as follows (Ramsbottom and Whitlow, 2003):

(a) Compartmentalised the cross-sections in the river reach at the flow-gauging weir, and/or in the floodplain, i.e., left bank and right bank floodplains, using vertical division lines.
(b) Calculate the rating for the channel section (or flow-gauging weir) using the SAM as described above.
(c) Calculate the cross-sectional area (*A*), wetted perimeter (*P*), and subsequently the hydraulic radius (*R*) for the channel at incremental levels of the stage above bankfull conditions. The latter calculations assume that there is no friction on the vertical lines for above bankfull flow conditions.
(d) Use the bankfull roughness coefficient values and S_o to extend the in-channel/structure rating above bankfull flow conditions.
(e) Establish separate ratings for the left bank and right bank floodplains. In using the same incremental levels as in Step (c), A, *P* and *R* should be calculated.
(f) Use the same S_o value as in Step (d) for the floodplains. Initial roughness coefficients can be determined using standard references, e.g., Chow (1959).
(g) Add the computed discharges for the channel (or structure) and floodplains at each stage interval to obtain the cumulative discharge, i.e., SD RC for the section.

The series of equations [Eqs. (2.53) – (2.63)] listed below could be used in Microsoft Excel to apply the SAM-MA and SAM-CHZ approaches in non-prismatic channels:

$$VH_u = \frac{\left(Q_{assumed}/A_u\right)^2}{2g} \tag{2.53}$$

$$VH_d = \frac{(Q_{assumed}/A_d)^2}{2g} \tag{2.54}$$

$$hf = f + [0.5x(VH_u - VH_d)] \quad \text{if} \quad VH_u > VH_d \tag{2.55}$$

$$hf = f + [1x(VH_u - VH_d)] \quad \text{if} \quad VH_u < VH_d \tag{2.56}$$

$$S_e = \frac{hf}{L} \tag{2.57}$$

$$K_u = \frac{A_u R_u^{2/3}}{n} \tag{2.58}$$

$$K_d = \frac{A_d R_d^{2/3}}{n} \tag{2.59}$$

$$K_u = A_u C \sqrt{R_u} \tag{2.60}$$

$$K_d = A_d C \sqrt{R_d} \tag{2.61}$$

$$K = \sqrt{K_u * K_d} \tag{2.62}$$

$$Q = K S_e^{1/2} \tag{2.63}$$

where A_u the upstream cross-sectional area (m^2), A_d the downstream cross-sectional area (m^2), C is the Chézy's roughness coefficient (m$^{0.5}$/s), f is the change in the channel water surface level between two cross-sections (m), g is the gravitational acceleration (m^2/s), h_f is the head loss (m), K is the conveyance, K_u is the upstream conveyance, K_d is the downstream conveyance, L is the length of the reach (m), n is the Manning's roughness coefficient (s/m$^{1/3}$), Q is the discharge (m^3/s), $Q_{assumed}$ is the assumed discharge for computation (m^3/s), R_u is the upstream hydraulic radius (m), R_d is the downstream hydraulic radius (m), S_e is the energy slope (m/m), VH_u is the upstream velocity head (m), and VH_d is the downstream velocity head (m).

2.5.6 Stepped backwater analysis

The SBA using the standard step computation method, applies to non-prismatic channels. Field survey data are required, e.g., the longitudinal river profile, cross-sections, and a detailed description of the roughness coefficients possibly applicable to each cross-section. The SBA calculations are done on a trial-and-error basis (Chow, 1959), or can be automated using solver functions in Microsoft Excel. All the computations are done within the gradually varied flow (GVF) regime.

The following assumptions apply to GVF (Chow, 1959):

(a) Hydrostatic distribution of pressure is over the whole channel.
(b) The flow is steady, i.e., the hydraulic characteristics remain constant for the time interval under consideration.
(c) The channel slope is insignificant.
(d) The depth of flow is equal to the normal flow depth.
(e) Pressure correction is equal to unity.
(f) No air entrapment occurs.
(g) If the channel is prismatic, it has a constant alignment and shape.
(h) The velocity distribution in the channel is fixed; therefore the velocity distribution coefficients are constant.
(i) The conveyance and section factors of the channel are exponential functions of the flow depth.
(j) Roughness coefficients are independent of the flow depth and are constant in the reach under consideration.

The following limitations are associated with GVF:

(a) The basic equation of GVF describes a gradual change in the water surface elevation, i.e., an insignificant slope. The challenge of numerical integration is to determine an appropriate step size from a spatial point of view (Malekabadi and Kalateh, 2019).
(b) The method assumes that the channel cross-section, channel slope and roughness coefficients remain constant; the opposite is evident in natural, non-prismatic channels (Moglen, 2015).

(c) The numerical aspects of the differential equation for GVF in open-channel flow computations allow for several solutions. Hence, it is possible to obtain two numerical solutions, especially in the case of the standard step method (Artichowicz and Ssymkiewicz, 2014).

In identifying possible cross-sections to be used in the SBA, the following criteria should be met (Thomason, 2019; Van der Spuy, 2022):

(a) Four to five cross-sections are enough for the water level to converge to the required accuracy.
(b) The number and frequency of cross-sections required are a function of the irregularity of the stream.
(c) The more irregular the stream, the more cross-sections are required to ensure a high level of accuracy.
(d) The distance between cross-sections is dependent on the riverbed slopes, with flatter slopes requiring more cross-sections, given that the flow profile convergence will be more distant.
(e) The cross-sections must represent the reach between them.

The series of equations [Eqs. (2.64) – (2.73)] listed below could be used in Microsoft Excel to apply the SBA-MA and SBA-CHZ approaches in non-prismatic channels:

$$K = \frac{AR^{2/3}}{n} \tag{2.64}$$

$$K = AC\sqrt{R} \tag{2.65}$$

$$F_R = \sqrt{\frac{Q^2B}{gA^3}} = 1 \tag{2.66}$$

$$v = \frac{Q}{A} \tag{2.67}$$

$$V_H = \frac{v^2}{2g} \tag{2.68}$$

$$T_{H1} = WSE + V_H \tag{2.69}$$

$$S_f = \left(\frac{Q}{K}\right)^2 \tag{2.70}$$

$$S_{favg} = \frac{S_{f1} + S_{f2}}{2} \tag{2.71}$$

$$S_{floss} = Lx\overline{S_f} \tag{2.72}$$

$$T_{H2} = T_{H1} + S_{floss} \tag{2.73}$$

where A is the wetted cross-sectional area of the channel (m^2), B is the top width of water in the channel (m), C is the Chézy's roughness coefficient (m$^{0.5}$/s), F_R is the Froude number, g is the gravitational acceleration (m^2/s), K is the conveyance, L is the length between two cross-sections (m), n is the Manning's roughness coefficient (s/m$^{1/3}$), Q is the discharge (m^3/s), R is the hydraulic radius (m), S_f is the friction slope (m/m), S_{favg} is the mean of the friction slope (m/m), S_{f1} is the downstream friction slope for supercritical flow/upstream friction slope for sub-critical flow (m/m), S_{f2} is the upstream friction slope for supercritical flow/downstream friction slope for sub-critical flow (m/m), S_{floss} is the friction loss between two cross-sections (m), T_{H1} is the total head before friction loss (m), T_{H2} is the total head after friction loss (m), v is the velocity at the cross-section (m/s), V_H is the velocity head (m) and *WSE* is the water surface elevation at the cross-section (m).

<u>Profile convergence for SBA:</u>

It is important to note that the starting water surface level or elevation in the SBA is regarded as unknown or indefinite; hence, several backwater profiles based on different arbitrary water surface levels should be computed until convergence occurs, i.e., the water levels correspond with the uniform flow profile and energy levels are in equilibrium. Therefore, if convergence is not reached (probably owing to insufficient cross-sectional survey data), additional and more distant (up- and/or downstream) cross-sections would be required (Thomason, 2019).

In this research at some of the flow-gauging sites under consideration, DWS had already established an arbitrary datum (reference level), and known water surface levels (e.g., flood marks). Subsequently, defining an arbitrary point to reach profile convergence as explained above was not required in these cases.

In general, the procedures to follow when hydraulic methods are used to develop SD relationships and/or to extend RCs to represent above-structure-limit flow conditions, are summarised in Figure 2.24:

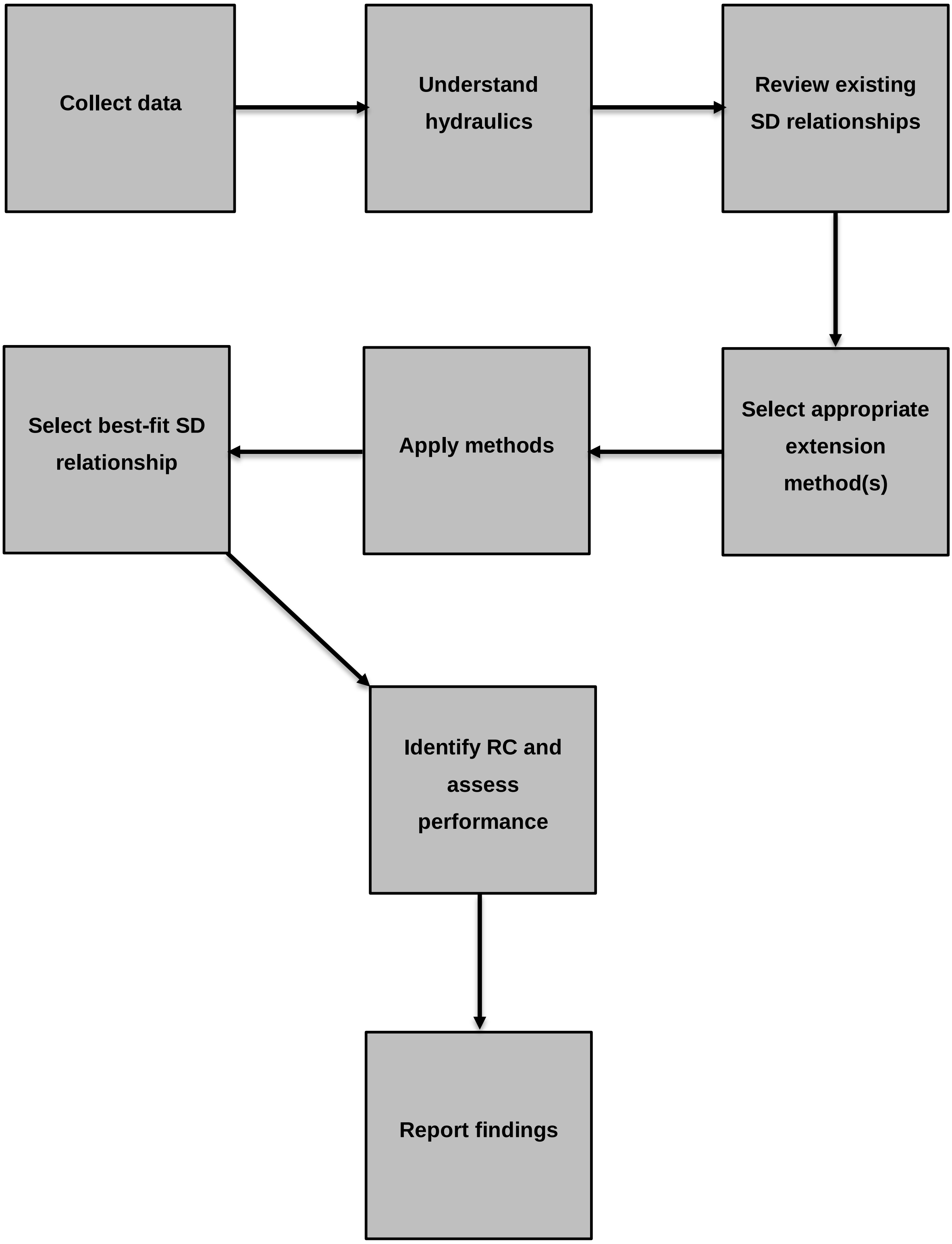

Figure 2.24: Hydraulic extension method procedure matrix

2.6 HEC-RAS

The USACE (2016) developed the Hydraulic Engineering Centre River Analysis System (HEC-RAS). The software can perform one-dimensional steady flow, two-dimensional unsteady flow, sediment transport, and water temperature/water quality modelling.

2.6.1 Development

The first versions of the HEC computer software emerged in the 1950s and 1960s. Bill Eichert developed the precursor to HEC-RAS (HEC-2) in 1964. The software was updated in 1966 and referred to as the *Backwater Any Cross-Section* software. Typically, the software application enabled the computation of water surface profiles in non-prismatic channels using various cross-sections. Hence, the latter software presented a significant step in developing modern computer programs for hydraulic analysis techniques (Maeder, 2015).

In the 1990s, Microsoft Windows and HEC's next-generation software were developed. The software development originated in the Linux's processor (UNIX) and later moved to Microsoft Windows. Visual Basic as the programming language rapidly migrated to MS-DOS. HEC-RAS Version 1.0 was released in August 1995, with subsequent updates every few years (Maeder, 2015).

The modern version of HEC-RAS builds on the advances from previous generations of the software. The software has many capabilities, which are discussed in the next section.

2.6.2 Capabilities and applications

HEC-RAS is capable of performing one- and two-dimensional hydraulic modelling for a complete flow network of natural and constructed channels, floodplain areas and levee protected areas. The software interface provides the following (USACE, 2016):

(a) File management.
(b) Data entry.
(c) Data entry for GIS interfaces.

(d) River analysis.

(e) Tabulation and graphical displays of river input and output data.

(f) Inundation mapping and animations.

(g) Reporting facilities.

(h) Online-help.

The steady flow analysis in HEC-RAS is based on the GVF theory. In applying the energy equation, energy losses are assessed by friction and contraction/ expansion coefficients. The momentum equation may be used in situations where the water surface profile varies rapidly, e.g., hydraulic jumps, hydraulics of bridges and evaluating profiles of rivers at confluences. The system can manage a complete network, a dendritic system and/or a full river reach. The effect of structures and obstructions may be considered in the modelling. Special features include multiple plan analyses, profile computations, bridge/culvert opening analyses, bridge scour analyses, split flow optimisation, and stable channel design and analysis (USACE, 2016).

Unsteady (US) flow analyses can either be based on one-dimensional, two dimensional, and combined one-two dimensional flow conditions throughout an entire network of open channels, floodplains, and alluvial fans. Essentially, the entire dynamic 1-D Saint-Venant equation using an implicit, finite differential method, is solved during the US flow analyses. Provision is made for supercritical, sub-critical, and mixed flow regimes. Special features of the US modelling component include extensive hydraulic structure capabilities such as: (i) dam break analysis, (ii) levee breaching and overtopping, (iii) pumping stations, (iv) navigation dam operations, (v) pressurised pipe systems, (vi) automated calibration features, (vii) user-defined rules, and (viii) combined 1-D and 2-D modelling.

Graphics and reporting include X-Y plots of the river schematic, cross-sections, profiles, RCs, hydrographs, and inundation mapping. A three-dimensional plot of multiple cross-sections is available. Tabular output is available in the form of pre-defined tables or user-defined tables. Graphical and tabular outputs can be printed directly or exported.

2.6.3 Limitations

The following limitations are associated with HEC-RAS (USACE, 2016):

(a) Steep bed slopes of above 10% produce errors.

(b) Multi-dimensional flow characteristics.

(c) Complex pipe systems.

2.6.4 HEC-RAS modelling tools for stage-discharge relationships

Standard hydraulic calculations can be performed manually for prismatic channels. However, as highlighted before, such computations become more challenging in natural non-prismatic channels where US flow dominates. Hence, the extension of any SD RC at a flow-gauging site would require US flow computation capabilities; however, the modelling tools available for the extension of SD RCs, are primarily one-dimensional (EA UK, 2002b).

In a 1-D model, the river system is represented by a series of cross-sections in any configuration, including loops and branches, while floodplains can be represented in the following ways (EA UK, 2002b):

(a) There is an extension to each river cross-section, and there are no embankments or high ground between the river and the floodplain.

(b) Floodplains having separate flow paths to the river, can be defined by different cross-sections.

(c) Floodplains can be viewed as static storage areas, where the flow path does not pass through the floodplain.

In 1-D modelling, the flow is assumed to be perpendicular; hence, the following apply (EA UK, 2002b):

(a) Lateral flows and velocities are neglected.

(b) The water level is constant across the cross-section.

(c) The flow occurs across the whole width of the cross-section unless part of the cross-section represents flood stage, which can be set in the model parameters.

Sound judgement and experience are required to justify (and prove) whether 1-D hydraulic modelling can be applied to extend SD RCs. Ultimately, such a decision will predominantly be controlled by the site hydraulics. In cases where limited data are available at a flow-gauging site, the guidelines below highlight when 1-D hydraulic modelling would not be appropriate (EA UK, 2002b):

(a) The approach conditions are not ideal for the structure, with little or no calibration data available. 1-D models would not be appropriate, given that the flow lines would not be parallel.

(b) The submergence of non-standard structures where the Navier Stokes equation can represent the submergence.

(c) Submergence which shallow water equations cannot represent.

(d) Complex non-standard structures with no or little calibration data.

(e) SD RCs are affected significantly by outflanking at the gauging site. 1-D models assume that the water level is constant across the floodplain, with no allowance for lateral flows.

(f) Wide floodplains with a significant difference in the velocity and water levels across the floodplain.

(g) No calibration data for embankments and other obstructions are available. 1-D models require roughness coefficients for these non-standard structures.

(h) Complex floodplains significantly impact the rating; however, very little topographical data are available. Without this information, floodplain flows may be in error in the model and lead to uncertainties in the total flow.

(i) Finally, the transition between in-bank and overbank flow, where interface occurs between the fast-moving channel and slow-moving floodplain flow. Typically, 3-D hydraulic effects occur; these effects can be significant at low flow depths, especially if floodplain flows are present.

2.6.5 HEC-RAS modelling best practices

CivilGEO (2022) recommends the following best practices applicable to defining, analysing, and reviewing a HEC-RAS model:

(a) The model results must be evaluated for consistency and accuracy.

(b) The cross-section detailed output warning messages should be evaluated, investigated and properly justified/motivated.

(c) The profile plot should be inspected, especially at roadway crossings. The energy grade line should be plotted along with the computed water surface elevations during this evaluation.

(d) Bridge opening results should be evaluated to ensure that the low chord clears the computed energy grade line elevation.

(e) Cross-sections should extend high enough to contain the defined discharge values. If not, the software will extend the cross-section ends vertically to contain the modelled flow.

(f) Cross-sections must be correctly positioned along a river reach to represent any changes in the river geometry. As a general rule, cross-sections should be spaced at five (5) times the channel width under consideration.

(g) Additional cross-sections should be included at locations where changes in discharge, slope, velocity, and/or roughness occur.

(h) Cross-sections just up- or downstream of roadway crossings (bridges and culverts), inline structures (dams and spillways), and levees (flood walls) are compulsory.

(i) Channels with steeper slopes would require more cross-sections.

(j) Streams that flow at high velocities may require cross-sections at approximately every 30 m.

(k) Large uniform rivers with flat slopes in rural areas would require cross-sections every 300 to 500 m.

(l) The review of any cross-sections where the computed water surface elevation is equal to critical depth is necessary. The flow regime at these cross-sections is likely to vary between super and/or sub-critical flow; hence, a mixed flow regime analysis should be performed.

(m) Downstream boundary inputs cannot have a flat or negative slope. If necessary, the downstream end of the model should be extended to provide a positive slope for the channel bed.

(n) The evaluation of ineffective flow areas elevations is necessary at roadway crossing structures. If a roadway structure is overtopped, the ineffective flow area on the downstream side of the structure should also be overtopped with flow being blocked-off.

(o) Commence with a simplified model setup to ensure the model is running successfully. Then add complexity to the model in iterative steps, confirming for each iteration that the model is running successfully to complete the overall modelling process.

2.6.6 Estimation of roughness parameters in HEC-RAS

Roughness parameters in HEC-RAS are primarily based on Manning's *n*-values. Typically, Manning's *n*-values need to be determined at each cross-section by comparing the observed (actual) stages during a flood, i.e., flood marks, with the simulated stages as estimated with the 1-D hydraulic models (steady flow) and/or other relevant hydraulic methods. The *n*-values are adjusted until the observed and simulated stages and discharges agree (Abbas *et al.*, 2020).

An overview of the flow-gauging site selection criteria and characteristics is provided in the next chapter.

CHAPTER 3 : FLOW-GAUGING SITE SELECTION

This chapter provides an overview of the selection criteria used to identify the 10-case study flow-gauging sites for the purpose of SD extensions using direct and indirect extension methods. In addition, the location, general characteristics, type of flow-gauging weirs, and extension methods used at each site are also elaborated on.

3.1 Selection Criteria

Initially, all the SD extension reports available from DWS, i.e., the *Discharge Table Improvement Reports*, were studied given that a standard SD rating table is regarded as the first step towards the extension of any SD relationship. As pilot case study, a total of 10 flow-gauging sites in Limpopo (LP), Gauteng (GP), Free State (FS), Mpumalanga (MP), KwaZulu-Natal (KZN) and the Western Cape (WC) provinces were selected based on the range of possible site conditions present. In terms of the hydrometric and geometric data requirements, the selection of the flow-gauging sites was based on and considered all aspects related to streamflow data, hydraulic conditions, and geometric properties as listed below:

(a) **Streamflow data:** Record length, data quality, flow duration curves to highlight the occurrence and frequency of minimum and maximum flow ranges, and the number of standard and extended SD relationship tables/curves available.

(b) **Hydraulic conditions:** Modular and/or submerged flow conditions, variable submergence due to backwater effects and vegetative growth, identification of possible hydraulic controls, sediment transport, unsteady flow conditions, and the influence of in-bank and out-of-bank flow paths.

(c) **Geometric properties:** Type of flow-gauging weir, e.g., sharp/broad-crested, Crump, hydro-flumes, broad-crested flank walls, flood/natural sections, overall river topography and layout, river channel and flood plain geometry, position of control points within the river system (especially at high flows), availability of survey data, e.g., cross-sections, longitudinal sections, previous flood surveys, and the previous/current allocation of site-specific roughness parameters (typical range possible to account for seasonal variability).

3.2 Flow-Gauging Site Characteristics

As shown in Figure 3.1, the 10 flow-gauging sites are located in secondary drainage regions A4, A6, C2, C5, H5, J1, K2, V1 and X3.

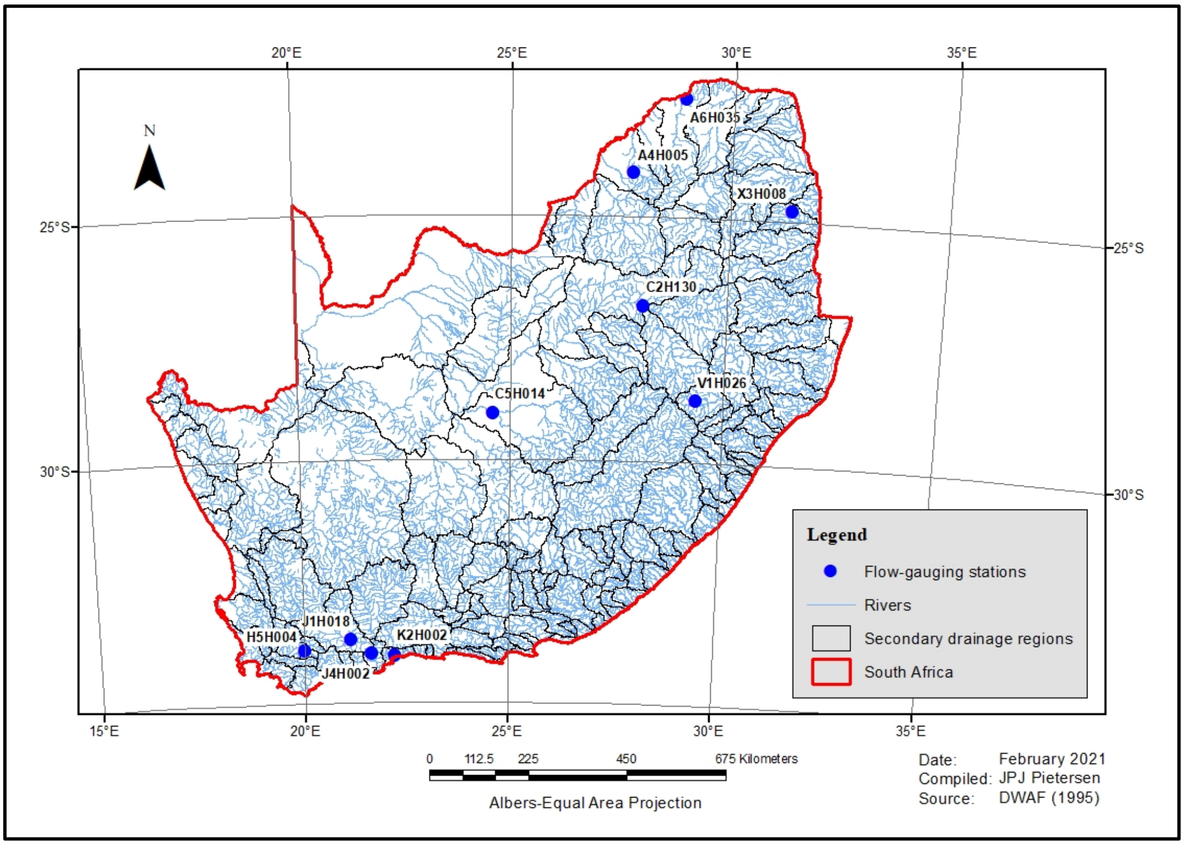

Figure 3.1: Location of the 10 flow-gauging sites in South Africa

Typically, the chosen flow-gauging sites are characterised by complex flow (hydraulic) conditions and are not necessarily sites that had gradual changes in geometric properties. Ultimately, the sites chosen are inclusive of the following problem areas: (i) submergence, (ii) estimation problems, (iii) complex geometry, and (iv) unsuitable sites for the construction of flow-gauging weirs.

As detailed in Chapter 4, a variety of direct extension (benchmark) and indirect extension methods was applied at each of the 10 flow-gauging sites.

Table 3.1 contains a summary of all the relevant characteristics present at each flow-gauging site.

Table 3.1: Summary of flow-gauging site characteristics

Case study	Site	Latitude Longitude	Period of record	River Province	Type of structure	Structural limit (*Q* & *H*)	Benchmark method	Indirect methods
1	A4H005	24°04'58"S 27°46'23"E	1962/08/27 to present	Mokolo LP	Compound weir 5 Sharp crests 6 Broad crests	Q = 115 m^3/s H = 1.4 m	Level pool (back) routing	SE, LE & VE
2	A6H035	22°32'0.7"S 28°53'51.1"E	1995/02/02 to present	Mogalakwena LP	Compound weir 4 Sharp crests	Q = 153 m^3/s H = 1.3 m	Level pool (back) routing	SE, LE & VE
3	C2H003 (C2H130)	28°49'11"S 28°03'49"E	1924/01/29 to present	Vaal GP	C2H003 Compound weir 8 Sharp crests C2H130 Flood section (FS)	Q = 481 m^3/s H =2.2 m	Level pool (back) routing	SE, LE & VE
4	C5H014	29°02'33"S 24°35'57"E	1969/07/03 to present	Riet FS	Compound weir Broad-crest V-Crump	Q = 90 m^3/s H = 1 m	SBA	SE, LE, VE, SAM, SBA & HEC-RAS
5	H5H004	33°53'52"S 20°00'46"E	1970/03/24 to present	Bree WC	Compound weir Hydro-flume 2 Sharp crests	Q = 81 m^3/s H = 1.4 m	SBA	SE, LE, VE, SAM, SBA & HEC-RAS
6	J1H018	33°41'05"S 21°08'46"E	1982/04/07 to present	Touws WC	Compound weir V-Crump (low) 4 Crumps	Q = 131 m^3/s H = 2 m	SBA	SE, LE, VE, SAM, SBA & HEC-RAS
7	J4H002	34°01'02.2"S 21°45'24"E	1964/05/01 to present	Gourits WC	Natural flood section (FS) at bridge	N/A	SBA	SE, LE, VE, SAM, SBA & HEC-RAS
8	K2H002	34°01'40"S 22°13'21"E	1961/05/05 to present	Groot Brak WC	Compound weir 4 Sharp crests	Q = 55 m^3/s H = 1.5 m	Wolwedans Dam spillage	SE, LE & VE
9	V1H026	28°43'15"S 29°21'33"E	1967/08/01 to present	Tugela KZN	Compound weir 4 Sharp crests Hydro-flume	Q = 98 m^3/s H =1.2 m	Hydrograph analysis	SE, LE & VE
10	X3H008	24°46'08"S 31°23'24"E	1967/09/01 to present	Sand MP	Compound weir Sharp crest Hydro-flume Broad-crested flank walls	Q = 76 m^3/s H = 1.95 m	SBA	SE, LE, VE, SAM, SBA & HEC-RAS

The detailed methodology adopted in meeting the specific objectives of this research is discussed in the next chapter.

CHAPTER 4 : METHODOLOGY

This chapter presents the methodology adopted to extend the observed SD relationships to above-structure-limit conditions using the various indirect, hydraulic extension methods and one-dimensional HEC-RAS modelling as discussed in Chapter 2. The hydraulic methods considered and elaborated on in this chapter are the: (i) SE, (ii) LE, (iii) three different VE methods, (iv) SAM using the MA and CHZ approaches, and (v) SBA using the MA and CHZ approaches.

4.1 Case Study Approach

The 10 flow-gauging sites as identified and discussed in Chapter 3 were used as case study flow-gauging sites to enable the comparison between the indirect extension and direct extension (benchmark) methods applied at each site in an attempt to model the SD relationships. According to Rowley (2002), such case studies would help to answer “How?” and “Why?” questions, especially when descriptive and explanatory research are conducted. Hence, in each case study, the following aspects were investigated: (i) site characteristics and hydraulics, (ii) existing SD relationships and associated data available, and (iii) suitability of the various indirect extension methods.

4.2 Data Collection for the Extension of Rating Curves

As discussed in Chapter 3 (*cf.* Section 3.1), data were collected based on the hydrometric and geometric requirements for the extension of SD relationships. Initially, all the SD extension reports available from the DWS (Directorate of Surface and Groundwater Information, Flood Studies), i.e., the *Discharge Table Improvement Reports*, were studied given that a standard SD rating table is regarded as the first step towards the extension of any SD relationship. In general, flow data were obtained directly from the DWS website (https://www.dws.gov.za/Hydrology/) for modelling purposes.

As highlighted in Chapter 3, in terms of the hydrometric and geometric data requirements, all aspects related streamflow data, hydraulic conditions, and geometric properties were considered.

4.3 Processing of Geometric Data

As highlighted in Chapter 2 (*cf.* Section 2.4.3), the processing of geometric data, e.g., wetted perimeter, wetted area, and hydraulic radius, was done by using the Windows Cross-Section Professional (WinXSPRO; Hardy *et al.*, 2005), which is essentially a channel cross-section analyser as shown in Figure 4.1:

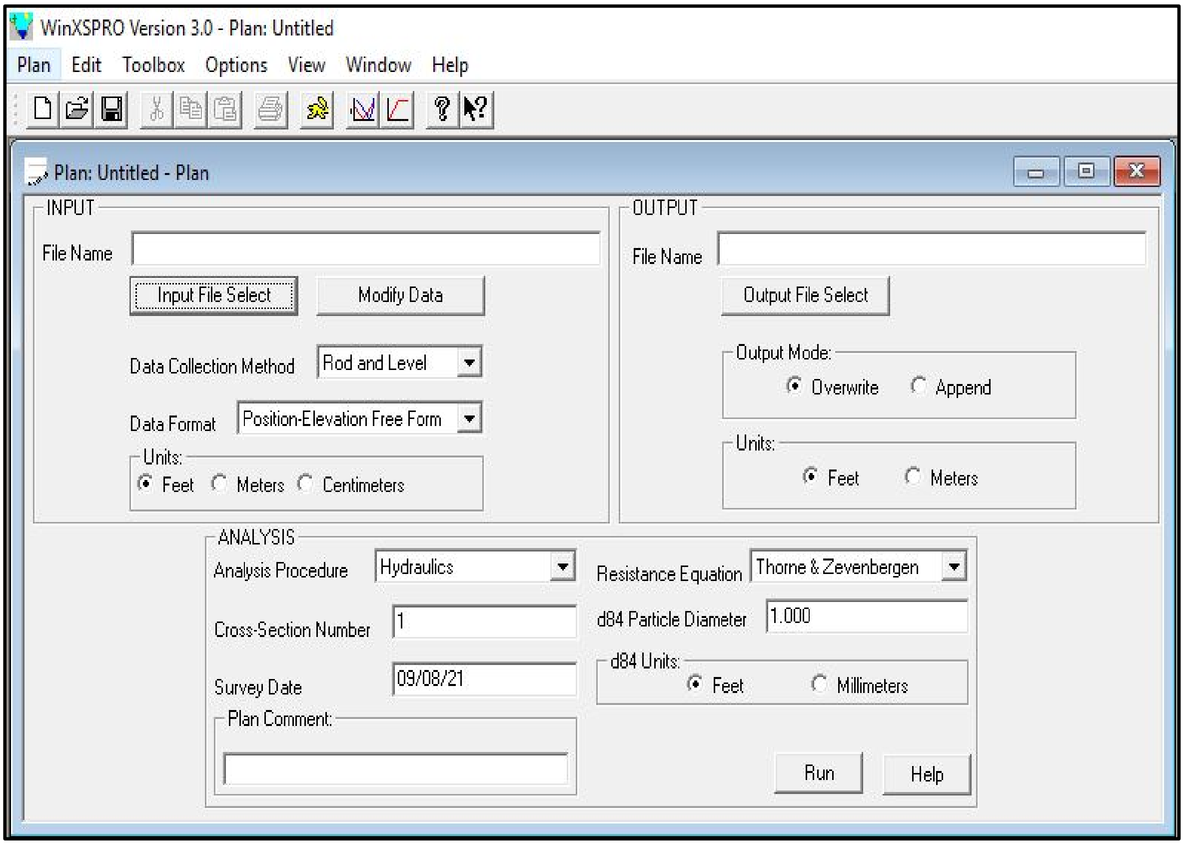

Figure 4.1: WinXSPRO user-interface (Hardy *et al.*, 2005)

Prior to the use of WinXSPRO, all the files were generated in Microsoft Excel with Position-Elevation Free Form as the data format. Each line in the worksheet has associated station-elevation pairs (x & y values) separated by tabs (tab-delimited). In each case, the MS Excel file was saved and renamed to *.sec for further analyses in WinXSPRO using *hydraulic* as the analysis procedure, while all the output units are specified to be in *meters*. WinXSPRO generates an output cross-section, as shown in Figure 4.2, that visually displays the cross-section in meters with the stage on the y-axis and the horizontal position on the x-axis (Hardy *et al.*, 2005).

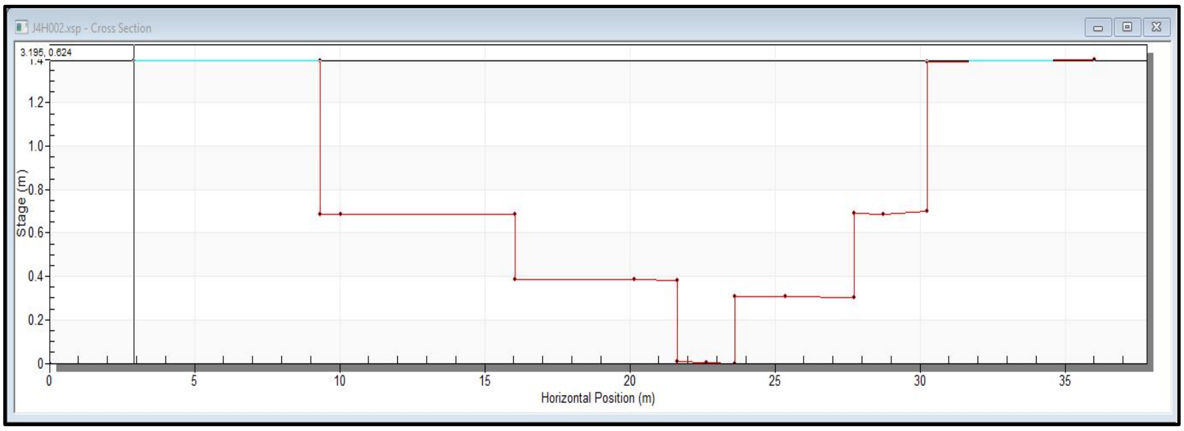

Figure 4.2: Example of a cross-section at J4H002 (Case study 7)

In addition, a Stage and Section Editor, as displayed in Figure 4.3, enabled the definition of the low stage, high stage, channel slopes, and the stage increment to be used, while a boundary section functionality enabled the sub-division of cross-sections into sub-sections, if required.

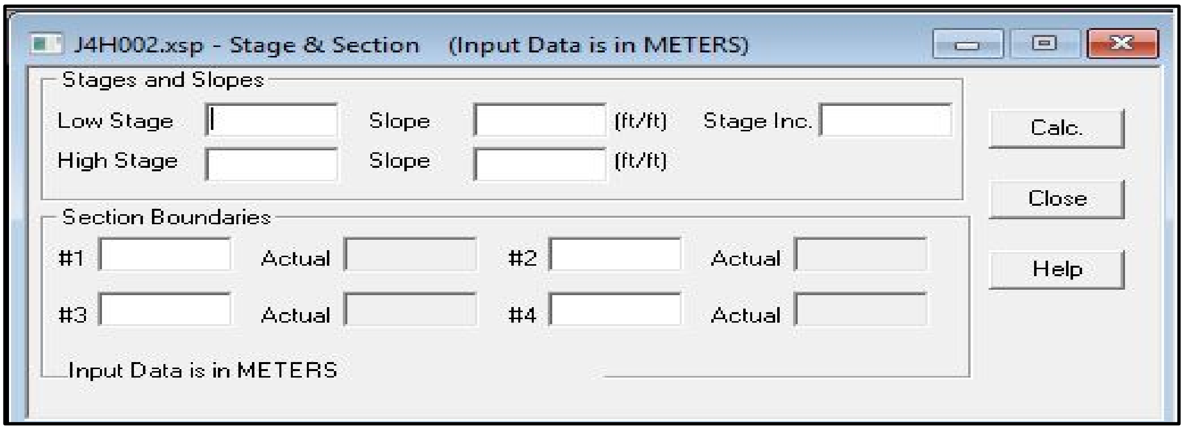

Figure 4.3: Stage and Section Editor at J4H002 (Case study 7)

A typical WinXSPRO output screen is shown in Figure 4.4. In this research, the outputs related to stage (*H*), area (*A*), wetted perimeter (*P*), and hydraulic radius (*R*), were used in the further computations. All the geometric properties applicable to each flow-gauging site are listed in Tables A.1–10, Appendix A.

```
*******************************WinXSPRO*********************************
C:\Winxspro_64bit\x3s1.out
Input File:              C:\Winxspro_64bit\x3s1.sec
Run Date:                05/20/20
Analysis Procedure:      Hydraulics
Cross Section Number:    1
Survey Date:             05/20/20


Subsections/Dividing positions
A /  76.95/

Resistance Method:       Thorne and Zevenbergen
            D84:         1.000 mm



Unadjusted horizontal distances used


 STAGE  #SEC      AREA    PERIM   WIDTH   R        DHYD         SLOPE                n     VAVG       Q
  (m)             (sq m)    (m)    (m)     (m)       (m)        (m/m)                       (m/s)    (cms)
  0.10    T       0.13     3.29    3.26   0.04     0.04         1.0000            0.015    7.91       1.05
  0.20    T       0.77     9.56    9.51   0.08     0.08         1.0000            0.015   12.66       9.77
  0.30    T       2.14    20.36   20.28   0.11     0.11         1.0000            0.015   15.22      32.59
  0.40    T       4.98    34.26   34.15   0.15     0.15         1.0000            0.015   18.79      93.51
```

Figure 4.4: Example of WinXSPRO output at X3H008 (Case study 10)

4.4 Development and Application of Semi-automated Extension Tools

A specific objective of this research was to develop semi-automated extension tools in Microsoft Excel to automate some procedures associated with the extension of SD relationships. The semi-automated tools consist of different functions (as applicable to each hydraulic extension method) to ultimately provide peak discharges at specific stages above the structural limit. The following worksheets are available in the semi-automated toolkit:

(a) Data/information input sheets for SE, LE and VE methods.

(b) SE method.

(c) LE method.

(d) VE-SA.

(e) VE-HRA.

(f) VE MA.

(g) SAM-MA/SAM-CHZ.

(h) SBA-MA/SBA-CHZ.

4.4.1 Simple extension and logarithmic extension

The SE and LE methods were used to extend the existing SD relationships to the above-structure-limit conditions using the SD rating equation associated with the highest limb of the RC, whether the plot is based on standard or log-transformed data.

Similar input is required by the SE and LE methods. The analyses were conducted and automated in two distinctive phases: (i) up to structural limit, and (ii) above structural limit. Rating curves, for the whole *H*-range were generated automatically, while any trend line evaluations were done manually to determine the best-fit polynomial function based on the coefficient of determination (r^2) and the estimated discharge (m^3/s). In each case, the best trend line equation was used for the required extension.

In the case of the LE method, the rating up to structural limit is log-transformed when a first-order polynomial function is applied to the data set. The trend line equation was then used to extend the rating, followed by the linear transformation to result in the final rating values.

Above procedures associated with the SE and LE methods are summarised in the flow diagram as shown in Figure 4.5. Apart from the detailed results included and discussed in Chapter 5, the SE and LE SD extensions for above-structure-limit conditions are listed in Tables A.11–20, Appendix A, and shown in Figures B.1–20, Appendix B.

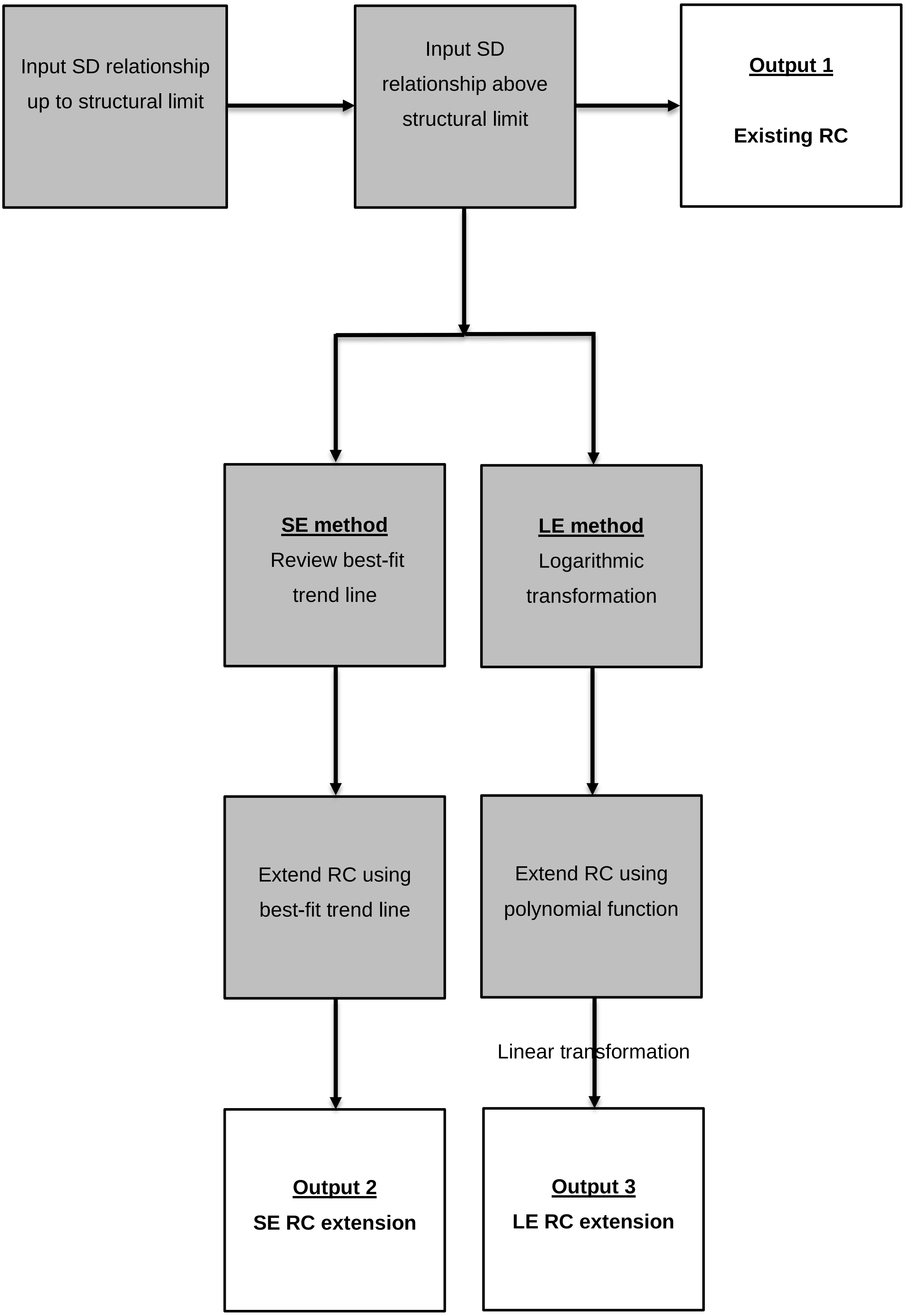

Figure 4.5: SE and LE procedure matrix

4.4.2 Velocity extension

The different approaches to the VE method, i.e., SA, HRA and MA, use various channel and hydraulic parameters to extend SD relationships to high flow regions. All VE methods shared an input worksheet, with inputs for *H*, *A*, *R,* and velocity (*v*) up to structural limit and separate inputs for above-structure-limit geometric properties. Essentially, first-order polynomial equations were generated (*cf.* Chapter 2, Section 2.5.4) to enable the RC fitting and subsequent extension of SD relationships for above-structure-limit conditions. The procedures associated with the different VE methods are summarised in the flow diagram as shown in Figure 4.6. Apart from the detailed results included and discussed in Chapter 5, the VE SD extensions for above-structure-limit conditions are listed in Tables A.11–20, Appendix A, and shown in Figures B.21–50, Appendix B.

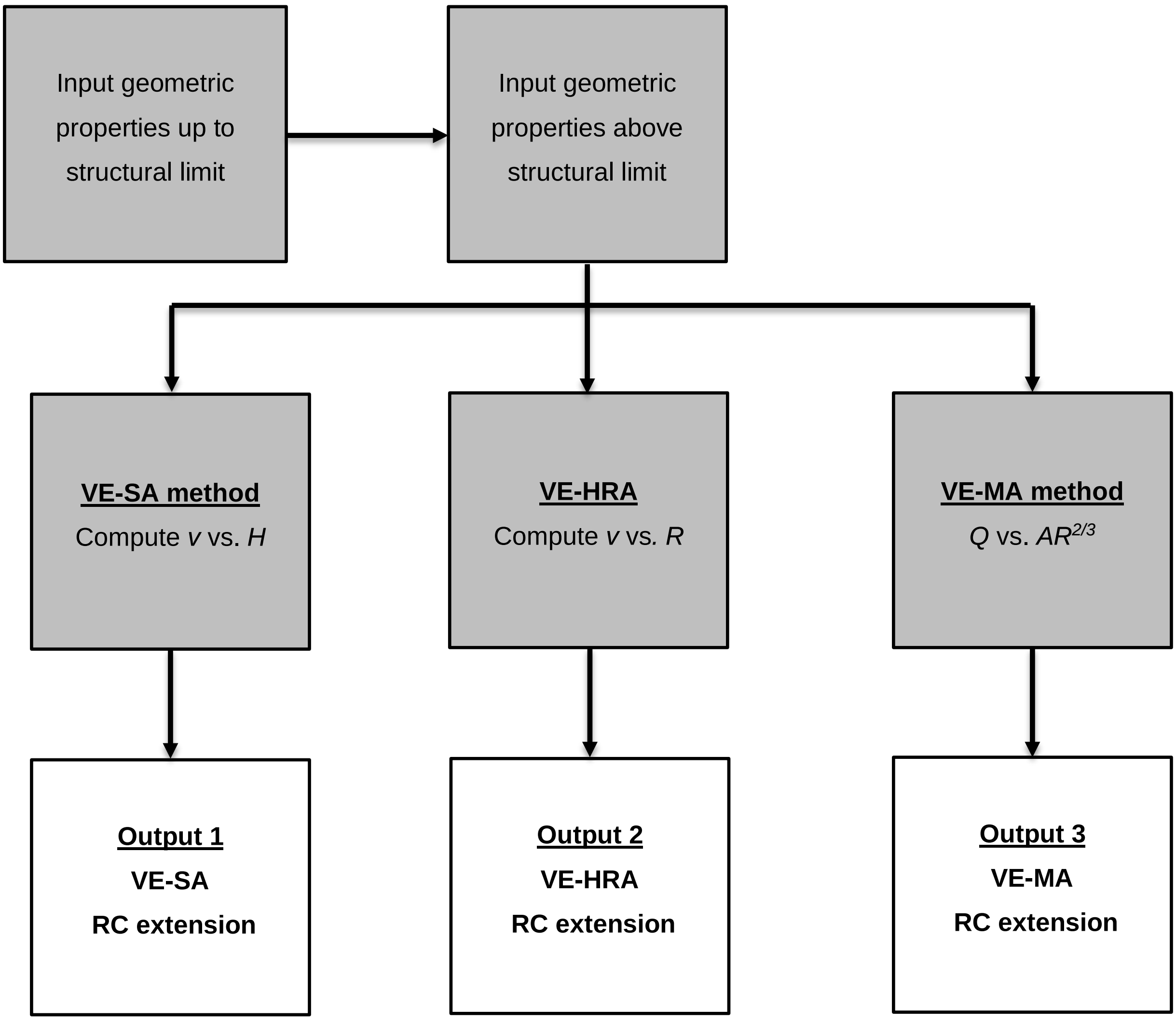

Figure 4.6: VE procedure matrix

4.4.3 Slope area method

The different approaches to the SAM, i.e., SA and DCM, use *A*, *R*, water surface elevations, Manning's *n*-values, and Chézy's *C*-values to extend SD relationships to high flow regions. According to Ramsbottom and Whitlow (2003), the description of the SAM theory is correct; however, the application thereof, as depicted in Table 4.1, is incorrect. In Table 4.1, *Q*-SAM represents the extension using the SAM, while *Q*-rating represents the SD relationship associated with the existing rating up to structural limit.

Table 4.1: Application of the SAM (after Ramsbottom and Whitlow, 2003)

Stage (m)	*A* (m^2)	*R* (m)	S_0 (m/m)	*n* ($s/m^{1/3}$)	*Q*-SAM (m^3/s)	*Q*-rating (m^3/s)
3.8	136.9	3.475	0.0002	0.035	126.898	125.348
4	144.2	3.543	0.0002	0.035	135.413	135.42
4.2	151.7	3.603	0.0002	0.035	144.068	145.744
4.4	159.6	3.677	0.0002	0.035	153.642	156.314
4.6	169.7	2.325	0.0002	0.035	120.328	167.125
4.8	187.4	1.938	0.0002	0.035	117.701	182.126
5	206.5	2.015	0.0002	0.035	133.096	202.381
5.2	226.8	2.096	0.0002	0.035	150.095	223.976
5.4	248.3	2.18	0.0002	0.035	168.678	246.944
5.6	270.7	2.302	0.0002	0.035	190.688	271.317
5.8	293.7	2.452	0.0002	0.035	215.766	297.128
6	317	2.598	0.0002	0.035	242.088	324.408
6.2	340.8	2.744	0.0002	0.035	269.897	353.187
6.4	365.1	2.888	0.0002	0.035	299.205	383.498
6.6	398.9	3.036	0.0002	0.035	330.223	-
6.8	414.8	3.183	0.0002	0.035	362.701	-
7	440.2	3.33	0.0002	0.035	396.621	-
7.2	466	3.475	0.0002	0.035	431.987	-
7.4	492.1	3.618	0.0002	0.035	468.644	-
7.6	518.7	3.761	0.0002	0.035	506.91	-
7.8	545.6	3.9	0.0002	0.035	546.209	-
8	572.8	4.037	0.0002	0.035	586.764	-
8.2	599.2	4.164	0.0002	0.035	626.652	-
8.4	627.2	4.299	0.0002	0.035	670.019	-
8.6	655.2	4.43	0.0002	0.035	714.098	-
8.8	683.2	4.558	0.0002	0.035	758.855	-
9	711.2	4.682	0.0002	0.035	804.257	-
9.2	739.2	4.8	0.0002	0.035	850.272	-
9.4	767.2	4.921	0.0002	0.035	896.872	-
9.5	781.2	4.979	0.0002	0.035	920.383	-

Essentially, the SAM is not a simplified computation where Manning's equation for open-channel flow is used to determine discharges at different stages.

The correct methodology (Chow, 1959), and as applied in this research, entails the following:

(a) Determine the upstream and downstream conveyance from known geometric and hydrometric properties (using separate worksheets for SAM-MA and SAM-CHZ).

(b) Compute the average conveyance.

(c) Determine the energy slope by assuming the velocity head equals zero.

(d) Calculate the corresponding discharge and assumed discharge.

(e) Repeat Step (d) until the assumed and computed discharges are in equilibrium.

Steps (a) to (e) were also automated in Microsoft Excel, with the iteration in Step (e) conducted using Visual Basic for Applications (VBA) and the *GOAL SEEK* function. The above-listed steps and procedures associated with the SAM, are summarised in the flow diagram as shown in Figure 4.7. Apart from the detailed results included and discussed in Chapter 5, the SAM SD extensions for above-structure-limit conditions are listed in Tables A.11–20, Appendix A, while the detailed SAM computations are listed in Tables A.21–30, Appendix A.

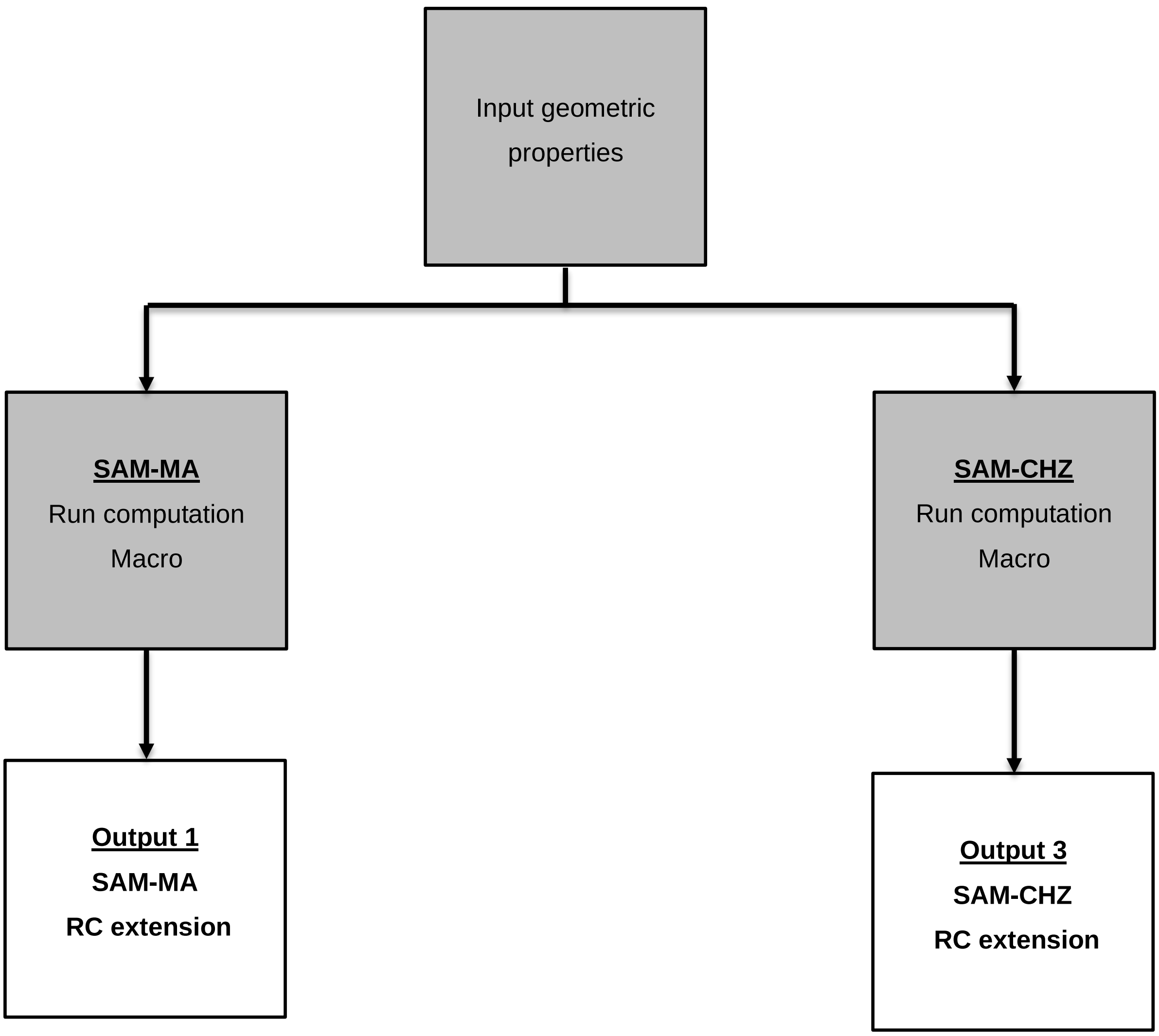

Figure 4.7: SAM procedure matrix

4.4.4 Stepped backwater analysis

The SBA worksheet developed has two different toolkits for SBA-MA and SBA-CHZ and is based on the methodology proposed by Chow (1959), i.e., the standard step method for natural (non-prismatic) channels. The Froude number for each cross-section is determined to define the flow regime, i.e., super- and/or sub-critical flow. The worksheets are inclusive of the following columns:

(a) Cross-section number.
(b) Discharge.
(c) Water surface width.
(d) Water surface elevation.
(e) Water area.
(f) Hydraulic radius.

(g) Hydraulic radius$^{2/3}$.

(h) Manning's *n* (including eddy losses) for SBA-MA and Chézy's *C* for SBA-CHZ worksheets.

(i) Conveyance.

(j) Froude number.

(k) Velocity.

(l) Velocity head.

(m) Total head before friction losses.

(n) Friction slope.

(o) Average slope.

(p) Distance between reaches.

(q) Total head after friction losses.

The computations in the worksheet were done in accordance with the description in Chapter 2 (*cf.* Section 2.5.6). Essentially, trail-and-error calculations were used until channel profile convergence was reached, i.e., the profile approximates the uniform depth profile and energy levels are in equilibrium.

The above-listed steps and procedures associated with the SBA are summarised in the flow diagram as shown in Figure 4.8. Apart from the detailed results included and discussed in Chapter 5, the SBA SD extensions for above-structure-limit conditions are listed in Tables A.11–20, Appendix A, while the detailed SBA computations are listed in Tables A.31–40, Appendix A.

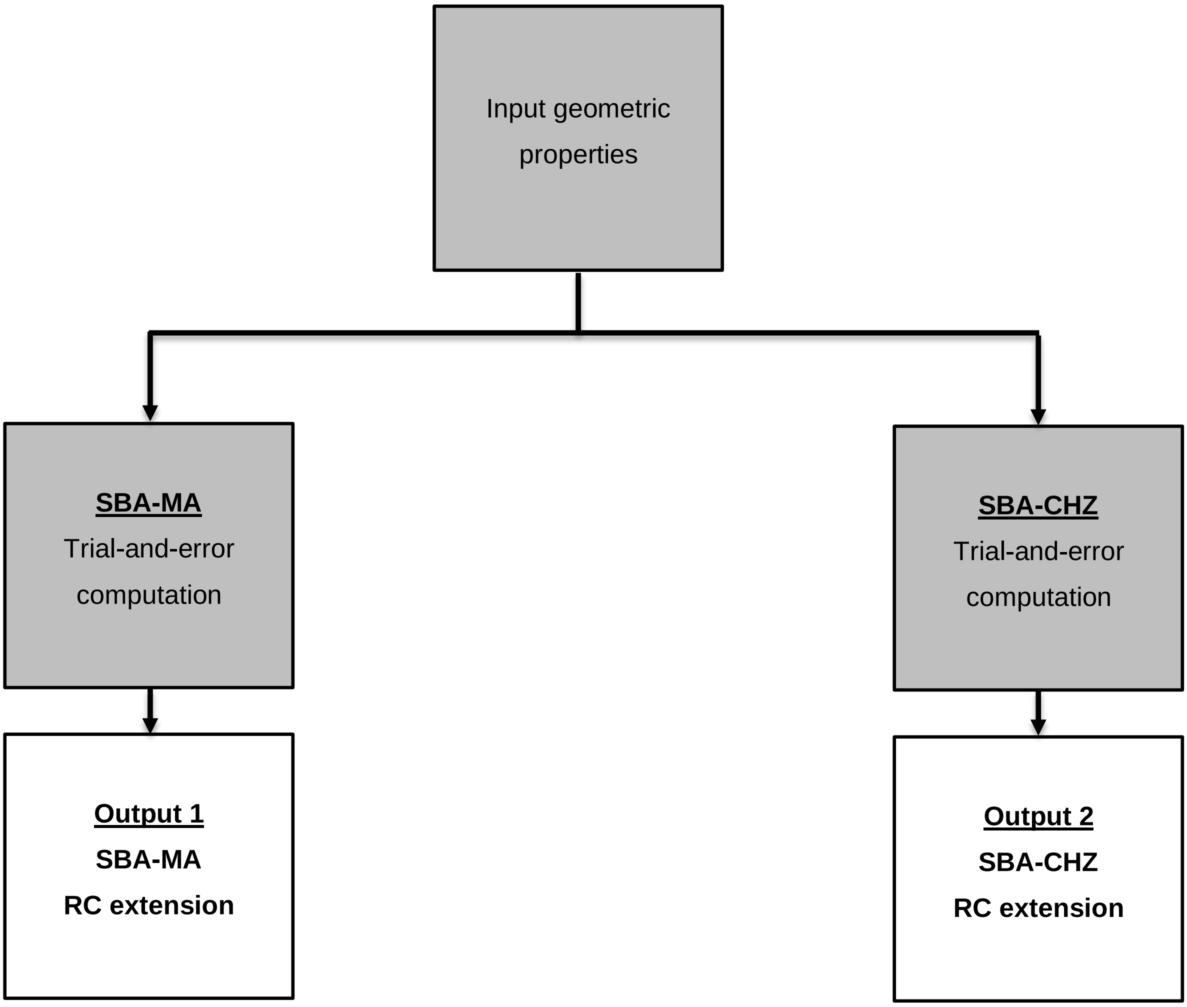

Figure 4.8: SBA procedure matrix

4.5 HEC-RAS Modelling

This section provides an overview of the modelling procedure followed to extend RCs in HEC-RAS. The modelling in HEC-RAS was limited to steady flow (S) analyses at the flood sections only, given that the calibration data at the flow-gauging weirs are regarded as unsuitable for RC extensions at above-structure-limit conditions. In addition, the calibration data also lack the information required to conduct an unsteady flow (US) analysis for the full range of flows at the various flow-gauging sites under consideration.

4.5.1 Working with projects in HEC-RAS

Projects in HEC-RAS are used to create river hydraulics applications. The *Project* is a cluster of files used to build a model (USACE, 2016). In creating a new project, a title and file name were assigned to ensure that all the associated data are stored automatically under the same file name, while only the file extensions differ. The management of all created files was done through the user-interface in HEC-RAS.

4.5.2 Entering and editing of geometric data

Geometric data can be entered directly or developed in the Aeronautical Reconnaissance Coverage Geographic Information System (ArcGIS) environment and then entered in HEC-RAS (USACE, 2016). Geometric data were entered by selecting *Geometric Data* from the Edit menu in the main HEC-RAS window. An optional map background layer was loaded along with cross-section data, the river network/system, and any hydraulic structure data for the gauging sites under consideration. Before entering any geometric data, the user has to decide whether the model to be used should be georeferenced or not. In this research, to enable any form of mapping, the models were georeferenced.

River systems were drawn on a reach-by-reach basis. The *River Reach* function allows the user to draw a reach from upstream to downstream in the positive flow direction. Typically, after a river reach is drawn, *River* and *Reach* identifiers are assigned, while the interface automatically forms junctions as the reaches join. Figure 4.9 is illustrative of a typical river schematic of the Sand River at X3H008.

Upon completion of the river schematic as shown in Figure 4.9, the cross-section and hydraulic structure data were entered by commencing at the highest river station upstream to the lowest river station downstream.

Figure 4.10 is illustrative of a typical cross-section entered at flow-gauging site X3H008.

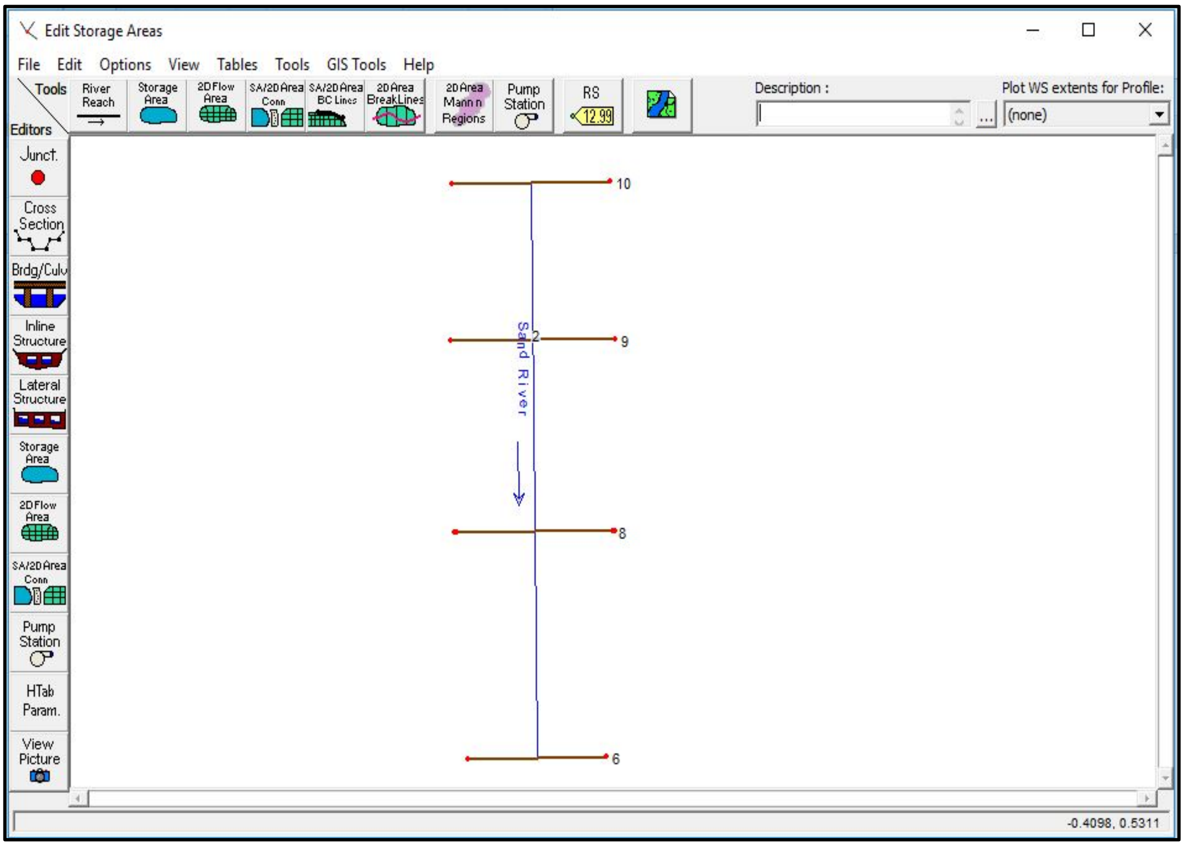

Figure 4.9: River schematic at X3H008 (Case study 10)

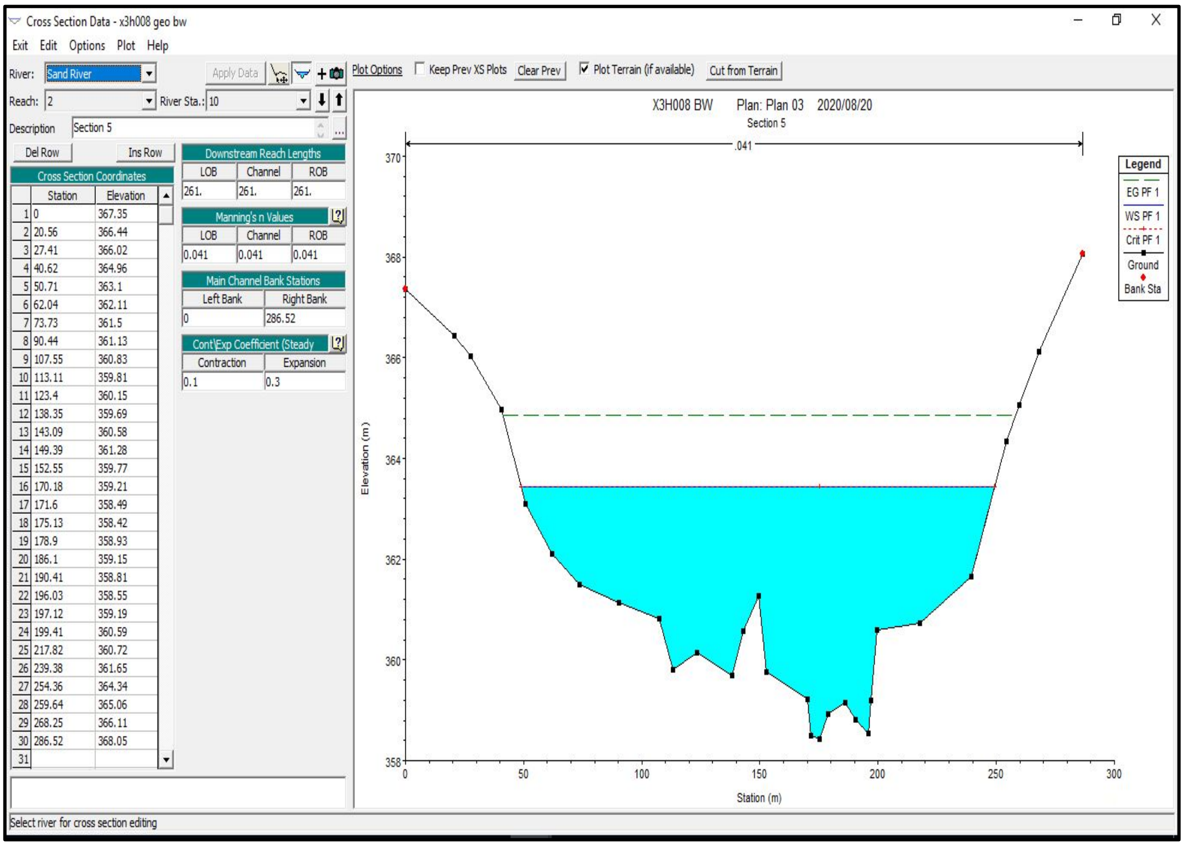

Figure 4.10: Cross-section data editor (Cross-section 5, X3H008, Case study 10)

4.5.3 Performing steady flow analyses

This subsection highlights how steady flow (S) analyses were conducted. The number of profiles to be computed, the peak flow data (for each river reach and every profile), and the necessary boundary conditions were defined for each analysis. The flow data were entered upstream to downstream in each river reach, as shown in Figure 4.11.

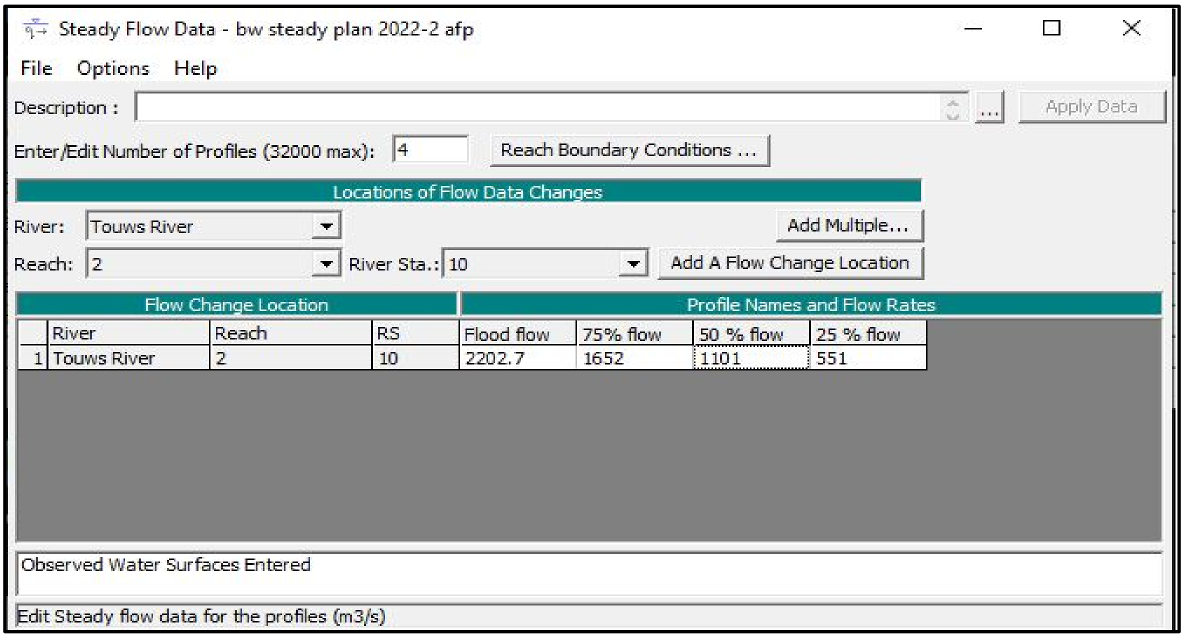

Figure 4.11: Steady flow data at J1H018 (Case study 6)

The desired flow regime, i.e., sub-critical, supercritical, and/or mixed flow, was defined prior to the actual simulation run, as shown in Figure 4.12. In other words, the boundary conditions for each analysis were specified, i.e., upstream (supercritical flow), downstream (sub-critical flow), and/or up and downstream (mixed flow). Typically, the known water surface elevations (up- and downstream) were used as the default boundary conditions at most of the gauging sites under consideration. In the absence of these known water surface elevations, the *critical depth* was entered as the downstream boundary condition, given that sub-critical flow conditions ($F_R < 1$) were present at all the flow-gauging sites (case studies) under consideration.

A typical steady flow analysis computation screen is shown in Figure 4.13:

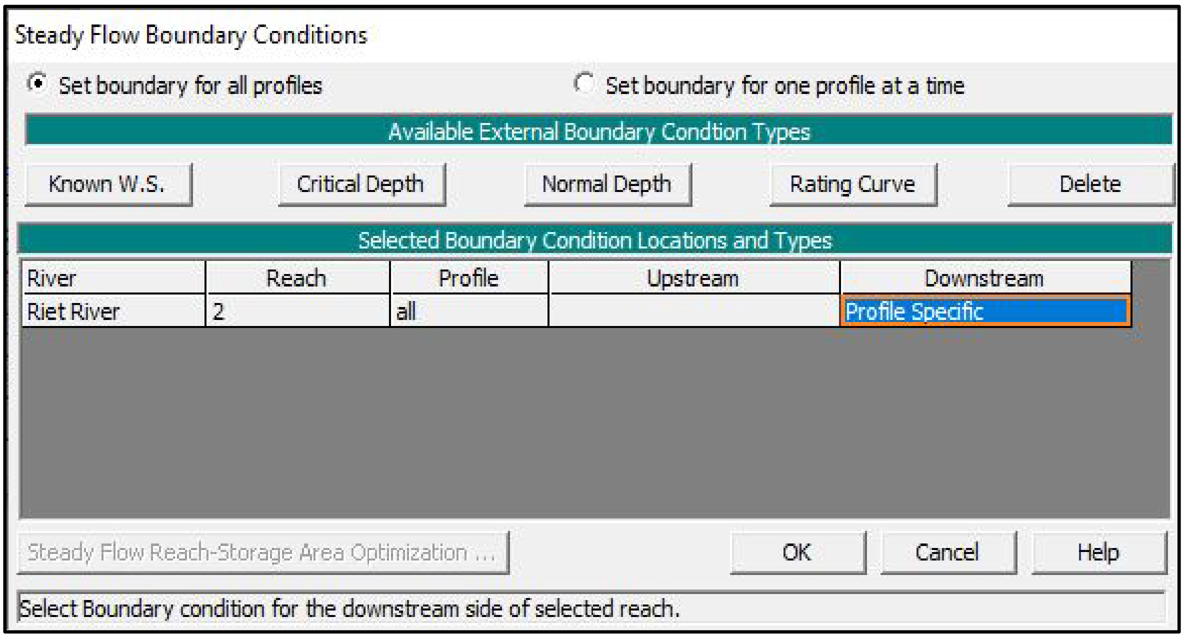

Figure 4.12: Steady flow boundary conditions at C5H014 (Case study 4)

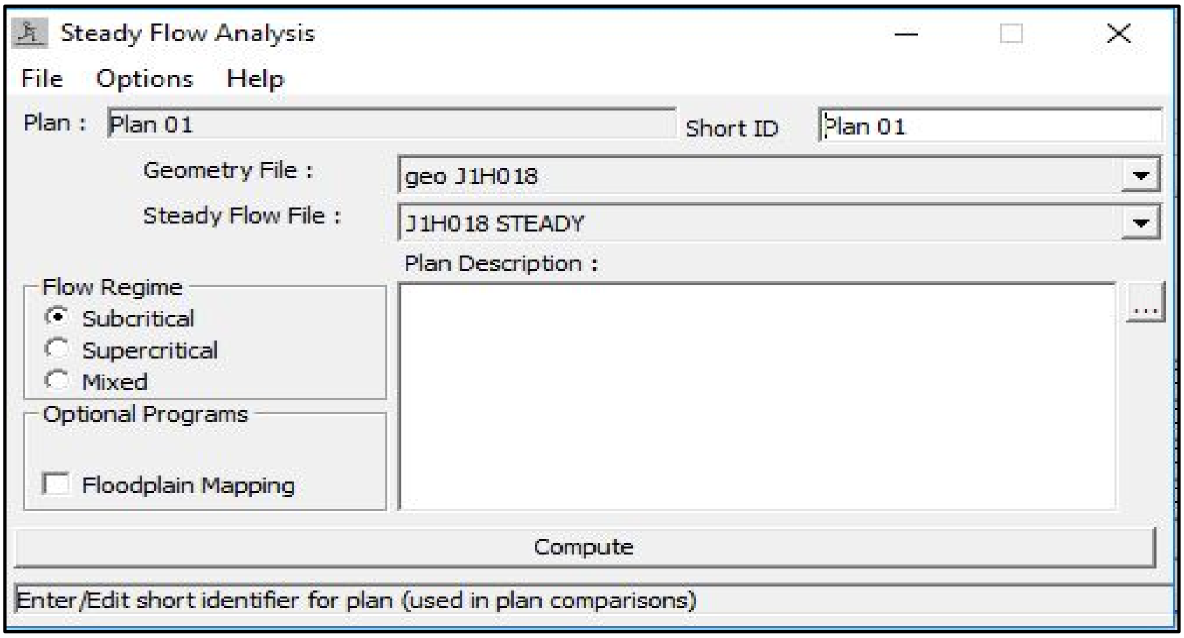

Figure 4.13: Steady flow analysis at J1H018 (Case study 6)

Apart from the detailed results included and discussed in Chapter 5, the HEC-RAS SD extensions for above-structure-limit conditions are listed in Tables A.11–20, Appendix A, while the observed versus simulated water surface profiles are shown in Figures B.51–55, Appendix B.

4.5.4 Determination of Manning's *n*-values in HEC-RAS

In Chapter 2 (*cf*. Section 2.6.5), the estimation of Manning's *n*-values was discussed. However, the three methods available to estimate *n*-values could not be applied owing to the unavailability of data. Essentially, as explained in Section 4.5.3, steady flow analysis was conducted, and simulated water surface levels were compared to the observed water levels, while adjusting the Manning's *n*-values until equilibrium was reached. The different water levels and Manning's *n*-values associated with the different simulations which reached the desired state of equilibrium are listed in Table 4.2.

Table 4.2: Observed versus simulated stage levels based on different Manning's *n*-values at C5H014 (Case study 4)

Cross-sections	*n*-values Initial (Final)	Observed stage (m)	Initial model stage (m)	Final model stage (m)
4	0.040 (0.024)	104.73	105.53	104.74
3	0.044 (0.027)	104.28	105.24	104.30
2	0.074 (0.054)	103.84	104.72	103.80
1	0.069 (0.054)	103.49	103.49	103.49

It should be noted that the *observed stage* in Table 4.2 has associated peak discharges, which in turn, are also known given that the SD relationships associated with the benchmark data sets were already being extended.

4.5.5 Viewing results in HEC-RAS

Upon completion of all the simulation runs in HEC-RAS, the results can be viewed. Several output variables are available under the *View* option in the main window: (i) cross-section plots, (ii) RC plots, (iii) and hydraulic tables.

Figure 4.19 shows an example of a cross-section plot. This output can be used to compare the output at different flood sections (FSs). The latter output can also be used for the verification of roughness coefficients. Figure 4.20 is illustrative of the same results as contained in Figure 4.19; however, only in a tabular format. Both Figures 4.19 and 4.20 are useful when comparisons need to be drawn between steady flow analyses and hydraulically correct extension methods (e.g., SBA and SAM), as well as for the allocation of representative roughness coefficients.

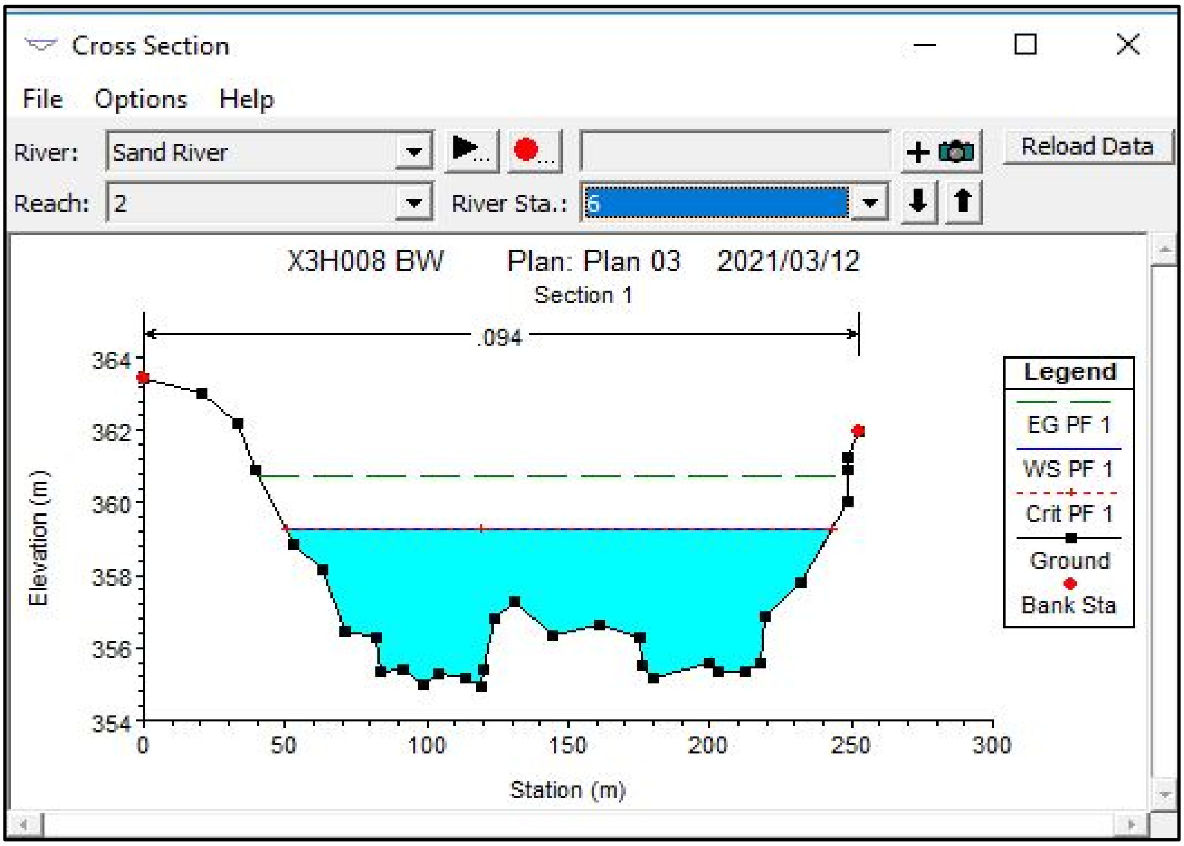

Figure 4.14: Cross-section plot (Cross-section 1, X3H008, Case study 10)

Cross Section Output

File Type Options Help

River: Riet River Profile: Flood Flow

Reach 2 RS: 7 Plan: Plan 23

Plan: Plan 23 Riet River 2 RS: 7 Profile: Flood Flow

		Element	Left OB	Channel	Right OB
E.G. Elev (m)	104.23	Element	Left OB	Channel	Right OB
Vel Head (m)	0.75	Wt. n-Val.		0.054	
W.S. Elev (m)	103.49	Reach Len. (m)			
Crit W.S. (m)	101.14	Flow Area (m2)		1338.36	
E.G. Slope (m/m)	0.004142	Area (m2)		1338.36	
Q Total (m3/s)	5128.30	Flow (m3/s)		5128.30	
Top Width (m)	230.54	Top Width (m)		230.54	
Vel Total (m/s)	3.83	Avg. Vel. (m/s)		3.83	
Max Chl Dpth (m)	8.99	Hydr. Depth (m)		5.81	
Conv. Total (m3/s)	79679.7	Conv. (m3/s)		79679.7	
Length Wtd. (m)		Wetted Per. (m)		232.18	
Min Ch El (m)	94.50	Shear (N/m2)		234.16	
Alpha	1.00	Stream Power (N/m s)		897.26	
Frctn Loss (m)		Cum Volume (1000 m3)			
C & E Loss (m)		Cum SA (1000 m2)			

Figure 4.15: Detailed output table (Cross-section 4, C5H014, Case study 4)

The extension of SD relationships and their associated RCs using different indirect estimation methods are central to this research. Therefore, of particular interest is the viewing of RCs as an output from the modelling procedure. Figure 4.16 shows the RC plot and the information from this plot could be used in further analyses (as described in Chapter 2, Section 2.5.1) to determine a SD relationship for steady flow conditions at a flood section, i.e., S (FS).

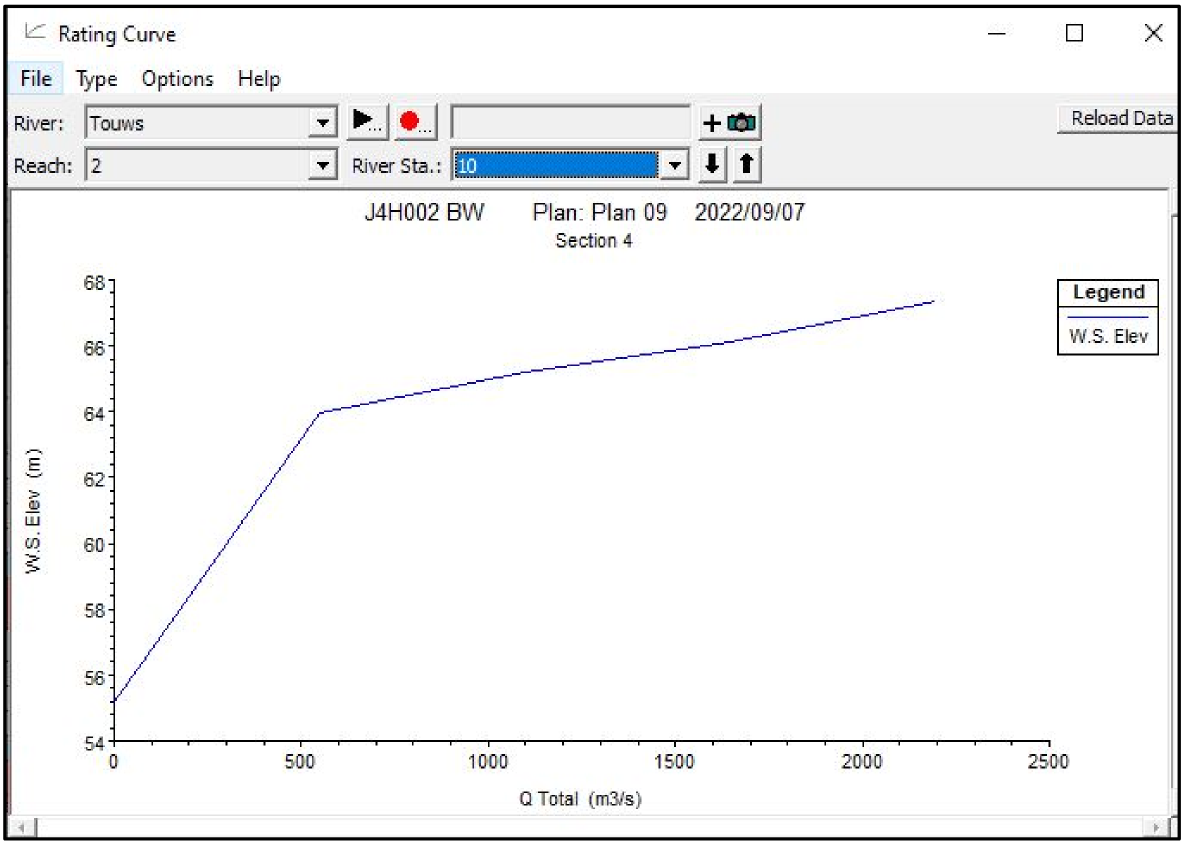

Figure 4.16: RC output under steady flow conditions at J4H002 (Case study 7)

4.6 Evaluation of Model Performance

A ranking-based selection procedure was developed to evaluate and select the best performing indirect (hydraulic) extension methods at each flow-gauging site. In other words, the indirect extension method's estimation results were compared to the at-site/benchmark extension results at each site (*i*) by considering a large set of quantitative GOF criteria to assess each method's accuracy and bias. Typically, the standard error of the estimate [SE_E, Eq. (4.1)], mean absolute relative error [*MARE*, Eq. (4.2)], root mean square error [*RMSE*, Eq. (4.3)], coefficient of determination [r^2, Eq. (4.4)], Nash-Sutcliffe coefficient [*NSE*, Eq. (4.5)], and the *z*-test [Eq. (4.6)], were used to compare and assess the indirect extension methods' results to those of the at-site direct extension (benchmark) methods. The *z*-test indicates how many standard deviations a sample scores above or below the mean, and the results are classified as: (i) similar ($0 \leq z \leq 2$), (ii) marginally different ($2 < z \leq 2.5$), (iii) significantly different ($2.5 < z \leq 3$), and (iv) unacceptable ($z > 3$).

Each indirect hydraulic extension method was ranked against the different assessment criteria and summed and/or averaged to provide the overall performance. Finally, the overall rankings and associated relative frequency of the various *z*-test ranking clusters (as defined in (i) to (iv) above) were used to establish the hierarchical order of the various indirect extension methods.

$$SE_E = \left[\frac{1}{(N-2)}\left(\sum_{i=1}^{N}\left(Q_{Ei}-\overline{Q_E}\right)^2 - \frac{\left(\sum_{i=1}^{N}\left(Q_{Bi}-\overline{Q_B}\right)\left(Q_{Ei}-\overline{Q_E}\right)\right)^2}{\sum_{i=1}^{N}\left(Q_{Ei}-\overline{Q_B}\right)^2}\right)\right]^{0.5} \tag{4.1}$$

$$MARE = 100\left[\frac{1}{N}\sum_{i=1}^{N}\frac{\left|Q_{Ei}-Q_{Bi}\right|}{Q_{Bi}}\right] \tag{4.2}$$

$$RMSE = \sqrt{\frac{\sum_{i=1}^{N}\left(Q_{Bi}-Q_{Ei}\right)^2}{N}} \tag{4.3}$$

$$r^2 = \left[\frac{\sum_{i=1}^{N}\left(Q_{Bi}-\overline{Q_B}\right)\left(Q_{Ei}-\overline{Q_E}\right)}{\sqrt{\sum_{i=1}^{N}\left(Q_{Bi}-\overline{Q_B}\right)^2\sum_{i=1}^{N}\left(Q_{Ei}-\overline{Q_E}\right)^2}}\right]^2 \tag{4.4}$$

$$NSE = 1-\left[\frac{\sum_{i=1}^{N}\left(Q_{Bi}-Q_{Ei}\right)^2}{\sum_{i=1}^{N}\left(Q_{Bi}-\overline{Q_B}\right)^2}\right] \tag{4.5}$$

$$z = \frac{\overline{Q_{Bi}}-\overline{Q_{Ei}}}{\sqrt{\sigma_{Bi}+\sigma_{Ei}}} \tag{4.6}$$

where SE_E is the standard error of the estimate (m^3/s), *MARE* is the mean absolute relative error (%), *RMSE* is the root mean square error, r^2 is the coefficient of determination, *NSE* is the Nash-Sutcliffe coefficient, *N* is the sample size, Q_{Bi} is the at-site benchmark discharge (m^3/s), $\overline{Q_B}$ is the mean of the at-site benchmark discharge (m^3/s), Q_{Ei} is the estimated/indirect discharge using the various indirect extension methods (m^3/s). $\overline{Q_E}$ is the mean of the estimated/indirect discharge using the various indirect extension methods (m^3/s), σ_{Bi} is the standard deviation of the at-site benchmark discharge, and σ_{Ei} is the standard deviation of the estimated/ indirect discharge using the various indirect extension methods/modelling.

The results associated with each case study gauging site are presented and discussed in the next chapter.

CHAPTER 5 : RESULTS AND DISCUSSION

In this chapter, the results associated with each case study are presented. The discussions focus on the research aim, i.e., to evaluate and compare a selection of indirect extension methods, e.g., hydraulic and one-dimensional modelling methods with direct extension (benchmark) methods, e.g., at-site conventional current gaugings and other appropriate methods, in order to establish the best-fit and most appropriate SD extension method to be used in South Africa.

5.1 Case Studies

In each case study, the following aspects are investigated and discussed, namely: (i) site characteristics and hydraulics, (ii) existing SD relationships and associated data available, and (iii) the suitability of the various indirect extension methods, using GOF criteria and a ranking-based selection procedure.

5.1.1 Gauging weir A4H005

Site characteristics and hydraulics:

Gauging weir A4H005 is located in the Mokolo River, Limpopo Province. The weir was constructed in 1962. As shown in Figure 5.1, the structure is a compound weir consisting of five sharp-crested notches and six broad-crested notches (Matji, 1993).

Figure 5.1: Gauging weir A4H005 in the Mokolo River

<u>Existing SD relationships and associated data:</u>

The structural limit is at a stage of 1.4 m (gauge plate (GP) reading) with an associated discharge of 115 m^3/s. In the latest DWS Calibration Report, level pool (back) routing was used as the benchmark SD extension method. Subsequently, all the other indirect extension methods were compared against the latter method up to a stage of 3.4 m and corresponding discharge of 1 205 m^3/s. The most recent cross-sectional survey of the gauging weir was conducted on 13 November 1992. The current (existing) SD relationship table (DT3) applicable to A4H005 is listed in Table 5.1, and shown in Figure 5.2 (Matji, 1993).

Table 5.1: DT3 at A4H005 (Van der Spuy, 2006)

Stage (m)	Stage increments (m)/ Discharge (m^3/s)									
	0	**0.1**	**0.2**	**0.3**	**0.4**	**0.5**	**0.6**	**0.7**	**0.8**	**0.9**
0	0.0	0.2	-	2.6	-	-		28.6	-	-
1	-	-	-	-	-	-	-	-	-	-
2	-	-	-	-	512.4	579.7	647.0	714.8	782.9	851.3
3	920.0	989.0	1058.3	1127.9	1197.8	-	-	-	-	-

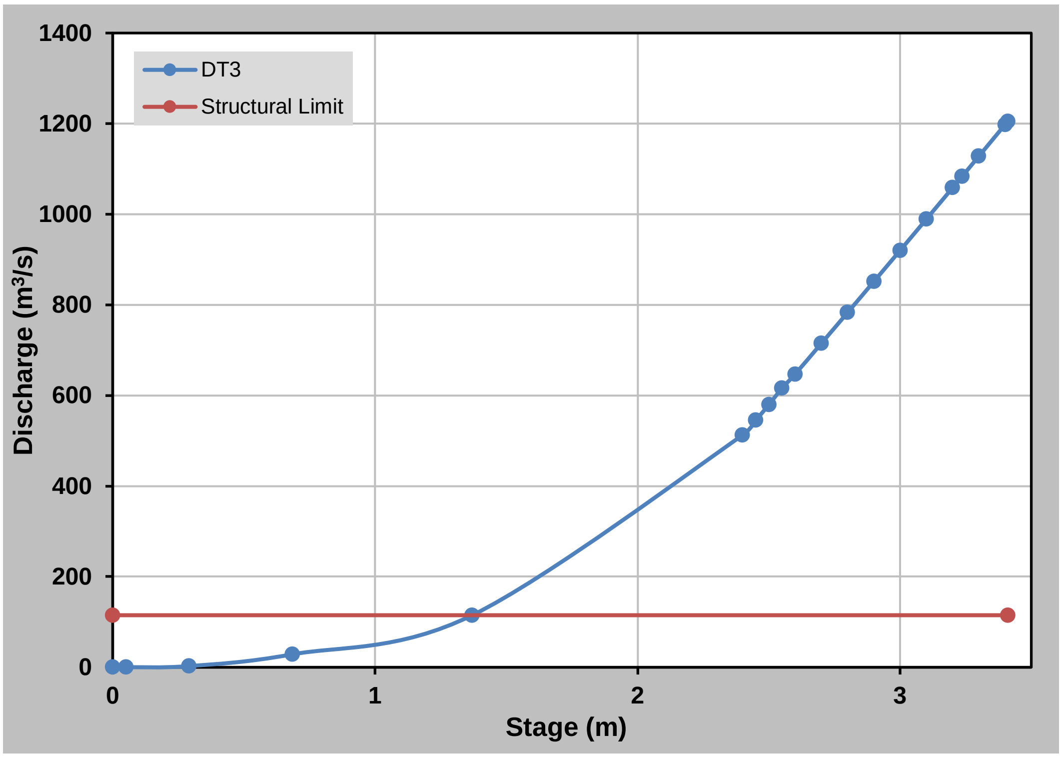

Figure 5.2: Benchmark at-site SD relationship (DT3) at A4H005

<u>Suitability of indirect extension methods:</u>

The current information available at the site is insufficient to apply the SAM, SBA, and HEC-RAS modelling. Consequently, the evaluation of the indirect extension methods was limited to the SE, LE and VE methods based on the survey data used during the calibration of the weir. The results pertained to the SD RC extension using all the above methods are shown in Figure 5.3. The GOF statistics applicable to each method are listed in Table 5.2.

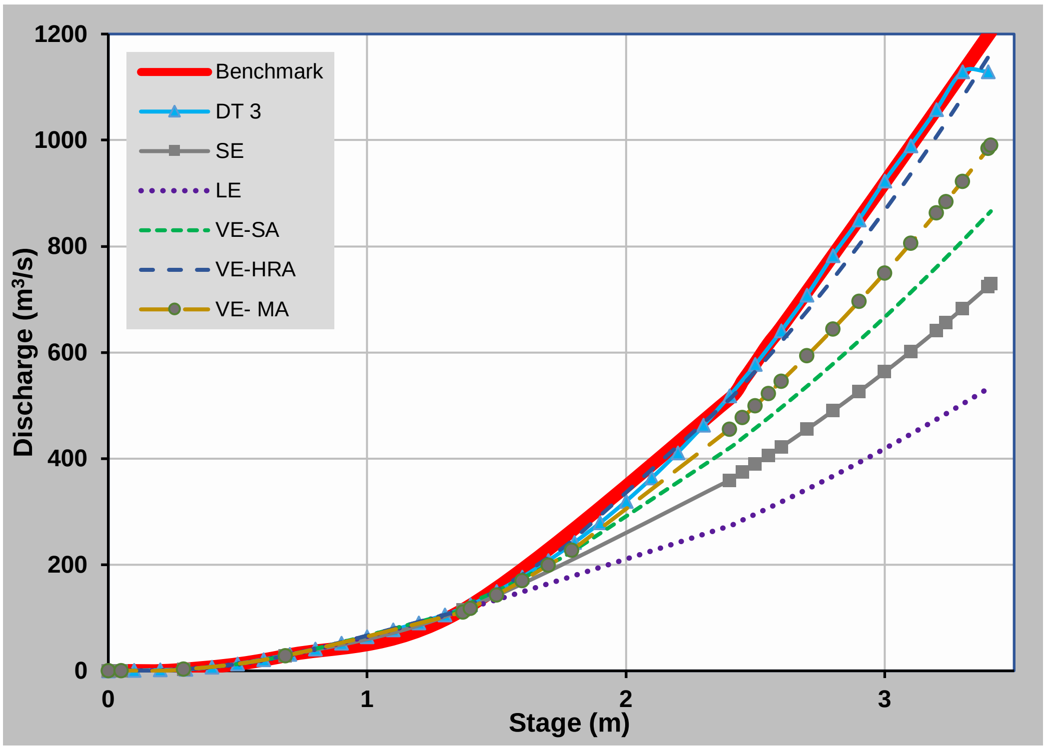

Figure 5.3: Indirect SD extensions in comparison to the benchmark rating at A4H005

In Table 5.2, it is evident that all methods underestimated the SD relationships in comparison to the Q_{Bi} benchmark SD values. The LE method performed the worst; with underestimated Q_{Ei} peak values and a *MARE* of 52.7%

Table 5.2: GOF results at A4H005

Criteria	**SE**	**LE**	**VE**			**SAM**		**SBA**		**HEC-RAS S (FS)**
			SA	**HRA**	**MA**	**MA**	**CHZ**	**MA**	**CHZ**	
Sample size (*N*)	15	15	15	15	15	-	-	-	-	-
Average	535	398	632	819	709	-	-	-	-	-
Standard deviation	132	93	159	232	190	-	-	-	-	-
SE_E [Eq. (4.1); m^3/s]	5.3	3.4	6.2	10.9	8.0	-	-	-	-	-
SE_E ranking	2	1	3	5	4	-	-	-	-	-
MARE [Eq. (4.2); %]	36.7	52.7	25.3	4.0	16.6	-	-	-	-	-
MARE ranking	4	5	3	1	2	-	-	-	-	-
RMSE [Eq. (4.3)]	339.2	480.4	238.7	39.6	156.1	-	-	-	-	-
RMSE ranking	4	5	3	1	2	-	-	-	-	-
r^2 [Eq. (4.4)]	0.999	0.999	0.999	0.998	0.998	-	-	-	-	-
r^2 ranking	3	1	2	5	4	-	-	-	-	-
NSE [Eq. (4.5)]	-1.04	-3.10	-0.01	0.97	0.57	-	-	-	-	-
NSE ranking	4	5	3	1	2	-	-	-	-	-
Z-test [Eq. (4.6)]	16.5	24.8	11.1	1.6	7.0	-	-	-	-	-
Z-test ranking	4	5	3	1	2	-	-	-	-	-
Sum of rankings	**21**	**22**	**17**	**14**	**16**	**-**	**-**	**-**	**-**	**-**
Overall ranking	**4**	**5**	**3**	**1**	**2**	**-**	**-**	**-**	**-**	**-**

MA (Manning's approach); CHZ (Chézy's approach); S (Steady flow); and FS (Flood section)

Based on the GOF statistics, the different versions of the VE methods performed the best with an *NSE* = 0.972 in the case of the VE-HRA method. In addition, the *z*-test values of the VE-MA and VE-SA methods are 7 and 11.1 deviations, respectively. Despite the fact that the latter two methods are respectively ranked in the 2nd and 3rd position, they demonstrated a good correlation between velocity vs. the hydraulic radius and velocity vs. stage. However, such a good correlation does not necessarily result in a high correlation between the Q_{Ei} and Q_{Bi} values. The SE (4th) and LE (5th) methods performed poorly as extension methods, with high *z*-test deviations ranging between 16.5 and 24.8. In summary, the GOF statistics at A4H005 highlighted the methods' inability to replicate the Q_{Bi} values, despite the high r^2 values > 0.99 evident. The negative *NSE* results associated with the SE, LE, and VE-SA and methods are indicative of their poor estimates when the observed mean Q_{Bi} values are considered.

5.1.2 Gauging weir A6H035

<u>Site characteristics and hydraulics:</u>

Gauging weir A6H035 is located in the Mogalakwena River, Limpopo Province. The weir has been operational since 1995, and the gauging weir structure was constructed on an old retaining wall at Leniesrus. As shown in Figure 5.4, it has four sharp-crested notches with a combined length of 74.5 m (Masekela, 2013).

Figure 5.4: Gauging weir A6H035 in the Mogalakwena River

Existing SD relationships and associated data:

The structural limit is at 1.3 m (GP reading) with an associated discharge of 148 m^3/s. In the latest DWS Calibration Report, level pool (back) routing was used as the benchmark SD extension method. Subsequently, all the other indirect extension methods were compared against the latter method up to a stage of 2.6 m and corresponding discharge of 715 m^3/s. The most recent cross-sectional survey of the gauging weir was conducted on 16 November 2012. The current (existing) SD relationship table (DT4) applicable to A6H035 is listed in Table 5.3, and shown in Figure 5.5 (Mahlangu, 1995; Roux *et al.*, 2014).

Table 5.3: DT4 at A6H035 (Roux *et al.*, 2014)

Stage (m)	Stage increments (m)/ Discharge (m^3/s)									
	0	**0.1**	**0.2**	**0.3**	**0.4**	**0.5**	**0.6**	**0.7**	**0.8**	**0.9**
0	0.0	0.9	2.5	4.5	9.5	16.6	25.3	36.7	50.5	66.4
1	84.2	104.0	125.6	147.9	172.6	199.5	228.8	260.8	295.8	334.0
2	375.8	421.2	470.8	524.6	583.0	646.3	714.7	-	-	-

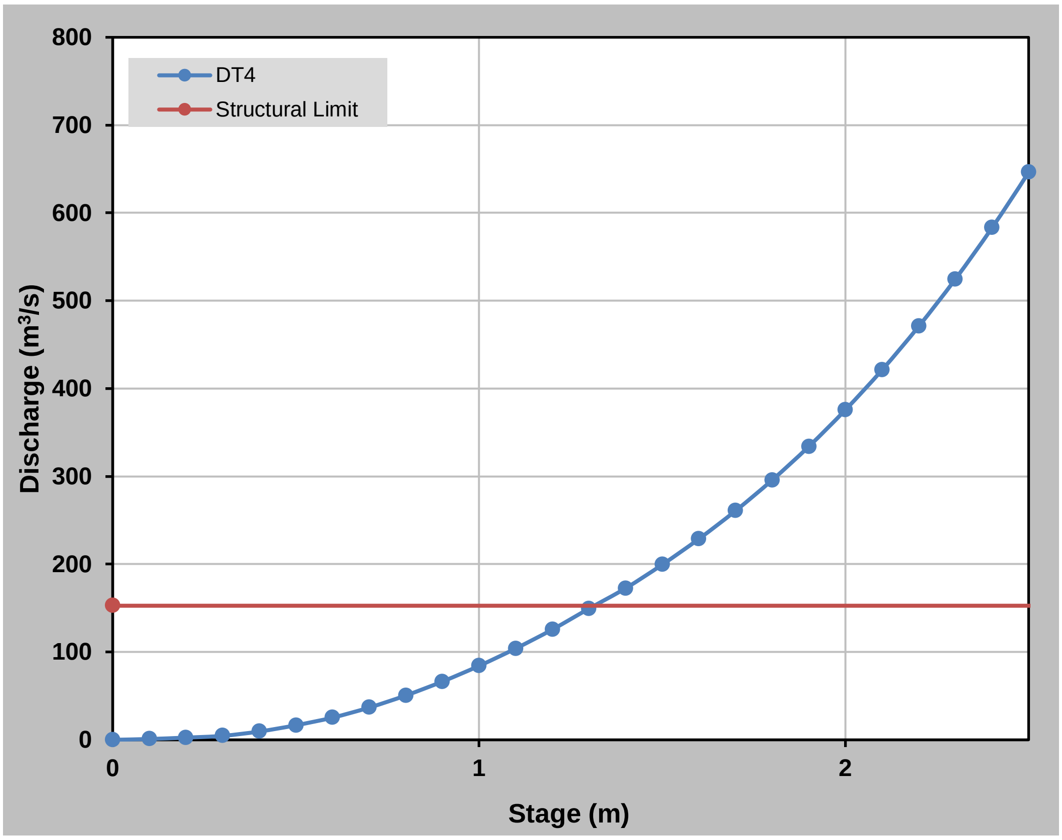

Figure 5.5: Benchmark at-site SD relationship (DT4) at A6H035

<u>Suitability of indirect extension methods:</u>

The current information available at the site is insufficient to apply the SAM, SBA, and HEC-RAS modelling. Consequently, the evaluation of the indirect extension methods was limited to the SE, LE and VE methods based on the survey data used during the calibration of the weir. The results pertained to the SD RC extension using all the above methods are shown in Figure 5.6. The GOF statistics applicable to each method are listed in Table 5.4.

In Table 5.4, all the methods at the site, except the VE-MA method, underestimated the SD relationships in comparison to the Q_{Bi} benchmark SD values. The overestimations of the VE-MA are significant with the *MARE* = 1 557%. The latter high *MARE* value is ascribed to the method's inability to correctly reflect the relationship between discharge and the geometric properties of the channel/river. Based on the GOF statistics, the LE method is ranked in the 1st position, despite having a *z*-test value = 3.2, which confirms the poor simulation of the benchmark

SD relationship. The SE, VE-HRA and VE-SA methods also did not replicate the SD relationship well at $H > 1.3$ m, with $61\% \leq RMSE \leq 169\%$.

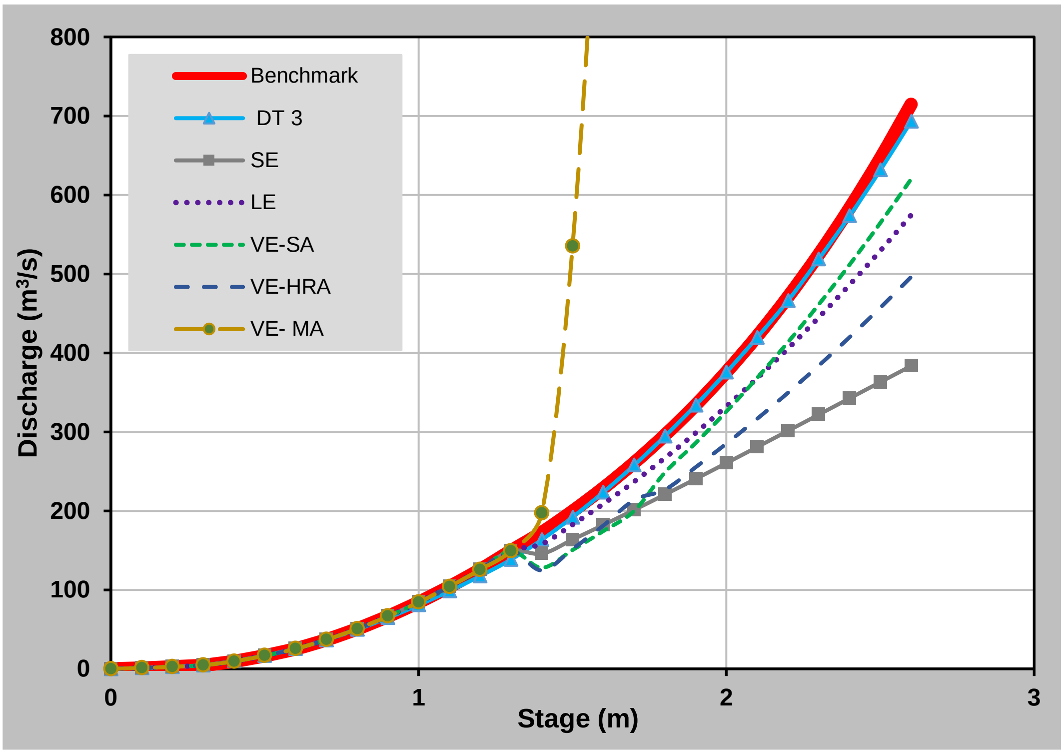

Figure 5.6: Indirect SD extensions in comparison to the benchmark rating at A6H035

Table 5.4: GOF results at A6H035

Criteria	SE	LE	VE			SAM		SBA		HEC-RAS S (FS)
			SA	HRA	MA	MA	CHZ	MA	CHZ	
Sample size (*N*)	13	13	13	13	13	-	-	-	-	-
Average	262	346	342	297	8341	-	-	-	-	-
Standard deviation	78	136	163	119	7490	-	-	-	-	-
SE_E [Eq. (4.1); m³/s]	9.8	7.2	7.7	8.8	808.9	-	-	-	-	-
SE_E ranking	4	1	2	3	5	-	-	-	-	-
MARE [Eq. (4.2); %]	30.8	12.5	16.6	25.2	1556.7	-	-	-	-	-
MARE ranking	4	1	2	3	5	-	-	-	-	-
RMSE [Eq. (4.3)]	169.4	68.9	61.4	119.0	10602.6	-	-	-	-	-
RMSE ranking	4	2	1	3	5	-	-	-	-	-
r^2 [Eq. (4.4)]	0.985	0.997	0.998	0.995	0.989	-	-	-	-	-
r^2 ranking	5	2	1	3	4	-	-	-	-	-
NSE [Eq. (4.5)]	-0.01	0.83	0.87	0.50	-3943.25	-	-	-	-	-
NSE ranking	4	2	1	3	5	-	-	-	-	-
Z-test [Eq. (4.6)]	8.8	3.2	3.2	6.1	90.7	-	-	-	-	-
Z-test ranking	4	1	2	3	5	-	-	-	-	-
Sum of rankings	**25**	**9**	**9**	**18**	**29**	**-**	**-**	**-**	**-**	**-**
Overall ranking	**4**	**1**	**2**	**3**	**5**	**-**	**-**	**-**	**-**	**-**

MA (Manning's approach); CHZ (Chézy's approach); S (Steady flow); and FS (Flood section)

In summary, the GOF statistics at A6H035 highlighted the methods' inability to replicate the Q_{Bi} values, despite the high r^2 values > 0.98 evident. The large z-test values (3.2 ≤ *deviations* ≤ 90.7) confirmed the significant variance displayed when attempting to extend the extend SD relationships to above-structure-limit conditions.

5.1.3 Gauging weir C2H003

Site characteristics and hydraulics:

As shown in Figure 5.7, gauging weir C2H003 is located in the Vaal River, Gauteng Province, while C2H130 is a flood section (FS) associated with C2H003. The weir has been operational since 1924 and it is a multiple-notch (eight notches) sharp-crested weir.

Figure 5.7: Gauging weir C2H003 in the Vaal River

Existing SD relationships and associated data:

The structural limit is at 2.2 m (GP reading) with an associated discharge of 481 m^3/s. In the latest DWS Calibration Report, level pool (back) routing was used as the benchmark SD extension method. Subsequently, all the other indirect extension methods were compared against the latter method up to a stage of 4.0 m and corresponding discharge of 1 711 m^3/s. The most recent cross-sectional survey of the gauging weir was conducted on 12 November 1996. The current (existing) SD relationship table (DT5) applicable to C2H003 is listed in Table 5.5 and shown in Figure 5.8 (Mathole 1998; Rademeyer and Van der Spuy, 2014).

Table 5.5: DT5 at C2H003 (Rademeyer and Van der Spuy, 2014)

Stage (m)	Stage increments (m)/ Discharge (m^3/s)									
	0	**0.1**	**0.2**	**0.3**	**0.4**	**0.5**	**0.6**	**0.7**	**0.8**	**0.9**
0	0.0	0.2	1.1	3.1	6.4	11.3	18.0	26.6	37.5	50.6
1	68.2	85.1	105.1	105.1	128.5	155.1	218.2	254.6	294.3	337.3
2	383.6	433.1	497.1	569.4	641.3	712.5	783.1	853.2	922.6	991.5
3	1060.0	1128.0	1195.0	1261.0	1327.0	1393.0	1458.0	1522.0	1585.0	1649.0
4	1711.0	-	-	-	-	-	-	-	-	-

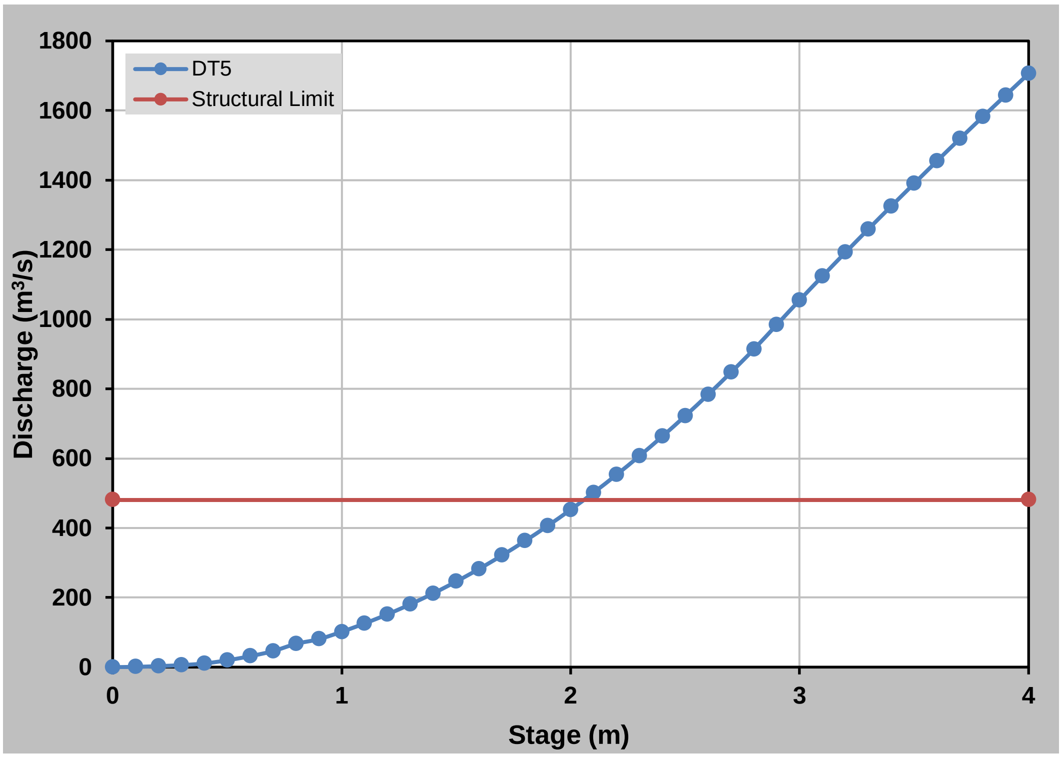

Figure 5.8: Benchmark at-site SD relationship (DT5) at C2H003

<u>Suitability of indirect extension methods:</u>

The current information available at the site is insufficient to apply the SAM, SBA, and HEC-RAS modelling. Consequently, the evaluation of the indirect extension methods was limited to the SE, LE and VE methods based on the survey data used during the calibration of the weir. The results pertained to the SD RC extension using all the above methods are shown in Figure 5.9. The GOF statistics applicable to each method are listed in Table 5.6.

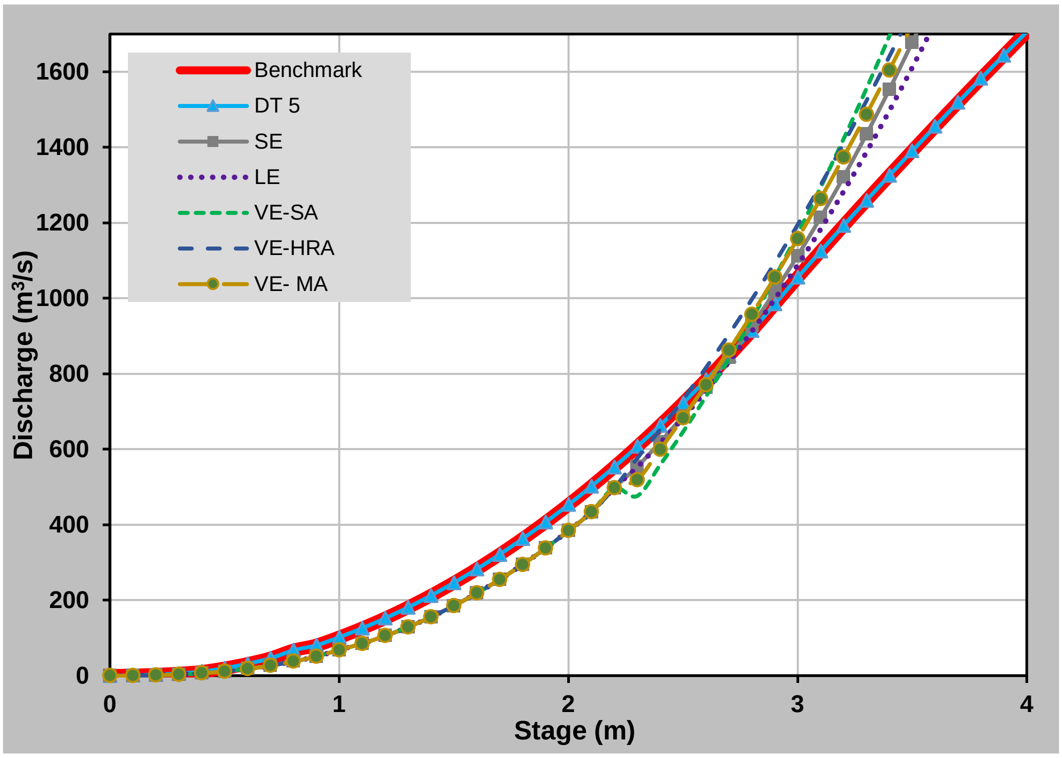

Figure 5.9: Indirect SD extensions in comparison to the benchmark rating at C2H003

Table 5.6: GOF results at C2H003

Criteria	SE	LE	VE			SAM		SBA		HEC-RAS S (FS)
			SA	HRA	MA	MA	CHZ	MA	CHZ	
Sample size (*N*)	18	18	18	18	18	-	-	-	-	-
Average	1345	1297	1433	1410	1368	-	-	-	-	-
Standard deviation	582	539	687	586	588	-	-	-	-	-
SE_E [Eq. (4.1); m³/s]	86.6	73.3	86.9	65.4	59.2	-	-	-	-	-
SE_E ranking	4	3	5	2	1	-	-	-	-	-
MARE [Eq. (4.2); %]	14.0	11.1	22.8	18.3	16.5	-	-	-	-	-
MARE ranking	2	1	5	4	3	-	-	-	-	-
RMSE [Eq. (4.3)]	297.0	233.8	428.3	342.3	312.0	-	-	-	-	-
RMSE ranking	2	1	5	4	3	-	-	-	-	-
r^2 [Eq. (4.4)]	0.979	0.983	0.985	0.988	0.990	-	-	-	-	-
r^2 ranking	5	4	3	2	1	-	-	-	-	-
NSE [Eq. (4.5)]	0.27	0.55	-0.51	0.04	0.20	-	-	-	-	-
NSE ranking	2	1	5	4	3	-	-	-	-	-
Z-test [Eq. (4.6)]	6.3	4.8	8.7	8.4	7.0	-	-	-	-	-
Z-test ranking	2	1	5	4	3	-	-	-	-	-
Sum of rankings	**17**	**11**	**28**	**20**	**14**	**-**	**-**	**-**	**-**	**-**
Overall ranking	**3**	**1**	**5**	**4**	**2**	**-**	**-**	**-**	**-**	**-**

MA (Manning's approach); CHZ (Chézy's approach); S (Steady flow); and FS (Flood section)

In Table 5.6, it is evident that all the methods overestimated the SD relationships in comparison to the Q_{Bi} benchmark SD values. Based on the GOF statistics, the LE method is regarded as the most appropriate with *MARE* = 11.1%, while the VE-SA method is regarded as the most inappropriate extension method. However, in all cases, the *z*-test values ranged between 4.8 and 8.7, thereby confirming that most of the methods under consideration fail to replicate the SD relationship. Given the complex site and river reach geometry, none of the methods applied is regarded as being hydraulically correct.

5.1.4 Gauging weir C5H014

Site characteristics and hydraulics:

Gauging weir C5H014 is located in Riet River, Free State Province and has been operational since 1969. As shown in Figure 5.10, the structure is a compound weir consisting of a broad-crest and V-Crump. Variable submergence conditions exist (especially at higher flows) and are caused by excessive reed growth downstream of the gauging weir (Hattingh and Masekela, 2017). In principle, the reed growth will significantly impact on the associated drag and velocity coefficients, resulting in an increase of resistance with flow depth when the plants are partially submerged. The effect of this on the flow conditions by using appropriate roughness coefficients and obscure details, e.g., modulus of plant stiffness, relative plant density, stem cross-section and deflected plant height, need to be determined (Freeman *et al.,* 2000). However, the latter vegetative information is unavailable and the methodology as outlined in Chapter 4 and associated with the SAM, SBA, and HEC-RAS modelling, was adopted.

Figure 5.10: Gauging weir C5H014 in the Riet River (Hattingh & Masekela, 2017)

Existing SD relationships and associated data:

The structural limit is at a stage of 1.0 m (GP reading) with an associated discharge of 90 m^3/s. In the latest DWS Calibration Report, the SBA was used as the benchmark SD extension method. Subsequently, all the other indirect extension methods were compared against the latter method up to a stage of 4.99 m and corresponding discharge of 5 128 m^3/s. The most recent cross-sectional survey of the gauging weir was conducted on 15 February 2009. The current (existing) SD relationship table (DT2) applicable to C5H014 is listed in Table 5.7, and shown in Figure 5.11 (Roux *et al.*, 2015; Hattingh and Masekela, 2017). The following specific values apply to DT2: (i) Structural limit (H = 1.0 m, Q = 90 m^3/s), and (ii) Rating limit (H = 4.99 m, Q = 5 128.3 m^3/s).

Table 5.7: DT2 at C5H014 (Roux *et al.*, 2015)

Stage (m)	Stage increments (m)/ Discharge (m^3/s)									
	0	0.1	0.2	0.3	0.4	0.5	0.6	0.7	0.8	0.9
0	0.0	0.1	0.3	0.8	1.6	2.8	6.9	20.1	62.0	86.5
1	90.4	113.6	139.9	169.4	202.3	238.6	278.5	322.0	369.2	423.0
2	483.3	549.7	622.3	701.0	785.9	876.9	974.1	1077.4	1186.9	1302.6
3	1424.4	1552.4	1686.5	1826.8	1973.2	2125.8	2284.5	2449.4	2620.5	2979.7
4	2981.0	3170.5	3366.2	3568.0	3776.0	3390.1	4210.4	4436.8	4669.4	4908.2

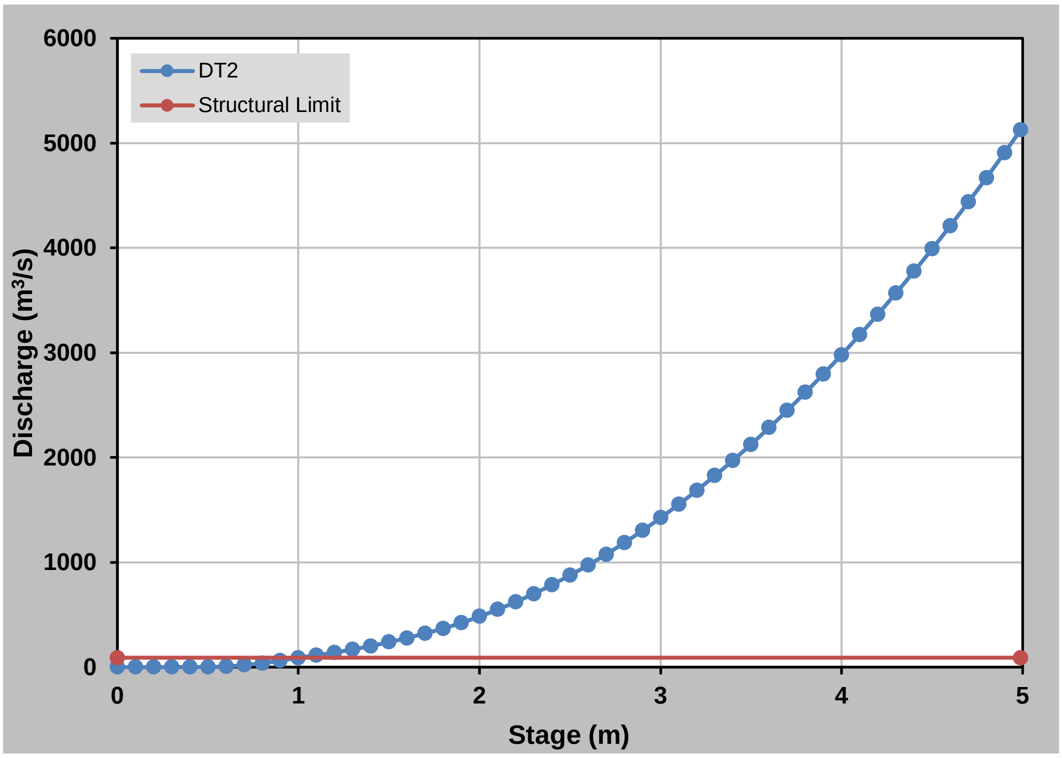

Figure 5.11: Benchmark at-site SD relationship (DT2) at C5H014

Suitability of indirect extension methods:

Based on the current information available at site, the evaluation of the indirect extension methods was based on all the methods considered in this research, including HEC-RAS modelling for steady flow conditions. The results pertained to the SD RC extension using all the above methods are shown in Figure 5.12. The GOF statistics are listed in Table 5.8.

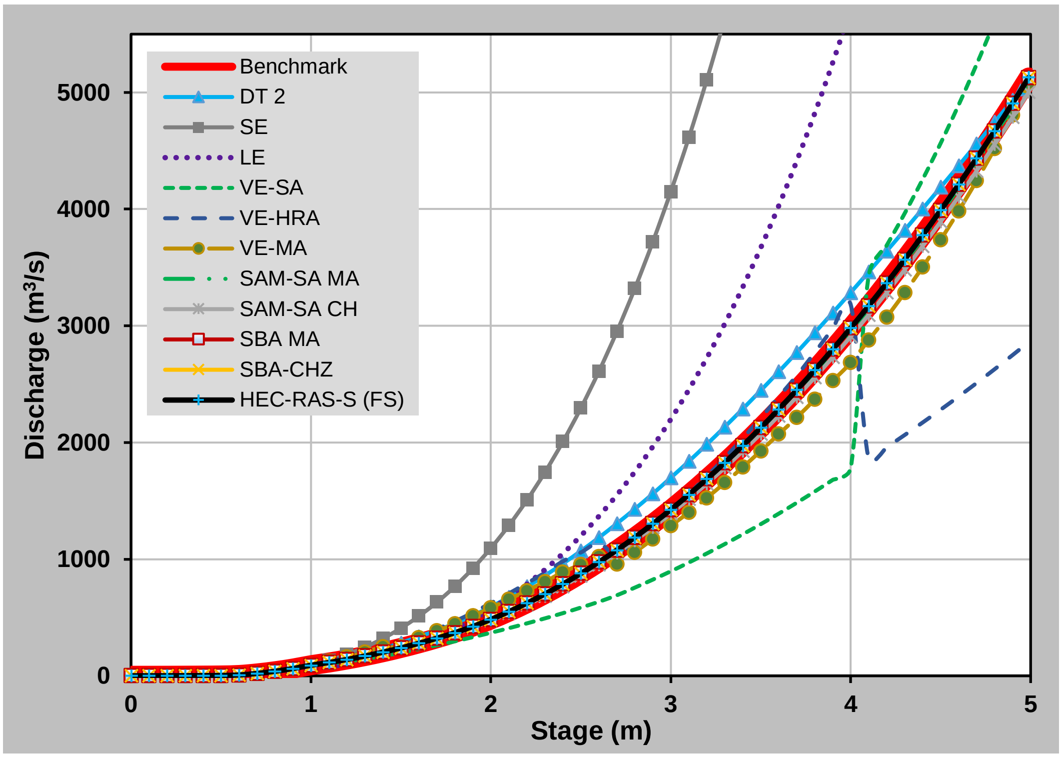

Figure 5.12: Indirect SD extensions in comparison to the benchmark rating at C5H014

Table 5.8: GOF results at C5H014

Criteria	SE	LE	VE			SAM		*SBA		HEC-RAS S (FS)
			SA	HRA	MA	MA	CHZ	MA	CHZ	
Sample size (*N*)	40	40	40	40	40	40	40	40	40	40
Average	6540	3616	1760	1528	1813	1881	1848	1894	1894	1894
Standard deviation	6250	3546	1894	931	1438	1532	1506	1543	1543	1544
SE_E [Eq. (4.1); m³/s]	547.5	388.4	540.8	446.0	136.3	0.0	0.0	0.0	0.0	0.0
SE_E ranking	10	7	9	8	6	4	3	2	1	5
MARE [Eq. (4.2); %]	185.8	60.4	25.4	22.4	12.3	0.7	2.4	0.0	0.0	0.0
MARE ranking	10	9	8	7	6	4	5	2	1	3
RMSE [Eq. (4.3)]	6577.1	2633.7	607.5	912.4	190.6	17.3	59.2	0.0	0.0	0.5
RMSE ranking	10	9	7	8	6	4	5	2	1	3
r^2 [Eq. (4.4)]	0.993	0.988	0.921	0.777	0.991	1.000	1.000	1.000	1.000	1.000
r^2 ranking	6	8	9	10	7	4	1	3	2	5
NSE [Eq. (4.5)]	-17.63	-1.99	0.84	0.64	0.98	1.00	1.00	1.00	1.00	1.00
NSE ranking	10	9	7	8	6	4	5	2	1	3
Z-test [Eq. (4.6)]	52.6	24.1	2.3	7.4	1.5	0.2	0.8	0.0	0.0	0.0
Z-test ranking	10	9	7	8	6	4	5	2	1	3
Sum of rankings	**56**	**51**	**47**	**49**	**37**	**24**	**24**	**13**	**7**	**22**
Overall ranking	**10**	**9**	**7**	**8**	**6**	**4**	**5**	**2**	**1**	**3**

*Benchmark method; MA (Manning's approach); CHZ (Chézy's approach); S (Steady flow); and FS (Flood section)

In Table 5.8, all the indirect SD extension methods, except the VE-MA (*H* > 6.3 m), provided estimated discharge (Q_{Ei}) values that exceed the at-site benchmark discharges (Q_{Bi}). The latter overestimations using the SE and LE methods were evident for stages (*H*) > 1 m (60% ≤ *MARE* ≤ 186%). Given that the SBA-CHZ method is used as the benchmark method (default ranking = 1) at this site, the SBA-MA demonstrated the second-best overall ranking, followed by the HEC-RAS S (FS), SAM-CHZ, and SAM-MA methods. HEC-RAS S (FS) ranked 3rd overall with an *RMSE* of 0.5. Considering that steady flow modelling in HEC-RAS is based on the SBA, the similarity in results is to be expected. By considering the individual GOF statistics, the latter SAM-CHZ and SAM-MA methods also proved to be equally accurate by being interchangeably ranked in the top five positions. Overall, the SE method is the most inappropriate method with the poorest ranking for all the GOF statistics under consideration.

Overall, the hydraulically correct methods resulted in the lowest SE_E, *MARE, RMSE*, and *z*-test values. All the methods demonstrated a high degree of association, with r^2 values > 0.78. However, as demonstrated previously, this serves to highlight that there is a high correlative trend between the estimated Q_{Ei} values as suggested by the various extension methods and the benchmark Q_{Bi} values. Hence, the *NSE* results should also be considered, whereas the SE and LE methods demonstrated the lowest *NSE* values, despite their r^2 values ≈ 0.99.

5.1.5 Gauging weir H5H004

Site characteristics and hydraulics:

Gauging weir H5H004 is located in the Breë River, Western Cape Province. The weir has been operational since 1970. As shown in Figure 5.13, the structure is a compound weir consisting of a hydro-flume and two sharp-crested notches (Hadebe, 2001).

Existing SD relationships and associated data:

The structural limit is at a stage of 1.4 m (GP reading), with an associated discharge of 81 m^3/s. In the latest DWS Calibration Report, the SBA and SAM were used as the benchmark and verification SD extension methods, respectively. Subsequently, all the other indirect extension methods were compared against the latter methods up to a stage of 8.0 m and corresponding discharge of 2 137 m^3/s. The most recent cross-sectional survey of the gauging weir was conducted on 23 May 2000, while five FSs were used in the analyses.

The current (existing) SD relationship table (DT6) applicable to H5H004 is listed in Table 5.9, and shown in Figure 5.14 (Hadebe, 2001; Wessels *et al.*, 2018).

Figure 5.13: Gauging weir H5H004 in the Breë River

Table 5.9: DT6 at H5H004 (Wessels *et al.*, 2018)

Stage (m)	Stage increments (m)/ Discharge (m^3/s)									
	0	**0.1**	**0.2**	**0.3**	**0.4**	**0.5**	**0.6**	**0.7**	**0.8**	**0.9**
0	0.0	0.1	0.4	1.1	2.2	5.1	9.9	16.5	23.3	31.5
1	41.2	52.5	63.0	72.2	81.4	90.6	99.9	109.1	118.4	127.7
2	139.9	153.8	169.0	185.5	203.3	222.7	243.7	266.5	291.1	317.6
3	335.2	349.7	364.7	380.1	395.9	412.2	428.9	446.0	463.6	481.6
4	500.1	519.1	538.6	558.5	578.9	599.8	621.2	643.1	655.5	688.4
5	711.9	735.8	760.3	785.4	811.0	835.7	861.9	890.1	920.6	953.2
6	988.0	1024.9	1064.0	1105.2	1148.6	1194.2	1241.9	1291.8	1343.8	1398.0
7	1454.4	1512.9	1573.6	1636.5	1701.5	1768.6	1838.0	1909.5	1983.1	2136.9
8	2136.9	-	-	-	-	-	-	-	-	-

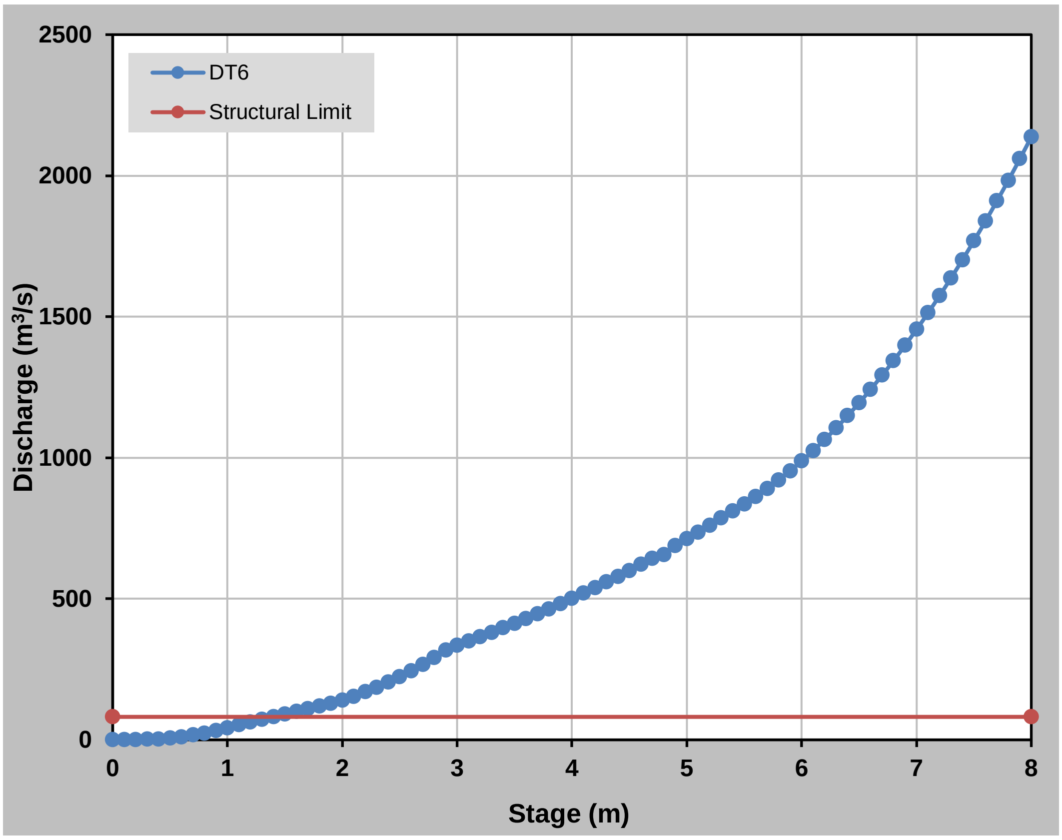

Figure 5.14: Benchmark at-site SD relationship (DT6) at H5H004

<u>Suitability of indirect extension methods:</u>

Based on the current information available at site, the evaluation of the indirect extension methods was based on all the methods considered in this research, including HEC-RAS modelling for steady flow conditions. The results pertained to the SD RC extension using all the above methods are shown in Figure 5.15. The GOF statistics are listed in Table 5.10.

In Table 5.10, the SE, LE, VE-SA, VE-HRA, SAM-MA, SAM-CHZ and HEC-RAS S (FS) methods provided estimated discharge (Q_{Ei}) values that exceed the at-site benchmark discharges (Q_{Bi}). The latter overestimations were evident for H > 1.4 m (2.4 ≤ *RMSE* ≤ 8 522). Given that the SBA methods are used as benchmark, the SBA-CHZ method is ranked by default = 1, followed by the SBA-MA method ranked in the second position. The HEC-RAS S (FS), SAM-CHZ and SAM-MA methods also proved to be more accurate than the other indirect extension methods, which in general, failed to replicate the hydraulic conditions at the site. Overall, the

SE method is regarded as the most inappropriate method with the poorest ranking for all the GOF statistics under consideration.

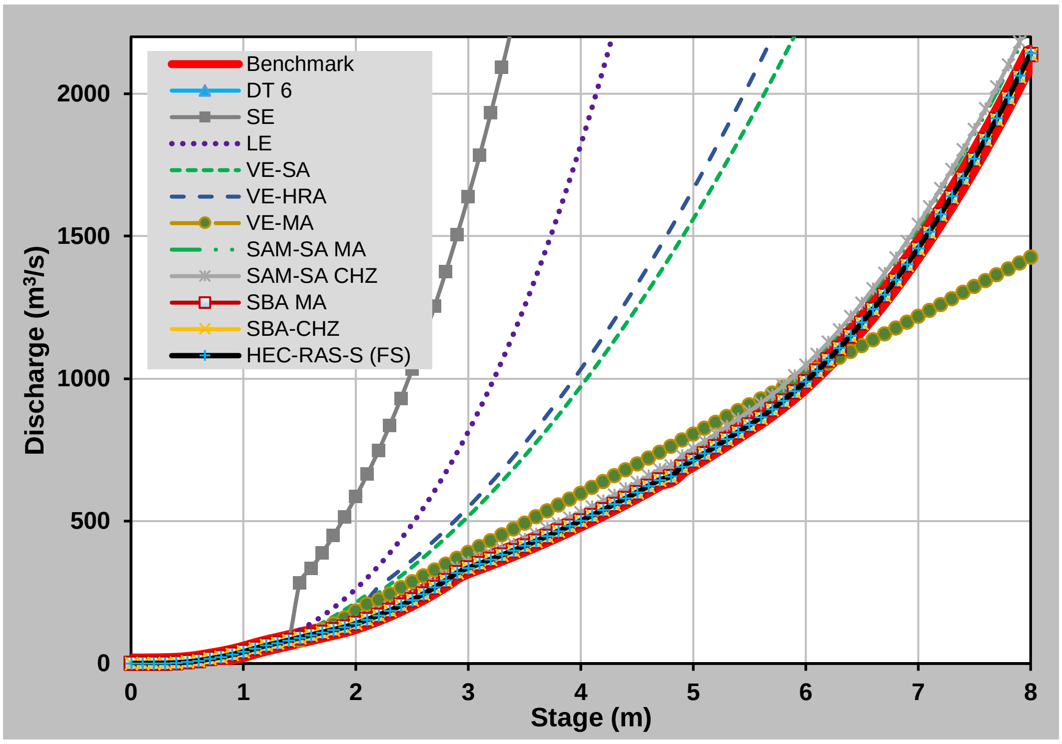

Figure 5.15: Indirect SD extensions in comparison to the benchmark rating at H5H004

Table 5.10: GOF results at H5H004

Criteria	SE	LE	VE			SAM		*SBA		HEC-RAS S (FS)
			SA	HRA	MA	MA	CHZ	MA	CHZ	
Sample size (*N*)	66	66	66	66	66	66	66	66	66	66
Average	7211	4132	1643	1761	752	833	841	793	793	795
Standard deviation	6211	3718	1209	1310	398	591	597	563	563	564
SE_E [Eq. (4.1); m³/s]	469.1	300.5	142.5	150.0	105.6	0.1	0.2	0.0	0.0	0.0
SE_E ranking	10	9	7	8	6	4	5	2	1	3
MARE [Eq. (4.2); %]	662.8	320.7	93.0	104.1	17.0	5.1	6.0	0.0	0.0	0.2
MARE ranking	10	9	7	8	6	4	5	2	1	3
RMSE [Eq. (4.3)]	8522.1	4578.5	1069.3	1223.4	209.7	49.1	58.2	0.0	0.0	2.4
RMSE ranking	10	9	7	8	6	4	5	2	1	3
r^2 [Eq. (4.4)]	0.994	0.994	0.986	0.987	0.931	1.000	1.000	1.000	1.000	1.000
r^2 ranking	6	7	9	8	10	4	5	2	1	3
NSE [Eq. (4.5)]	-231.84	-66.21	-2.67	-3.80	0.86	0.99	0.99	1.00	1.00	1.00
NSE ranking	10	9	7	8	6	4	5	2	1	3
Z-test [Eq. (4.6)]	78.0	51.0	20.2	22.4	1.3	1.2	1.4	0.0	0.0	0.1
Z-test ranking	10	9	7	8	5	4	6	2	1	3
Sum of rankings	**56**	**52**	**44**	**48**	**39**	**24**	**31**	**12**	**6**	**18**
Overall ranking	**10**	**9**	**7**	**8**	**6**	**4**	**5**	**2**	**1**	**3**

*Benchmark method; MA (Manning's approach); CHZ (Chézy's approach); S (Steady flow); and FS (Flood section)

Overall, the hydraulically correct methods resulted in the lowest SE_E, *MARE, RMSE*, and *z*-test values. All the methods demonstrated a high degree of association with r^2 values > 0.93; however, as highlighted before, this only confirms a high correlative trend between the estimated Q_{Ei} values as suggested by the various extension methods and the benchmark Q_{Bi} values. For example, the SE and LE methods are ranked in the 6th and 7th positions, respectively when r^2 values are considered; however, for all the other GOF statistics under consideration, they are ranked in the last positions, i.e., 9th and 10th.

5.1.6 Gauging weir J1H018

Site characteristics and hydraulics:

Gauging weir J1H018 is located in the Touws River at Okkerskraal, Western Cape Province. The weir has been operational since 1982. As shown in Figure 5.16, the structure is a compound weir consisting of a V-Crump (low notch) and four horizontal notches (Bennie *et al.*, 2015).

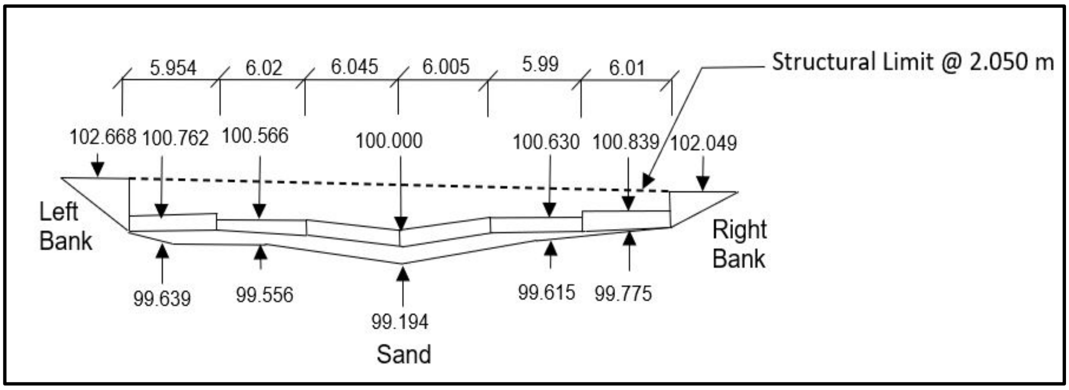

Figure 5.16: Cross-section of compounded weir J1H018 in the Touws River (upstream)

Existing SD relationships and associated data:

The structural limit is at a stage of 2.05 m (GP reading) with an associated discharge of 131 m³/s. In the latest DWS Calibration Report, the SBA method was used as the benchmark SD extension method. Subsequently, all the other indirect extension methods were compared against the latter method up to a stage of 7.0 m and corresponding discharge of 2 203 m³/s. The most recent cross-sectional survey of the gauging weir was conducted on 25 August 2005. The current (existing) SD relationship table (DT3) applicable to J1H018 is listed in Table 5.11, and shown in Figure 5.17 (Bennie *et al.*, 2015).

Table 5.11: DT3 at J1H018 (Bennie *et al.*, 2015)

Stage (m)	Stage increments (m)/ Discharge (m^3/s)									
	0	**0.1**	**0.2**	**0.3**	**0.4**	**0.5**	**0.6**	**0.7**	**0.8**	**0.9**
0	0.0	0.1	0.3	0.8	1.6	2.8	4.5	7.3	11.1	16.3
1	22.8	30.3	38.7	47.8	57.8	68.4	79.7	91.7	104.3	117.5
2	131.2	142.8	155.2	167.7	180.3	193.1	206.2	219.6	233.5	247.9
3	262.9	278.5	294.9	312.0	330.1	349.1	369.2	390.3	412.7	436.3
4	461.2	487.5	515.4	544.7	575.8	608.5	643.0	679.4	717.7	758.1
5	800.5	845.0	891.9	941.0	992.5	1046.5	1103.0	1162.1	1223.9	1288.5
6	1335.9	1426.2	1499.5	1575.9	1655.4	1738.2	1824.2	1913.6	2006.4	2102.7
7	2202.7	-	-	-	-	-	-	-	-	-

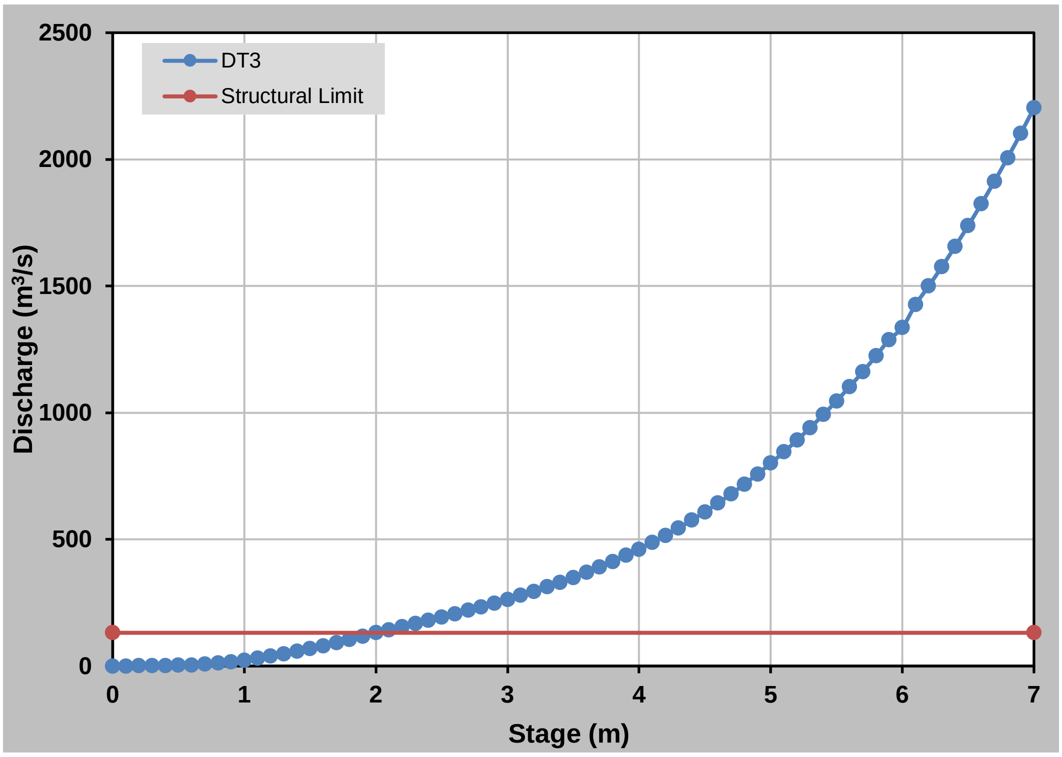

Figure 5.17: Benchmark at-site SD relationship (DT3) at J1H018

<u>Suitability of indirect extension methods:</u>

Based on the current information available at site, the evaluation of the indirect extension methods was based on all the methods considered in this research, including HEC-RAS modelling for steady flow conditions. The results pertained to the SD RC extension using all the above methods are shown in Figure 5.18. The GOF statistics are listed in Table 5.12.

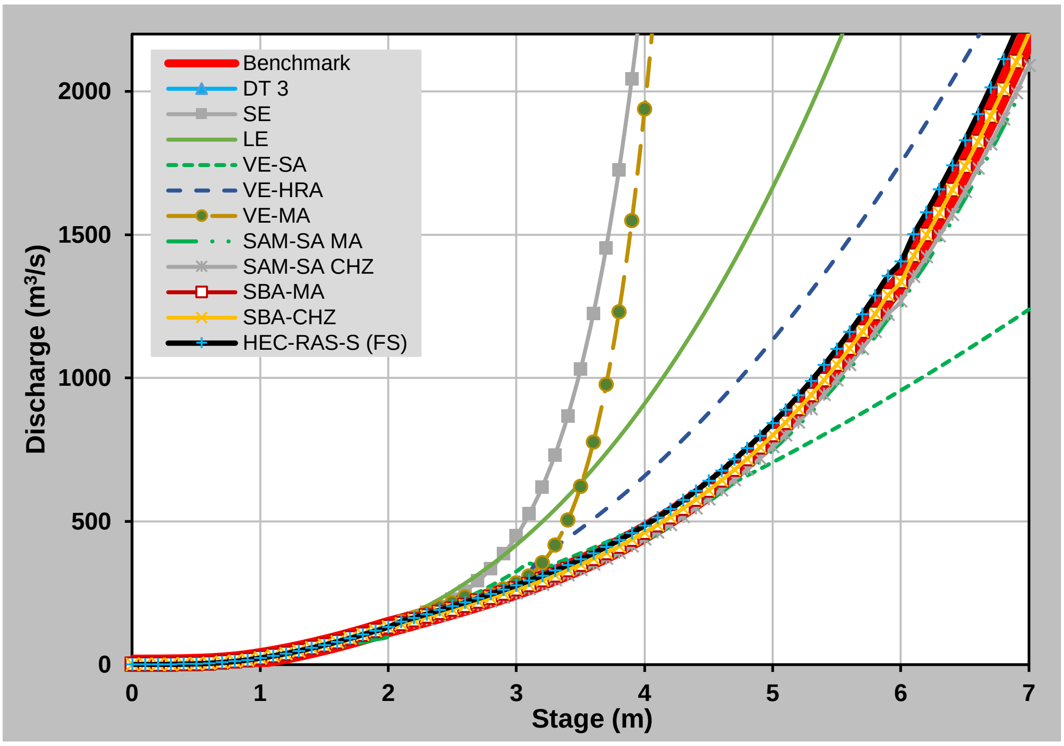

Figure 5.18: Indirect SD extensions in comparison to the benchmark rating at J1H018

Table 5.12: GOF results at J1H018

Criteria	SE	LE	VE			SAM		*SBA		HEC-RAS S (FS)
			SA	HRA	MA	MA	CHZ	MA	CHZ	
Sample size (*N*)	50	50	50	50	50	50	50	50	50	50
Average	19997	1588	637	1049	23845	762	774	815	815	858
Standard deviation	27780	1189	323	716	33805	558	567	597	597	628
SE_E [Eq. (4.1); m³/s]	7593.9	87.7	67.4	84.4	9216.7	0.0	0.0	0.0	0.0	0.0
SE_E ranking	9	8	6	7	10	4	3	2	1	5
MARE [Eq. (4.2); %]	1351.7	84.4	17.6	29.2	1577.4	6.5	5.1	0.0	0.0	5.2
MARE ranking	9	8	6	7	10	5	3	2	1	4
RMSE [Eq. (4.3)]	33064.6	972.1	337.0	272.6	40157.0	65.3	51.2	0.0	0.0	52.7
RMSE ranking	9	8	7	6	10	5	3	2	1	4
r^2 [Eq. (4.4)]	0.927	0.995	0.957	0.986	0.927	1.000	1.000	1.000	1.000	1.000
r^2 ranking	10	6	8	7	9	4	3	2	1	5
NSE [Eq. (4.5)]	-973.021	0.158	0.899	0.934	-1435.695	0.996	0.998	1.000	1.000	0.998
NSE ranking	9	8	7	6	10	5	3	2	1	4
Z-test [Eq. (4.6)]	113.9	18.3	5.9	6.4	124.2	1.6	1.2	0.0	0.0	1.2
Z-test ranking	9	8	6	7	10	5	3	2	1	4
Sum of rankings	**55**	**46**	**40**	**40**	**59**	**28**	**18**	**12**	**6**	**26**
Overall ranking	**9**	**8**	**6**	**7**	**10**	**4**	**3**	**2**	**1**	**5**

*Benchmark method; MA (Manning's approach); CHZ (Chézy's approach); S (Steady flow); and FS (Flood section)

In Table 5.12, the SE, LE, VE-HRA, VE-MA, SAM-MA, SAM-CHZ and HEC-RAS S (FS) methods provided estimated discharge (Q_{Ei}) values that exceed the at-site benchmark discharges (Q_{Bi}). The VE-SA method underestimated the Q_{Ei} values. The SE and VE-MA methods are regarded as the most inappropriate methods, with *MARE* values of 1 352% and 1 577%, respectively. Given that the SBA methods are used as benchmark, the SBA-CHZ method is ranked by default = 1, followed by the SBA-MA method ranked in the second position. HEC-RAS S (FS) is ranked in the 5th position and is based on the SBA with a *MARE* = 5.2%. The latter lower ranking could be ascribed to the insufficient number of cross-sections and steep channel bed slopes (S_o) between cross-sections 2 and 3. The SAM-CHZ and SAM-MA methods also proved to be more accurate than the other indirect extension methods, which, in general, failed to replicate the hydraulic conditions at the site. Overall, the VE-MA method is regarded as the most inappropriate method with the poorest ranking for all the GOF statistics under consideration.

Overall, the hydraulically correct methods resulted in the lowest SE_E, *MARE, RMSE*, and *z*-test values. In terms of r^2 values, the SE method demonstrated the poorest results, while a high correlative trend between the estimated Q_{Ei} values as suggested by the various other extension methods and the benchmark Q_{Bi} values was evident, i.e., $r^2 > 0.92$. The *NSE* results should also be considered; the VE-MA method demonstrated the lowest *NSE* value, despite an r^2 value ≈ 0.93.

5.1.7 Gauging site J4H002

<u>Site characteristics and hydraulics:</u>

Gauging site J4H002 is located in the Gourits River, Western Cape Province. Owing to problems with sedimentation, no weir was constructed, but a natural FS at a bridge has been used since 1964 (*cf.* Figure 5.19).

<u>Existing SD relationships and associated data:</u>

In the latest DWS Calibration Report, the SBA method was used as the benchmark SD extension method. Subsequently, all the other indirect extension methods were compared against the latter method up to a stage of 7.8 m and corresponding discharge of 2 782 m^3/s. The most recent cross-sectional survey of the site was conducted on 30 June 1969, while four FSs were used in the analyses. The current (existing) SD relationship table (DT6) applicable to J4H002 is listed in Table 5.12, and shown in Figure 5.20 (Van Wyk *et al.*, 2015).

Figure 5.19: Natural FS J4H002 in the Gourits River

Table 5.13: DT6 at J4H002 (Van Wyk *et al.*, 2015)

Stage (m)	Stage increments (m)/ Discharge (m^3/s)									
	0	**0.1**	**0.2**	**0.3**	**0.4**	**0.5**	**0.6**	**0.7**	**0.8**	**0.9**
0	0.0	0.0	0.0	0.0	0.0	0.0	0.0	0.0	0.1	0.1
1	0.2	0.3	0.5	0.7	1.1	1.5	2.1	2.9	3.9	5.1
2	6.6	8.5	10.7	13.4	16.7	20.5	25.0	30.3	36.5	43.6
3	51.8	61.2	71.9	84.1	97.8	113.4	130.8	150.3	172.1	196.4
4	223.4	253.2	286.2	322.5	362.5	406.3	454.3	492.6	533.9	577.4
5	623.1	671.0	721.0	773.3	827.8	884.4	943.3	1004.3	1067.5	1133.0
6	1200.6	1270.4	1342.4	1416.6	1493.0	1571.6	1652.3	1735.3	1820.4	1907.8
7	1997.3	2089.1	2183.0	2279.1	2377.4	2477.9	2580.6	2685.5	-	-

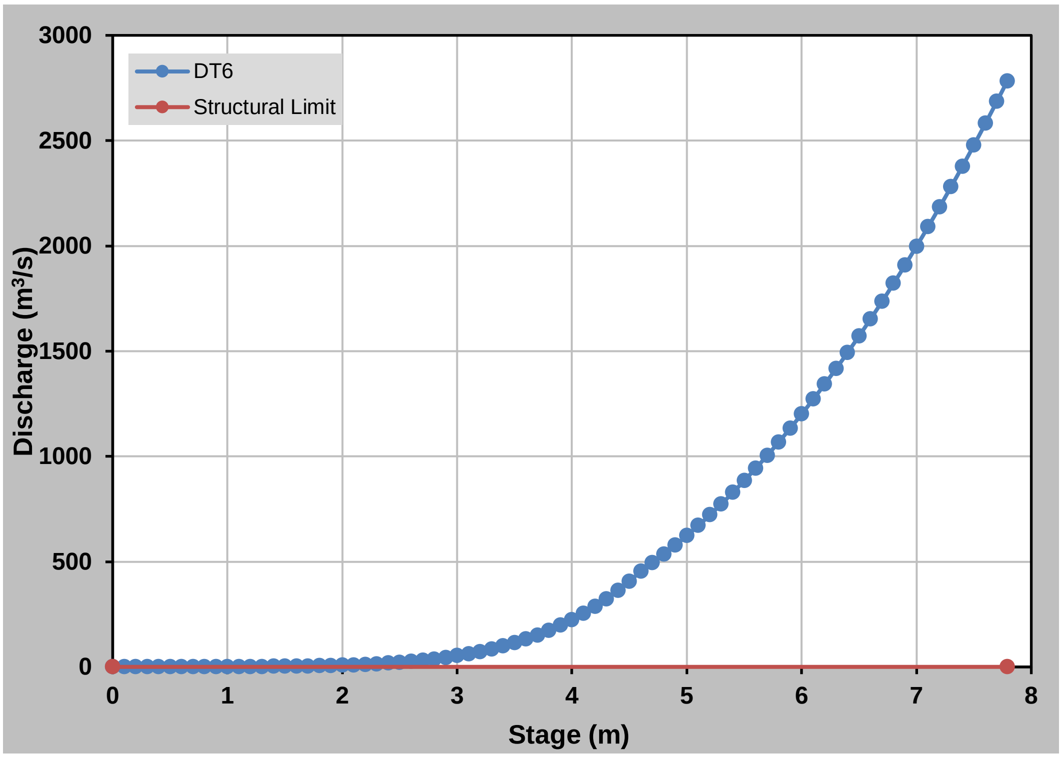

Figure 5.20: Benchmark at-site SD relationship (DT6) at J4H002

Suitability of indirect extension methods:

Based on the current information available at the site, the evaluation and comparison of the indirect extension methods included the following methods: SE, LE, VE, SAM, SBA, and HEC-RAS modelling under steady flow conditions. The results pertained to the SD RC extension using all the above methods are shown in Figure 5.21. The GOF statistics are listed in Table 5.14.

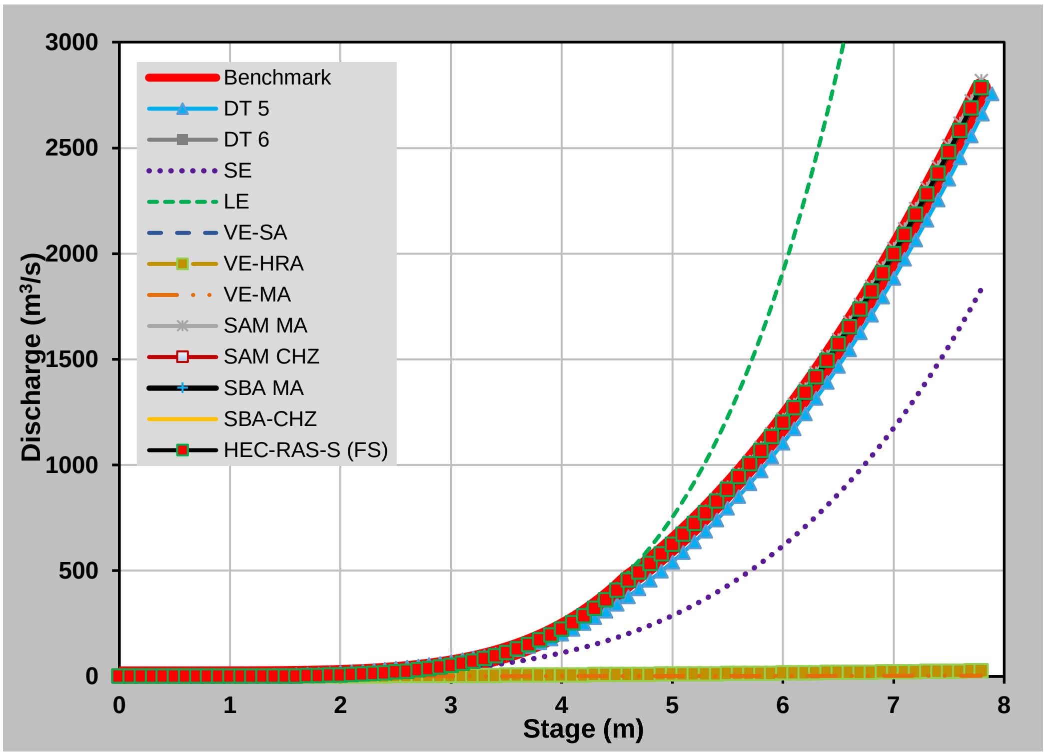

Figure 5.21: Indirect SD extensions in comparison to the benchmark rating at J4H002

Table 5.14: GOF results at J4H002

Criteria	SE	LE	VE			SAM		*SBA		HEC-RAS S (FS)
			SA	HRA	MA	MA	CHZ	MA	CHZ	
Sample size (*N*)	67	67	67	67	67	67	67	68	68	68
Average	428	1450	758	9	2	768	757	747	747	747
Standard deviation	519	1983	844	7	1	856	843	843	843	844
SE_E [Eq. (4.1); m³/s]	51.4	375.4	9.7	149.2	310.9	9.8	9.7	0.0	0.0	0.0
SE_E ranking	7	10	5	8	9	6	4	2	1	3
MARE [Eq. (4.2); %]	37.2	58.8	16.6	92.6	95.0	18.2	16.5	0.0	0.0	0.1
MARE ranking	7	8	4	9	10	6	4	2	1	3
RMSE [Eq. (4.3)]	535.8	1436.7	344.1	1119.7	1128.4	346.8	343.9	0.0	0.0	0.9
RMSE ranking	7	10	4	8	9	6	4	2	1	3
r^2 [Eq. (4.4)]	0.990	0.965	1.000	0.967	0.855	1.000	1.000	1.000	1.000	1.000
r^2 ranking	7	9	4	8	10	6	4	2	1	1
NSE [Eq. (4.5)]	0.596	-1.904	0.833	-0.764	-0.792	0.831	0.834	1.000	1.000	1.000
NSE ranking	7	10	4	8	9	6	4	2	1	3
Z-test [Eq. (4.6)]	8.6	13.2	0.3	25.3	25.7	0.5	0.3	0.0	0.0	0.0
Z-test ranking	7	8	5	9	10	6	4	2	1	3
Sum of rankings	**42**	**55**	**26**	**50**	**57**	**36**	**24**	**12**	**6**	**16**
Overall ranking	**7**	**9**	**5**	**8**	**10**	**6**	**4**	**2**	**1**	**3**

*Benchmark method; MA (Manning's approach); CHZ (Chézy's approach); S (Steady flow); and FS (Flood section)

In Table 5.14, the LE,VE-SA, SAM-SA, and HEC-RAS S (FS) methods provided estimated discharge (Q_{Ei}) values that exceeded the at-site benchmark discharges (Q_{Bi}) throughout the whole rating. The LE overestimations were evident for stages (H) > 4.5 m ($MARE$ = 59%). All the other methods underestimated the Q_{Bi} values for the entire rating. Overall, the VE-MA is the most inappropriate method with the poorest ranking for all the GOF statistics under consideration.

Overall, the hydraulically correct methods resulted in the lowest SE_E, *MARE, RMSE*, and *z*-test values. All the methods demonstrated a high degree of association, with r^2 values > 0.86; however, as shown previously, this only highlights a high correlative trend between the estimated Q_{Ei} values as suggested by the various extension methods and the benchmark Q_{Bi} values. Hence, the *NSE* results should also be considered, whereas the LE and VE-MA methods demonstrated the lowest *NSE* values, despite their $0.86 \leq r^2 \leq 0.97$.

5.1.8 Gauging weir K2H002

<u>Site characteristics and hydraulics:</u>

Gauging weir K2H002 is located downstream of the Wolwedans Dam in the Groot Brak River, Western Cape Province. The weir has been operational since 1961 and is subjected to submergence due to either tidal action or variable water levels in the river as a result of various different discharges being released from the dam. As shown in Figure 5.22, the structure is a compound weir consisting of four sharp-crested notches (Roux and Van der Spuy, 2012).

<u>Existing SD relationships and associated data:</u>

The structural limit is at a stage of 1.5 m (GP reading) with an associated discharge of 55 m^3/s. In the latest DWS Calibration Report, the Wolwedans Dam spillage and allowance for weir submergence were used as the benchmark SD extension method. Subsequently, all the other indirect extension methods were compared against the latter method up to a stage of 4.6 m and corresponding discharge of 428 m^3/s. The most recent cross-sectional survey of the gauging weir was conducted on 14 January 1983. The current (existing) SD relationship table (DT5) applicable to K2H002 is listed in Table 5.15, and shown in Figure 5.23 (Keuris, 1991; Roux and Van der Spuy, 2012).

Figure 5.22: Gauging weir K2H002 in the Groot Brak River

Table 5.15: DT5 at K2H002 (Roux and Van der Spuy, 2012)

Stage (m)	Stage increments (m)/ Discharge (m^3/s)									
	0	**0.1**	**0.2**	**0.3**	**0.4**	**0.5**	**0.6**	**0.7**	**0.8**	**0.9**
0	0.0	0.4	1.2	2.5	5.0	8.4	12.3	16.7	20.5	24.3
1	28.8	33.7	38.8	44.0	49.2	54.4	61.1	68.4	76.1	84.1
2	92.5	101.2	110.2	119.6	129.4	139.4	149.8	160.6	171.7	183.1
3	194.9	207.0	219.5	232.3	245.5	258.9	272.8	287.0	301.5	316.3
4	331.5	347.1	362.9	379.2	395.7	412.6	-	-	-	-

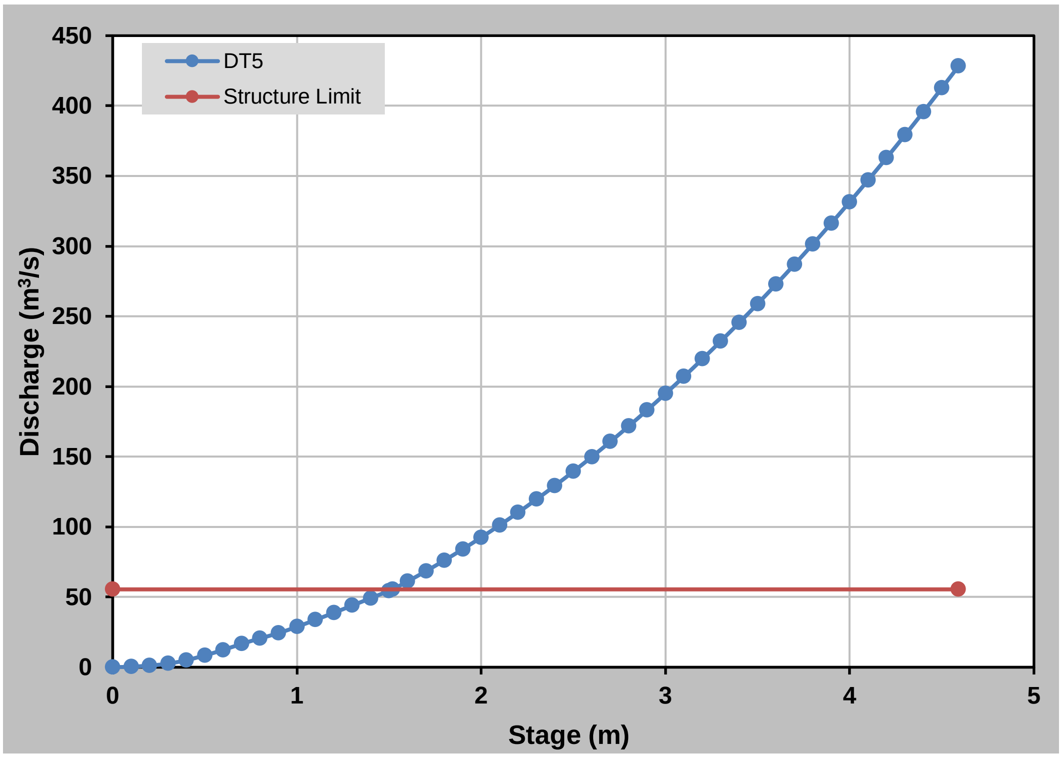

Figure 5.23: Benchmark at-site SD relationship (DT3) at K2H002

<u>Suitability of indirect extension methods:</u>

The current information available at the site is insufficient to apply the SAM, SBA, and HEC-RAS modelling. Consequently, the evaluation of the indirect extension methods was limited to the SE, LE and VE methods based on the survey data used during the calibration of the weir. The results pertained to the SD RC extension using all the above methods are shown in Figure 5.24. The GOF statistics applicable to each method are listed in Table 5.16.

In Table 5.16, all the methods, except the LE method, underestimated the SD relationships in comparison to the Q_{Bi} benchmark SD values. In considering all the GOF criteria, the SE method is ranked in the 1st position, with the *MARE* = 6% and *NSE* = 0.97. However, the SE method is regarded as not being hydraulically correct, given the transition of flows into the overbank flow zone. The VE-MA method performed the worst; with underestimated Q_{Ei} values for H > 1.6 m (*MARE* = 34%).

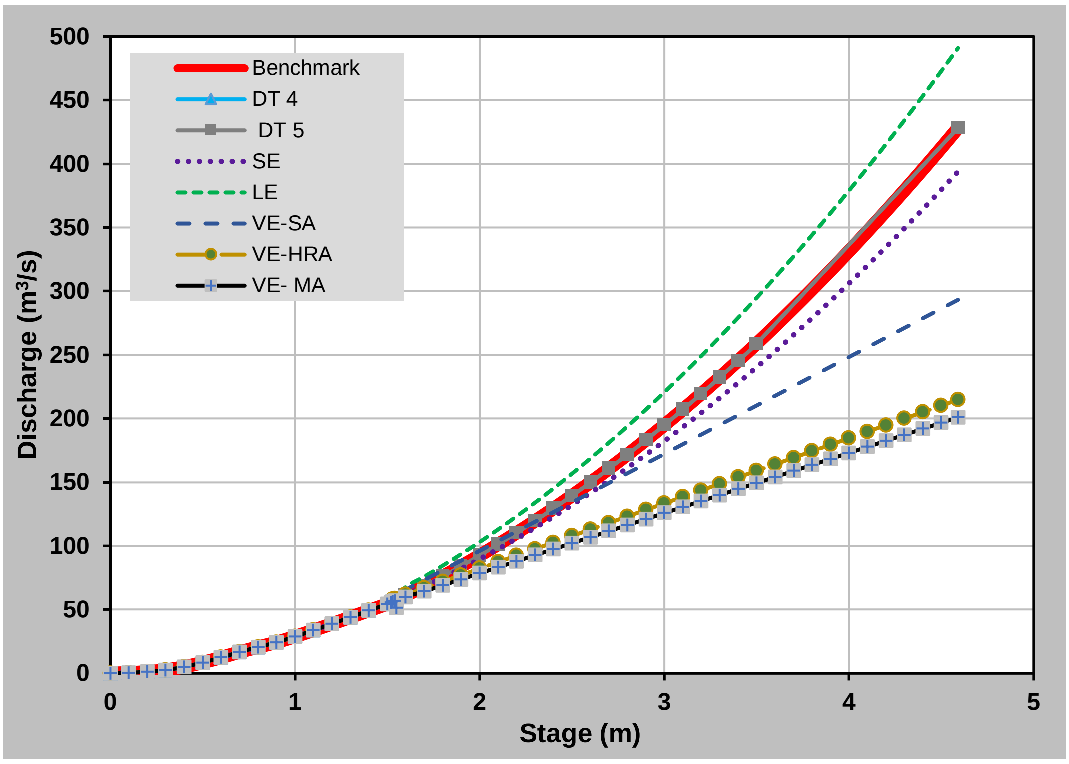

Figure 5.24: Indirect SD extensions in comparison to the benchmark rating at K2H002

Table 5.16: GOF results at K2H002

Criteria	SE	LE	VE			SAM		SBA		HEC-RAS S (FS)
			SA	HRA	MA	MA	CHZ	MA	CHZ	
Sample size (*N*)	31	31	31	31	31	-	-	-	-	-
Average	206	251	180	138	130	-	-	-	-	-
Standard deviation	102	130	69	47	43	-	-	-	-	-
SE_E [Eq. (4.1); m³/s]	0.1	0.4	7.8	5.2	4.8	-	-	-	-	-
SE_E ranking	1	2	5	4	3	-	-	-	-	-
MARE [Eq. (4.2); %]	5.8	13.1	14.5	30.2	33.9	-	-	-	-	-
MARE ranking	1	2	3	4	5	-	-	-	-	-
RMSE [Eq. (4.3)]	18.2	34.8	59.7	104.9	113.4	-	-	-	-	-
RMSE ranking	1	2	3	4	5	-	-	-	-	-
r^2 [Eq. (4.4)]	1.000	1.000	0.988	0.988	0.988	-	-	-	-	-
r^2 ranking	1	2	5	3	3	-	-	-	-	-
NSE [Eq. (4.5)]	0.97	0.90	0.71	0.10	-0.05	-	-	-	-	-
NSE ranking	1	2	3	4	5	-	-	-	-	-
Z-test [Eq. (4.6)]	1.0	1.9	3.0	6.5	7.2	-	-	-	-	-
Z-test ranking	1	2	3	4	5	-	-	-	-	-
Sum of rankings	**6**	**12**	**22**	**23**	**26**	**-**	**-**	**-**	**-**	**-**
Overall ranking	**1**	**2**	**3**	**4**	**5**	**-**	**-**	**-**	**-**	**-**

MA (Manning's approach); CHZ (Chézy's approach); S (Steady flow); and FS (Flood section)

In summary, the GOF statistics at K2H002 highlighted the methods' inability to replicate the Q_{Bi} values, despite the high r^2 values > 0.98 evident. The negative *NSE* results associated with the VE-MA method are indicative of the poor estimates when the observed mean Q_{Bi} values are considered.

5.1.9 Gauging weir V1H026

<u>Site characteristics and hydraulics:</u>

Gauging weir V1H026 is located in the Tugela River at Kleine Waterval, KwaZulu-Natal Province. The weir was constructed in 1967. Sediment deposition is a problem at the site, but submergence is accounted for from a GP reading of 1.026 m. As shown in Figure 5.25, the structure is a compound weir consisting of four sharp-crested notches and a hydro-flume (Sorour, 1992).

Figure 5.25: Gauging weir V1H026 in the Tugela River

<u>Existing SD relationships and associated data:</u>

The structural limit is at a stage of 1.2 m (GP reading) with an associated discharge of 98 m^3/s. In the latest DWS Calibration Report, a hydrograph analysis was used as the benchmark SD extension method. Subsequently, all the other indirect extension methods were compared against the latter method up to a stage of 4.7 m and corresponding discharge of 2 148 m^3/s. The most recent cross-sectional survey of the gauging weir was conducted in March (date unclear) (Sorour, 1992; Oakes and Van der Spuy, 2018).

The current (existing) SD relationship table (DT4) applicable to V1H026 is listed in Table 5.17 and shown in Figure 5.26.

Table 5.17: DT4 at V1H026 (Oakes and Van der Spuy, 2018)

Stage (m)	Stage increments (m)/ Discharge (m^3/s)									
	0	**0.1**	**0.2**	**0.3**	**0.4**	**0.5**	**0.6**	**0.7**	**0.8**	**0.9**
0	0.0	0.3	0.8	1.5	3.8	8.2	15.8	25.4	36.8	50.0
1	64.6	80.6	97.9	117.5	139.3	163.2	189.3	217.6	248.0	280.6
2	314.2	349.9	388.5	429.5	472.7	518.2	566.0	616.3	668.9	723.9
3	781.3	841.2	903.6	968.4	1035.8	1105.6	1178.1	1253.1	1330.6	1410.8
4	1493.6	1579.0	1667.1	1757.8	1851.3	1851.3	1947.4	2046.2	2147.8	-

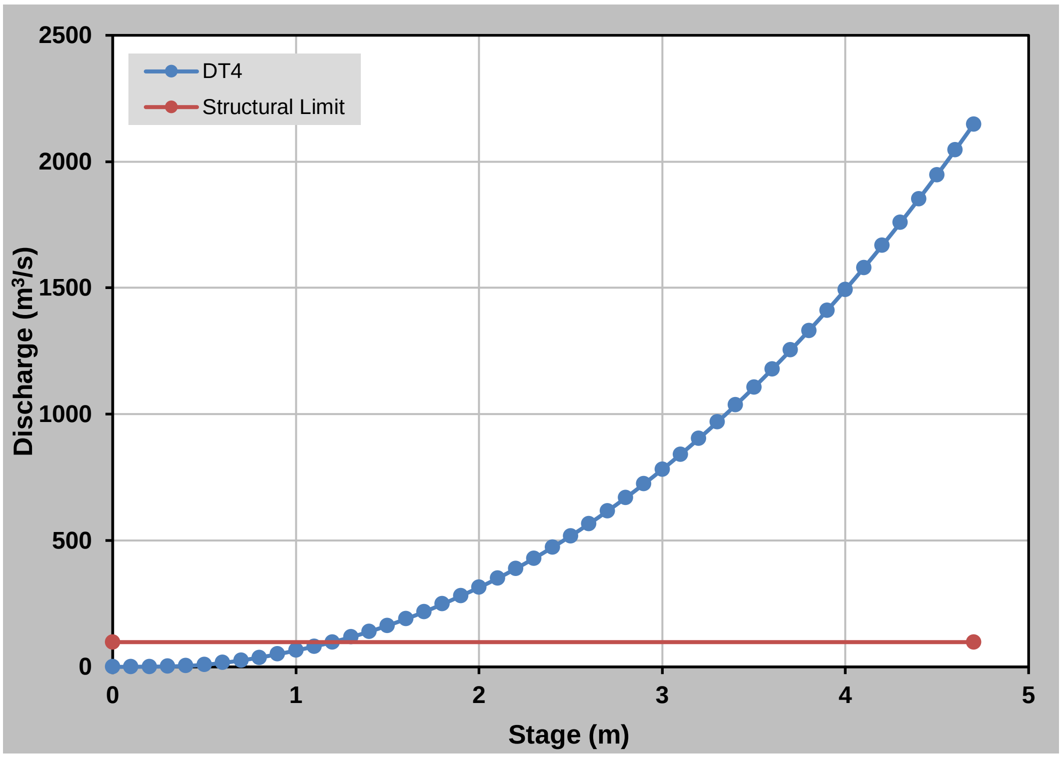

Figure 5.26: Benchmark at-site SD relationship (DT4) at V1H026

<u>Suitability of indirect extension methods:</u>

The current information available at the site is insufficient to apply the SAM, SBA, and HEC-RAS modelling. Consequently, the evaluation of the indirect extension methods was limited to the SE, LE and VE methods based on the survey data used during the calibration of the weir. The results pertained to the SD RC extension using all the above methods are shown in Figure 5.27. The GOF statistics applicable to each method are listed in Table 5.18.

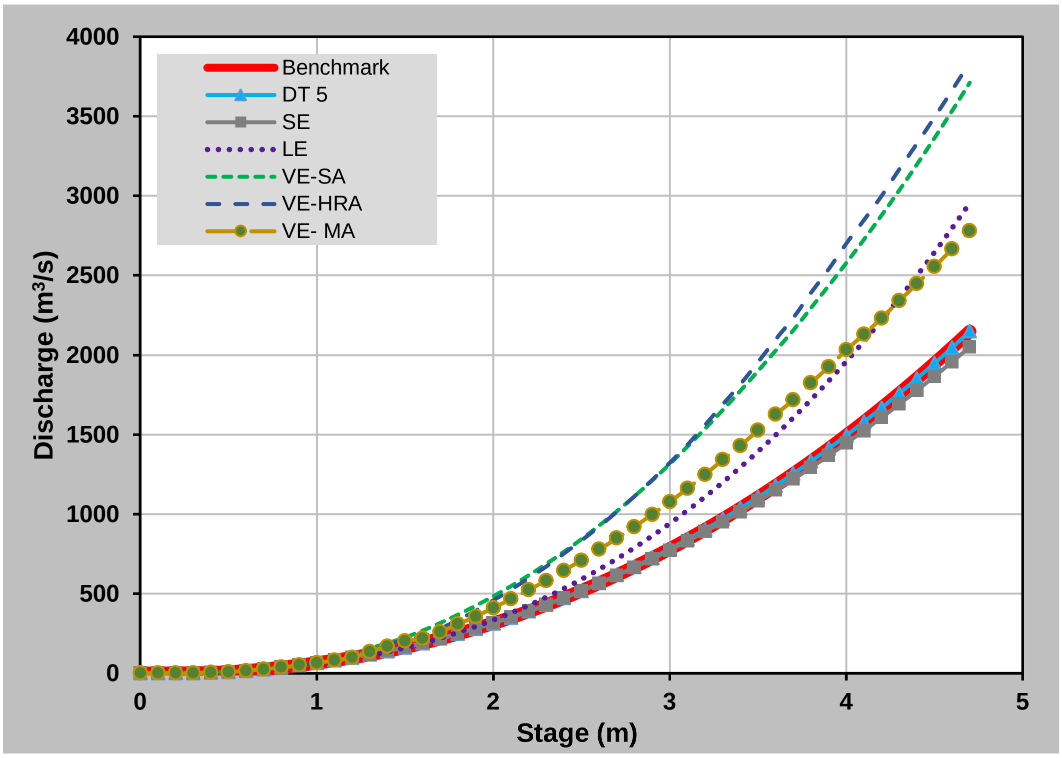

Figure 5.27: Indirect SD extensions in comparison to the benchmark rating at V1H026

Table 5.18: GOF results at V1H026

Criteria	SE	LE	VE			SAM		SBA		HEC-RAS S (FS)
			SA	HRA	MA	MA	CHZ	MA	CHZ	
Sample size (*N*)	35	35	35	35	35	-	-	-	-	-
Average	883	1150	1534	1569	1216	-	-	-	-	-
Standard deviation	588	864	1090	1150	823	-	-	-	-	-
SE_E [Eq. (4.1); m³/s]	7.6	34.2	7.9	20.3	35.6	-	-	-	-	-
SE_E ranking	1	4	2	3	5	-	-	-	-	-
MARE [Eq. (4.2); %]	1.9	19.4	62.8	62.4	32.6	-	-	-	-	-
MARE ranking	1	2	5	4	3	-	-	-	-	-
RMSE [Eq. (4.3)]	38.1	345.5	781.5	846.1	371.7	-	-	-	-	-
RMSE ranking	1	2	4	5	3	-	-	-	-	-
r^2 [Eq. (4.4)]	1.000	0.998	1.000	1.000	0.998	-	-	-	-	-
r^2 ranking	2	4	1	3	5	-	-	-	-	-
NSE [Eq. (4.5)]	1.00	0.68	-0.65	-0.93	0.63	-	-	-	-	-
NSE ranking	1	2	4	5	3	-	-	-	-	-
Z-test [Eq. (4.6)]	0.7	6.3	15.2	15.8	8.2	-	-	-	-	-
Z-test ranking	1	2	4	5	3	-	-	-	-	-
Sum of rankings	**7**	**16**	**20**	**25**	**22**	**-**	**-**	**-**	**-**	**-**
Overall ranking	**1**	**2**	**3**	**5**	**4**	**-**	**-**	**-**	**-**	**-**

MA (Manning's approach); CHZ (Chézy's approach); S (Steady flow); and FS (Flood section)

In Table 5.18, all the methods except the VE-SA and VE-HRA methods, underestimated the SD relationships in comparison to the Q_{Bi} benchmark SD values. In considering all the GOF criteria, the SE method is ranked in the 1st position, with the *MARE* = 8% and *NSE* = 0.99. However, the SE method is regarded as not being hydraulically correct, given the transition of flows into the overbank flow zone. The VE-SA method is ranked in the 3rd position, with overestimations above H > 1.2 m. Overall, the VE-HRA method is the most inappropriate method with the poorest ranking for all the GOF statistics under consideration.

In summary, the GOF statistics at V1H026 highlighted the methods' inability to replicate the Q_{Bi} values, despite the high r^2 values > 0.97 evident. The latter high r^2 values only highlight a high correlative trend between the estimated Q_{Ei} values as suggested by the various extension methods and the benchmark Q_{Bi} values. Hence, the *NSE* results should also be considered, whereas the VE-HRA and VE-MA methods demonstrated the lowest *NSE* values, despite their r^2 values ≈ 0.98.

5.1.10 Gauging weir X3H008

Site characteristics and hydraulics:

Gauging weir X3H008 is located in the Sand River, Mpumalanga Province. The weir was constructed in 1967. As shown in Figure 5.28, the structure consists of a sharp-crest, hydro-flume, and broad-crested flank walls (Mathole, 1999).

Figure 5.28: Gauging weir X3H008 in the Sand River

Existing SD relationships and associated data:

The structural limit is at a stage of 1.95 m (GP reading), with an associated discharge of 76 m^3/s. In the latest DWS Calibration Report, the SBA was used as the preferred SD extension method. Hence, the SBA was also used as a benchmark against which the other indirect extension methods were compared up to a stage of 5.4 m and corresponding discharge of 2 972 m^3/s. The most recent cross-sectional survey of the gauging weir was conducted on 07 August, but the year is unclear. Five FSs were used in the SBA. The current (existing) SD relationship table (DT10) applicable to X3H008 is listed in Table 5.19, and the existing SD relationship is shown in Figure 5.29 (Mathole, 1999; Nathanael *et al.*, 2018).

Table 5.19: DT10 at X3H008 (Nathanael *et al.*, 2018)

Stage (m)	Stage increments (m)/ Discharge (m^3/s)									
	0	**0.1**	**0.2**	**0.3**	**0.4**	**0.5**	**0.6**	**0.7**	**0.8**	**0.9**
0	0.0	0.2	0.6	1.1	1.8	2.8	4.7	7.1	9.9	13.0
1	16.5	20.3	24.4	28.7	34.1	39.1	45.4	52.7	61.0	70.2
2	84.7	107.6	137.0	172.4	213.8	261.2	315.2	372.1	429.1	488.9
3	552.8	618.7	688.0	760.3	836.0	914.0	995.0	1 080.0	1 167.0	1 258.0
4	1351.0	1448.0	1548.0	1650.0	1756.0	1865.0	1976.0	2091.0	2209.0	2330.0
5	2453.0	2580.0	2710.0	2843.0	2972.0	-	-	-	-	-

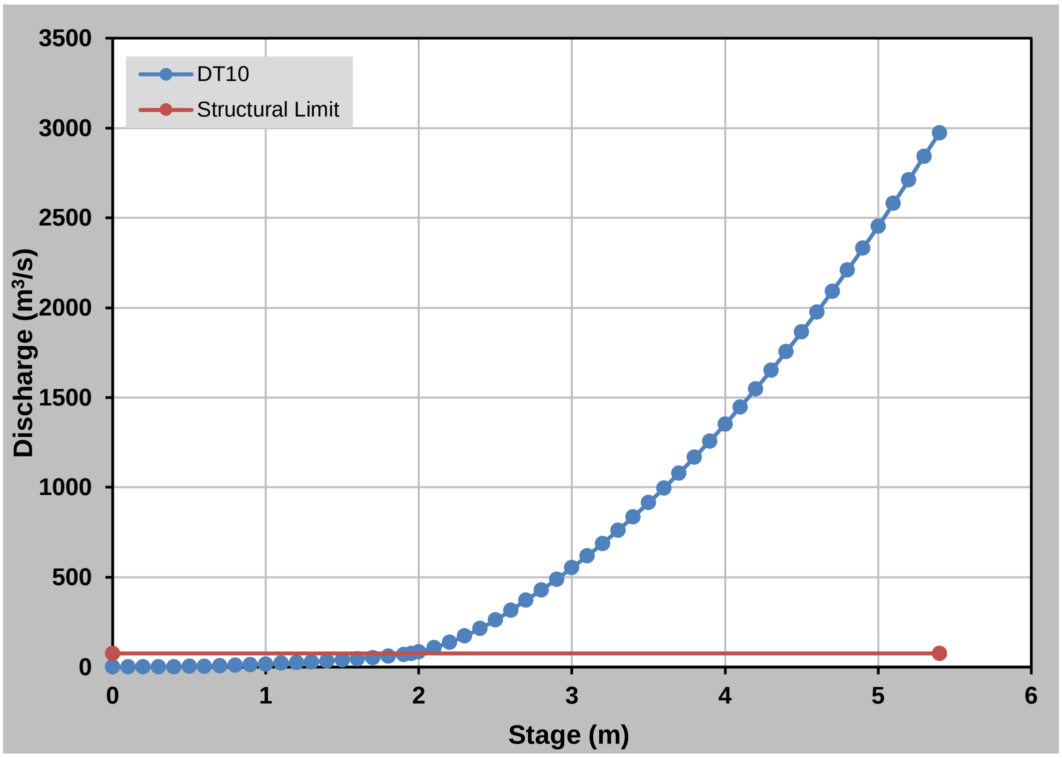

Figure 5.29: Benchmark at-site SD relationship (DT10) at X3H008

<u>Suitability of indirect extension methods:</u>

Based on the current information available at X3H008, the evaluation and comparison of the indirect SD extension methods included all the methods. The SD RC extension results using all the above methods are shown in Figure 5.30. The GOF statistics applicable to each method are listed in Table 5.20.

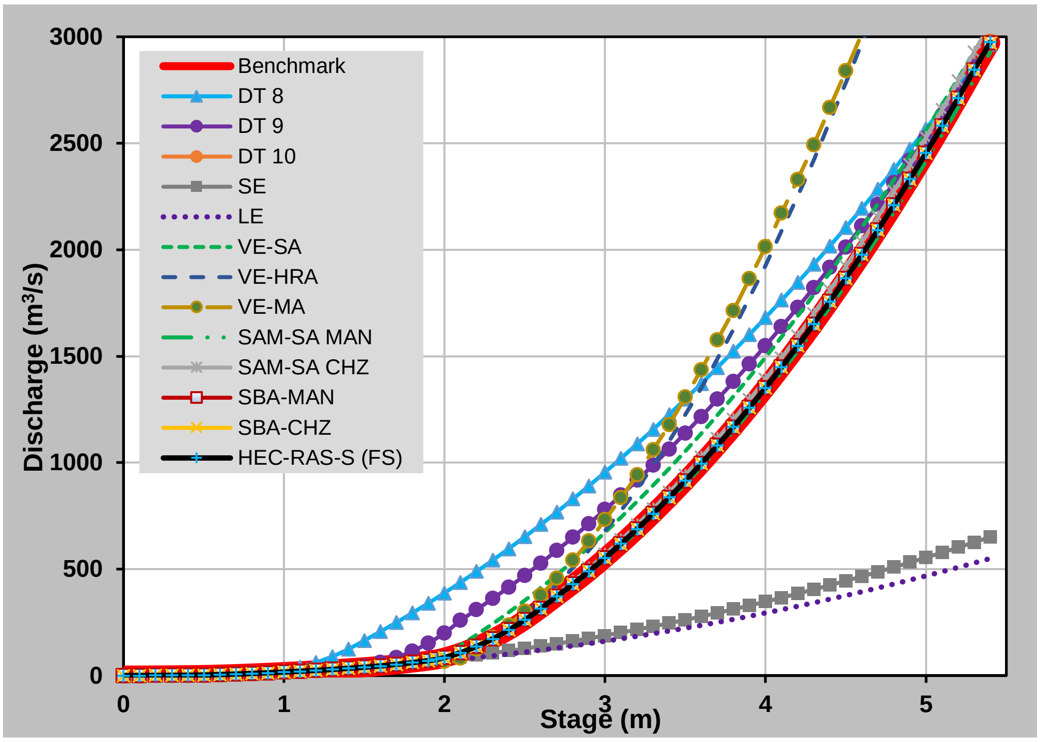

Figure 5.30: Indirect SD extensions in comparison to the benchmark rating at X3H008

Table 5.20: GOF results at X3H008

Criteria	SE	LE	VE			SAM		*SBA		HEC-RAS S (FS)
			SA	HRA	MA	MA	CHZ	MA	CHZ	
Sample size (*N*)	35	35	35	35	35	35	35	35	35	35
Average	319	271	1348	1809	1839	1217	1273	1235	1235	1236
Standard deviation	174	146	899	1436	1414	877	917	890	890	891
SE_E [Eq. (4.1); m^3/s]	5.7	4.4	31.2	66.3	27.0	0.0	0.2	0.0	0.0	0.0
SE_E ranking	7	6	9	10	8	3	5	2	1	4
MARE [Eq. (4.2); %]	65.4	70.2	16.3	35.0	39.7	1.5	3.0	0.0	0.0	0.1
MARE ranking	9	10	6	7	8	4	5	2	1	3
RMSE [Eq. (4.3)]	1156.5	1211.5	116.8	788.4	794.7	22.8	0.0	0.0	0.0	1.3
RMSE ranking	9	10	6	7	8	5	3	2	1	4
r^2 [Eq. (4.4)]	0.999	0.999	0.999	0.998	1.000	1.000	1.000	1.000	1.000	1.000
r^2 ranking	8	7	9	10	6	4	5	2	1	3
NSE [Eq. (4.5)]	-0.74	-0.91	0.98	0.19	0.18	1.00	1.00	1.00	1.00	1.00
NSE ranking	9	10	6	7	8	5	3	2	1	4
Z-test [Eq. (4.6)]	28.1	30.0	2.7	11.9	12.6	0.4	0.9	0.0	0.0	0.0
Z-test ranking	9	10	6	7	8	4	5	2	1	3
Sum of rankings	**51**	**53**	**42**	**48**	**46**	**25**	**26**	**12**	**6**	**21**
Overall ranking	**9**	**10**	**6**	**8**	**7**	**4**	**5**	**2**	**1**	**3**

*Benchmark method; MA (Manning's approach); CHZ (Chézy's approach); S (Steady flow); and FS (Flood section)

In Table 5.20, the various indirect SD extension methods, except for the SE and LE methods, provided estimated discharge (Q_{Ei}) values that exceed the at-site benchmark discharges (Q_{Bi}). The latter underestimations using the SE and LE methods were evident for stages (H) > 2 m (65% ≤ *MARE* ≤ 70%). Given that the SBA-CHZ method is used as the benchmark method (default ranking = 1) at this site, the SBA-MA demonstrated the second-best overall ranking, followed by the HEC-RAS S (FS) modelling in the 3rd position. By considering the individual GOF statistics, the latter SAM-CHZ and SAM-MA methods also proved to be equally accurate by being interchangeably ranked at either the 4th or 5th position. Overall, the LE method is the most inappropriate method with the poorest ranking for all the GOF statistics under consideration.

Overall, the hydraulically correct methods resulted in the lowest SE_E, *MARE, RMSE*, and *z*-test values. All the methods demonstrated a high degree of association, with r^2 values > 0.99; however, as shown previously, this highlights a high correlative trend between the estimated Q_{Ei} values as suggested by the various extension methods and the benchmark Q_{Bi} values. Hence, the *NSE* results should also be considered, whereas the VE-HRA and VE-MA methods demonstrated the lowest *NSE* values of ±0.19 despite their r^2 values ≈ 0.99.

5.2 Summary of Results

The overall ranking results are listed in Table 5.21.

Table 5.21: Summary of the GOF-based rankings at the 10 flow-gauging sites

Gauging site	SE	LE	VE			SAM		SBA		HEC-RAS S (FS)
			SA	HRA	MA	MA	CHZ	MA	CHZ	
A4H005	4	5	3	1	2	-	-	-	-	-
A6H035	4	1	2	3	5	-	-	-	-	-
C2H003 (C3H130)	3	1	5	4	2	-	-	-	-	-
C5H014	10	9	7	8	6	4	5	2	1	3
H5H004	10	9	7	8	6	4	5	2	1	3
J1H018	9	8	6	7	10	4	3	2	1	5
J4H002	7	9	5	8	10	6	4	2	1	3
K2H002	1	2	3	4	5	-	-	-	-	-
V1H026	1	2	3	5	4	-	-	-	-	-
X3H008	9	10	6	8	7	4	5	2	1	3
Avg. Rankings	**5.8**	**5.6**	**4.7**	**5.6**	**5.7**	**4.4**	**4.4**	**2**	**1.2**	**3.4**
Overall ranking	**10**	**8**	**6**	**7**	**9**	**5**	**4**	**2**	**1**	**3**

The overall ranking results listed in Table 5.21 highlight that the SBA, SAM, and 1-D HEC-RAS steady flow modelling performed the best. The other indirect extension methods were characterised by larger statistical differences between the at-site benchmark values (Q_{Bi}) and the modelled values (Q_{Ei}). The VE-MA and SE methods are regarded as the least appropriate methods, ranked in the 9th and 10th positions, respectively.

The SBA, SAM, and 1-D HEC-RAS steady flow modelling are therefore regarded as the most appropriate indirect estimation methods to reflect the hydraulic conditions during high discharges at a flow-gauging site. In general, any extension method must be hydraulically correct if it is to be used as a robust approach to extend SD RCs beyond the structural limit. The extension of a RC is significantly more affected by the site (and river reach) geometry, initial hydraulic conditions, flow regimes and level of submergence at high discharges, than the actual extension method used.

In addition to the above, the individual performances of each method at the 10 flow-gauging sites under consideration, are summarised in the subsequent sections.

5.2.1 SE performance

The SE method is ranked overall in the 10th position. The method tends to either over- or underestimate the at-site benchmark discharges (Q_{Bi}). At K2H002 and V1H026, it provided satisfactory results due to no changes in the geometry or hydraulic conditions above the structural limit. This method is not suited to extend SD relationships at sites with complex hydraulics or geometry, and the use thereof should be limited to gauging sites with adequate data and reasonably simple site characteristics and hydraulics. It demonstrated the poorest performance at C5H014 and H5H004.

5.2.2 LE performance

The LE method is ranked overall in the 8th position. The method tends to either over- or underestimate the at-site benchmark discharges (Q_{Bi}). At A6H035, there are no apparent transitions beyond/above the structural limit; hence, the subsequent number one ranking at this site. The LE method performed marginally better than the SE method at all the gauging sites under consideration, except at A4H005, J4H002, K2H002, V1H026 and X3H008. However, this method is not recommended for significant extensions above the structural limit; typically, in these above-structure-limit ranges, it proved to result in estimated discharges (Q_{Ei}) significantly different from the benchmark discharges (Q_{Bi}).

5.2.3 VE performance

The VE-SA (6th position) and VE-HRA (7th position) methods performed better than the VE-MA method (9th position); however, the application of all these methods was limited by data availability. The VE methods require a complete cross-section of the weir at high flows, and such data sets were not available at most of the sites under consideration, except at A4H005 where these methods were ranked as the top three methods. Hence, based on the promising results achieved at some of the gauging sites, the VE methods should be considered more often when SD relationships need to be extended. The VE methods are also simpler to apply as opposed to the often-preferred SAM and SBA methods.

5.2.4 SAM performance

The SAM-CHZ is ranked overall in the 4th position, while the SAM-MA is ranked in the 5th position. In comparison to the SE, LE and VE methods, it is hydraulically more correct. At J1H018 and J4H002, the SAM-CHZ proved to be hydraulically more correct (3rd to 4th position) and agreed well with the SBA. By considering the individual GOF statistics, the SAM-CHZ and SAM-MA methods also proved to be equally accurate at gauging sites C5H014, H5H004 and X3H008 by being interchangeably ranked at either the 4th or 5th position. The SAM also requires what is referred to as SAM cross-sections, with specific hydraulic conditions as discussed in Chapter 2 (*cf.* Section 2.5.5). Hence, if the cross-sections available at the site do not meet the above criteria, then the SAM performance is affected accordingly.

5.2.5 SBA performance

The SBA-CHZ is overall ranked in the 1st position, while the SBA-MA is ranked in the 2nd position. However, the SBA was also used as the preferred benchmark method at 50% of the flow-gauging sites under consideration. The latter preferential use and associated rankings were also confirmed by Roux and Rademeyer (2015): "*From experience, DWS Flood Studies regard the SBA method as superior to the SAM when flood peaks need to be estimated*." The latter statement, as highlighted in Chapter 2, is also supported in international literature. The SBA is also less affected by hydraulic conditions than the SAM and is therefore regarded as a more versatile method.

The Chézy's absolute roughness (k_s) version of the SBA, i.e., SBA-CHZ is preferred to the Manning's *n*-value version (SBA-MA). This is ascribed to the fact that Manning's *n*-value is expressed in non-measurable units, i.e., s/m$^{1/3}$, and constant for a given discharge associated with a specific velocity and hydraulic radius. Equation (2.2) makes allowance for changes in the Chézy's roughness coefficient C (m$^{0.5}$/s) as changes in the flow depth and subsequently the hydraulic radius (R) occur. As a result, channel profile convergence is normally achieved sooner when Chézy's C-value (function of k_s and R) is used in the SBA. Manning's *n*-value does vary with changes in the hydraulic radius; however, there is no explicit mathematical procedure to determine this. Additionally, it is also easier to visualise Chézy's absolute roughness (k_s) as it represents the sizes of irregularities on the channel beds and sides, expressed in millimetres.

It is also important to note that the starting water surface level/elevation in the SBA is regarded as unknown or indefinite; hence, several backwater profiles based on different arbitrary water surface levels should be computed until convergence occurs, i.e., the water levels correspond with the uniform flow profile and energy levels are in equilibrium. Therefore, if convergence is not reached (probably owing to insufficient cross-sectional survey data), additional and more distant (up- and/or downstream) cross-sections would be required. In this research at some of the flow-gauging sites under consideration, DWS had already established an arbitrary datum (reference level), and known water surface levels (e.g., flood marks). Subsequently, defining an arbitrary point to reach profile convergence was not required in these cases.

<u>Manning's *n*-value for flood flows:</u>

In assigning roughness parameters, i.e., Manning's *n*-values, it should not be limited to a cross-section, but it should rather be representative of the entire river reach under consideration (George *et al.*, 1989). Observations made in this research confirmed the difficulty in assigning Manning's *n*-values for a river reach and the cross-sections under consideration. Hence, based on Figure 5.31, it is evident that various input parameters (excluding eddy losses) need to be considered when assigning *n*-values during high flows. Given that eddy losses, especially in non-prismatic channels, cannot be easily quantified, these losses are normally included as part of the friction loss component (Chow, 1959). Irrespective of the method used, e.g., SAM, SBA and/or HEC-RAS, if representative and correct *n*-values are assigned, then comparable results will be achieved.

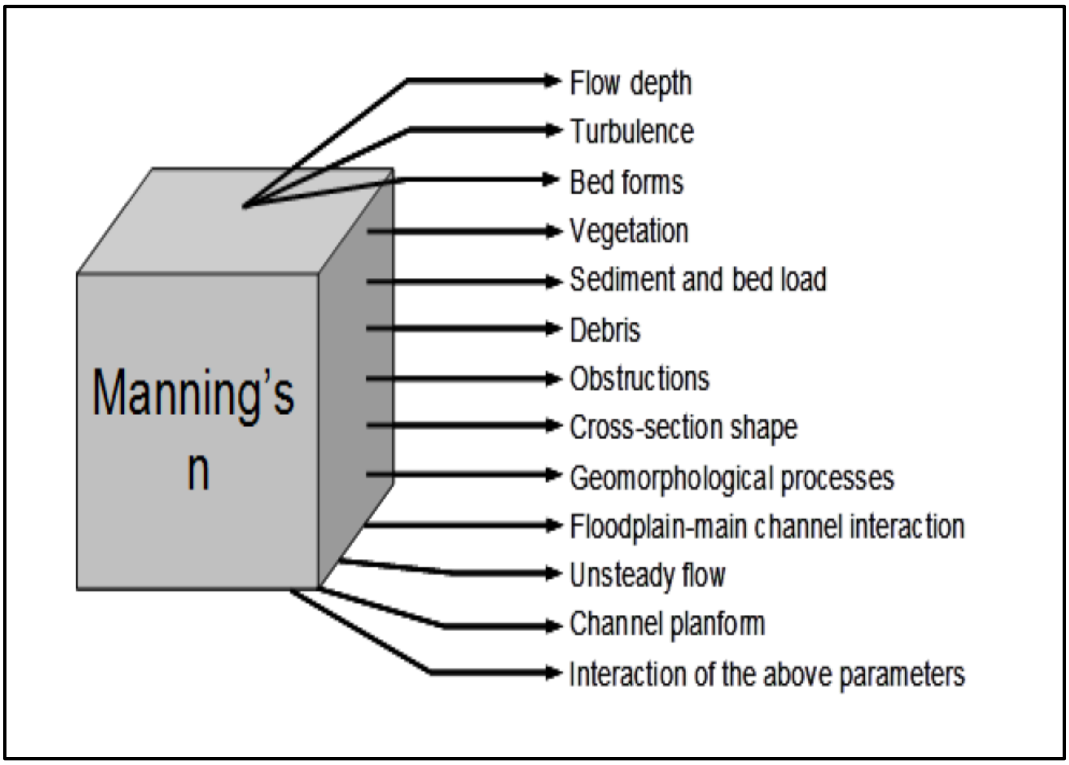

Figure 5.31: Input parameters affecting Manning's *n*-value selection for flood flows (Lumbroso and Gaume, 2012)

5.2.6 HEC-RAS performance

In general, the HEC-RAS steady flow modelling is limited by data suitability and availability. It was evident that the HEC-RAS results improved as the number of more detailed and distant cross-sections increased. Therefore, by having a continuous surface, i.e., digital terrain model, from which high-accuracy cross-sections can be extracted, the modelling results can be improved significantly.

According to Price (2020): "*When you hit compute in a steady-state run, the model assumes that the given discharge has been running at that rate forever and ever – to infinity and beyond."* Price (2020) also indicated that steady flow computations are sufficient to extend SD relationships, despite the limitations; however, the software will provide an unrealistic linear SD relationship. In order to provide a more realistic and hydraulically correct simulation and SD RCs, known water surface levels, additional discharges, and additional cross-sections should be incorporated. Typically, owing to insufficient data being available, no HEC-RAS modelling was possible at gauging sites A4H005, A6H035, C2H003, K2H002, and V1H026. At the latter gauging sites, only calibration data up to the structural limit were available, subsequently resulting in discontinued flow at above-structure-limit conditions. In applying HEC-RAS at data deficient gauging sites, overestimations will typically occur up to the structural limit, while above-structure-limit flows will either be under- or overestimated.

The next chapter provides the conclusions and general recommendations for future research.

CHAPTER 6 : CONCLUSIONS AND RECOMMENDATIONS

This chapter contains a synthesised discussion of the research results presented in Chapter 5. The conclusions and recommendations for future research are included at the end of this chapter.

6.1 Research Aim

The overall aim of this research was to assess and compare a selection of indirect extension methods (e.g., hydraulic and one-dimensional modelling methods) with direct extension (benchmark) methods (e.g., at-site conventional current gaugings, hydrograph analyses and level pool routing techniques), in order to establish the best-fit and most appropriate SD extension method to be used in South Africa. In terms of the direct extension (benchmark) methods, the following approaches were used at the various flow-gauging sites: (i) dam spillage (K2H002), (ii) hydrograph analysis (V1H026), (iii) level pool (back) routing (A4H005, A6H035 and C2H130), and (iv) SBA (C5H014, H5H004, J1H018, J4H002 and X3H008).

The investigation applicable to the research assumptions is summarised in the next section.

6.2 Research Assumptions

<u>*Assumption 1*</u>: *The SAM and by extension, the DCM, are more appropriate and hydraulically correct than the other SD extension methods available.*

Assumption 1 was rejected, given that the SAM-CHZ and SAM-MA were ranked overall in the 4th and 5th position, respectively. In comparison to the SE, LE and VE methods, the SAM proved to be hydraulically more correct. However, the SAM also requires what is referred to as SAM cross-sections, with the specific hydraulic conditions as discussed in Chapter 2 (*cf.* Section 2.5.5). Hence, if the cross-sections available at the site do not meet the above criteria, then the SAM performance will be affected accordingly. In addition, another drawback of the method is that roughness coefficients for between-reaches are also required.

<u>Assumption 2:</u> The SBA is more accurate than the SAM.

Assumption 2 was confirmed, given that the SBA-CHZ was ranked in the 1st position overall, while the SBA-MA was ranked in the 2nd position. The SBA was used as the preferred benchmark method at 50% of the flow-gauging sites under consideration given that the SBA is less affected by hydraulic conditions than the SAM and is therefore regarded as a more versatile method.

<u>Assumption 3:</u> One-dimensional hydraulic models (e.g., HEC-RAS) better illustrate the actual hydraulic conditions in a river reach than hydraulic methods.

Assumption 3 was rejected, given that the HEC-RAS steady flow modelling was ranked in the 3rd position overall. In principle, the HEC-RAS steady flow modelling is also based on the SBA; hence, the latter performance was expected. However, the steady flow modelling was in general limited by data suitability and availability. It was evident that the HEC-RAS results improved as the number of more detailed and distant cross-sections increased. Therefore, having a continuous surface, i.e., digital terrain model, from which high-accuracy cross-sections can be extracted, the modelling results can be improved significantly.

6.3 Specific Objectives

The specific objectives were addressed successfully and ensured that the overall research aim was achieved. The details are listed below:

(a) The literature review conducted is inclusive of both the fundamental theory, as well as the latest advances applicable to the extension of SD relationships.
(b) Ten (10) appropriate DWS flow-gauging sites were identified and selected to enable the benchmarking and comparisons between the direct and indirect extension methods.
(c) The semi-automated extension tool was developed successfully and enabled the consistent application of the various hydraulic methods with limited manual user input.
(d) One-dimensional HEC-RAS modelling was conducted successfully at each flow-gauging site by considering steady flow conditions.

(e) The indirect extension methods' results were compared and independently assessed against the direct SD measurements/estimates at each site. Based on the overall GOF-based rankings, the SBA, SAM, and 1-D HEC-RAS steady flow modelling were identified as the most appropriate indirect estimation methods to reflect the hydraulic conditions during high discharges at a flow-gauging site. The remaining indirect extension methods were characterised by larger statistical differences between the at-site benchmark values (Q_{Bi}) and the modelled values (Q_{Ei}). The SE method was identified as the least appropriate method.

6.4 Major Findings

An enhanced methodology was developed to assess and compare a selection of indirect extension methods with direct extension (benchmark) methods in order to establish the best-fit and most appropriate SD extension method to be used in South Africa. The significant findings are detailed in the subsequent sections.

6.4.1 Data quantity and quality

An increase in the quantity and quality of the data inevitably reduced the statistical differences between the at-site benchmark values (Q_{Bi}) and the modelled values (Q_{Ei}). For example, at flow-gauging sites A4H005 and C5H014, where more complete data sets and detailed geometric data were available, the extension of the SD RCs improved accordingly, while the more sensitive methods, e.g., VE methods also performed better.

It was evident that the data requirements as specified in scientific literature, are unduly generic. Hence, the following observations were made when the indirect extension methods were applied at the various flow-gauging sites:

(a) The SE and LE methods need to include all transitions, overbank flow, changes from modular to submerged flow conditions, and any control changes. Literature highlighted that vegetation and cross-section changes are not accounted for in these methods; however, any of these changes actually also qualifies as a change in the geometric properties of a cross-section. Furthermore, any re-orientations in a cross-section would also result in significant changes when stage and the hydraulic radius are considered. However, the latter aspects will not be apparent during the application of these extension methods.

(b) The VE methods require a cross-section at the weir or flow-gauging site that covers the entire flow range. However, standard calibration surveys do not necessarily include cross-section details up to these high stages, while practical constraints, e.g., high flow velocities, water depths, danger to staff required to enter the river reach, and operational difficulties further exacerbate the situation during high flows.

(c) In the case of the HEC-RAS modelling, the data required for a simulation run and the calibration thereof represent a paradox. Firstly, the model requires survey data covering the full range of flows at a maximum flow depth. Such data are unavailable at sites where the SD RC is only applicable up to the structural limit of the flow-gauging weir. Similarly, the discharges at these high stages (above-structure-limit conditions), are also unavailable. Secondly, the data required for calibration purposes are also non-existent, except in cases where flood surveys were conducted to include the high watermarks and associated roughness coefficients.

6.4.2 Roughness coefficients

The Chézy's absolute roughness (k_s) version of the SBA, i.e., SBA-CHZ is preferred to the Manning's *n*-value version (SBA-MA). This is ascribed to the fact that Manning's *n*-value is expressed in non-measurable units, i.e., s/m$^{1/3}$, and is constant for a given discharge associated with a specific velocity and hydraulic radius. Equation (2.2) makes allowance for changes in the Chézy's roughness coefficient C (m$^{0.5}$/s) as changes in the flow depth and subsequently the hydraulic radius (R) occur. As a result, channel profile convergence is normally achieved sooner when Chézy's C-value (function of k_s and R) is used in the SBA. Manning's *n*-value does vary with changes in the hydraulic radius; however, there is no explicit mathematical procedure to determine this. Additionally, it is also easier to visualise Chézy's absolute roughness (k_s) as it represents the sizes of irregularities on the channel beds and sides, expressed in millimetres.

Observations made during this research confirmed the difficulty in assigning Manning’s *n*-values for a river reach and the cross-sections under consideration. Hence, the combined influence of various input parameters, e.g., flow depth, turbulence, bed forms, vegetation, sedimentation and bed load, debris, obstructions, cross-section shape, geomorphological processes, and floodplain-main channel interactions needs to be considered when assigning *n*-values during high flows.

6.4.3 Site-specific method versus robust extension method

The SBA, SAM, and 1-D HEC-RAS steady flow modelling are regarded as the most appropriate indirect estimation methods to reflect the hydraulic conditions during high discharges at a specific flow-gauging site. In general, any extension method must be hydraulically correct if it is to be used as a robust approach to extend SD RCs beyond the structural limit.

The extension of a RC is significantly more affected by the site (and river reach) geometry, initial hydraulic conditions, flow regimes and level of submergence at high discharges, than the actual extension method used. Hence, there is no one-size-fits-all approach available for the extension of SD RCs in South Africa.

6.5 Recommendations for Future Research

Based on the literature reviewed and the results obtained from this research, the following aspects are recommended for future research:

(a) **Manning’s and Chézy’s roughness coefficients for flood flows:** The selection for Manning’s *n*-values for SD extension methods needs to be reviewed. Lumbroso and Gaume (2012) highlighted that flow conditions differ significantly during flash floods. The current methodology used to decide on appropriate Manning’s *n*-values, without further verifications, contributes to the potential over- or underestimation of peak discharges during flash floods. Despite the fact that Chézy’s approach is preferred (*cf.* Section 6.4.2), channel roughness may vary over a wide range, and such investigations for Chézy’s *C*-values have not been done to the same degree as for the Darcy-Weisbach’ s friction factor (Chaudhry, 2008). Hence, future studies should focus on the influence which channel shape and river reach characteristics could have on Chézy's *C*-values as highlighted in Chapter 5 (*cf.* Section 5.2).

(b) **Scale models of a river reach in flood:** A scale model of a typical river reach subjected to flooding will eliminate data variability. Such scale models will also ensure that SD extension methods can be assessed, verified and the applicability of each method will be better justified.

(c) **Hydrograph analyses for RC extension:** Oakes and Van der Spuy (2018) used hydrograph analysis to extend SD RCs. Hence, the extensive use of such hydrograph analyses should be further investigated and propagated.

(d) **Hydrodynamic models for RC extension:** Shao *et al.* (2018) conducted SD extensions using a hydrodynamic model to produce synthetic SD relationships for above-structure-limit conditions. Box cut transformations were used to calibrate the synthetic RCs with regression residuals that are typically distributed. The method includes statistical uncertainty analyses and would assist decision-makers in establishing whether the accuracy achieved is acceptable or not. This method needs to be reviewed for possible implementation in South Africa.

(e) **ANN for RC extension:** This method allows for the extension of a SD RC with no prior knowledge or information about the phenomenon of interest (Sivapragasam and Muttil, 2004). ANN enables the extension of RCs when data are limited. This method needs to be reviewed for possible implementation in South Africa.

(f) **SVM for RC extension:** Sivapragasam and Muttil (2004) demonstrated that SVM is an approximate implementation of the structural risk minimisation (SRM) principle, which stipulates that the generalisation ability of learning machines depends more on capacity concepts than merely the dimensionality of the space or the number of free parameters of the loss function. Sivapragasam and Muttil (2004) highlighted that SVM outperforms ANN when extending SD relationships, while SVM has only two input parameters compared to the tedious ANN architecture. This method can be used as a SE method and needs to be reviewed for possible implementation in South Africa.

6.6 Conclusions

The achievement of the overall research aim, assumptions and specific objectives has been discussed in this chapter. By improving the quality of all input data and assigning more appropriate roughness coefficients in conjunction with the implementation of new or alternative SD extension methods, the improved extension of SD RCs is warranted to result in consistent and acceptable results.

CHAPTER 7 : REFERENCES

Abbas, SA, Al-Aboodi, AH and Ibrahim, HT. 2020. Identification of Manning's coefficient using HEC-RAS model: Upstream Al-Amarah Barrage. *Hindawi Journal of Engineering* 20: 7. DOI: https://doi.org/10.1155/2020/6450825

Ackers, P, White, WR, Perkins, JA and Harrison, AJM. 1978. *Weirs and Flumes for Flow Measurement*. John Wiley & Sons, Chichester, UK.

Akan, AO. 2006*. Open Channel Hydraulics*. Elsevier, Oxford, UK.

Artichowicz, W and Szymkiewicz, R. 2014. Computational issues of solving the 1-D steady gradually varied flow equation. *J Hydrol Hydromech, Sciendo, Poland* 62:226–233. DOI: 10.2478/johh-2014-0031

Bennie, R, Rademeyer, PF and Van der Spuy, D. 2015. *Discharge Rating Improvement of Rating Table Touws River at Okkerskraal (J1H018)*. Report No. J1H018DT-2015.06. Department of Water and Sanitation, Pretoria, RSA.

Brezinski, C and Zaglia, M. 1991. *Extension Methods: Theory and Practice.* Elsevier, Amsterdam, Netherlands.

British Standards Institution International Organisation for Standardisation (BSI ISO). 1998. *Measurement of Liquid Flow in Open Channels: Determination of the Stage-discharge Relation*. BSI ISO 1100-2.1998. London, UK.

British Standards Institution (BSI). 1981. BSI 3680: Part 4D: *Methods of Measurement of Liquid Flow in Open Channels: Compound Gauging Structures*. British Standards Institution, London, UK.

Chadwick, AJ and Morfett, JC. 2004. *Hydraulics in Civil and Environmental Engineering.* 4th ed*.* E & FN Spon, Chapman and Hall, London, UK.

Chaudhry, MH. 2008. *Open-channel Flow*. MA Springer, Boston, USA.

Chow, VT.1959. *Open-channel Hydraulics.* McGraw-Hill Book Company, New York, USA.

CivilGeo. 2022. HEC-RAS Modelling Best Practices . [Internet]. CivilGEO, Middleton, USA. Available from: https://knowledge.civilgeo.com/knowledge-base/hec-ras-modeling-best-practices/ [Accessed: 20 July 2022].

Dymond, JR and Christian, R .1982*.* Accuracy of discharge determined from a rating curve*. Hydrological Sciences Journal* 27 (4): 493–504. DOI: 10.1080/02626668209491128

Environmental Agency United Kingdom (EA UK). 2002a. *Stage 1 – Extension of Rating Curves at Gauging Stations*. Report No. 1. Environmental Agency, Bristol, UK.

Environmental Agency United Kingdom (EA UK). 2002b. *Stage 3 – Extension of Rating Curves at Gauging Stations using 1-D Hydraulic Models*. Report No. 3. Environmental Agency, Bristol, UK.

Environmental Agency United Kingdom (EA UK). 2003. *Stage 2 – Extension of Rating Curves at Gauging Stations using simple hydraulic techniques*. Report No. 2. Environmental Agency, Bristol, UK.

Freeman, GE, Rahmeyer, WJ and Copeland, RR. 2000. *Determination of Resistance due to Shrubs and Woody Vegetation*. Report No. 25. USACE Research and Development Centre, Washington, USA.

Gericke, OJ and Smithers, JC. 2017. Direct estimation of catchment response time parameters in medium to large catchments using observed streamflow data. *Hydrological Processes* 31 (5):1125–1143. DOI: 10.1002/hyp.11102

George, J, Arcement, JR and Schneider, VR. 1989. *Guide for selecting Manning's Roughness Coefficients for Natural and Flood Plains.* [Internet]. Water Supply Paper United States Geological Survey, 2339. Department of the Interior, Denver, USA. Available from:
https://pubs.usgs.gov/wsp/2339/report.pdf. [Accessed 07 September 2020].

Goodwill, I and Sleigh, A. 2009. *Fluid Mechanics: Open-channel Hydraulics Lecture Notes*. CIVE2400 Fluid Mechanics. University of Leeds, Leeds, UK.

Hadebe, XM. 2001. *Calibration Request (H5H004).* Report No. DT5. Department of Water Affairs and Forestry, Pretoria, RSA.

Hardy, T, Panja, P and Mathias, P. 2005. *WinXSPRO: A Channel Cross-Section Analyser.* United States Department of Agriculture, Forest Service, Rocky Mountains, USA.

Hattingh, WL and Masekela, LJ. 2017*. Calibration of Gauging Site (C5H014).* Report No. DT5*.* Department of Water and Sanitation, Pretoria, RSA.

Henderson, FM. 1966*. Open-channel Flow*, MacMillan, New York, USA.

Keuris, M. 1991*. Kalibrasieverslag (K2H002-A01).* Report No. DT4*.* Department of Water Affairs and Forestry, Pretoria, RSA.

Kriel, J.P. 1963. Deurstromingskoëffisiënte vir Hoekyster – Meetdamkruine. *The Civil Engineer in South Africa* 5(10).

Lambie, JC. 1978. *Measurement of Flow: Velocity Area Methods*. Hydrometry, John Wiley & Sons, Chichester, UK.

Lang, M, Pobanz, K, Renard, B, Renouf, E and Sauquet, E. 2010. Extension of rating curves by hydraulic modelling with application to flood frequency analysis. *Hydrological Sciences Journal 5*5 (6): 883–898. DOI: 10.1080/02626667.2010.504186

Leonard, J, Mietton, M, Najib, H and Gourbesville, P. 2009. Rating curve modelling with Manning's equation to manage instability and improve extension. *Hydrological Sciences Journal* 45 (5): 739–750. DOI: 10.1080/02626660009492374

Lindner, GA and Miller, AJ. 2012. Numerical modelling of stage-discharge relationships in urban streams. *J. Hydrol. Eng.* 17: 590–596.

Lumbroso, D and Gaume, E. 2012. Reducing the uncertainty in indirect estimates of extreme flash flood discharges*. Journal of Hydrology* 414. DOI: 10.1016/j.jhydrol.2011.08.048

Maeder, C. 2015. The Road to HEC-RAS. [Internet]. CivilGEO, Middleton, USA. Available from:https://www.civilgeo.com/blog/the-road-to-HEC-RAS/3:~:text=In%201964%2C%20Bill%20Eichert%20began,of%20Engineers%20

Tulsa%20District%20office.&text=This%20step%2Dbackwater%20program%20was,like%20computer%20language%20called%20WIZ [Accessed: 07 March 2021].

Mahlangu, D. 1995. *Kalibrasieversoek (A6H035).* Report No. DT3. Department of Water Affairs and Forestry, Pretoria, RSA.

Malekabadi, JM and Kalateh, F. 2019. Gradually varied flow profile based on adaptive pattern*. ISH Journal of Hydraulic Engineering* 25 (2): 223–231. DOI: 10.1080/09715010.2017.1408035

Marriot, M. 2016*. Nalluri & Featherstone's Civil Engineering Hydraulics*. Wiley Blackwell, West Sussex, UK.

Mathole, J. 1998. *Calibration Request (C2H130)*. Report No. DT5. Department of Water Affairs and Forestry, Pretoria, RSA.

Mathole, J. 1999. *Kalibrasieversoek (X3H008).* Report No. DT5*.* Department of Water Affairs and Forestry, Pretoria, RSA.

Matji, MP. 1993. *Evaluation Report (A4H005-A01)*. Report No. DT3*.* Department of Water Affairs and Forestry, Pretoria, RSA.

Masekela, J. 2013. *Calibration of Gauging Site (A6H035).* Report No. DT3. Department of Water and Sanitation, Pretoria, RSA.

Menné, TC. 1960. *The Role of Hydrology in Planning the Development of a Country.* Hydrological Research, Technical Report No. 9, Department of Water Affairs, Pretoria, RSA.

Moglen, GE. 2015. *Fundamentals of Open-channel Flow*. Taylor & Francis Group, Florida, USA.

Muzzammil, M, Alam, J and Zakwan, M. 2018. A worksheet approach for extension of rating curve parameters. *Germany Hydrologic Modelling* 36: 525–533 DOI: 10.1007/978-981-10-5801-1_36

Nathanael, JJ, Rademeyer, PF and Van der Spuy, D. 2018. *Discharge Rating Improvement of Rating Table and High Flow Data Sand River at Exeter.* Report No. X3H008DT-2018.12*.* Department of Water and Sanitation, Pretoria, RSA.

Oakes, EGM and Van der Spuy, D. 2018. *Validation of Improved Rating Tables and Expanded Information at Gauging Weirs V1H026 and V1H058 on the Tugela River*. Report No. V1H026DT-2018.09/V1H058DT-2018.09*.* Department of Water and Sanitation, Pretoria, RSA.

National Weather Service Hydrologic Services Division (NWS-HSD). 2018*. Stage-Discharge Relationships*. [Internet]. National Weather Service, Hydrologic Services Division, USA. Available from: http://users.humboldt.edu/finneyb/nws/lesson6.html [Accessed: 21 May 2018].

Petersen-Øverleir, A and Reitan, T. 2009. Accounting for rating curve imprecision in flood frequency analysis using likelihood-based methods. *Journal of Hydrology* 366 (2009): 89–100.

Price, K. 2020. *Rating Curves Part 1*. [Internet]. Surface Water Solutions, Kelmscott, Australia. Available from: https://www.surfacewater.biz/ratingtheory/3:~:text=1-D%20Rating%20Curves%20in%20HEC%2DRAS&text=You%20can%20click%20on%20the,stage%20and%20flow%20data%20graphically [Accessed 31 August 2020].

Rademeyer, PF and Van der Spuy, D. 2014. *Discharge Rating Improvement of Rating Table and High Flow Data, Vaal River at Elandsfontein.* Report No. C2H130DT-2014.09. Department of Water and Sanitation, Pretoria, RSA.

Ramsbottom, DM and Whitlow, CD. 2003. *Extension of Rating Curves at Gauging Stations: Best Practice Guidance Manual.* Environmental Agency, Bristol, UK.

Roux M, Rademeyer, PF and Van der Spuy, D. 2015. *Discharge Rating Improvement of Rating Table Riet River at Gauging Weir C5H014*. Report No. C500-H014-2015.03. Department of Water and Sanitation, Pretoria, RSA.

Roux, M and Van der Spuy, D. 2012. *Great Brak River K2H002 Extension of Discharge Table.* Report No. K200-H002-2012.10. Department of Water and Sanitation, Pretoria, RSA.

Roux, M, Rademeyer, PF and Van der Spuy, D. 2014. *Discharge Rating Extension of Rating Table 4, Mogalakwena River at A6H035.* Report No. A600-H035-2014.02. Department of Water and Sanitation, Pretoria, RSA.

Rowley, J. 2002. Using case studies in research. *Management Research News* 25 (1):16–27. DOI: https://doi.org/10.1108/01409170210782990

South African Roads Agency Limited (SANRAL). 2013. *Drainage Manual*. 6th ed. South African Roads Agency Limited, Pretoria, RSA.

Shao, Q, Dutta, D, Karim, F and Petheram, C. 2018. A method for extending stage-discharge relationships using a hydrodynamic model and quantifying the associated uncertainty. *Journal of Hydrology* 556 (2018): 154–172.

Sivapragasam, C and Muttil, N. 2004. Discharge rating curve extension: A new approach. *Water Resources Management* 19:505–520. DOI: 10.1007/s11269-005-6811-2

Sorour, J. 1992. *Kalibrasieversoek (V1H026).* Report No. DT2. Department of Water Affairs and Forestry, Pretoria, RSA.

Thomason, C. 2019. *Hydraulic Design Manual*. [Internet]. Texas Department of Transportation, Austin, USA.
Available from: http://onlinemanuals.txdot.gov/txdotmanuals/hyd/index.htm [Accessed: 10 May 2021].

United States Army Corps of Engineers (USACE). 2016. *HEC-RAS River Analysis System User's Manual.* Hydrologic Engineering Centre, Davis, California, USA. Available from: https://www.hec.usace.army.mil/software/hec-ras/documentation/HEC-RAS%205.0%20Users%20Manual.pdf [Accessed: 11 March 2020].

United States Army Corps of Engineers (USACE). 2019. *HEC-RAS River Analysis System Release Notes Version 5.0.7.* Hydrologic Engineering Centre, Davis, California, USA. Available from: https://www.hec.usace.army.mil/software/hec-ras/documentation/HEC-RAS_5.0.7_Release_Notes.pdf [Accessed: 11 March 2020].

United States Geological Survey (USGS). 2020. *How Stream Flow is Measured.* [Internet]. United States Geology Survey, Virginia, USA. Available from: https://www.usgs.gov/special-topic/water-science-school/science/how-streamflow-measured?qt-science_center_objects=03qt-science_center_objects [Accessed: 9 October 2020].

United States Geological Survey (USGS). 2021*.* Water Watch: Customised Rating Curve Builder. [Internet]. United States Geology Survey, Virginia, USA. Available from: https://waterwatch.usgs.gov/?m=mkrc&sno=16414200 [Accessed: 8 March 2021].

Van der Spuy, D. 1999*. Interim Guidelines on Flood Surveys.* Directorate Hydrology, Flood Studies (unpublished). Department of Water Affairs and Forestry, Pretoria, RSA.

Van der Spuy, D. 2006*. Improvement of DT Gauging Weir A4H005*. Report No. A4H005DT-2006. Department of Water Affairs and Forestry, Pretoria, RSA.

Van der Spuy, D. 2022. *Personal Communication*. Department of Water and Sanitation, Pretoria, RSA.

Van Heerden, JJ, Van der Spuy, D and Le Roux, PJ. 1986. *Manual for the Planning, Design and Operation of River Gauging Stations*. Department of Water Affairs, Pretoria, RSA.

Van Wyk, N, Rademeyer, PF and Van der Spuy, D. 2015. *Discharge Rating Improvement of Rating Table Gouritz River at The Poort (J4H002)*. Report No. J4H002DT-2015.09. Department of Water and Sanitation, Pretoria, RSA.

Wessels, P. 1999. *Flow-gauging Structures in South African Streams.* Directorate Hydrology, Engineering Services. Department of Water Affairs and Forestry, Pretoria, RSA.

Wessels, P. 2001. *Flow-gauging structures in South African streams: Part 1*. Directorate-Hydrology Services. Department of Water Affairs and Forestry, Pretoria, RSA.

Wessels, P and Rooseboom, A. 2009a. Flow-gauging structures in South African rivers. Part 1: An Overview. *Water SA* 35 (1) 1–10.

Wessels, P and Rooseboom, A. 2009b. Flow-gauging structures in South African rivers. Part 2: Calibration*. Water SA* 35 (1) 11–20.

Wessels A, Rademeyer, PF and Van der Spuy, D. 2018. *Discharge Rating Improvement of Rating Table Breë River at Wolvendrift (H5H004).* Report No. H5H004DT-2018.01. Department of Water and Sanitation, Pretoria, RSA.

World Meteorological Organisation (WMO). 2008. *Guide to Hydrological Practices Volume 1: Hydrology – From Measurement to Hydrological Information.* 6th ed*.* World Meteorological Organisation, Geneva, Switzerland.

APPENDIX A: TABULATED INFORMATION AND RESULTS

Table A.1: Geometric properties at A4H005

Stage (*H*, m)	Area (*A*, m^2)	Hydraulic radius (*R*, m)
1.400	82.470	0.740
1.500	92.920	0.830
1.600	103.420	0.920
1.700	113.960	1.010
1.790	123.490	1.090

Table A.2: Geometric properties at A6H035

Stage (*H*, m)	Area (*A*, m^2)	Hydraulic radius (*R*, m)
1.320	74.740	0.630
1.330	75.940	0.600
1.340	77.160	0.610
1.350	78.390	0.620

Table A.3: Geometric properties at C2H003 (C2H130)

Stage (*H*, m)	Area (*A*, m^2)	Hydraulic radius (*R*, m)
2.2	240.76	0.95
2.3	263.76	1.04
2.4	286.78	1.13
2.5	309.83	1.22
2.6	332.9	1.31
2.7	356	1.39
2.8	379.13	1.48
2.9	402.35	1.56
2.92	406.99	1.58

Table A.4: Geometric properties at C5H014

Stage (*H*, m)	Area (*A*, m^2)	Hydraulic radius (*R*, m)
1.1	93.58	0.57
1.2	110.02	0.67
1.3	126.27	0.77
1.4	142.52	0.87
1.5	159.98	0.73
1.6	179.02	0.93
1.7	198.08	1.03
1.8	217.15	1.12
1.9	236.23	1.22
2	255.3	1.32
2.1	274.41	1.41
2.2	293.66	1.5
2.3	313.05	1.58
2.4	332.58	1.67
2.5	532.58	1.7
2.6	373.58	1.73
2.7	396.48	1.43
2.8	424	1.51
2.9	451.81	1.6
3	479.84	1.68
3.1	508.49	1.75
3.2	537.37	1.83
3.3	566.52	1.91
3.4	595.91	1.99
3.5	625.71	2.07
3.6	655.75	2.15
3.7	686.09	2.22
3.8	716.72	2.3
3.9	747.65	2.38
4	778.83	2.45

Table A.5: Geometric properties at H5H004

Stage (*H*, m)	Area (*A*, m²)	Hydraulic radius (*R*, m)
1.5	51.01	0.71
1.6	57.53	0.8
1.7	64.05	0.89
1.8	70.58	0.97
1.9	77.12	1.06
2	83.66	1.15
2.1	90.21	1.24
2.12	91.57	1.2

Table A.6: Geometric properties at J1H018

Stage (*H*, m)	Area (*A*, m²)	Hydraulic radius (*R*, m)
2.1	55.1	1.39
2.2	58.77	1.48
2.3	62.43	1.57
2.4	66.09	1.66
2.5	69.76	1.74
2.6	73.42	1.83
2.7	77.51	1.57
2.8	82.16	1.63
2.9	86.88	1.7
3	91.69	1.76
3.1	96.58	1.83

Table A.7: Geometric properties at J4H002

Stage (*H*, m)	Area (*A*, m²)	Hydraulic radius (*R*, m)
1.1	13.26	0.57
1.2	15.35	0.66
1.3	17.44	0.74
1.4	19.6	0.55

Table A.8: Geometric properties at K2H002

Stage (*H*, m)	Area (*A*, m²)	Hydraulic radius (*R*, m)
1.53	35.2	0.88
1.54	35.51	0.88
1.55	35.81	0.74

Table A.9: Geometric properties at V1H026

Stage (*H*, m)	Area (*A*, m²)	Hydraulic radius (*R*, m)
1.3	50.17	0.64
1.4	57.41	0.72
1.5	64.66	0.8
1.6	72.67	0.76
1.7	81.39	0.84
1.8	90.17	0.93
1.9	99.02	1.01
2	107.92	1.1
2.1	116.91	1.18
2.2	126	1.26
2.3	135.19	1.33
2.4	144.47	1.41
2.5	153.9	1.48
2.6	163.47	1.55
2.7	173.19	1.62
2.8	183.05	1.69
2.9	193.05	1.76
3	203.19	1.83

Stage (*H*, m)	Area (*A*, m²)	Hydraulic radius (*R*, m)
3.1	213.44	1.9
3.2	223.69	1.98
3.3	233.93	2.06
3.4	244.15	2.13
3.5	254.32	2.21
3.6	264.46	2.29
3.7	274	2.36
3.8	284.61	2.44
3.9	294.61	2.51
4	304.6	2.59
4.1	314.63	2.65
4.2	324.74	2.71
4.3	334.94	2.78
4.4	345.22	2.84
4.5	355.59	2.9
4.6	366.03	2.96
4.7	376.57	3.02
4.8	387.19	3.08
4.9	397.9	3.13
5	408.72	3.19
5.1	419.64	3.24
5.2	430.66	3.29
5.3	441.79	3.35
5.4	453.02	3.4
5.5	464.36	3.45
5.6	475.8	3.51
5.7	487.35	3.56
5.8	499	3.61
5.9	510.75	3.67
6	522.57	3.73
6.1	534.47	3.79
6.2	546.45	3.85
6.3	558.49	3.91
6.4	570.62	3.97
6.5	582.81	4.03
6.6	595.08	4.09
6.7	607.43	4.15
6.8	619.83	4.21
6.9	632.27	4.27
7	644.77	4.34
7.1	657.31	4.41
7.2	669.86	4.48
7.3	682.41	4.55
7.4	694.97	4.63
7.5	707.53	4.7
7.6	720.1	4.78
7.7	732.67	4.85
7.8	745.22	4.92

Table A.10: Geometric properties at X3H008

Stage (*H*, m)	Area (*A*, m²)	Hydraulic radius (*R*, m)
2	47.85	0.38
2.1	66.56	0.32
2.2	87.1	0.41
2.3	107.77	0.51
2.4	128.57	0.6
2.5	149.49	0.69
2.6	170.54	0.79
2.7	191.72	0.88
2.8	213.03	0.97
2.9	234.45	1.06
3	255.98	1.16
3.1	277.62	1.25
3.2	299.32	1.34
3.3	321.06	1.44
3.4	342.83	1.53
3.5	364.62	1.63
3.6	386.45	1.72

Stage (*H*, m)	Area (*A*, m²)	Hydraulic radius (*R*, m)
3.7	408.31	1.82
3.8	430.2	1.91
3.9	452.12	2.01
4	474.08	2.1
4.1	496.06	2.2
4.2	518.09	2.29
4.3	540.16	2.38
4.4	562.26	2.48
4.5	584.42	2.57
4.6	606.61	2.66
4.7	628.84	2.75
4.8	651.12	2.985
4.9	673.44	2.94
5	695.8	3.03
5.1	718.2	3.12
5.2	740.64	3.21
5.3	763.11	3.31
5.4	785.6	3.4
5.5	808.12	3.49
5.6	830.67	3.59
5.7	853.24	3.68
5.8	875.84	3.77
5.9	898.46	3.87
6	921.11	3.96
6.1	943.79	4.05
6.2	966.49	4.14
6.3	989	4.24

Table A.11: SD extension for above-structure-limit conditions at A4H005

H (m)	Discharge (m³/s)									
	SE	LE	VE-SA	VE-HRA	VE-MA	SAM-MA	SAM-CHZ	SBA-MA	SBA-CHZ	HEC-RASS (FS)
2.4	358.9	273.0	419.8	511.6	455.4	-	-	-	-	-
2.5	374.2	284.0	438.3	537.7	477.3	-	-	-	-	-
2.5	389.7	295.2	457.2	564.5	499.7	-	-	-	-	-
2.6	405.6	306.6	476.4	591.9	522.5	-	-	-	-	-
2.6	421.9	318.3	496.1	620.0	545.8	-	-	-	-	-
2.7	455.3	342.1	536.4	678.0	593.9	-	-	-	-	-
2.8	489.9	366.8	578.3	738.7	643.9	-	-	-	-	-
2.9	525.8	392.4	621.7	801.9	695.8	-	-	-	-	-
3.0	563.1	418.7	666.5	867.7	749.6	-	-	-	-	-
3.1	601.5	445.9	712.9	936.1	805.4	-	-	-	-	-
3.2	641.3	473.8	760.7	1007.0	863.0	-	-	-	-	-
3.2	655.9	484.1	778.3	1033.2	884.2	-	-	-	-	-
3.3	682.3	502.6	810.1	1080.6	922.6	-	-	-	-	-
3.4	724.6	532.2	860.9	1156.7	984.0	-	-	-	-	-
3.4	728.9	535.2	866.1	1164.4	990.3	-	-	-	-	-

Table A.12: SD extension for above-structure-limit conditions at A6H035

H (m)	Discharge (m³/s)									
	SE	LE	VE-SA	VE-HRA	VE-MA	SAM-MA	SAM-CHZ	SBA-MA	SBA-CHZ	HEC-RASS (FS)
1.4	145.6	158.0	128.0	124.6	197	-	-	-	-	-
1.5	163.6	182.4	150.4	151.6	535	-	-	-	-	-
1.6	182.1	208.7	174.4	181.3	1150	-	-	-	-	-
1.7	201.1	236.8	199.8	213.6	2044	-	-	-	-	-
1.8	220.6	266.8	248.4	226.8	3216	-	-	-	-	-
1.9	240.4	298.6	285.8	255.2	4666	-	-	-	-	-
2.0	260.4	332.4	325.8	285.1	6394	-	-	-	-	-
2.1	280.8	368.0	368.4	316.6	8400	-	-	-	-	-
2.2	301.2	405.4	413.5	349.5	10684	-	-	-	-	-
2.3	321.8	444.8	461.3	383.9	13247	-	-	-	-	-
2.4	342.4	486.1	511.6	419.8	16087	-	-	-	-	-
2.5	362.9	529.3	564.5	457.2	19206	-	-	-	-	-
2.6	383.4	574.4	620.0	496.1	22602	-	-	-	-	-

Table A.13: SD extension for above-structure-limit conditions at C2H003 (C2H130)

H (m)	Discharge (m³/s)									
	SE	LE	VE-SA	VE-HRA	VE-MA	SAM-MA	SAM-CHZ	SBA-MA	SBA-CHZ	HEC-RASS (FS)
2.3	553.5	552.2	476.0	575.6	519.0	-	-	-	-	-
2.4	618.4	615.5	558.0	651.4	599.1	-	-	-	-	-
2.5	688.1	683.1	645.8	731.4	682.9	-	-	-	-	-
2.6	762.6	754.9	739.4	815.6	770.4	-	-	-	-	-
2.7	842.1	831.2	838.6	904.0	861.6	-	-	-	-	-
2.8	926.8	911.9	943.6	996.6	956.5	-	-	-	-	-
2.9	1016.9	997.3	1054.3	1093.3	1055.2	-	-	-	-	-
3.0	1112.4	1087.3	1170.8	1194.3	1157.5	-	-	-	-	-
3.1	1213.6	1182.2	1293.0	1299.5	1263.5	-	-	-	-	-
3.2	1320.6	1281.8	1420.9	1408.9	1373.3	-	-	-	-	-
3.3	1433.5	1386.5	1554.6	1522.5	1486.7	-	-	-	-	-
3.4	1552.5	1496.1	1694.0	1640.2	1603.8	-	-	-	-	-
3.5	1677.8	1610.9	1839.1	1762.2	1724.7	-	-	-	-	-
3.6	1809.5	1730.9	1989.9	1888.4	1849.2	-	-	-	-	-
3.7	1947.8	1856.1	2146.5	2018.7	1977.5	-	-	-	-	-
3.8	2092.9	1986.7	2308.8	2153.3	2109.4	-	-	-	-	-
3.9	2244.8	2122.7	2476.9	2292.0	2245.1	-	-	-	-	-
4.0	2403.8	2264.3	2650.7	2435.0	2384.5	-	-	-	-	-

Table A.14: SD extension for above-structure-limit conditions at C5H014

H (m)	Discharge (m³/s)									
	SE	LE	VE-SA	VE-HRA	VE-MA	SAM-MA	SAM-CHZ	SBA-MA	SBA-CHZ	HEC-RASS (FS)
1.1	132.2	78.5	99.8	126.4	122.9	112.8	110.8	113.6	113.6	113.6
1.2	182.9	104.8	122.0	164.6	160.7	138.9	136.5	139.9	139.9	139.9
1.3	245.0	136.7	145.3	207.3	202.1	168.2	165.3	169.4	169.4	169.5
1.4	319.6	174.9	170.0	254.7	247.2	200.9	197.4	202.3	202.3	202.4
1.5	407.9	219.9	197.6	253.3	246.9	236.9	232.8	238.6	238.6	238.7
1.6	511.1	272.5	228.6	335.5	324.3	276.5	271.7	278.5	278.5	278.6
1.7	630.2	333.3	261.3	400.1	384.0	319.7	314.1	322.0	322.0	322.1
1.8	766.3	403.0	295.6	467.0	444.9	366.6	360.2	369.2	369.2	369.3
1.9	920.8	482.3	331.5	542.4	512.3	420.0	412.7	423.0	423.0	423.1
2.0	1094.6	571.9	369.1	623.3	583.4	479.8	471.5	483.3	483.3	483.4
2.1	1288.9	672.5	408.2	705.8	655.1	545.8	536.3	549.7	549.7	549.8
2.2	1504.9	784.9	449.3	793.8	730.5	617.8	607.1	622.3	622.3	622.4
2.3	1743.8	909.7	492.1	882.6	806.0	696.0	683.9	701.0	701.0	701.1
2.4	2006.5	1047.9	536.8	981.2	888.4	780.3	766.7	785.9	785.9	786.0
2.5	2294.4	1200.0	882.1	1594.5	1439.1	870.7	855.5	876.9	876.9	877.1
2.6	2608.5	1367.0	634.5	1134.8	1021.6	967.2	950.4	974.1	974.1	974.3
2.7	2950.0	1549.6	690.1	1031.4	955.0	1069.7	1051.2	1077.4	1077.4	1077.6
2.8	3320.0	1748.6	755.8	1152.3	1058.9	1178.4	1158.0	1186.9	1186.9	1187.1
2.9	3719.7	1964.7	824.4	1287.0	1172.7	1293.3	1270.9	1302.6	1302.6	1302.9
3.0	4150.1	2198.9	895.8	1422.6	1286.5	1414.3	1389.7	1424.4	1424.4	1424.7
3.1	4612.6	2451.9	970.7	1559.3	1400.8	1541.3	1514.6	1552.4	1552.4	1552.7
3.2	5108.1	2724.6	1048.5	1710.4	1525.1	1674.5	1645.4	1686.5	1686.5	1686.8
3.3	5637.8	3017.8	1129.2	1869.1	1654.2	1813.8	1782.3	1826.8	1826.8	1827.2
3.4	6202.9	3332.4	1212.9	2035.4	1788.2	1959.1	1925.1	1973.2	1973.2	1973.6
3.5	6804.5	3669.2	1299.9	2209.9	1927.6	2110.7	2074.0	2125.8	2125.8	2126.2
3.6	7443.7	4029.2	1390.0	2392.3	2071.8	2268.2	2228.9	2284.5	2284.5	2285.0
3.7	8121.8	4413.1	1483.2	2572.8	2214.4	2432.0	2389.7	2449.4	2449.4	2449.9
3.8	8839.8	4821.8	1579.6	2771.1	2368.4	2601.8	2556.7	2620.5	2620.5	2621.0
3.9	9598.9	5256.3	1679.3	2977.6	2527.5	2777.8	2729.6	2797.7	2797.7	2798.3
4.0	10400.2	5717.5	1782.1	3181.1	2684.2	2959.8	2908.4	2981.0	2981.0	2981.6
4.1	11244.8	6206.2	3431.5	1858.0	2878.0	3147.9	3093.3	3170.5	3170.5	3171.1
4.2	12134.0	6723.3	3689.5	1959.6	3075.0	3342.2	3284.2	3366.2	3366.2	3366.9
4.3	13068.8	7269.9	3964.0	2064.1	3283.7	3542.6	3481.1	3568.0	3568.0	3568.7
4.4	14050.4	7846.8	4255.9	2171.3	3504.5	3749.1	3684.0	3776.0	3776.0	3776.7
4.5	15079.9	8454.9	4565.7	2281.4	3737.9	3961.7	3892.9	3990.1	3990.1	3990.9
4.6	16158.5	9095.3	4894.2	2394.2	3984.4	4180.4	4107.8	4210.4	4210.4	4211.2
4.7	17287.3	9768.8	5242.0	2509.9	4244.4	4405.2	4328.7	4436.8	4436.8	4437.7
4.8	18467.4	10476.4	5609.8	2628.3	4518.5	4636.1	4555.7	4669.4	4669.4	4670.3
4.9	19700.1	11219.0	5998.3	2749.6	4807.0	4873.2	4788.6	4908.2	4908.2	4909.2
5.0	20855.3	11918.2	6366.2	2861.1	5079.5	5091.8	5003.4	5128.3	5128.3	5129.3

Table A.15: SD extension for above-structure-limit conditions at H5H004

H (m)	Discharge (m³/s)									
	SE	**LE**	**VE-SA**	**VE-HRA**	**VE-MA**	**SAM-MA**	**SAM-CHZ**	**SBA-MA**	**SBA-CHZ**	**HEC-RAS (FS)**
1.5	282.0	117.3	102.0	82.7	81.5	95.2	96.0	90.6	90.6	90.8
1.6	332.6	140.5	121.4	101.7	99.3	104.9	105.9	99.9	99.9	100.1
1.7	388.2	166.5	142.3	122.6	118.4	114.7	115.7	109.1	109.1	109.4
1.8	448.9	195.3	164.7	144.4	138.0	124.4	125.5	118.4	118.4	118.7
1.9	515.0	227.2	188.6	169.1	159.7	134.2	135.4	127.7	127.7	128.0
2.0	586.5	262.3	213.9	195.7	182.8	147.0	148.3	139.9	139.9	140.2
2.1	663.7	300.6	240.8	224.2	207.1	161.6	163.0	153.8	153.8	154.2
2.2	746.7	342.4	248.2	269.2	223.7	177.5	179.1	169.0	169.0	169.4
2.3	835.7	387.7	277.2	299.0	244.4	194.9	196.6	185.5	185.5	185.9
2.4	930.8	436.7	307.5	330.3	265.1	213.6	215.5	203.3	203.3	203.8
2.5	1032.2	489.5	339.1	363.1	285.9	234.0	236.1	222.7	222.7	223.3
2.6	1140.1	546.2	372.1	397.4	306.6	256.1	258.3	243.7	243.7	244.3
2.7	1254.7	607.0	406.4	433.1	327.3	280.0	282.4	266.5	266.5	267.1
2.8	1376.1	672.0	442.0	470.4	348.1	305.8	308.5	291.1	291.1	291.8
2.9	1504.5	741.3	479.0	509.1	368.8	333.7	336.7	317.6	317.6	318.4
3.0	1640.0	815.0	517.2	549.3	389.5	352.2	355.3	335.2	335.2	336.0
3.1	1782.9	893.3	556.8	591.0	410.3	367.5	370.7	349.7	349.7	350.6
3.2	1933.3	976.2	597.8	634.2	431.0	383.2	386.6	364.7	364.7	365.6
3.3	2091.3	1063.9	640.0	678.9	451.7	399.4	402.9	380.1	380.1	381.0
3.4	2257.2	1156.6	683.6	725.1	472.4	416.0	419.7	395.9	395.9	396.9
3.5	2431.0	1254.2	728.4	772.7	493.2	433.1	436.9	412.2	412.2	413.2
3.6	2613.1	1357.0	774.6	821.8	513.9	450.6	454.6	428.9	428.9	429.9
3.7	2803.4	1465.1	822.2	872.4	534.6	468.6	472.8	446.0	446.0	447.1
3.8	3002.3	1578.5	871.0	924.5	555.4	487.1	491.4	463.6	463.6	464.7
3.9	3209.8	1697.4	921.2	978.1	576.1	506.0	510.5	481.6	481.6	482.8
4.0	3426.2	1822.0	972.7	1033.2	596.8	525.5	530.1	500.1	500.1	501.4
4.1	3651.6	1952.2	1025.5	1089.7	617.6	545.4	550.2	519.1	519.1	520.4
4.2	3886.1	2088.3	1079.7	1147.8	638.3	565.9	570.9	538.6	538.6	539.9
4.3	4130.0	2230.3	1135.2	1207.3	659.0	586.8	592.0	558.5	558.5	559.8
4.4	4383.4	2378.4	1192.0	1268.3	679.8	608.2	613.6	578.9	578.9	580.3
4.5	4646.5	2532.7	1250.1	1330.8	700.5	630.2	635.8	599.8	599.8	601.2
4.6	4919.4	2693.2	1309.5	1394.8	721.2	652.7	658.5	621.2	621.2	622.7
4.7	5202.4	2860.2	1370.3	1460.2	741.9	675.7	681.7	643.1	643.1	644.7
4.8	5495.5	3033.6	1432.4	1527.2	762.7	688.7	694.8	655.5	655.5	657.1
4.9	5799.0	3213.7	1495.8	1595.6	783.4	723.3	729.7	688.4	688.4	690.1
5.0	6113.0	3400.5	1560.5	1665.5	804.1	748.0	754.6	711.9	711.9	713.6
5.1	6437.7	3594.1	1626.6	1736.9	824.9	773.1	780.0	735.8	735.8	737.6
5.2	6773.2	3794.7	1694.0	1809.8	845.6	798.9	806.0	760.3	760.3	762.2
5.3	7119.8	4002.3	1762.7	1884.2	866.3	825.2	832.5	785.4	785.4	787.3
5.4	7477.5	4217.0	1832.7	1960.0	887.1	852.1	859.6	811.0	811.0	812.9
5.5	7846.7	4439.1	1904.1	2037.3	907.8	878.1	885.9	835.7	835.7	837.8
5.6	8227.3	4668.5	1976.8	2116.2	928.5	905.6	913.6	861.9	861.9	864.0
5.7	8619.6	4905.3	2050.8	2196.5	949.3	935.3	943.6	890.1	890.1	892.3
5.8	9023.8	5149.8	2126.1	2278.3	970.0	967.3	975.8	920.6	920.6	922.8
5.9	9440.1	5402.0	2202.8	2361.5	990.7	1001.5	1010.4	953.2	953.2	955.5
6.0	9868.5	5661.9	2280.7	2446.3	1011.5	1038.0	1047.2	988.0	988.0	990.4
6.1	10309.3	5929.8	2360.0	2532.6	1032.2	1076.9	1086.4	1024.9	1024.9	1027.4
6.2	10762.6	6205.6	2440.6	2620.3	1052.9	1117.9	1127.8	1064.0	1064.0	1066.6
6.3	11228.7	6489.6	2522.6	2709.5	1073.6	1161.2	1171.5	1105.2	1105.2	1107.9
6.4	11707.6	6781.7	2605.9	2800.2	1094.4	1206.8	1217.5	1148.6	1148.6	1151.4
6.5	12199.5	7082.2	2690.4	2892.4	1115.1	1254.7	1265.9	1194.2	1194.2	1197.1
6.6	12704.7	7391.2	2776.4	2986.1	1135.8	1304.9	1316.4	1241.9	1241.9	1244.9
6.7	13223.2	7708.6	2863.6	3081.2	1156.6	1357.3	1369.3	1291.8	1291.8	1295.0
6.9	14301.1	8369.5	3042.0	3276.0	1177.3	1468.9	1481.9	1398.0	1398.0	1347.1
7.0	14860.7	8713.1	3133.3	3375.6	1198.0	1528.1	1541.7	1454.4	1454.4	1401.4
7.1	15434.5	9065.6	3225.8	3476.7	1218.8	1589.6	1603.7	1512.9	1512.9	1458.0
7.2	16022.4	9427.2	3319.6	3579.3	1239.5	1653.4	1668.0	1573.6	1573.6	1516.6
7.3	16624.7	9798.0	3414.8	3683.3	1260.2	1719.5	1734.7	1636.5	1636.5	1577.5
7.4	17241.6	10177.9	3511.3	3788.9	1281.0	1787.8	1803.6	1701.5	1701.5	1640.5
7.5	17873.2	10567.2	3609.1	3895.9	1301.7	1858.3	1874.7	1768.6	1768.6	1705.7
7.6	18519.6	10966.0	3708.3	4004.4	1322.4	1931.2	1948.3	1838.0	1838.0	1772.9
7.7	19181.2	11374.2	3808.8	4114.4	1343.1	2006.3	2024.1	1909.5	1909.5	1842.5
7.8	19857.9	11792.2	3910.6	4225.9	1363.9	2083.6	2102.1	1983.1	1983.1	1914.2
7.9	20550.1	12219.8	4013.7	4338.9	1384.6	2163.3	2182.4	2058.9	2058.9	1988.0
8	21257.8	12657.3	4118.1	4453.4	1405.3	2245.2	2265.1	2136.9	2136.9	2063.9

Table A.16: SD extension for above-structure-limit conditions at J1H018

H (m)	Discharge (m³/s)									
	SE	LE	VE-SA	VE-HRA	VE-MA	SAM-MA	SAM-CHZ	SBA-MA	SBA-CHZ	HEC-RAS (FS)
2.1	146.3	159.4	145.7	151.1	147.3	133.5	135.5	142.8	142.8	150.3
2.3	181.2	203.9	177.7	187.0	163.5	156.8	159.2	167.7	167.7	176.5
2.5	227.0	255.5	212.6	225.7	180.4	180.6	183.3	193.1	193.1	203.2
2.6	256.3	284.1	231.1	246.8	198.0	192.8	195.7	206.2	206.2	217.0
2.7	291.4	314.6	251.8	232.2	215.4	205.4	208.5	219.6	219.6	231.1
2.8	334.0	347.1	275.2	253.0	234.3	218.4	221.6	233.5	233.5	245.7
2.9	385.8	381.7	299.7	276.1	223.4	231.8	235.3	247.9	247.9	260.9
3.0	448.8	418.3	325.5	299.2	242.6	245.8	249.5	262.9	262.9	276.6
3.1	525.6	457.1	352.6	324.6	263.6	260.4	264.4	278.5	278.5	293.1
3.2	618.7	498.1	333.6	380.5	284.6	275.7	279.9	294.9	294.9	310.3
3.3	731.4	541.3	351.6	410.3	307.4	291.8	296.2	312.0	312.0	328.4
3.4	867.2	586.8	370.0	441.4	353.9	308.7	313.3	330.1	330.1	347.4
3.5	1029.8	634.6	388.6	474.0	416.1	326.5	331.4	349.1	349.1	367.4
3.6	1223.8	684.9	407.6	508.0	502.8	345.2	350.4	369.2	369.2	388.5
3.7	1453.8	737.5	426.9	543.5	620.2	365.0	370.5	390.3	390.3	410.7
3.8	1725.3	792.7	446.4	580.3	775.4	385.9	391.7	412.7	412.7	434.2
3.9	2044.1	850.4	466.4	618.6	976.1	407.9	414.1	436.3	436.3	459.1
4.0	2416.6	910.6	486.6	658.3	1230.5	431.3	437.7	461.2	461.2	485.3
4.1	2849.8	973.5	507.1	699.4	1547.7	455.9	462.7	487.5	487.5	513.0
4.2	3351.3	1039.0	527.9	741.9	1937.4	481.9	489.2	515.4	515.4	542.3
4.3	3929.4	1107.3	549.1	785.9	2409.9	509.4	517.0	544.7	544.7	573.2
4.4	4593.1	1178.3	570.6	831.3	2976.2	538.4	546.5	575.8	575.8	605.9
4.5	5352.2	1252.1	592.4	878.1	3648.0	569.0	577.6	608.5	608.5	640.3
4.6	6216.9	1328.8	614.5	926.3	4437.8	601.3	610.3	643.0	643.0	676.7
4.7	7198.5	1408.4	636.9	975.9	5358.4	635.3	644.9	679.4	679.4	714.9
4.8	8309.2	1490.9	659.6	1026.9	6423.7	671.1	681.2	717.7	717.7	755.3
4.9	9561.8	1576.4	682.7	1079.4	7647.9	708.9	719.5	758.1	758.1	797.7
5.0	10970.1	1664.9	706.0	1133.3	9046.2	748.5	759.8	800.5	800.5	842.3
5.1	12548.9	1756.5	729.7	1188.6	10634.3	790.2	802.1	845.0	845.0	889.2
5.2	14313.9	1851.2	753.7	1245.4	12428.5	834.0	846.5	891.9	891.9	938.5
5.3	16281.8	1949.0	778.0	1303.5	14445.9	879.9	893.1	941.0	941.0	990.2
5.4	18470.3	2050.1	802.6	1363.1	16704.2	928.1	942.0	992.5	992.5	1044.4
5.5	20898.4	2154.3	827.5	1424.1	19221.9	978.6	993.3	1046.5	1046.5	1101.2
5.6	23586.0	2261.9	852.8	1486.5	22017.9	1031.4	1046.9	1103.0	1103.0	1160.7
5.7	26554.3	2372.8	878.3	1550.3	25112.1	1086.7	1103.0	1162.1	1162.1	1222.9
5.8	29825.7	2487.1	904.2	1615.6	28524.9	1144.5	1161.7	1223.9	1223.9	1287.9
5.9	33423.7	2604.7	930.4	1682.3	32277.2	1204.9	1223.0	1288.5	1288.5	1355.9
6.0	37373.4	2725.8	956.9	1750.3	36391.0	1249.2	1268.0	1335.9	1335.9	1405.8
6.1	41700.9	2850.4	983.7	1819.9	40888.5	1333.6	1353.7	1426.2	1426.2	1500.8
6.2	46434.0	2978.6	1010.8	1890.8	45793.0	1402.2	1423.3	1499.5	1499.5	1577.9
6.3	51601.6	3110.3	1038.3	1963.1	51128.1	1473.6	1495.8	1575.9	1575.9	1658.3
6.4	57234.4	3245.6	1066.0	2036.9	56918.4	1548.0	1571.2	1655.4	1655.4	1742.0
6.5	63364.5	3384.5	1094.1	2112.1	63188.8	1625.4	1649.8	1738.2	1738.2	1829.1
6.6	70025.4	3527.2	1122.5	2188.7	69965.2	1705.8	1731.5	1824.2	1824.2	1919.6
6.7	77252.5	3673.6	1151.2	2266.8	77274.1	1789.4	1816.3	1913.6	1913.6	2013.7
6.8	85082.7	3823.7	1180.2	2346.2	85142.5	1876.2	1904.4	2006.4	2006.4	2111.3
6.9	93554.6	3977.7	1209.5	2427.1	93598.3	1966.2	1995.8	2102.7	2102.7	2212.7
7.0	102708.7	4135.5	1239.2	2509.4	102669.9	2059.8	2090.7	2202.7	2202.7	2317.9

Table A.17: SD extension for above-structure-limit conditions at J4H002

H (m)	Discharge (m³/s)									
	SE	LE	VE-SA	VE-HRA	VE-MA	SAM-MA	SAM-CHZ	SBA-MA	SBA-CHZ	HEC-RAS (FS)
1.3	0.7	0.8	0.7	0.3	0.5	0.8	0.7	0.7	0.7	0.7
1.4	1.0	1.1	1.1	0.4	0.6	1.1	1.1	1.1	1.1	1.1
1.5	1.4	1.6	1.5	0.5	0.6	1.6	1.5	1.5	1.5	1.5
1.6	1.9	2.2	2.1	0.6	0.7	2.2	2.1	2.1	2.1	2.1
1.7	2.5	3.0	2.9	0.7	0.7	2.9	2.9	2.9	2.9	2.9
1.8	3.3	4.0	3.9	0.8	0.7	3.9	3.9	3.9	3.9	3.9
1.9	4.2	5.3	5.1	0.9	0.8	5.2	5.1	5.1	5.1	5.1
2.0	5.3	6.9	6.6	1.1	0.8	6.7	6.6	6.6	6.6	6.6
2.1	6.6	8.9	8.5	1.2	0.9	8.6	8.5	8.5	8.5	8.5
2.2	8.2	11.2	10.7	1.3	0.9	10.9	10.7	10.7	10.7	10.7
2.3	10.0	14.1	13.4	1.5	0.9	13.6	13.4	13.4	13.4	13.4
2.4	12.1	17.6	16.7	1.6	1.0	16.9	16.7	16.7	16.7	16.7
2.5	14.5	21.6	20.5	1.8	1.0	20.8	20.5	20.5	20.5	20.5
2.6	17.2	26.4	25.0	2.0	1.1	25.4	25.0	25.0	25.0	25.1
2.7	20.3	32.1	30.3	2.2	1.1	30.8	30.3	30.3	30.3	30.4
2.8	23.9	38.7	36.5	2.4	1.1	37.0	36.5	36.5	36.5	36.5
2.9	27.8	46.3	43.6	2.6	1.2	44.2	43.6	43.6	43.6	43.6
3.0	32.3	55.0	51.8	2.8	1.2	52.5	51.8	51.8	51.8	51.8
3.1	37.2	65.1	61.2	3.0	1.3	62.0	61.1	61.2	61.2	61.2
3.2	42.7	76.6	71.9	3.2	1.3	72.9	71.8	71.9	71.9	72.0
3.3	48.8	89.7	84.1	3.5	1.3	85.2	84.0	84.1	84.1	84.1
3.4	55.6	104.5	97.8	3.7	1.4	99.2	97.7	97.8	97.8	97.9
3.5	63.0	121.2	113.4	4.0	1.4	114.9	113.2	113.4	113.4	113.5
3.6	71.1	140.0	130.8	4.2	1.5	132.6	130.7	130.8	130.8	130.9
3.7	79.9	161.1	150.3	4.5	1.5	152.4	150.2	150.3	150.3	150.5
3.8	89.6	184.6	172.1	4.8	1.5	174.5	172.0	172.1	172.1	172.3
3.9	100.2	210.9	196.4	5.1	1.6	199.1	196.2	196.4	196.4	196.6
4.0	111.6	240.1	223.4	5.4	1.6	226.5	223.2	223.4	223.4	223.6
4.1	124.0	272.5	253.2	5.7	1.7	256.7	253.0	253.2	253.2	253.4
4.2	137.4	308.2	286.2	6.0	1.7	290.2	285.9	286.2	286.2	286.4
4.3	151.9	347.7	322.5	6.3	1.7	327.0	322.2	322.5	322.5	322.8
4.4	167.5	391.2	362.5	6.7	1.8	367.5	362.1	362.5	362.5	362.8
4.5	184.2	438.9	406.3	7.0	1.8	412.0	405.9	406.3	406.3	406.7
4.6	202.2	491.2	454.3	7.3	1.9	460.6	453.8	454.3	454.3	454.7
4.7	221.4	548.3	492.6	7.7	1.9	499.4	492.1	492.6	492.6	493.0
4.8	242.0	610.8	533.9	8.1	1.9	541.3	533.4	533.9	533.9	534.3
4.9	264.0	678.8	577.4	8.4	2.0	585.4	576.8	577.4	577.4	577.9
5.0	287.5	752.8	623.1	8.8	2.0	631.7	622.5	623.1	623.1	623.6
5.1	312.5	833.1	671.0	9.2	2.1	680.3	670.3	671.0	671.0	671.5
5.2	339.1	920.2	721.0	9.6	2.1	731.0	720.3	721.0	721.0	721.6
5.3	367.4	1014.5	773.3	10.0	2.2	784.0	772.5	773.3	773.3	773.9
5.4	397.4	1116.4	827.8	10.4	2.2	839.2	826.9	827.8	827.8	828.4
5.5	429.2	1226.4	884.4	10.8	2.2	896.7	883.5	884.4	884.4	885.1
5.6	462.9	1344.9	943.3	11.3	2.3	956.4	942.3	943.3	943.3	944.0
5.7	498.5	1472.5	1004.3	11.7	2.3	1018.2	1003.3	1004.3	1004.3	1005.1
5.8	536.2	1609.7	1067.5	12.2	2.4	1082.3	1066.4	1067.5	1067.5	1068.4
5.9	575.9	1756.9	1133.0	12.6	2.4	1148.7	1131.9	1133.0	1133.0	1133.9
6.0	617.8	1914.9	1200.6	13.1	2.4	1217.2	1199.4	1200.6	1200.6	1201.6
6.1	662.0	2084.0	1270.4	13.6	2.5	1288.0	1269.1	1270.4	1270.4	1271.4
6.2	708.5	2265.0	1342.4	14.0	2.5	1361.0	1341.0	1342.4	1342.4	1343.5
6.3	757.3	2458.3	1416.6	14.5	2.6	1436.2	1415.2	1416.6	1416.6	1417.7
6.4	808.7	2664.8	1493.0	15.0	2.6	1513.7	1491.5	1493.0	1493.0	1494.2
6.5	862.7	2885.0	1571.6	15.5	2.6	1593.4	1570.0	1571.6	1571.6	1572.9
6.6	919.3	3119.6	1652.3	16.0	2.7	1675.2	1650.6	1652.3	1652.3	1653.6
6.7	978.6	3369.4	1735.3	16.6	2.7	1759.4	1733.6	1735.3	1735.3	1736.7
6.8	1040.8	3634.9	1820.4	17.1	2.8	1845.6	1818.6	1820.4	1820.4	1821.9
6.9	1105.9	3917.1	1907.8	17.6	2.8	1934.3	1905.9	1907.8	1907.8	1909.3
7.0	1174.0	4216.6	1997.3	18.2	2.8	2025.0	1995.3	1997.3	1997.3	1998.9
7.1	1245.2	4534.3	2089.1	18.7	2.9	2118.1	2087.0	2089.1	2089.1	2090.8
7.2	1319.6	4871.0	2183.0	19.3	2.9	2213.3	2180.8	2183.0	2183.0	2184.7
7.3	1397.3	5227.5	2279.1	19.9	3.0	2310.7	2276.8	2279.1	2279.1	2280.9
7.4	1478.3	5604.7	2377.4	20.5	2.8	2410.4	2375.0	2377.4	2377.4	2379.3
7.5	1562.9	6003.5	2477.9	21.1	2.8	2512.3	2475.4	2477.9	2477.9	2479.9
7.6	1651.0	6424.8	2580.6	21.7	2.9	2616.4	2578.0	2580.6	2580.6	2582.7
7.7	1742.8	6869.6	2685.5	22.3	2.9	2722.7	2682.8	2685.5	2685.5	2687.6
7.79	1828.6	7290.8	2781.8	22.8	3.0	2820.4	2779.0	2781.8	2781.8	2784.0

Table A.18: SD extension for above-structure-limit conditions at K2H002

H (m)	Discharge (m³/s)									
	SE	LE	VE-SA	VE-HRA	VE-MA	SAM-MA	SAM-CHZ	SBA-MA	SBA-CHZ	HEC-RAS (FS)
1.6	61.4	67.7	65.7	61.7	59.6	-	-	-	-	-
1.7	68.0	75.9	73.3	66.8	64.3	-	-	-	-	-
1.8	74.9	84.5	80.9	71.9	69.0	-	-	-	-	-
1.9	82.1	93.6	88.5	77.1	73.8	-	-	-	-	-
2.0	89.7	103.0	96.1	82.2	78.5	-	-	-	-	-
2.1	97.5	112.9	103.7	87.3	83.2	-	-	-	-	-
2.2	105.7	123.2	111.3	92.4	87.9	-	-	-	-	-
2.3	114.2	134.0	118.9	97.5	92.7	-	-	-	-	-
2.4	123.0	145.1	126.5	102.7	97.4	-	-	-	-	-
2.5	132.1	156.7	134.2	107.8	102.1	-	-	-	-	-
2.6	141.5	168.7	141.8	112.9	106.8	-	-	-	-	-
2.7	151.2	181.1	149.4	118.0	111.6	-	-	-	-	-
2.9	171.6	207.1	164.6	128.3	116.3	-	-	-	-	-
3	182.3	220.8	172.2	133.4	121.0	-	-	-	-	-
3.1	193.3	234.8	179.8	138.5	125.7	-	-	-	-	-
3.2	204.6	249.2	187.4	143.6	130.5	-	-	-	-	-
3.3	216.2	264.1	195.0	148.7	135.2	-	-	-	-	-
3.4	228.1	279.3	202.6	153.9	139.9	-	-	-	-	-
3.5	240.3	294.9	210.3	159.0	144.7	-	-	-	-	-
3.6	252.9	311.0	217.9	164.1	149.4	-	-	-	-	-
3.7	265.7	327.4	225.5	169.2	154.1	-	-	-	-	-
3.8	278.9	344.2	233.1	174.3	158.8	-	-	-	-	-
3.9	292.4	361.4	240.7	179.4	163.6	-	-	-	-	-
4	306.2	379.1	248.3	184.6	168.3	-	-	-	-	-
4.1	320.3	397.1	255.9	189.7	173.0	-	-	-	-	-
4.2	334.7	415.5	263.5	194.8	177.7	-	-	-	-	-
4.3	349.4	434.3	271.1	199.9	182.5	-	-	-	-	-
4.4	364.5	453.4	278.7	205.0	187.2	-	-	-	-	-
4.5	379.8	473.0	286.4	210.2	191.9	-	-	-	-	-
4.59	393.9	490.9	293.2	214.8	196.6	-	-	-	-	-

Table A.19: SD extension for above-structure-limit conditions at V1H026

H (m)	Discharge (m³/s)									
	SE	LE	VE-SA	VE-HRA	VE-MA	SAM-MA	SAM-CHZ	SBA-MA	SBA-CHZ	HEC-RAS (FS)
1.3	119.1	111.5	154.9	141.3	136.5	-	-	-	-	-
1.5	165.7	160.6	225.4	214.2	167.7	-	-	-	-	-
1.7	220.1	220.9	316.1	279.7	201.6	-	-	-	-	-
1.9	282.5	293.4	424.0	392.5	218.5	-	-	-	-	-
2.1	352.9	378.7	547.1	525.0	260.6	-	-	-	-	-
2.3	431.6	477.6	686.4	670.0	308.0	-	-	-	-	-
2.5	518.5	590.7	842.7	834.2	356.6	-	-	-	-	-
2.6	565.1	652.9	927.6	921.6	410.6	-	-	-	-	-
2.7	613.8	718.8	1017.3	1014.0	465.4	-	-	-	-	-
2.8	664.6	788.7	1111.6	1111.4	523.4	-	-	-	-	-
2.9	717.5	862.5	1210.8	1214.0	581.6	-	-	-	-	-
3	772.7	940.4	1314.8	1321.9	645.6	-	-	-	-	-
3.1	829.9	1022.4	1423.6	1434.9	709.8	-	-	-	-	-
3.2	889.4	1108.6	1536.5	1559.3	777.1	-	-	-	-	-
3.3	951.0	1199.1	1653.4	1688.6	847.4	-	-	-	-	-
3.4	1014.8	1294.0	1774.2	1815.4	920.8	-	-	-	-	-
3.5	1080.8	1393.2	1898.7	1954.1	997.3	-	-	-	-	-
3.6	1149.1	1497.0	2027.0	2097.6	1077.0	-	-	-	-	-
3.7	1219.5	1605.4	2154.7	2232.7	1159.6	-	-	-	-	-
3.8	1292.3	1718.3	2294.7	2389.7	1248.7	-	-	-	-	-
3.9	1367.3	1836.0	2434.0	2537.6	1340.5	-	-	-	-	-
4	1444.5	1958.5	2577.2	2699.2	1430.2	-	-	-	-	-
4.1	1524.1	2085.7	2724.6	2846.6	1526.5	-	-	-	-	-
4.2	1606.0	2217.9	2876.8	2998.5	1625.1	-	-	-	-	-
4.3	1690.1	2355.1	3033.8	3165.3	1717.6	-	-	-	-	-
4.4	1776.6	2497.3	3195.6	3326.7	1823.9	-	-	-	-	-
4.5	1865.4	2644.6	3362.4	3492.8	1923.6	-	-	-	-	-
4.6	1956.6	2797.0	3534.0	3663.4	2030.6	-	-	-	-	-
4.7	2050.2	2954.7	3710.7	3838.9	2129.5	-	-	-	-	-

Table A.20: SD extension for above-structure-limit conditions at X3H008

H **(m)**	**Discharge (m³/s)**									
	SE	**LE**	**VE-SA**	**VE-HRA**	**VE-MA**	**SAM-MA**	**SAM-CHZ**	**SBA-MA**	**SBA-CHZ**	**HEC-RAS (FS)**
2	77.8	69.3	100.5	71.7	65.9	83.4	87.3	84.7	84.7	84.8
2.1	86.6	76.7	143.3	93.8	81.6	106.0	110.9	107.6	107.6	107.7
2.2	96.0	84.6	192.1	134.5	125.4	134.9	141.2	137.0	137.0	137.1
2.3	105.8	92.8	243.4	182.4	179.0	169.8	177.6	172.4	172.4	172.5
2.4	116.2	101.4	297.1	234.9	237.7	210.6	220.3	213.8	213.8	214.0
2.5	127.0	110.4	353.4	293.2	303.1	257.3	269.1	261.2	261.2	261.4
2.6	138.2	119.8	412.1	359.9	378.2	310.5	324.8	315.2	315.2	315.5
2.7	150.0	129.6	473.4	430.3	456.7	366.5	383.4	372.1	372.1	372.4
2.8	162.3	139.8	537.2	506.7	541.3	422.6	442.1	429.1	429.1	429.5
2.9	175.0	150.4	603.6	589.1	631.9	481.5	503.7	488.9	488.9	489.3
3	188.2	161.4	672.5	681.4	732.5	544.5	569.6	552.8	552.8	553.3
3.1	201.9	172.9	744.0	776.3	834.9	609.4	637.5	618.7	618.7	619.2
3.2	216.1	184.7	818.0	877.1	942.7	677.6	708.9	688.0	688.0	688.6
3.3	230.8	196.9	894.3	988.7	1060.8	748.9	783.4	760.3	760.3	761.0
3.4	246.0	209.6	973.0	1101.7	1179.3	823.4	861.4	836.0	836.0	836.7
3.5	261.6	222.6	1054.1	1226.1	1308.3	900.2	941.7	914.0	914.0	914.8
3.6	277.7	236.1	1137.5	1351.4	1437.1	980.0	1025.2	995.0	995.0	995.9
3.7	294.3	250.0	1223.4	1488.7	1576.6	1063.7	1112.8	1080.0	1080.0	1080.9
3.8	311.4	264.3	1311.7	1626.3	1715.3	1149.4	1202.4	1167.0	1167.0	1168.0
3.9	329.0	279.0	1402.3	1776.6	1865.0	1239.1	1296.2	1258.0	1258.0	1259.1
4	347.1	294.1	1495.4	1926.5	2013.5	1330.7	1392.0	1351.0	1351.0	1352.2
4.1	365.6	309.6	1590.9	2089.8	2173.1	1426.2	1491.9	1448.0	1448.0	1449.3
4.2	384.6	325.6	1688.9	2252.1	2331.1	1524.7	1595.0	1548.0	1548.0	1549.3
4.3	404.2	342.0	1789.3	2420.5	2493.6	1625.2	1700.1	1650.0	1650.0	1651.4
4.4	424.2	358.8	1892.1	2603.4	2667.7	1729.6	1809.3	1756.0	1756.0	1757.5
4.5	444.6	376.0	1997.5	2784.4	2839.5	1836.9	1921.6	1865.0	1865.0	1866.6
4.6	465.6	393.6	2105.3	2971.6	3015.7	1946.3	2036.0	1976.0	1976.0	1977.7
4.7	487.1	411.6	2215.6	3164.8	3196.2	2059.5	2154.5	2091.0	2091.0	2092.8
4.8	509.0	430.1	2328.5	3505.1	3495.4	2175.7	2276.0	2209.0	2209.0	2210.9
4.9	531.4	449.0	2443.8	3580.1	3578.7	2294.9	2400.7	2330.0	2330.0	2332.0
5	554.3	468.3	2561.6	3792.3	3772.6	2416.1	2527.4	2453.0	2453.0	2455.1
5.1	577.7	488.1	2681.9	4010.8	3970.7	2541.2	2658.3	2580.0	2580.0	2582.2
5.2	601.5	508.2	2804.7	4235.5	4173.1	2669.2	2792.2	2710.0	2710.0	2712.4
5.3	625.9	528.8	2930.1	4477.8	4388.5	2800.2	2929.3	2843.0	2843.0	2845.5
5.4	650.7	549.8	3057.8	4715.2	4599.3	2927.3	3062.2	2972.0	2972.0	2974.6

Table A.21: SAM-MA computations at flow-gauging site C5H014

Input variables	**Sections 1-2**	**Sections 2-3**	**Sections 3-4**	**Sections 4-5**
Manning's *n*-value (s/m$^{1/3}$)	0.038	0.041	0.041	-
Area upstream (*A* US, m^2)	1338.100	1387.550	1347.650	-
Area downstream (*A* DS, m^2)	1387.550	1347.650	1336.520	-
Hydraulic radius US (*R*, m)	5.760	6.690	6.540	-
Hydraulic radius DS (*R*, m)	6.690	6.540	7.140	-
Reach length (*L*, m)	195.000	230.000	240.000	-
Fall (Δh, m)	0.350	0.440	0.460	-
Channel slope (S_o, m/m)	0.002	0.002	0.002	-
$H_f \approx \Delta h$ (m)	0.378	0.402	0.448	-

Sections	**$v^2/2g$ US**	**$v^2/2g$ DS**	**H_f (m)**	**Energy slope (S_e, m/m)**	**$S_e^{1/2}$**	**Computed *Q* (m³/s)**
1 to 2	0.810	0.753	0.378	0.00194	0.044	5335.025
2 to 3	0.639	0.677	0.402	0.00175	0.042	4911.118
3 to 4	0.728	0.740	0.448	0.00187	0.043	5091.777
4 to 5	-	-	-	-	-	-

Table A.22: SAM-CHZ computations at flow-gauging site C5H014

Input variables	Sections 1-2	Sections 2-3	Sections 3-4	Sections 4-5
Chézy's *C*-value ($m^{0.5}/s$)	36	33	33	-
Area upstream (*A* US, m^2)	1338.10	1387.55	1347.65	-
Area downstream (*A* DS, m^2)	1387.55	1347.65	1336.52	-
Hydraulic radius US (*R*, m)	5.76	6.69	6.54	-
Hydraulic radius DS (*R*, m)	6.69	6.54	7.14	-
Reach length (*L*, m)	195	230	240	-
Fall (Δh, m)	0.350	0.440	0.460	-
Channel slope (S_o, m/m)	0.00179	0.00191	0.00192	-
$H_f \approx \Delta h$ (m)	0.379	0.403	0.448	-

Sections	$v^2/2g$ US	$v^2/2g$ DS	H_f (m)	Energy slope (S_e, m/m)	$S_e^{1/2}$	Computed *Q* (m^3/s)
1 to 2	0.826	0.768	0.379	0.002	0.044	5387.537
2 to 3	0.624	0.662	0.403	0.002	0.042	4855.097
3 to 4	0.703	0.714	0.448	0.002	0.043	5003.384
4 to 5	-	-	-	-	-	-

Table A.23: SAM-MA computations at flow-gauging site H5H004

Input variables	Sections 1-2	Sections 2-3	Sections 3-4	Sections 4-5
Manning's *n*-value ($s/m^{1/3}$)	0.015	0.017	0.021	0.032
Area upstream (*A* US, m^2)	532.160	566.110	542.400	521.550
Area downstream (*A* DS, m^2)	566.110	542.400	521.550	552.270
Hydraulic radius US (*R*, m)	2.890	2.790	3.140	3.760
Hydraulic radius DS (*R*, m)	2.790	3.140	3.760	3.440
Reach length (*L*, m)	147.000	191.000	161.000	234.000
Fall (Δh, m)	0.140	0.200	0.230	0.710
Channel slope (S_o, m/m)	0.001	0.001	0.001	0.003
$H_f \approx \Delta h$ (m)	0.227	0.150	0.178	0.761

Sections	$v^2/2g$ US	$v^2/2g$ DS	H_f (m)	Energy slope (S_e, m/m)	$S_e^{1/2}$	Computed *Q* (m^3/s)
1 to 2	1.497	1.323	0.227	0.00154	0.039	2883.831
2 to 3	0.563	0.613	0.150	0.00078	0.028	1881.286
3 to 4	0.637	0.689	0.178	0.00111	0.033	1917.795
4 to 5	0.945	0.842	0.761	0.00325	0.057	2245.242

Table A.24: SAM-CHZ computations at flow-gauging site H5H004

Input variables	Sections 1-2	Sections 2-3	Sections 3-4	Sections 4-5
Chézy's *C*-value ($m^{0.5}/s$)	77	71	59	39
Area upstream (*A* US, m^2)	532.16	566.11	542.40	521.55
Area downstream (*A* DS, m^2)	566.11	542.40	521.55	552.27
Hydraulic radius US (*R*, m)	2.89	2.79	3.14	3.76
Hydraulic radius DS (*R*, m)	2.79	3.14	3.76	3.44
Reach length (*L*, m)	147	191	161	234
Fall (Δh, m)	0.140	0.200	0.230	0.710
Channel slope (S_o, m/m)	0.00095	0.00105	0.00143	0.00303
$H_f \approx \Delta h$ (m)	0.219	0.149	0.177	0.762

Sections	$v^2/2g$ US	$v^2/2g$ DS	H_f (m)	Energy slope (S_e, m/m)	$S_e^{1/2}$	Computed *Q* (m^3/s)
1 to 2	1.361	1.203	0.219	0.001	0.039	2749.940
2 to 3	0.569	0.620	0.149	0.001	0.028	1891.551
3 to 4	0.646	0.698	0.177	0.001	0.033	1930.556
4 to 5	0.961	0.857	0.762	0.003	0.057	2265.120

Table A.25: SAM-MA computations at flow-gauging site J1H018

Input variables	Sections 1-2	Sections 2-3	Sections 3-4	Sections 4-5
Manning's *n*-value (s/m$^{1/3}$)	0.039	0.050	-	-
Area upstream (*A* US, m^2)	678.060	1012.800	-	-
Area downstream (*A* DS, m^2)	1012.800	850.440	-	-
Hydraulic radius US (*R*, m)	2.200	2.870	-	-
Hydraulic radius DS (*R*, m)	2.870	2.530	-	-
Reach length (*L*, m)	166.000	186.000	-	-
Fall (Δh, m)	0.525	0.699	-	-
Channel slope (S_o, m/m)	0.003	0.004	-	-
$H_f \approx \Delta h$ (m)	0.526	0.611	-	-

Sections	$v^2/2g$ US	$v^2/2g$ DS	H_f (m)	Energy slope (S_e, m/m)	$S_e^{1/2}$	Computed *Q* (m^3/s)
1 to 2	0.542	0.243	0.675	0.004	0.064	2503.658
2 to 3	0.211	0.299	0.611	0.003	0.057	2059.759
3 to 4	-	-	-	-	-	-
4 to 5	-	-	-	-	-	-

Table A.26: SAM-CHZ computations at flow-gauging site J1H018

Input variables	Sections 1-2	Sections 2-3	Sections 3-4	Sections 4-5
Chézy's *C*-value (m$^{0.5}$/s)	30	24	-	-
Area upstream (*A* US, m^2)	678	1012.80	-	-
Area downstream (*A* DS, m^2)	1013	850.44	-	-
Hydraulic radius US (*R*, m)	2	2.87	-	-
Hydraulic radius DS (*R*, m)	3	2.53	-	-
Reach length (*L*, m)	166	186	-	-
Fall (Δh, m)	1	0.699	-	-
Channel slope (S_o, m/m)	0	0.00376	-	-
$H_f \approx \Delta h$ (m)	1	0.608	-	-

Sections	$v^2/2g$ US	$v^2/2g$ DS	H_f (m)	Energy slope (S_e, m/m)	$S_e^{1/2}$	Computed *Q* (m^3/s)
1 to 2	0.631	0.283	0.699	0.004	0.065	2557.311
2 to 3	0.217	0.308	0.608	0.003	0.057	2090.720
3 to 4	-	-	-	-	-	-
4 to 5	-	-	-	-	-	-

Table A.27: SAM-MA computations at flow-gauging site J4H002

Input variables	Sections 1-2	Sections 2-3	Sections 3-4	Sections 4-5
Manning's *n*-value (s/m$^{1/3}$)	0.072	0.041	0.022	-
Area upstream (*A* US, m^2)	655.350	792.480	805.600	-
Area downstream (*A* DS, m^2)	792.480	805.600	629.690	-
Hydraulic radius US (*R*, m)	5.200	4.410	4.790	-
Hydraulic radius DS (*R*, m)	4.410	4.790	4.200	-
Reach length (*L*, m)	64.000	145.000	238.000	-
Fall (Δh, m)	0.618	0.387	0.227	-
Channel slope (S_o, m/m)	0.010	0.003	0.001	-
$H_f \approx \Delta h$ (m)	0.810	0.397	0.086	-

Sections	$v^2/2g$ US	$v^2/2g$ DS	H_f (m)	Energy slope (S_e, m/m)	$S_e^{1/2}$	Computed *Q* (m^3/s)
1 to 2	1.215	0.831	0.810	0.01266	0.112	3199.081
2 to 3	0.646	0.625	0.397	0.00274	0.052	2820.373
3 to 4	0.221	0.362	0.086	0.00036	0.019	1677.098
4 to 5	-	-	-	-	-	-

Table A.28: SAM-CHZ computations at flow-gauging site J4H002

Input variables	Sections 1-2	Sections 2-3	Sections 3-4	Sections 4-5
Chézy's *C*-value ($m^{0.5}/s$)	18	31	60	-
Area upstream (*A* US, m^2)	655.35	792.48	805.60	-
Area downstream (*A* DS, m^2)	792.48	805.60	629.69	-
Hydraulic radius US (*R*, m)	5.20	4.41	4.79	-
Hydraulic radius DS (*R*, m)	4.41	4.79	4.20	-
Reach length (*L*, m)	64	145	238	-
Fall (Δh, m)	0.618	0.387	0.227	-
Channel slope (S_o, m/m)	0.00966	0.00267	0.00095	-
$H_f \approx \Delta h$ (m)	0.809	0.397	0.083	-

Sections	$v^2/2g$ US	$v^2/2g$ DS	H_f (m)	Energy slope (S_e, m/m)	$S_e^{1/2}$	Computed *Q* (m^3/s)
1 to 2	1.209	0.827	0.809	0.013	0.112	3191.706
2 to 3	0.627	0.607	0.397	0.003	0.052	2778.999
3 to 4	0.225	0.369	0.083	0.0004	0.019	1694.431
4 to 5	-	-	-	-	-	-

Table A.29: SAM-MA computations at flow-gauging site X3H008

Input variables	Sections 1-2	Sections 2-3	Sections 3-4	Sections 4-5
Manning's *n*-value ($s/m^{1/3}$)	0.041	0.041	0.067	0.044
Area upstream (*A* US, m^2)	913.720	968.170	808.910	1250.660
Area downstream (*A* DS, m^2)	968.170	808.910	1250.660	917.160
Hydraulic radius US (*R*, m)	4.300	3.930	3.950	4.450
Hydraulic radius DS (*R*, m)	3.930	3.950	4.450	4.100
Reach length (*L*, m)	376.000	376.000	319.000	261.000
Fall (Δh, m)	0.859	1.030	1.600	0.599
Channel slope (S_o, m/m)	0.002	0.003	0.005	0.002
$H_f \approx \Delta h$ (m)	0.886	0.872	1.794	0.416

Sections	$v^2/2g$ US	$v^2/2g$ DS	H_f (m)	Energy slope (S_e, m/m)	$S_e^{1/2}$	Computed *Q* (m^3/s)
1 to 2	0.499	0.444	0.886	0.00236	0.049	2858.060
2 to 3	0.366	0.524	0.872	0.00232	0.048	2592.838
3 to 4	0.667	0.279	1.794	0.00562	0.075	2927.257
4 to 5	0.213	0.396	0.416	0.00159	0.040	2557.650

Table A.30: SAM-CHZ computations at flow-gauging site X3H008

Input variables	Sections 1-2	Sections 2-3	Sections 3-4	Sections 4-5
Chézy's *C*-value ($m^{0.5}/s$)	33	32	20	31
Area upstream (*A* US, m^2)	913.72	968.17	808.91	1250.66
Area downstream (*A* DS, m^2)	968.17	808.91	1250.66	917.16
Hydraulic radius US (*R*, m)	4.30	3.93	3.95	4.45
Hydraulic radius DS (*R*, m)	3.93	3.95	4.45	4.10
Reach length (*L*, m)	376	376	319	261
Fall (Δh, m)	0.859	1.030	1.600	0.599
Channel slope (S_o, m/m)	0.00228	0.00274	0.00502	0.00230
$H_f \approx \Delta h$ (m)	0.890	0.860	1.819	0.398

Sections	$v^2/2g$ US	$v^2/2g$ DS	H_f (m)	Energy slope (S_e, m/m)	$S_e^{1/2}$	Computed *Q* (m^3/s)
1 to 2	0.572	0.510	0.890	0.002	0.049	3062.198
2 to 3	0.393	0.563	0.860	0.002	0.048	2688.347
3 to 4	0.754	0.315	1.819	0.006	0.076	3110.513
4 to 5	0.234	0.435	0.398	0.002	0.039	2679.362

Table A.31: SBA-MA computations (sub-critical) at flow-gauging site C5H014

Section	Q (m³/s)	WSW (m)	WSE (m)	A (m²)	R (m)	$R^{2/3}$	n-value (s/m$^{1/3}$)	Conveyance K
4	5128.3	183.91	104.734	1336.520	7.140	3.708	0.040	123893.240
3	5128.3	204.19	104.275	1347.650	6.690	3.550	0.044	108994.908
2	5128.3	204.71	103.835	1387.550	6.540	3.497	0.074	65814.729
1	5128.3	230.66	103.486	1338.100	5.760	3.213	0.069	62453.540

Froude	v (m/s)	$v^2/2g$ (m)	H (m)	S_f (m/m)	Avg. S_f (m/m)	Reach L (m)	H_f (m)	H (m)
0.454	3.837	0.750	105.484	0.00171				105.484
0.473	3.805	0.738	105.013	0.00221	0.00196	240	0.471	105.484
0.453	3.696	0.696	104.531	0.00607	0.00414	230	0.953	105.484
0.454	3.833	0.749	104.235	0.00674	0.00641	195	1.249	105.484

Table A.32: SBA-CHZ computations (sub-critical) at flow-gauging site C5H014

Section	Q (m³/s)	WSW (m)	WSE (m)	A (m²)	R (m)	$R^{2/3}$	C-value (m$^{0.5}$/s)	Conveyance K
4	5128.3	183.91	104.734	1336.520	7.140	3.708	38	135708.8
3	5128.3	204.19	104.275	1347.650	6.690	3.550	29	102596.5
2	5128.3	204.71	103.835	1387.550	6.540	3.497	19	67391.77
1	5128.3	230.66	103.486	1338.100	5.760	3.213	19	61180.4

Froude	v (m/s)	$v^2/2g$ (m)	H (m)	S_f (m/m)	Avg. S_f (m/m)	Reach L (m)	H_f (m)	H (m)
0.454	3.837	0.750	105.484	0.001				105.484
0.473	3.805	0.738	105.013	0.002	0.002	240	0.471	105.484
0.453	3.696	0.696	104.531	0.006	0.004	230	0.953	105.484
0.454	3.833	0.749	104.235	0.007	0.006	195	1.250	105.484

Table A.33: SBA-MA computations (sub-critical) at flow-gauging site H5H004

Section	Q (m³/s)	WSW (m)	WSE (m)	A (m²)	R (m)	$R^{2/3}$	n-value (s/m$^{1/3}$)	Conveyance K
4	2195.7	158.05	107.200	552.210	3.440	2.279	0.033	38132.559
3	2195.7	137.00	106.410	521.550	3.760	2.418	0.029	43052.948
2	2195.7	170.47	106.260	542.400	3.140	2.144	0.049	23528.547
1	2195.7	206.37	106.050	566.110	2.790	1.982	0.031	35903.221

Froude	v (m/s)	$v^2/2g$ (m)	H (m)	S_f (m/m)	Avg. S_f (m/m)	Reach L (m)	H_f (m)	H (m)
0.679	3.976	0.806	108.006	0.00331				108.006
0.689	4.210	0.903	107.313	0.00260	0.00296	234	0.692	108.006
0.725	4.048	0.835	107.095	0.00871	0.00566	161	0.910	108.006
0.748	3.879	0.767	106.817	0.00374	0.00622	191	1.189	108.006

Table A.34: SBA-CHZ computations (sub-critical) at flow-gauging site H5H004

Section	Q (m³/s)	WSW (m)	WSE (m)	A (m²)	R (m)	$R^{2/3}$	C-value (m$^{0.5}$/s)	Conveyance K
4	2195.7	158.05	107.200	552.210	3.440	2.279	79	80911.56
3	2195.7	137.00	106.410	521.550	3.760	2.418	30	30499.2
2	2195.7	170.47	106.260	542.400	3.140	2.144	29	28042.5
1	2195.7	206.37	106.050	566.110	2.790	1.982	29	27592.35

Froude	v (m/s)	$v^2/2g$ (m)	H (m)	S_f (m/m)	Avg. S_f (m/m)	Reach L (m)	H_f (m)	H (m)
0.679	3.976	0.806	108.006	0.000736				108.006
0.689	4.210	0.903	107.313	0.00518	0.00296	234	0.693	108.006
0.725	4.048	0.835	107.095	0.00613	0.00566	161	0.911	108.006
0.748	3.879	0.767	106.817	0.00633	0.00622	191	1.190	108.007

Table A.35: SBA-MA computations (sub-critical) at flow-gauging site J1H018

Section	*Q* (m³/s)	*WSW* (m)	*WSE* (m)	*A* (m²)	*R* (m)	$R^{2/3}$	*n*-value (s/m$^{1/3}$)	Conveyance *K*
3	2202.7	296.91	104.650	850.060	2.530	1.857	0.022	71742.072
2	2202.7	350.90	104.355	1012.800	2.870	2.020	0.057	35595.659
1	2202.7	330.07	103.391	678.060	2.200	1.692	0.045	25265.955

Froude	*v* (m/s)	$v^2/2g$ (m)	*H* (m)	S_f (m/m)	Avg. S_f (m/m)	Reach *L* (m)	H_f (m)	*H* (m)
0.515	2.591	0.342	104.992	0.001				104.992
0.409	2.175	0.241	104.596	0.004	0.002	166.000	0.396	104.992
0.686	3.249	0.538	103.929	0.008	0.006	186.000	1.063	104.992

Table A.36: SBA-CHZ computations (sub-critical) at flow-gauging site J1H018

Section	*Q* (m³/s)	*WSW* (m)	*WSE* (m)	*A* (m²)	*R* (m)	$R^{2/3}$	*C*-value (m$^{0.5}$/s)	Conveyance *K*
3	2202.7	296.91	104.650	850.060	2.530	1.857	41.000	55436.231
2	2202.7	350.90	104.355	1012.800	2.870	2.020	22.722	38985.703
1	2202.7	330.07	103.391	678.060	2.200	1.692	24.127	24264.845

Froude	*v* (m/s)	$v^2/2g$ (m)	*H* (m)	S_f (m/m)	Avg. S_f (m/m)	Reach *L* (m)	H_f (m)	*H* (m)
0.515	2.591	0.342	104.992	0.002				104.992
0.409	2.175	0.241	104.596	0.003	0.002	166.000	0.396	104.992
0.686	3.249	0.538	103.929	0.008	0.006	186.000	1.063	104.992

Table A.37: SBA-MA computations (sub-critical) at flow-gauging site J4H002

Section	*Q* (m³/s)	*WSW* (m)	*WSE* (m)	*A* (m²)	*R* (m)	$R^{2/3}$	*n*-value (s/m$^{1/3}$)	Conveyance *K*
4	2195.7	137.73	67.337	629.690	4.200	2.603	0.018	91065.488
3	2195.7	165.27	67.110	805.600	4.790	2.842	0.060	37947.239
2	2195.7	177.34	66.723	792.480	4.470	2.714	0.089	24157.251
1	2195.7	123.70	66.105	655.380	5.200	3.001	0.160	12331.670

Froude	*v* (m/s)	$v^2/2g$ (m)	*H* (m)	S_f (m/m)	Avg. S_f (m/m)	Reach *L* (m)	H_f (m)	*H* (m)
0.521	3.487	0.62	67.957	0.000581				67.957
0.394	2.726	0.379	67.489	0.00335	0.00197	238	0.468	67.956
0.418	2.771	0.391	67.114	0.00826	0.00581	145	0.842	67.956
0.465	3.350	0.572	66.677	0.0317	0.01998	64.	1.279	67.956

Table A.38: SBA-CHZ computations (sub-critical) at flow-gauging site J4H002

Section	*Q* (m³/s)	*WSW* (m)	*WSE* (m)	*A* (m²)	*R* (m)	$R^{2/3}$	*C*-value (m$^{0.5}$/s)	Conveyance *K*
4	2195.7	137.73	67.337	629.690	4.200	2.603	71	91065.49
3	2195.7	165.27	67.110	805.600	4.790	2.842	22	37947.24
2	2195.7	177.34	66.723	792.480	4.470	2.714	14	24157.25
1	2195.7	123.70	66.105	655.380	5.200	3.001	8	12331.67

Froude	*v* (m/s)	$v^2/2g$ (m)	*H* (m)	S_f (m/m)	Avg. S_f (m/m)	Reach *L* (m)	H_f (m)	*H* (m)
0.521	3.487	0.620	67.957	0.00058				67.957
0.394	2.726	0.379	67.489	0.00335	0.00196	238	0.468	67.956
0.418	2.771	0.391	67.114	0.00826	0.00580	145	0.842	67.956
0.465	3.350	0.572	66.677	0.03170	0.01998	64	1.279	67.956

Table A.39: SBA-MA computations (sub-critical) at flow-gauging site X3H008

Section	*Q* (m^3/s)	*WSW* (m)	*WSE* (m)	*A* (m^2)	*R* (m)	$R^{2/3}$	*n*-value (s/$m^{1/3}$)	Conveyance *K*
5	2972	221.52	365.097	917.160	4.100	2.562	0.041	57303.852
4	2972	244.30	364.498	1250.660	4.450	2.705	0.070	48261.332
3	2972	201.55	362.898	808.910	3.950	2.499	0.065	31270.846
2	2972	242.03	361.868	968.170	3.930	2.490	0.074	32375.718
1	2972	209.73	361.009	913.720	4.30	2.644	0.094	25781.770

Froude	*v* (m/s)	$v^2/2g$ (m)	*H* (m)	S_f (m/m)	Avg. S_f (m/m)	Reach *L* (m)	H_f (m)	*H* (m)
0.508	3.240	0.535	365.632	0.00270				365.632
0.335	2.376	0.288	364.786	0.00379	0.00324	261	0.846	365.632
0.586	3.674	0.688	363.586	0.00903	0.00641	319	2.046	365.632
0.490	3.070	0.48	362.348	0.00843	0.00873	376	3.282	365.631
0.498	3.253	0.539	361.548	0.0133	0.0109	376	4.082	365.631

Table A.40: SBA-CHZ computations (sub-critical) at flow-gauging site X3H008

Section	*Q* (m^3/s)	*WSW* (m)	*WSE* (m)	*A* (m^2)	*R* (m)	$R^{2/3}$	*n*-value (s/$m^{1/3}$)	Conveyance *K*
5	2972	221.52	365.097	917.160	4.100	2.562	79	146711.5
4	2972	244.30	364.498	1250.660	4.450	2.705	14	38132.6
3	2972	201.55	362.898	808.910	3.950	2.499	22	36152.47
2	2972	242.03	361.868	968.170	3.930	2.490	15	28713.85
1	2972	209.73	361.009	913.720	4.30	2.644	15	28318.86

Froude	*v* (m/s)	$v^2/2g$ (m)	*H* (m)	S_f (m/m)	Avg. S_f (m/m)	Reach *L* (m)	H_f (m)	*H* (m)
0.508	3.240	0.535	365.632	0.00041				365.632
0.335	2.376	0.288	364.786	0.006074	0.003242	261	0.846	365.632
0.586	3.674	0.688	363.586	0.006758	0.006416	319	2.047	365.633
0.490	3.070	0.480	362.348	0.010713	0.008736	376	3.285	365.633
0.498	3.253	0.539	361.548	0.011014	0.010864	376	4.085	365.633

APPENDIX B: GRAPHICAL INFORMATION AND RESULTS

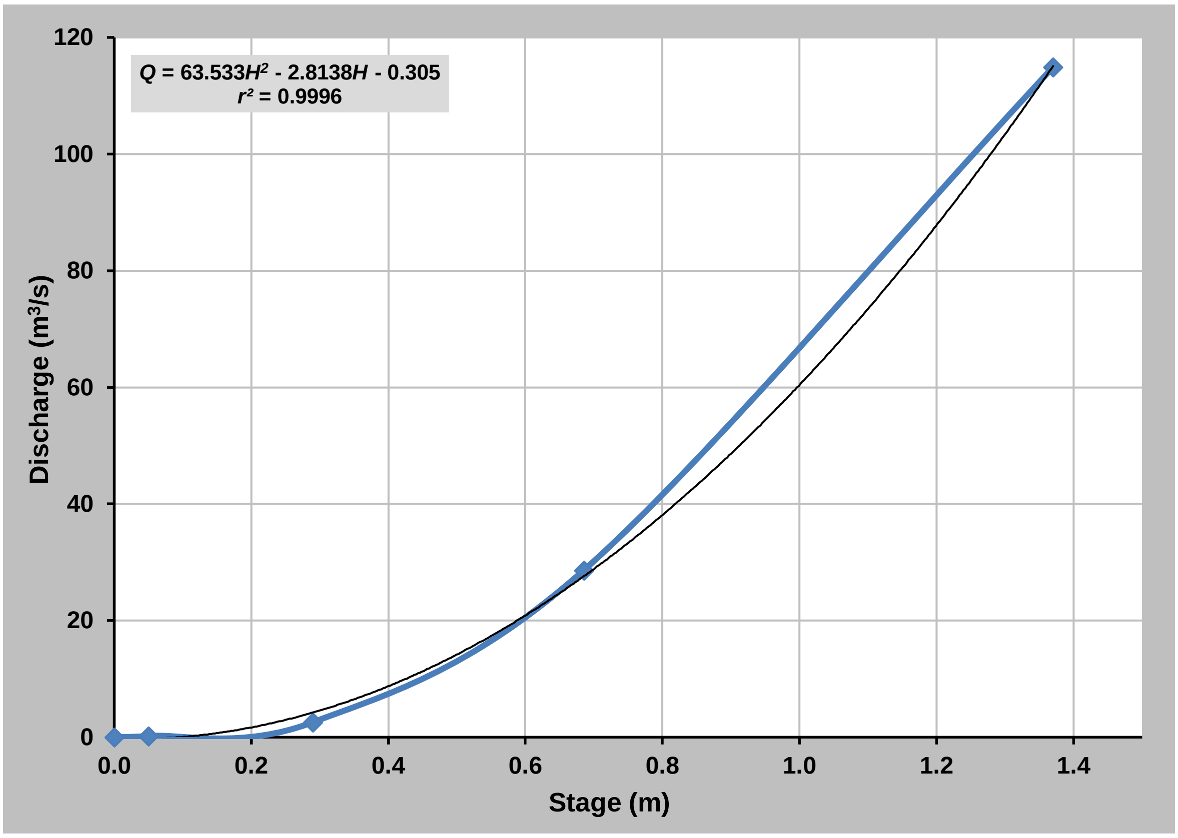

Figure B.1: SE RC estimation at flow-gauging site A4H005

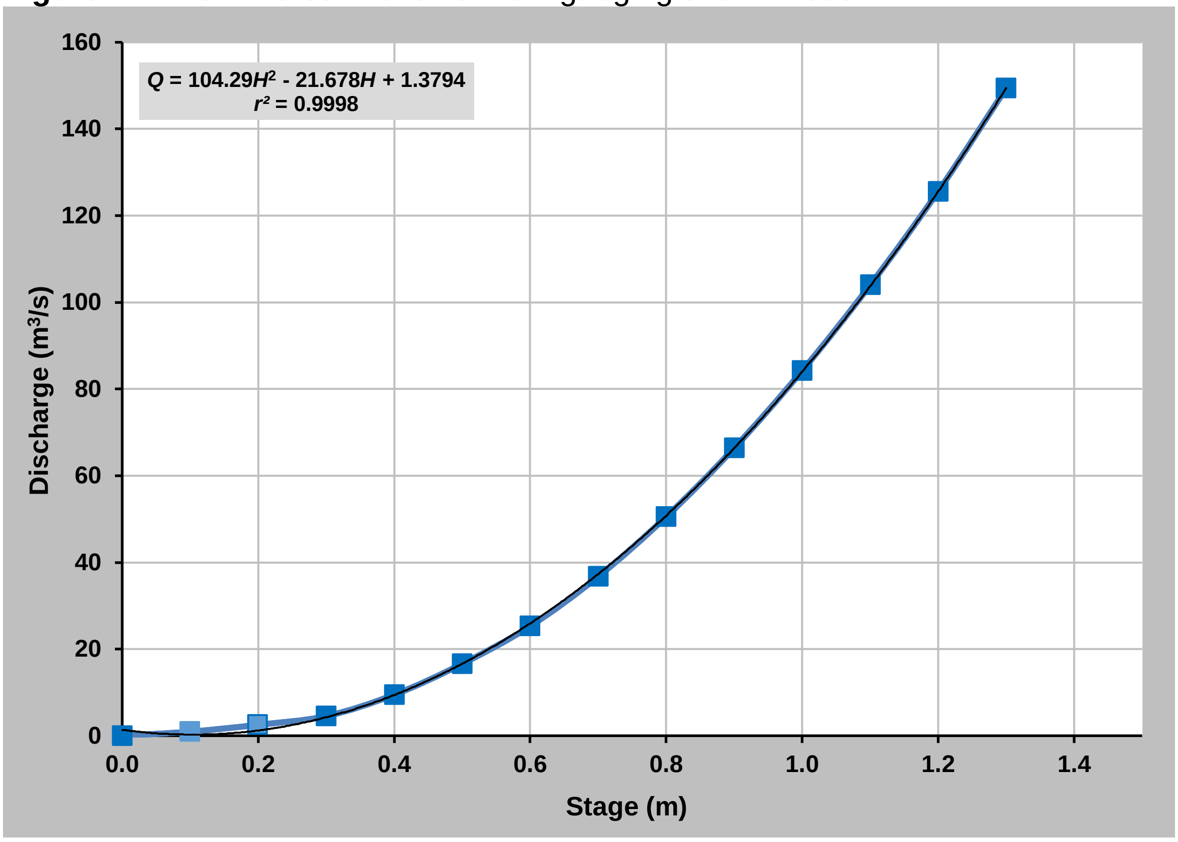

Figure B.2: SE RC estimation at flow-gauging site A6H035

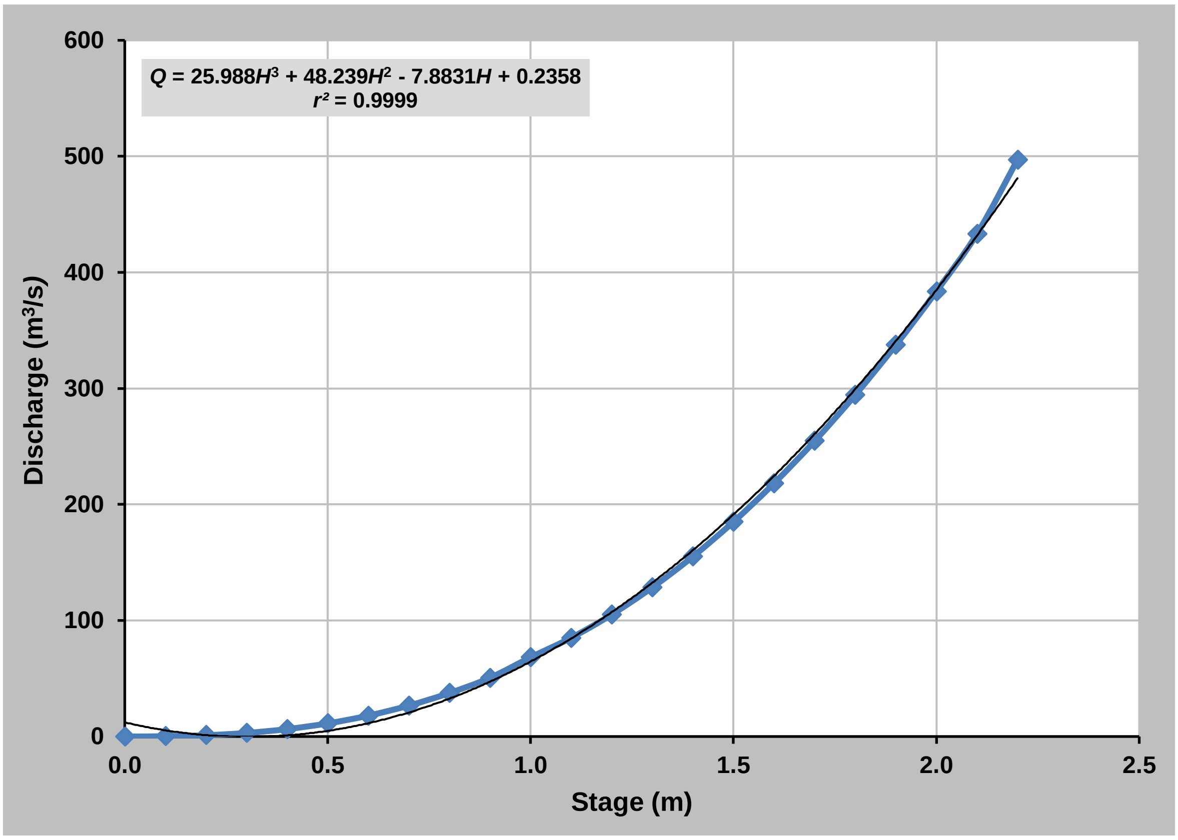

Figure B.3: SE RC estimation at flow-gauging site C2H003 (C2H130)

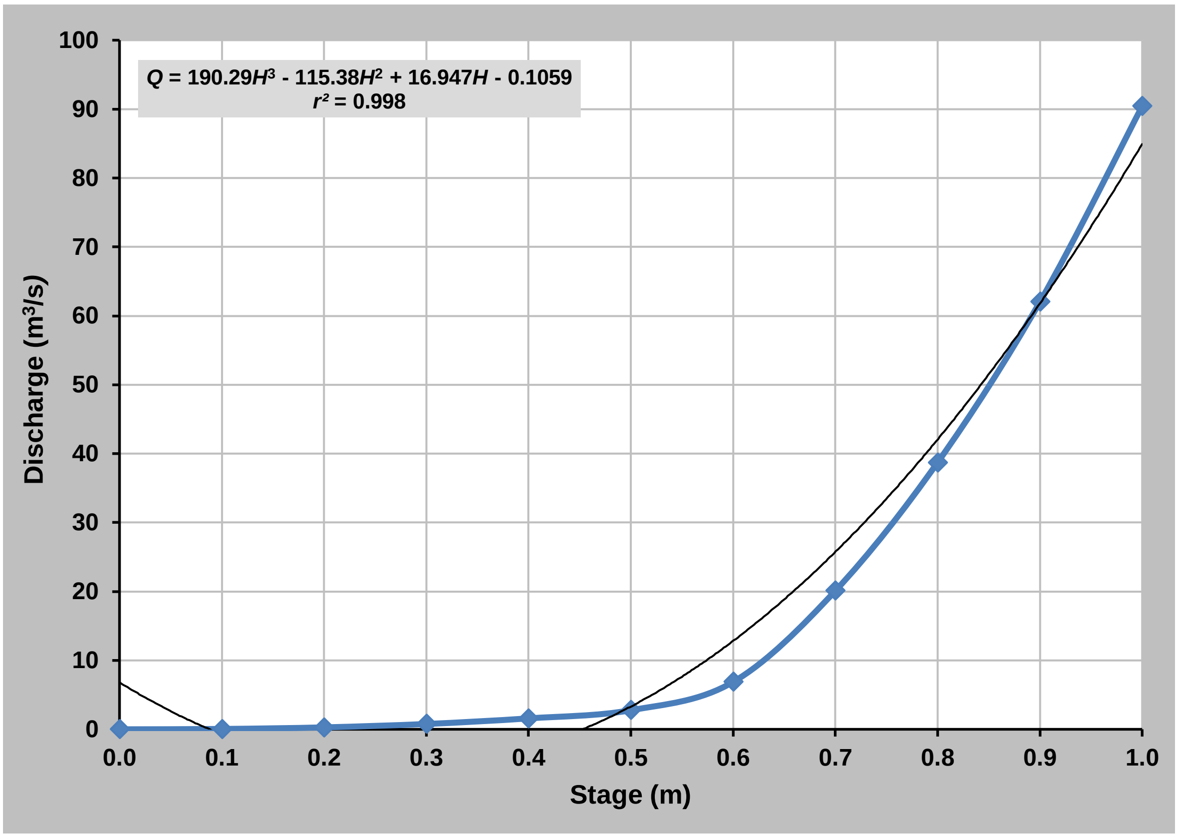

Figure B.4: SE RC estimation at flow-gauging site C5H014

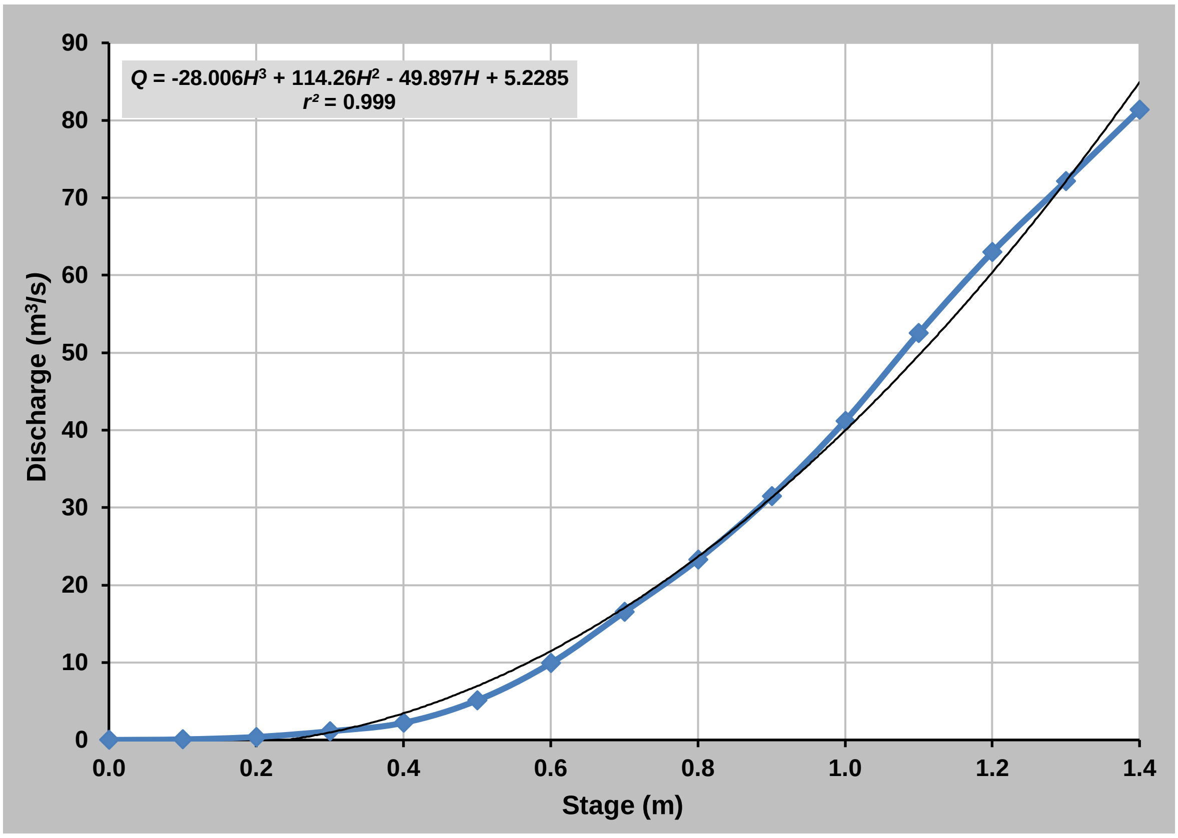

Figure B.5: SE RC estimation at flow-gauging site H5H004

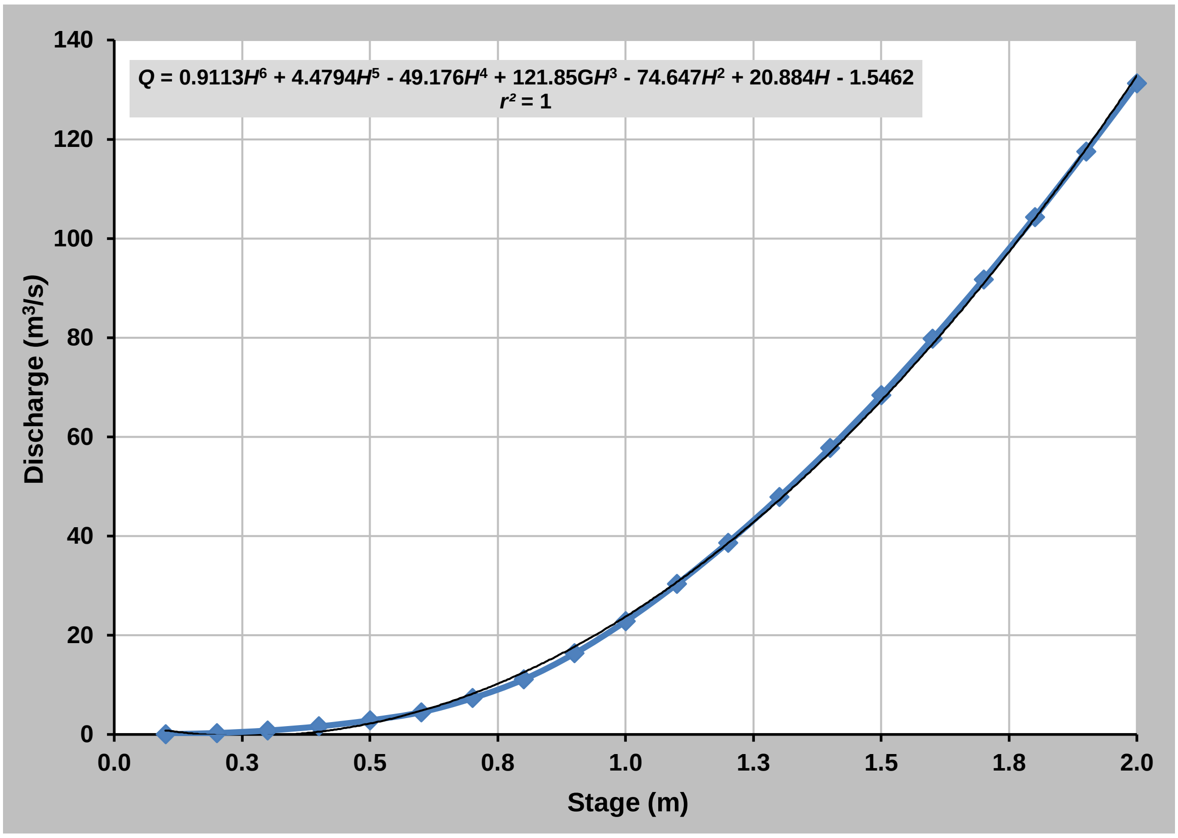

Figure B.6: SE RC estimation at flow-gauging site J1H018

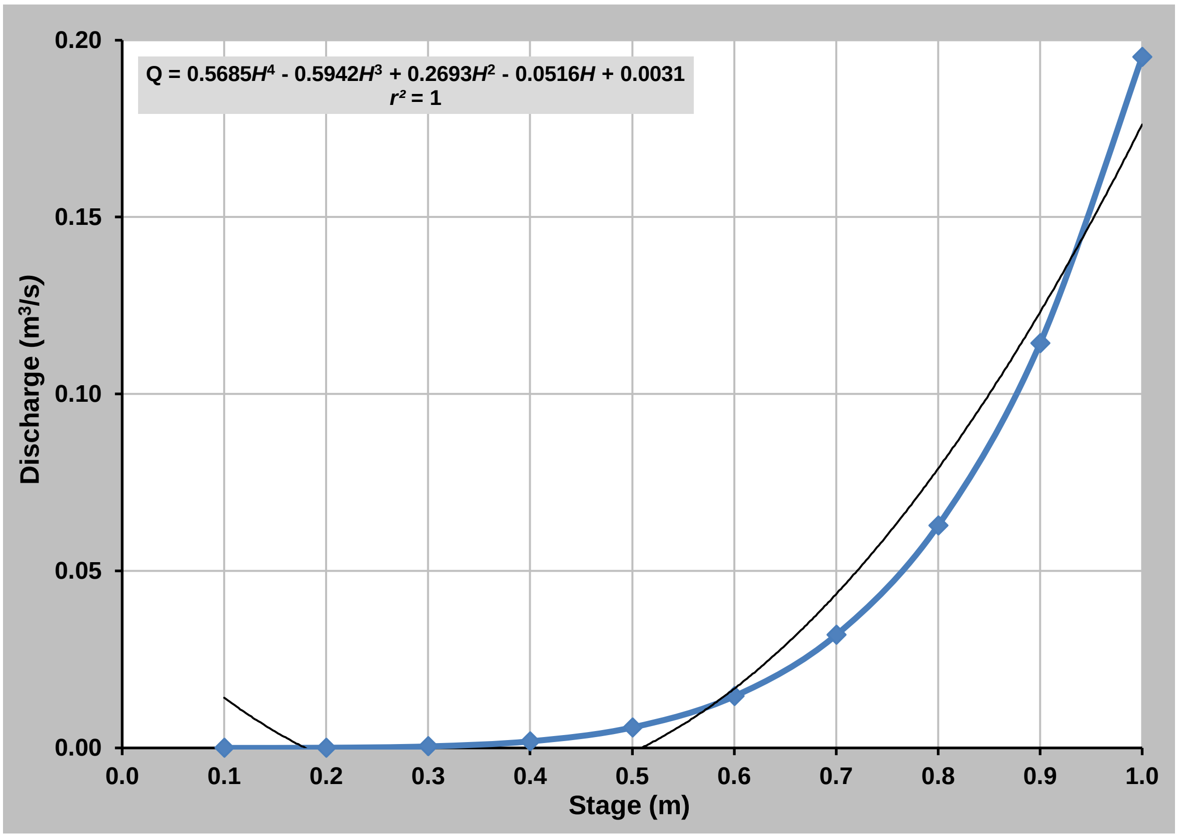

Figure B.7: SE RC estimation at flow-gauging site J4H002

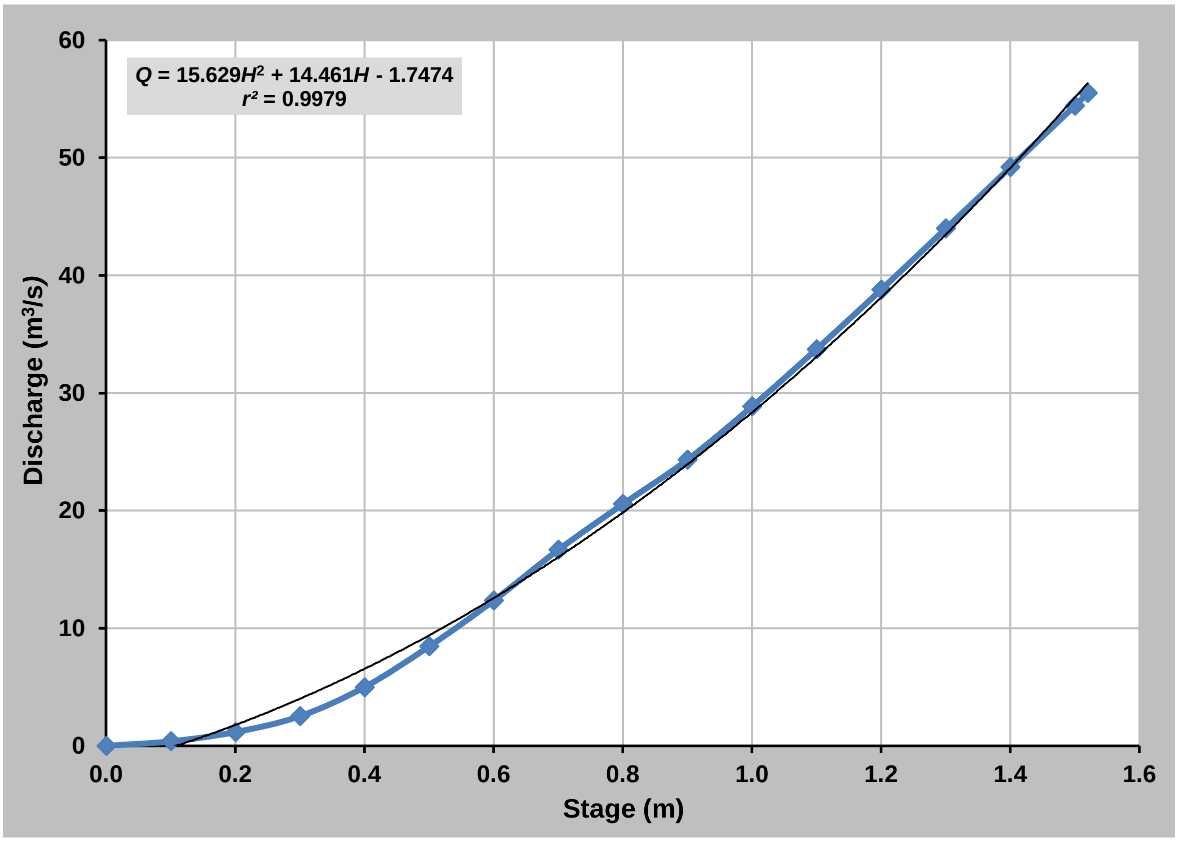

Figure B.8: SE RC estimation at flow-gauging site K2H002

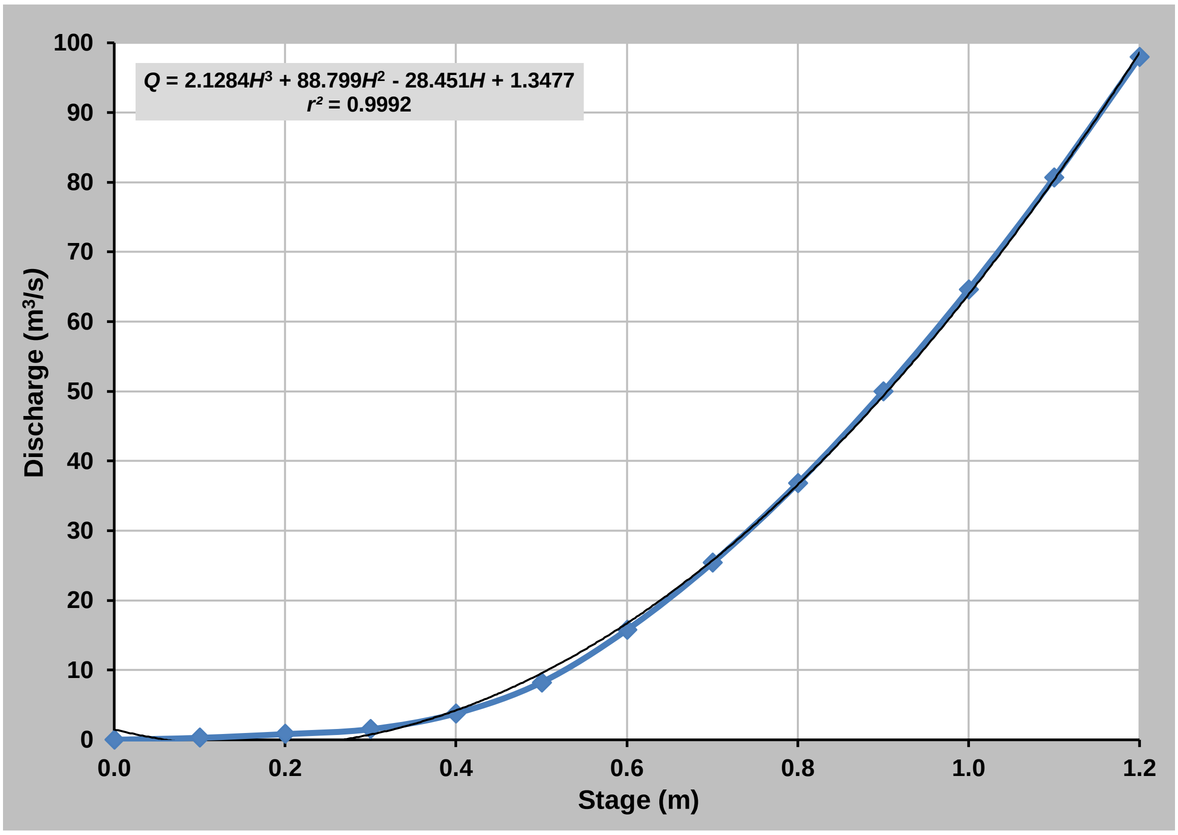

Figure B.9: SE RC estimation at flow-gauging site V1H026

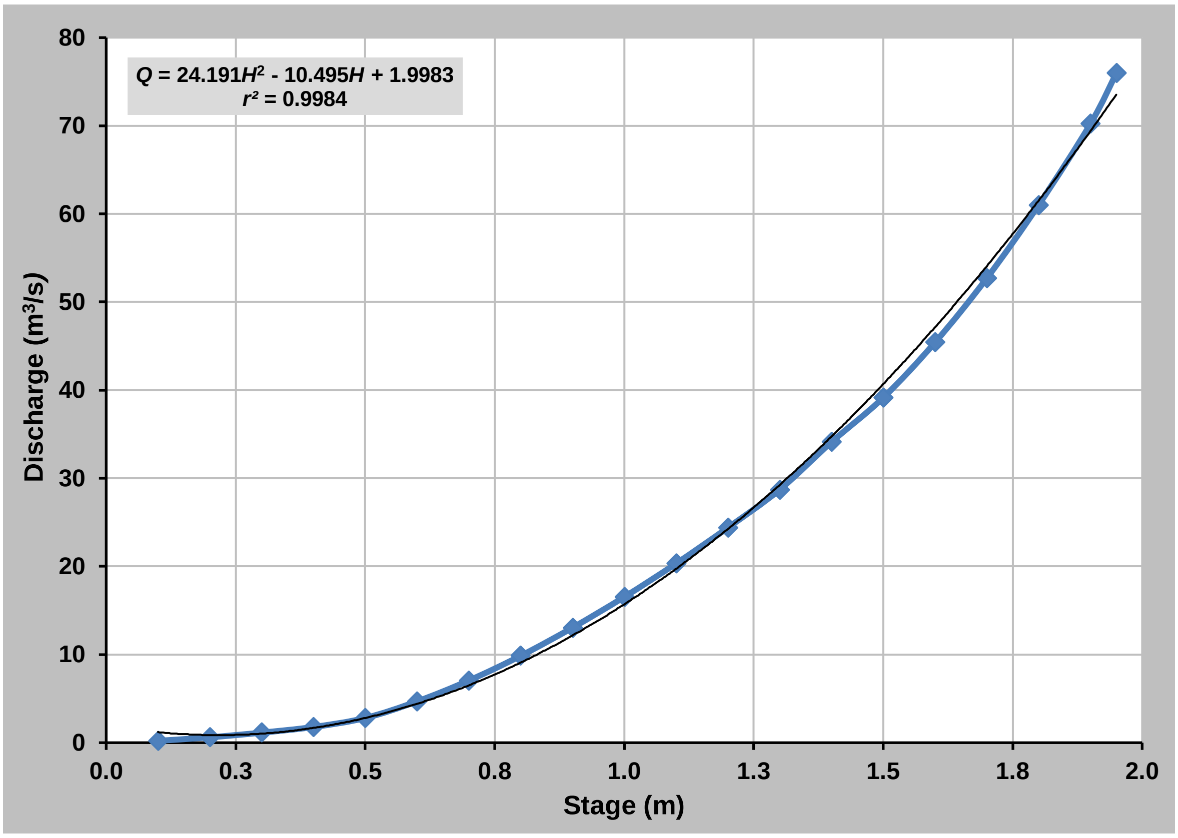

Figure B.10: SE RC estimation at flow-gauging site X3H008

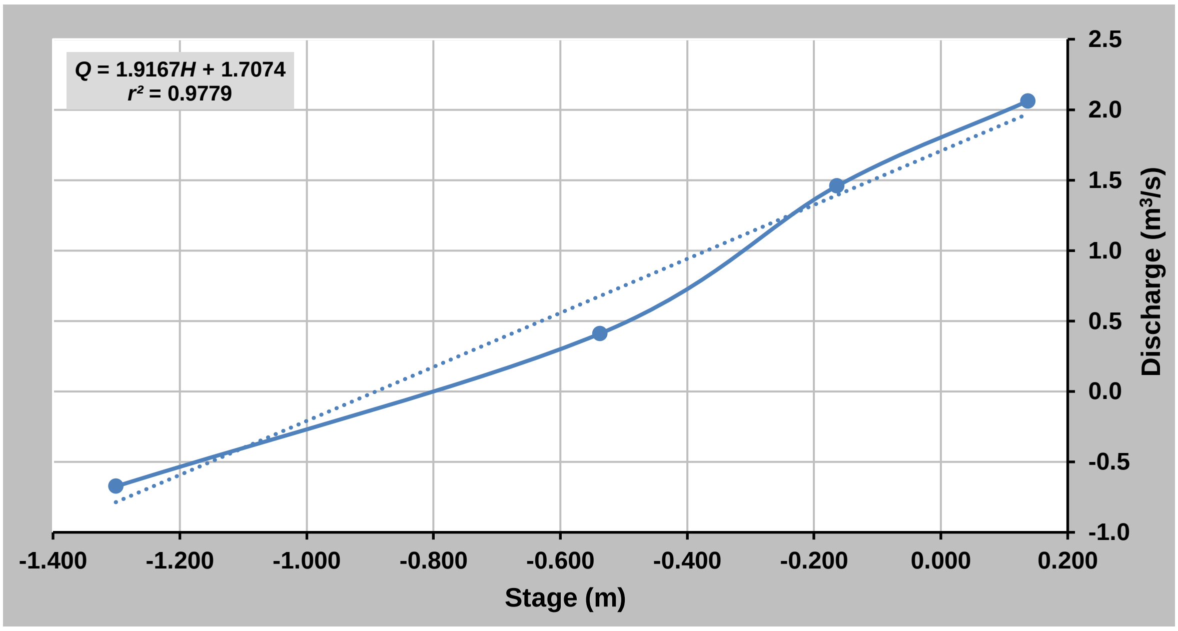

Figure B.11: LE RC estimation at flow-gauging site A4H005

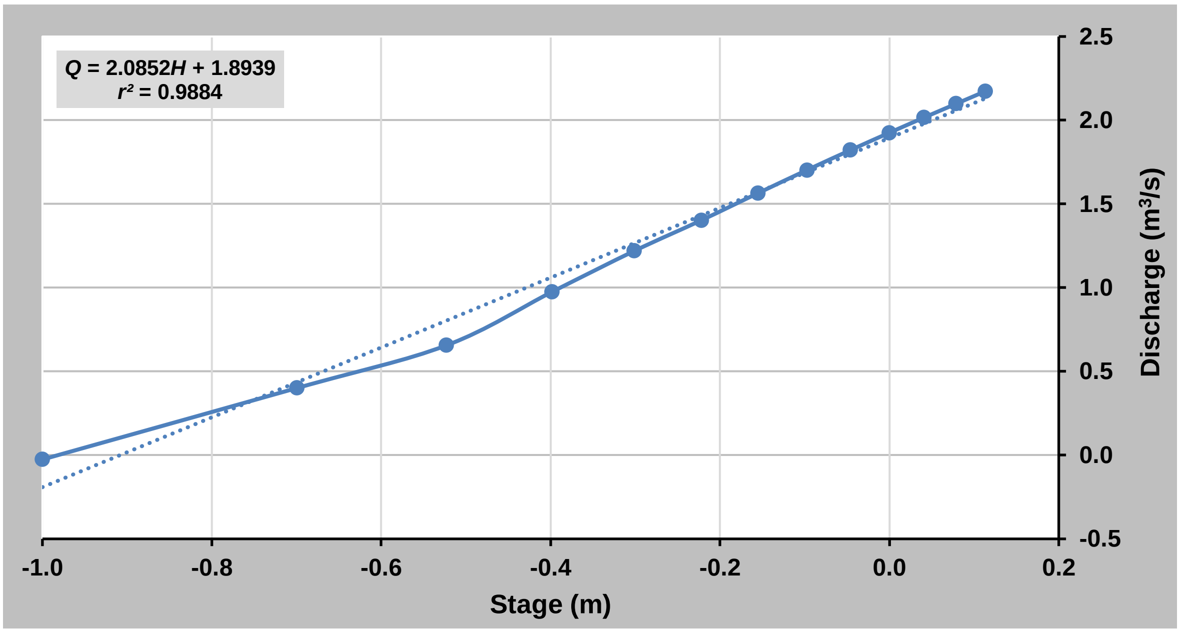

Figure B.12: LE RC estimation at flow-gauging site A6H035

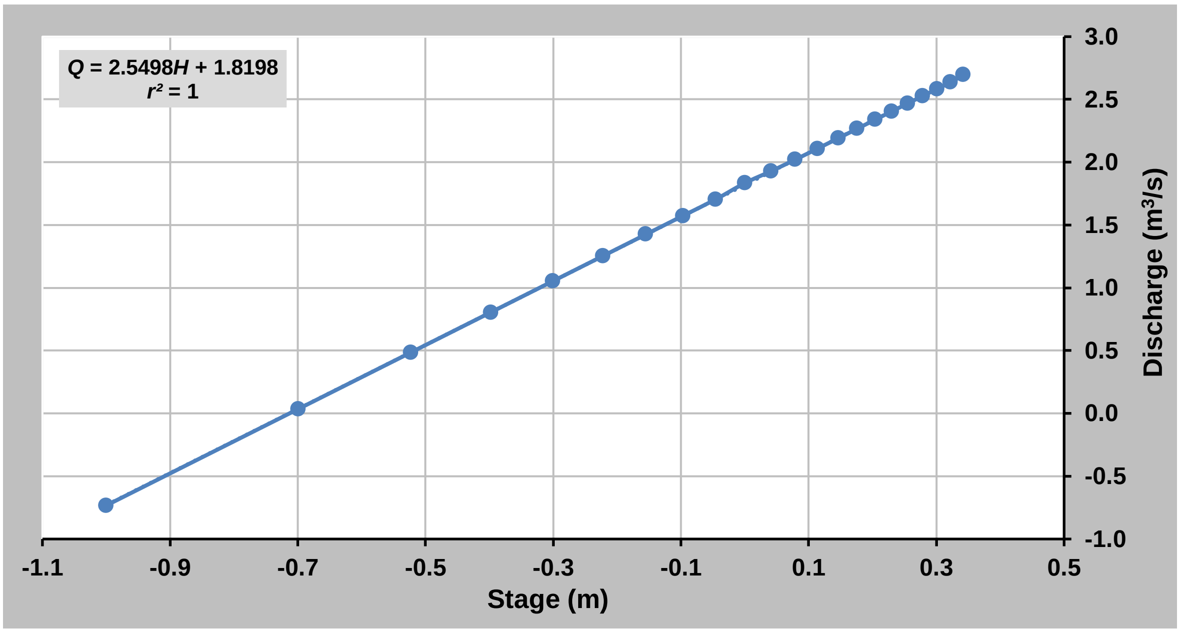

Figure B.13: LE RC estimation at flow-gauging site C2H003 (C2H130)

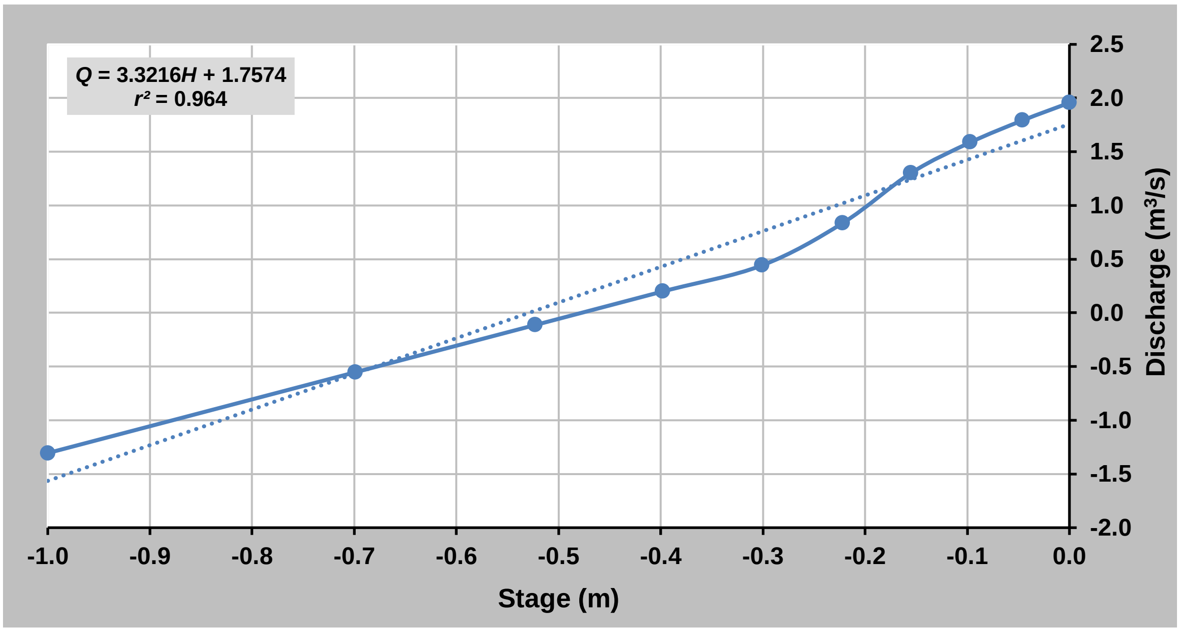

Figure B.14: LE RC estimation at flow-gauging site C5H014

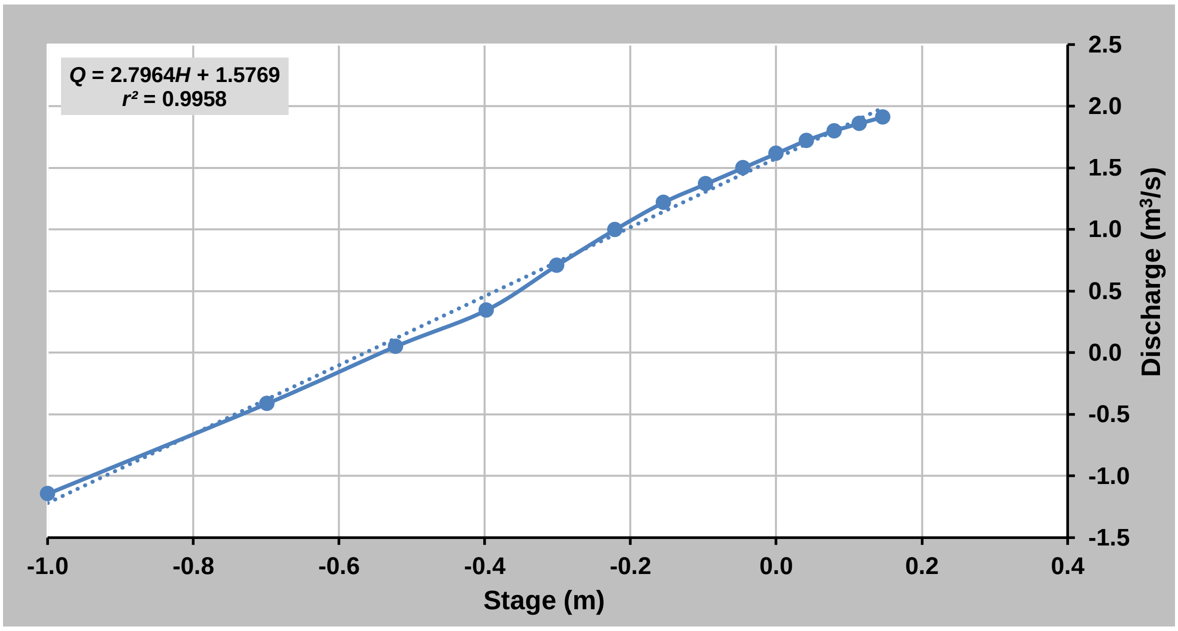

Figure B.15: LE RC estimation at flow-gauging site H5H004

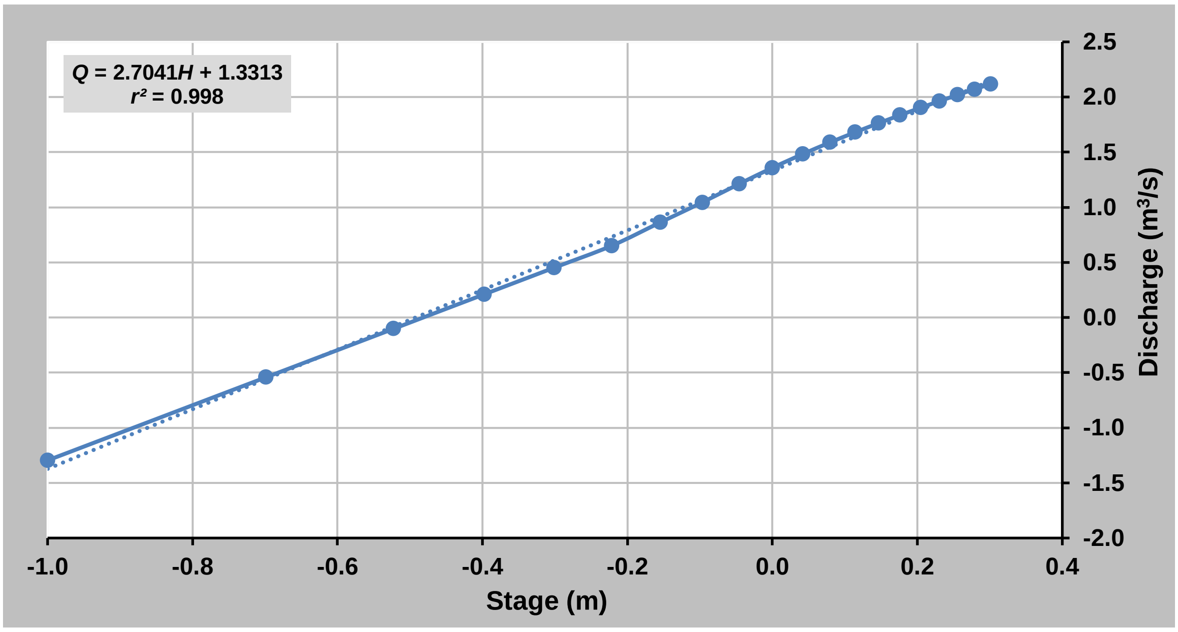

Figure B.16: LE RC estimation at flow-gauging site J1H018

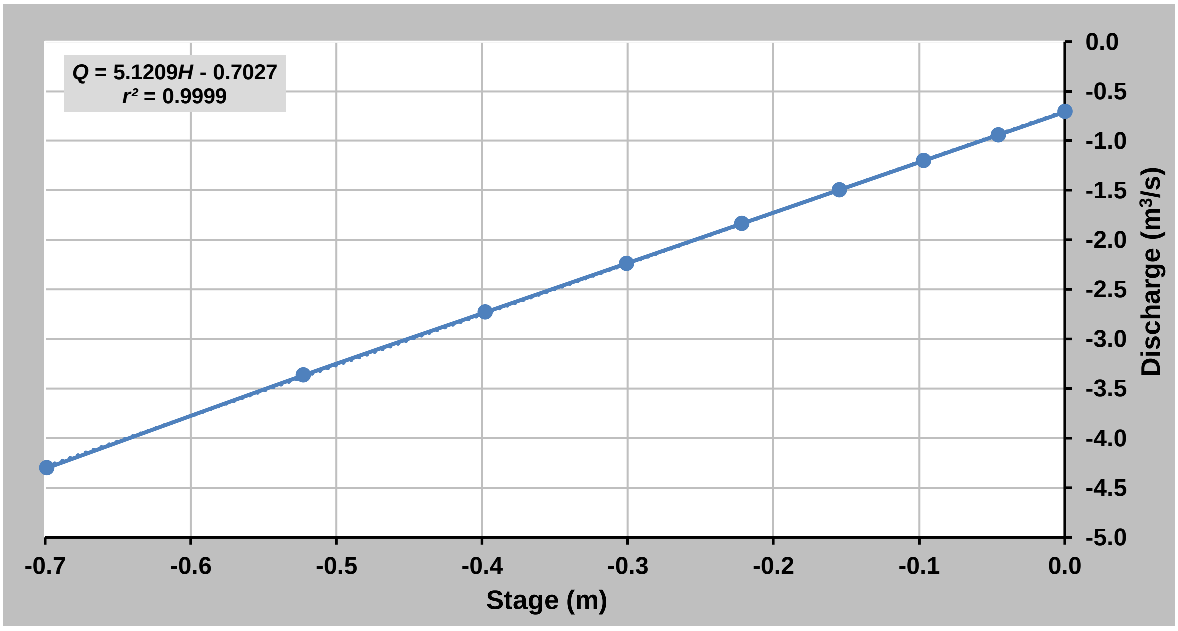

Figure B.17: LE RC estimation at flow-gauging site J4H002

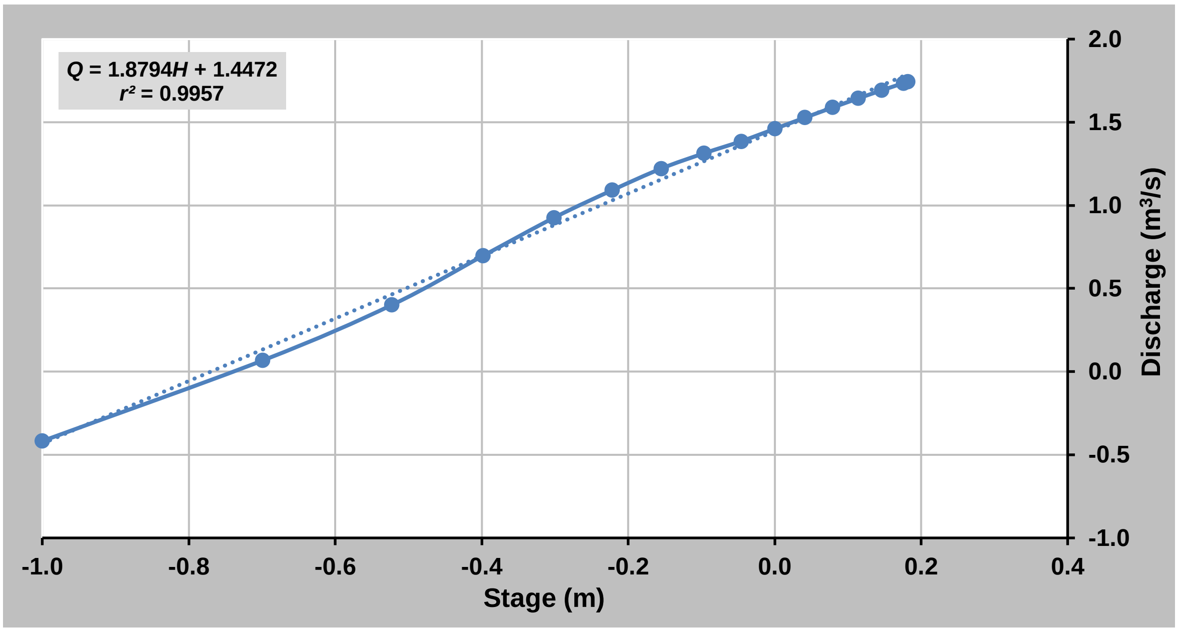

Figure B.18: LE RC estimation at flow-gauging site K2H002

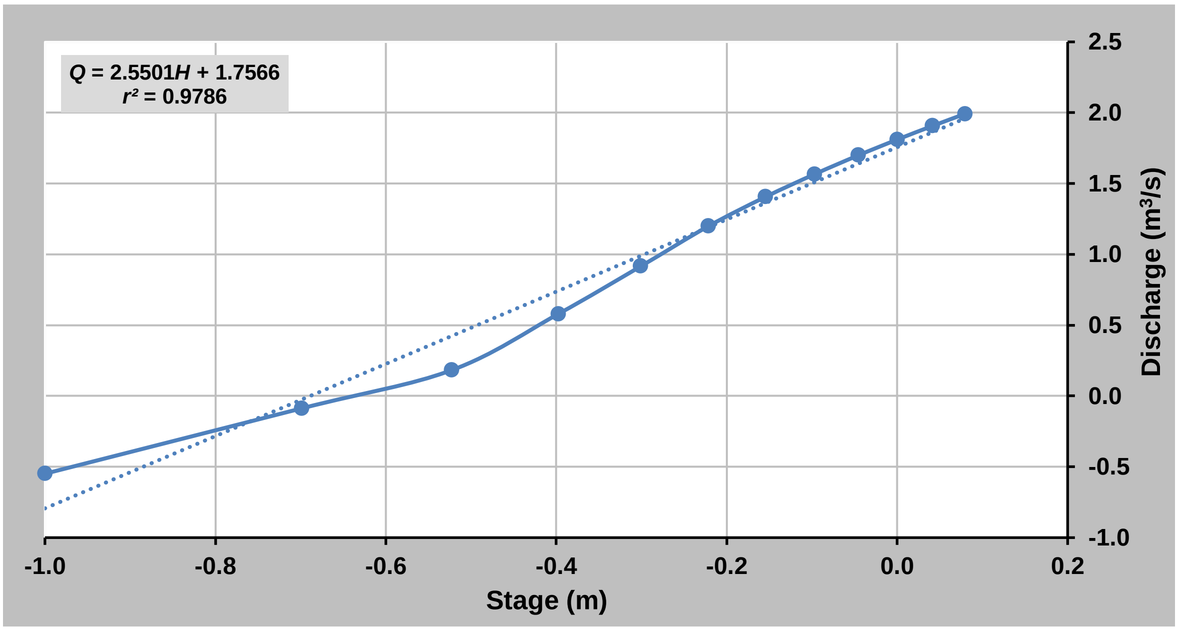

Figure B.19: LE RC estimation at flow-gauging site V1H026

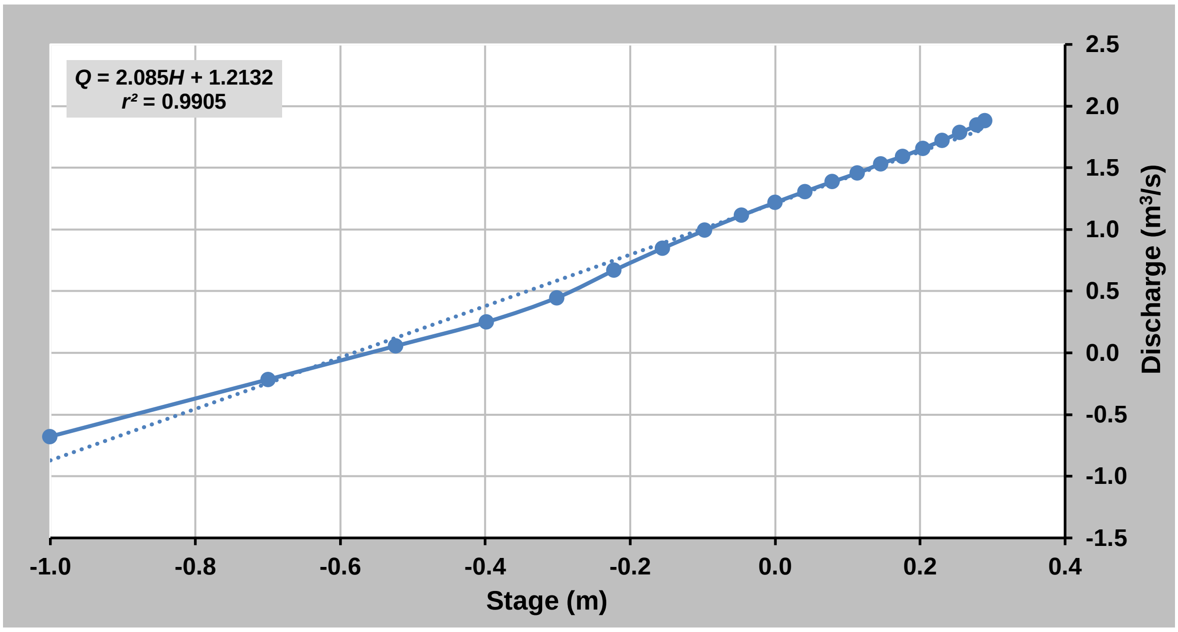

Figure B.20: LE RC estimation at flow-gauging site X3H008

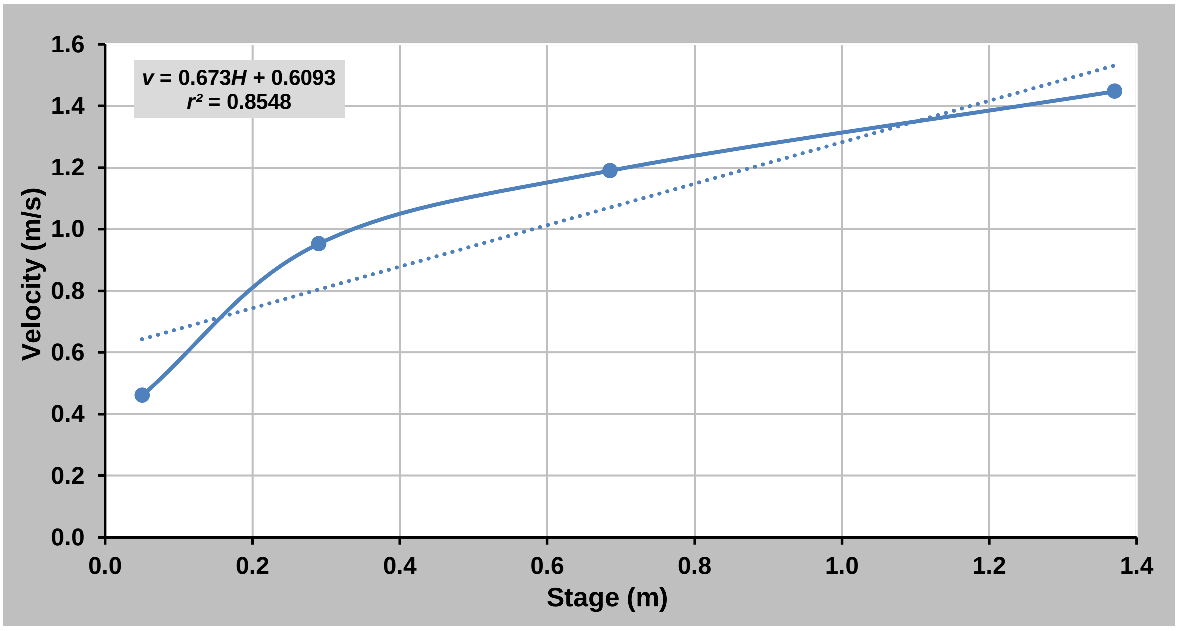

Figure B.21: Velocity versus stage at flow-gauging site A4H005 (VE-SA)

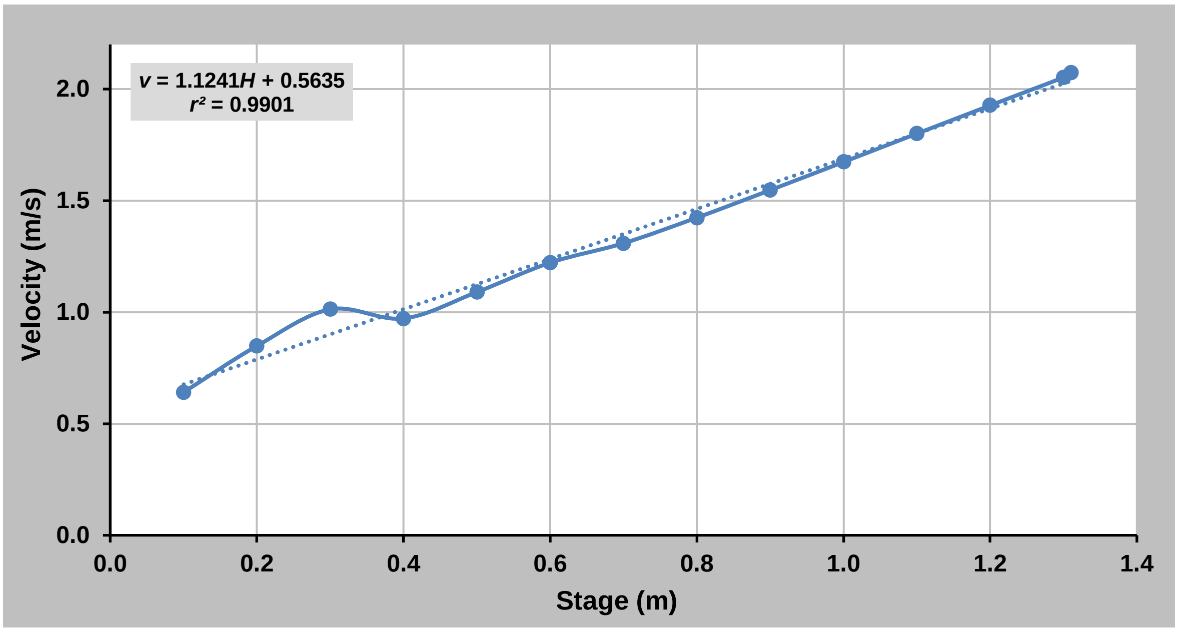

Figure B.22: Velocity versus stage at flow-gauging site A6H035 (VE-SA)

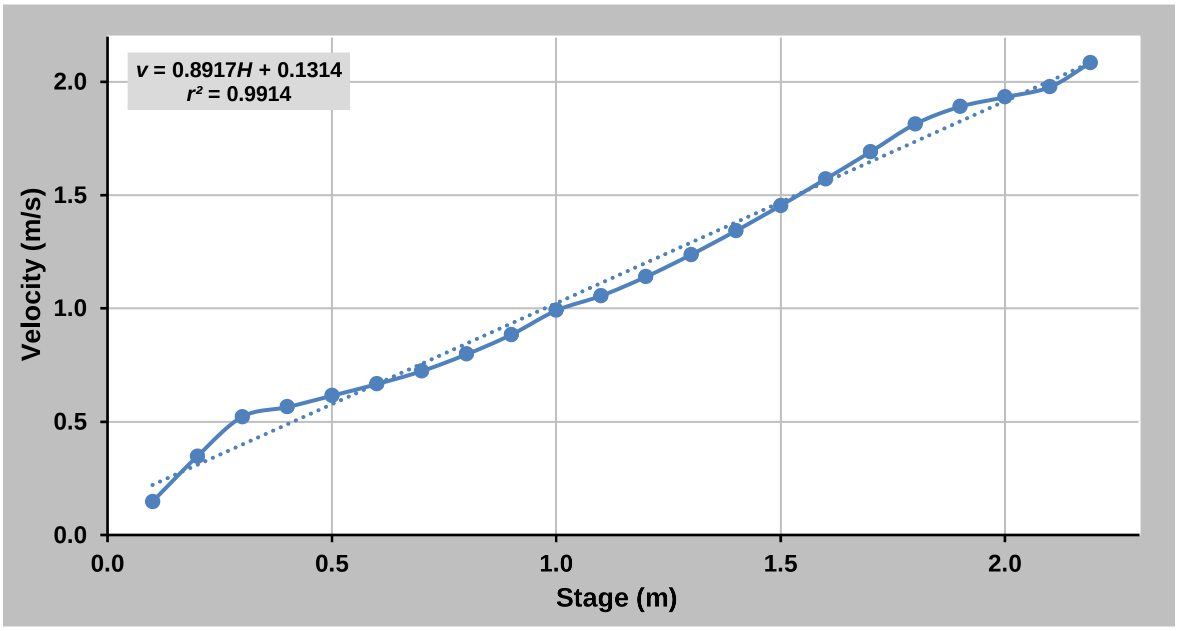

Figure B.23: Velocity versus stage at flow-gauging site C2H003/C2H130 (VE-SA)

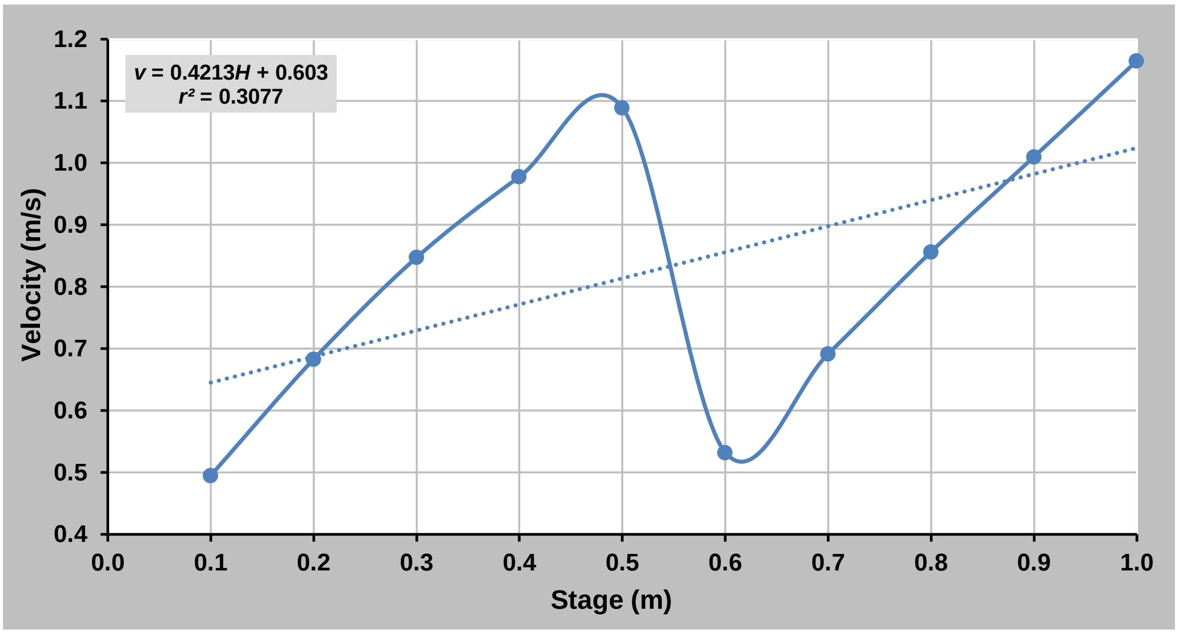

Figure B.24: Velocity versus stage at flow-gauging site C5H014 (VE-SA)

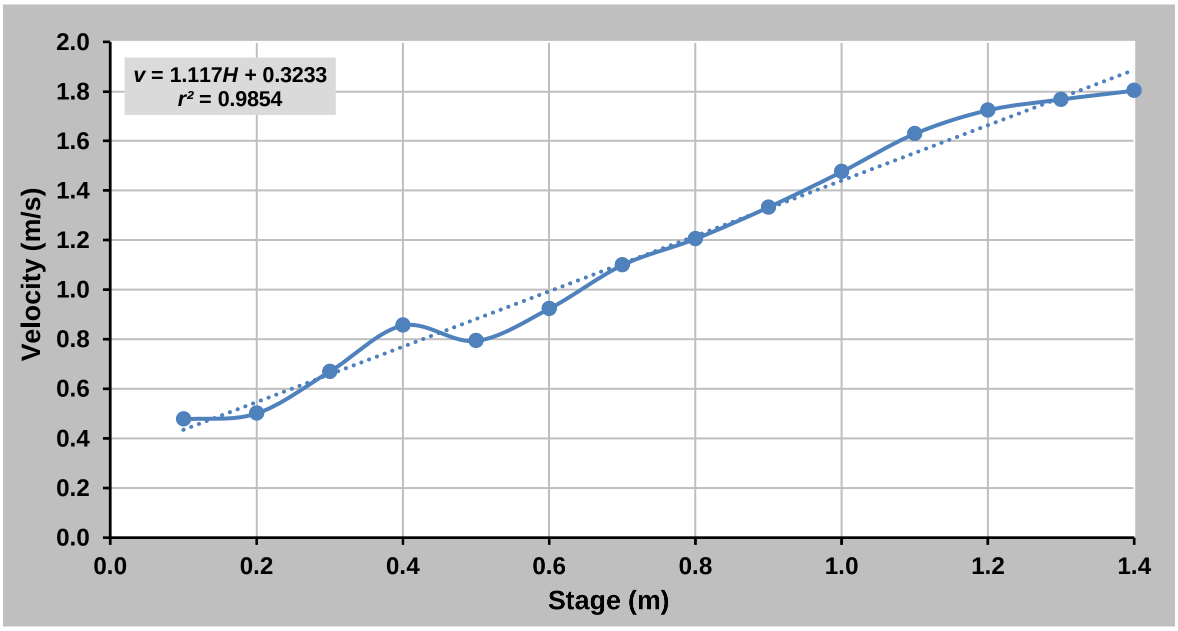

Figure B.25: Velocity versus stage at flow-gauging site H5H004 (VE-SA)

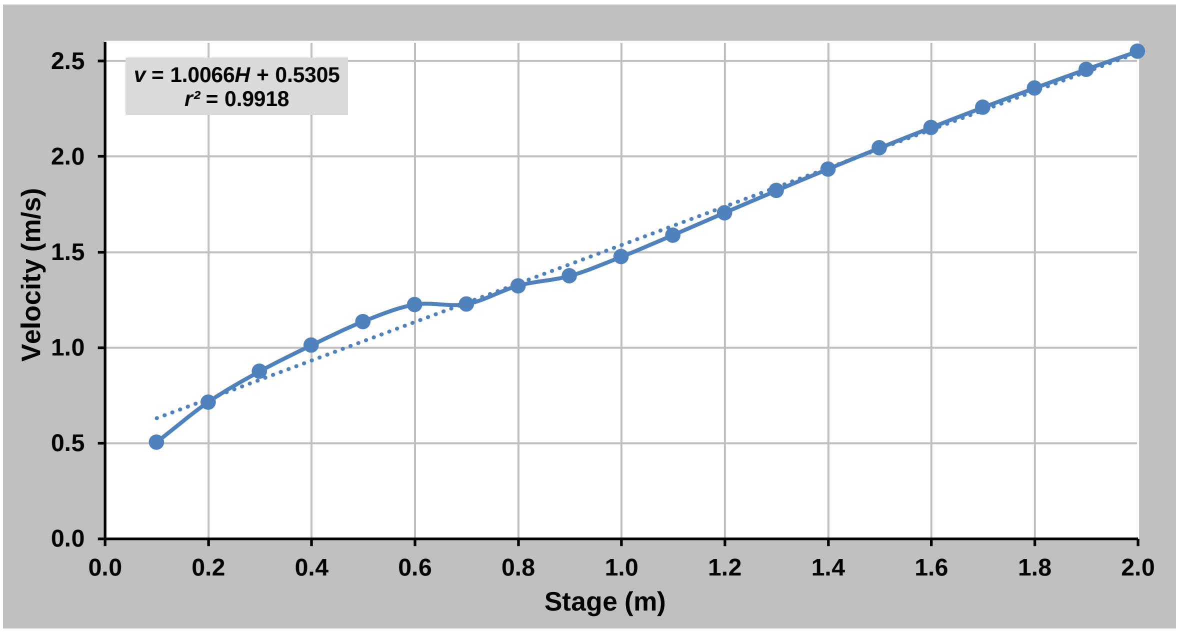

Figure B.26: Velocity versus stage at flow-gauging site J1H018 (VE-SA)

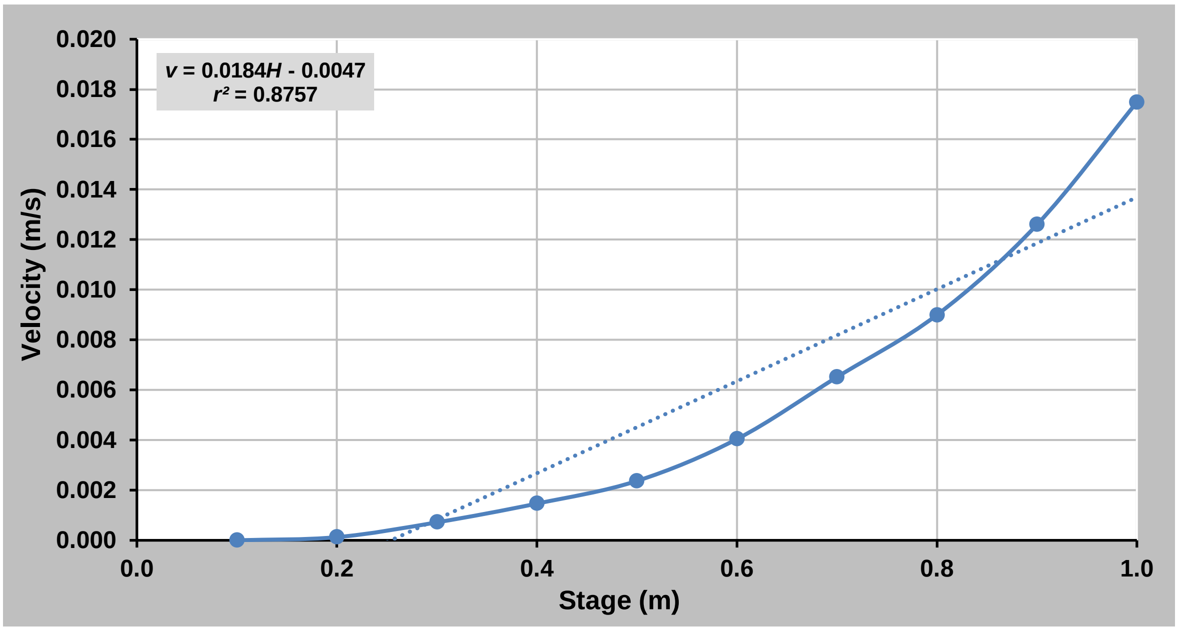

Figure B.27: Velocity versus stage at flow-gauging site J4H002 (VE-SA)

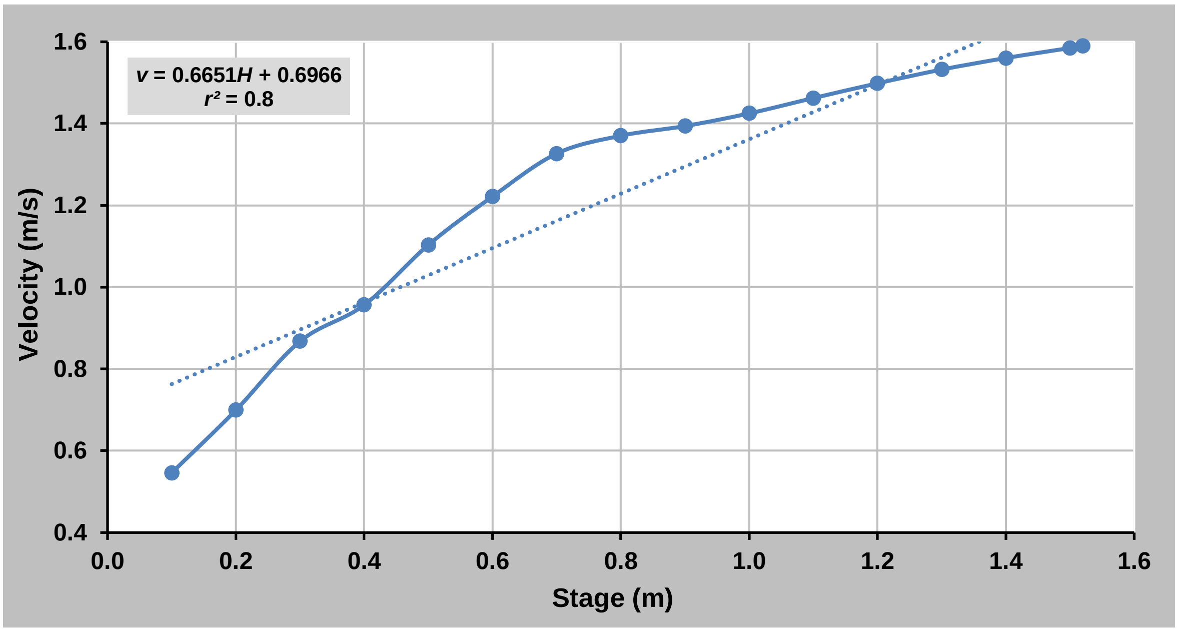

Figure B.28: Velocity versus stage at flow-gauging site K2H002 (VE-SA)

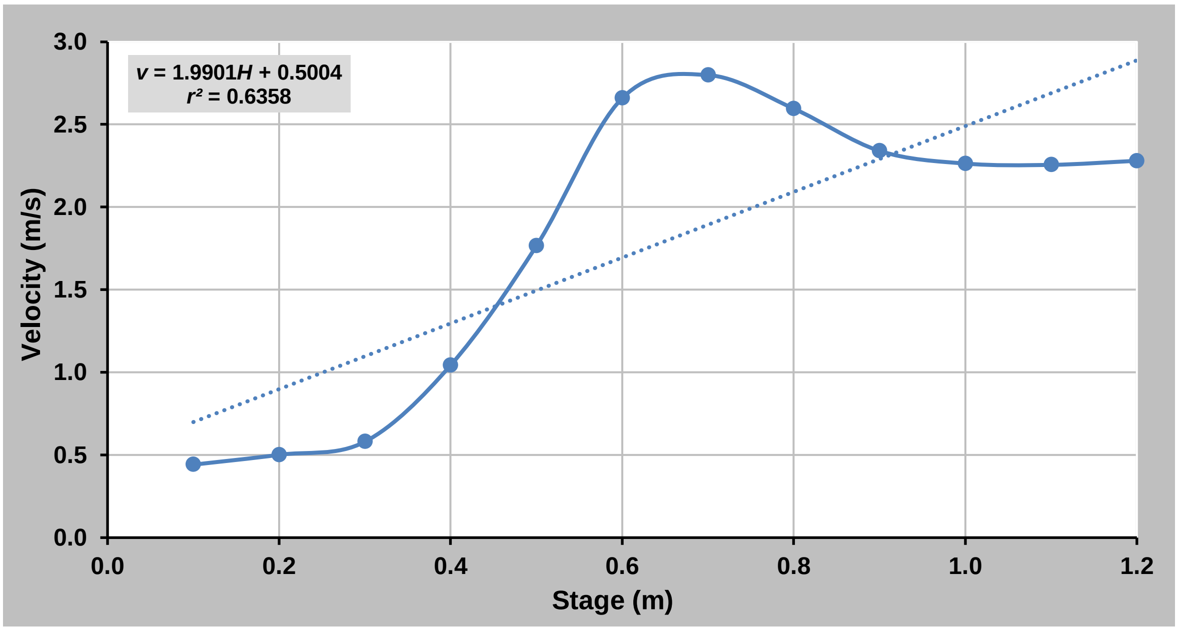

Figure B.29: Velocity versus stage at flow-gauging site V1H026 (VE-SA)

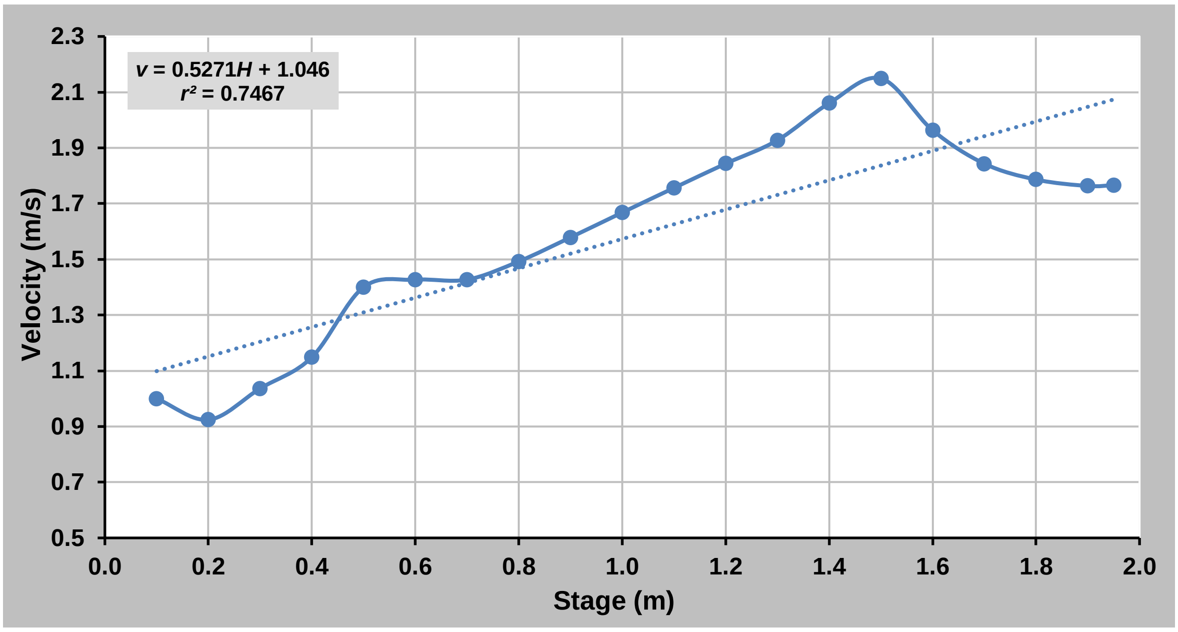

Figure B.30: Velocity versus stage at flow-gauging site X3H008 (VE-SA)

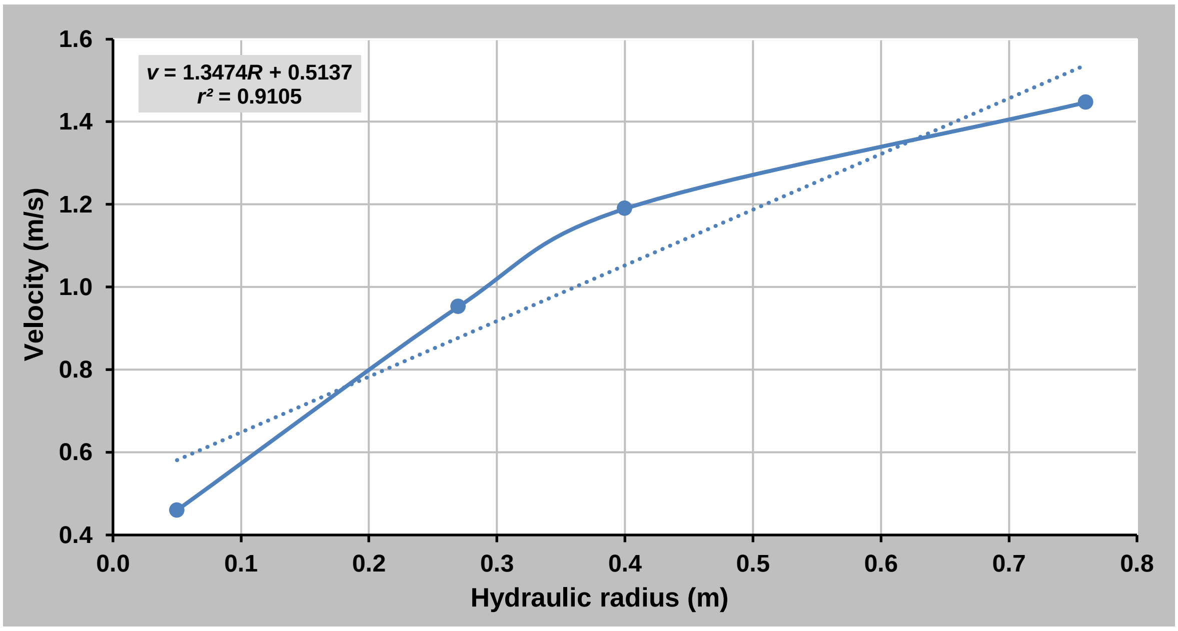

Figure B.31: Velocity vs. hydraulic radius at flow-gauging site A4H005 (VE-HRA)

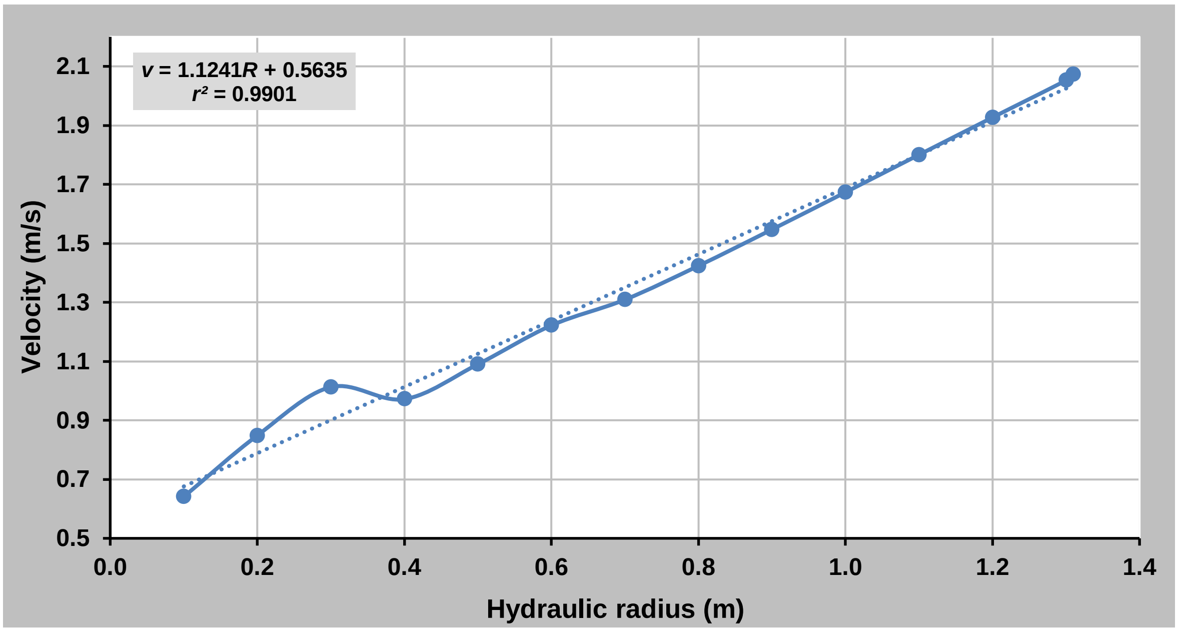

Figure B.32: Velocity vs. hydraulic radius at flow-gauging site A6H035 (VE-HRA)

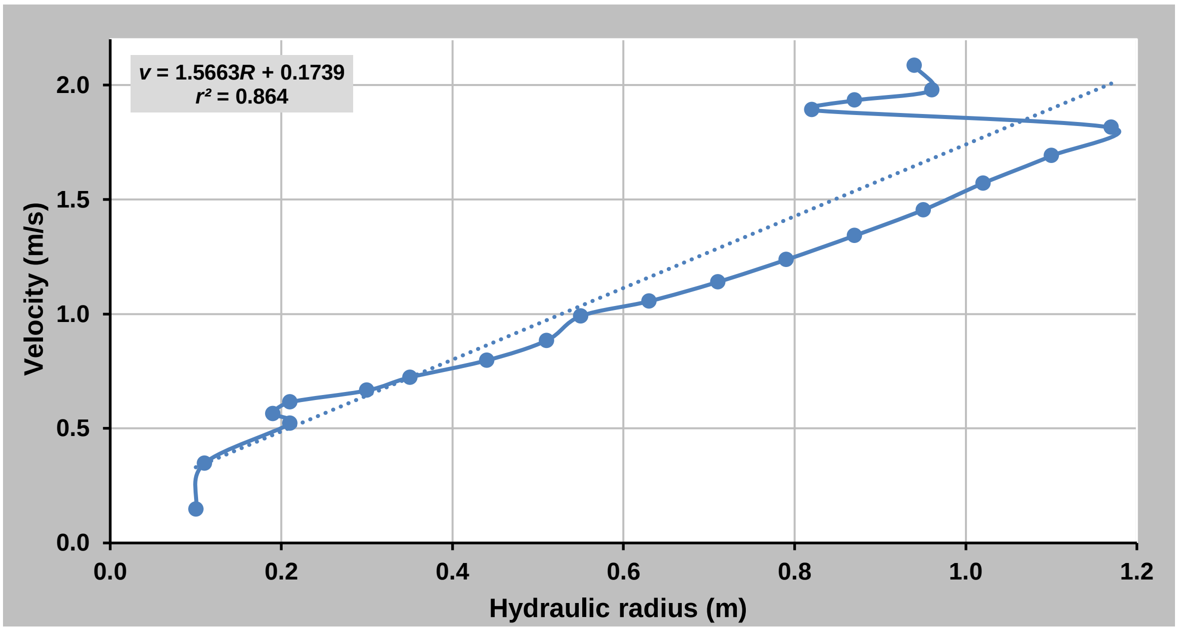

Figure B.33: Velocity vs. hydraulic radius at flow-gauging site C2H003 (VE-HRA)

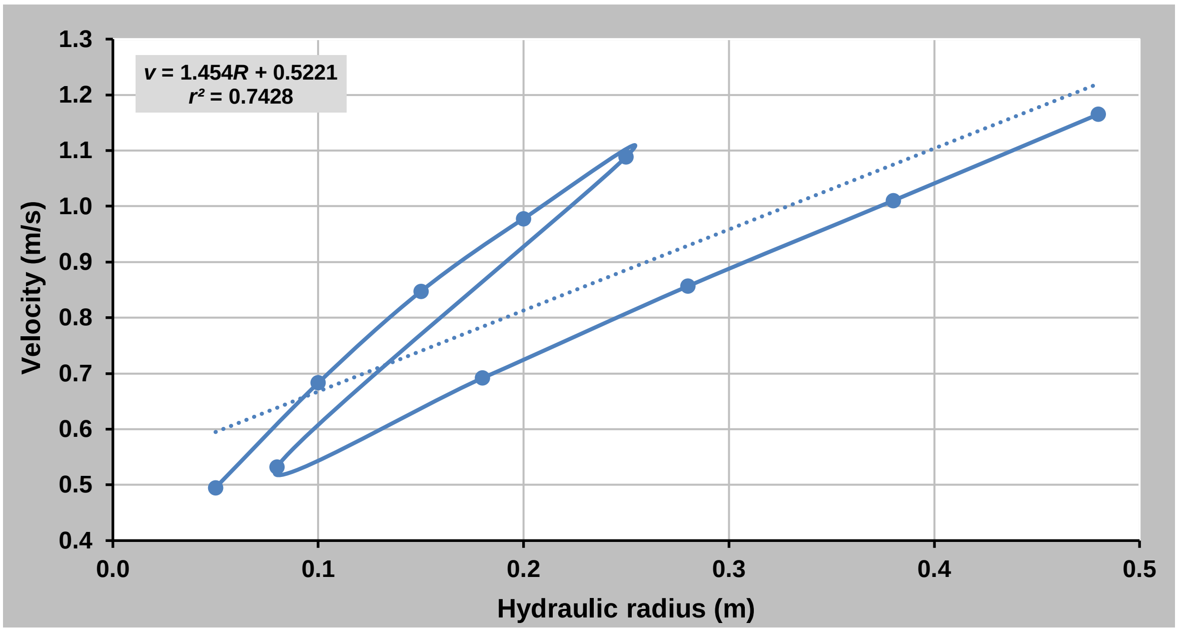

Figure B.34: Velocity vs. hydraulic radius at flow-gauging site C5H014 (VE-HRA)

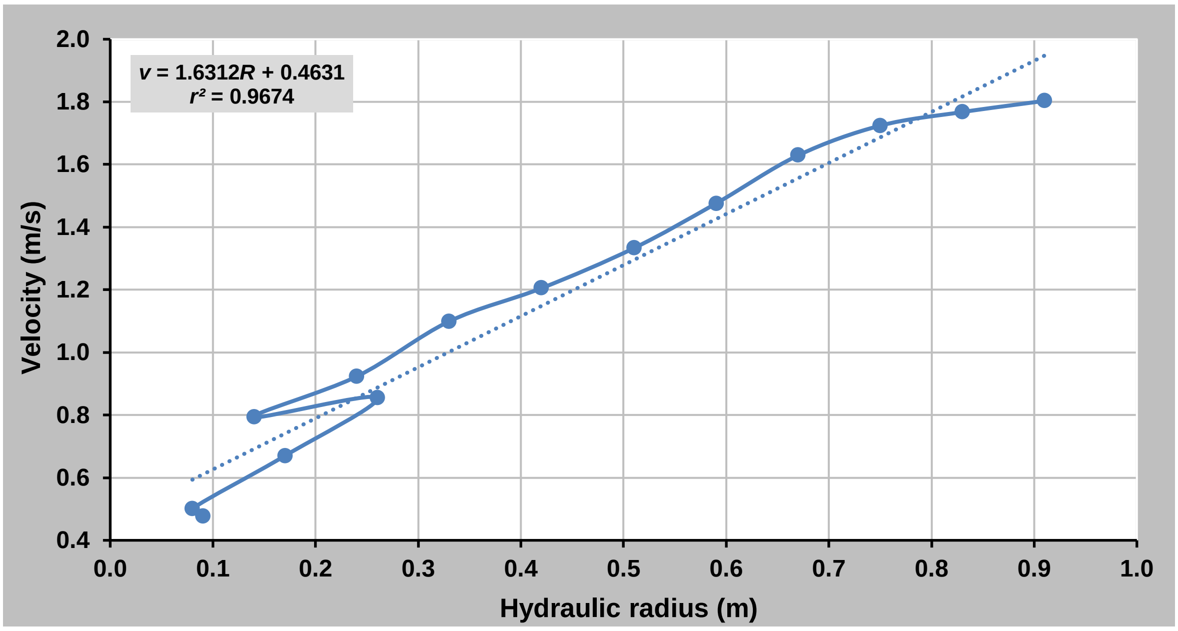

Figure B.35: Velocity vs. hydraulic radius at flow-gauging site H5H004 (VE-HRA)

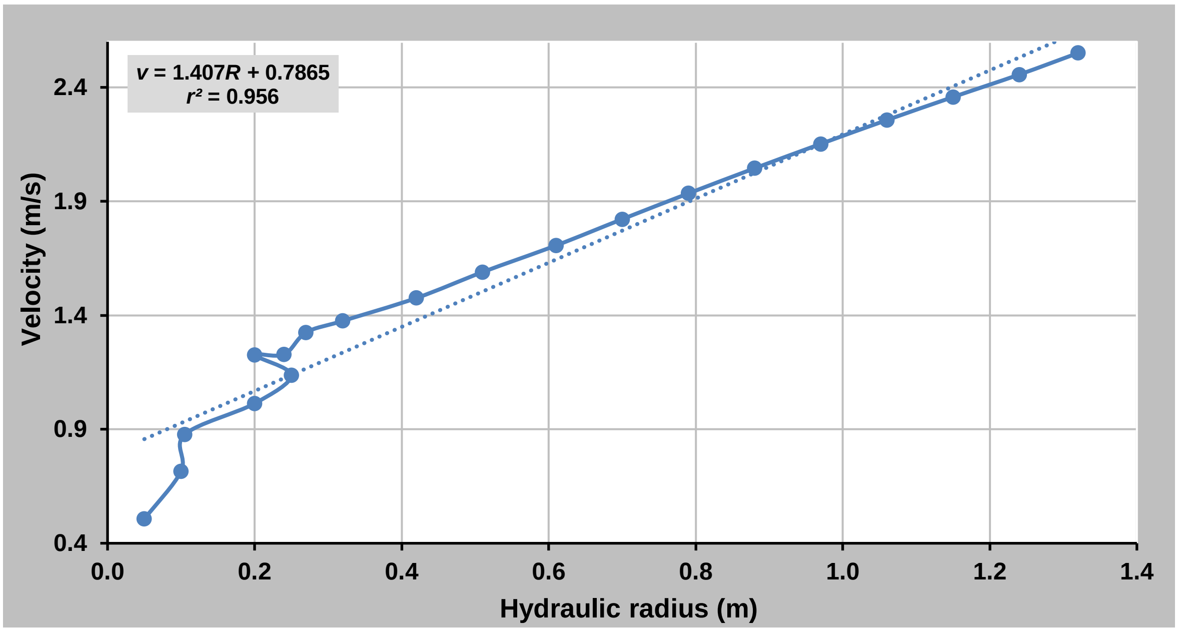

Figure B.36: Velocity vs. hydraulic radius at flow-gauging site J1H018 (VE-HRA)

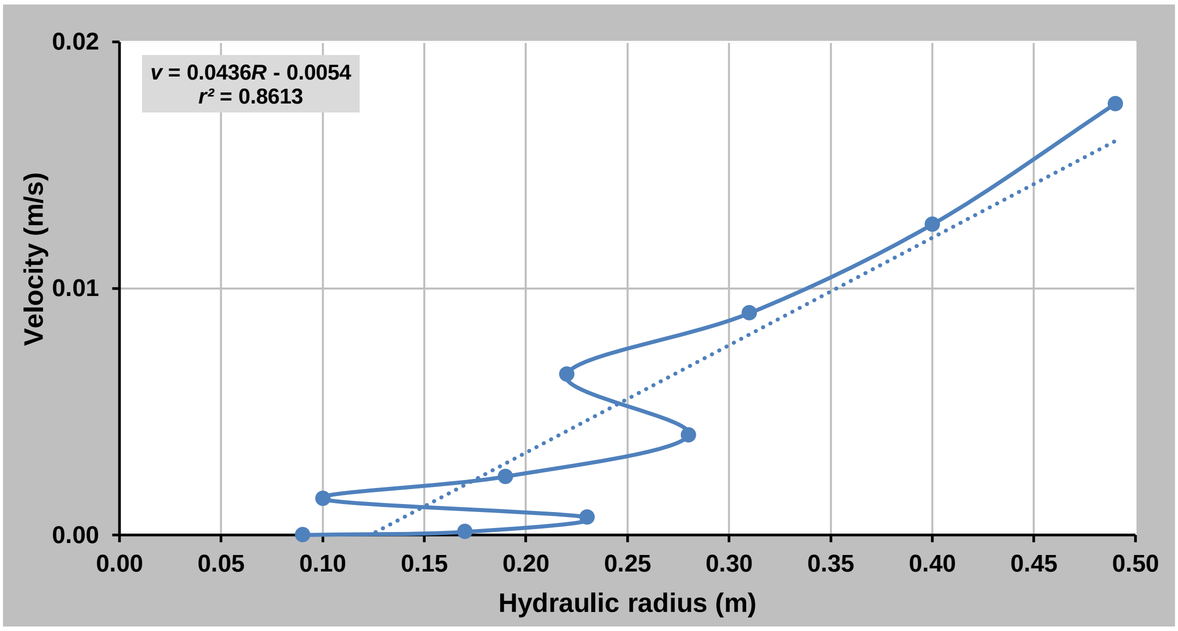

Figure B.37: Velocity vs. hydraulic radius at flow-gauging site J4H002 (VE-HRA)

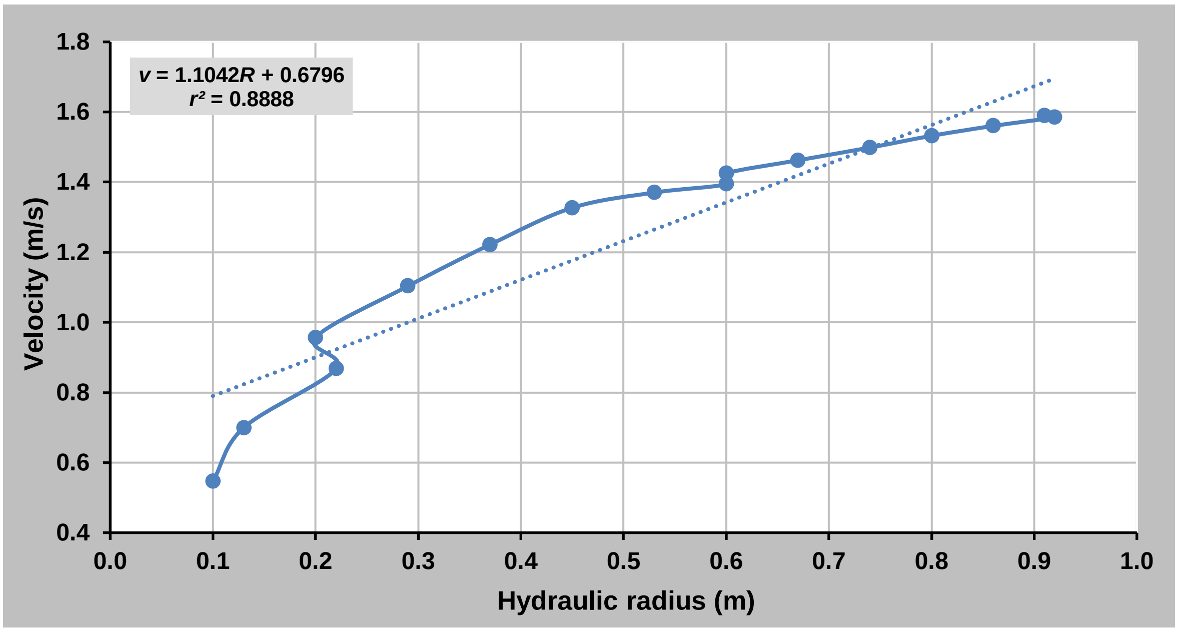

Figure B.38: Velocity vs. hydraulic radius at flow-gauging site K2H002 (VE-HRA)

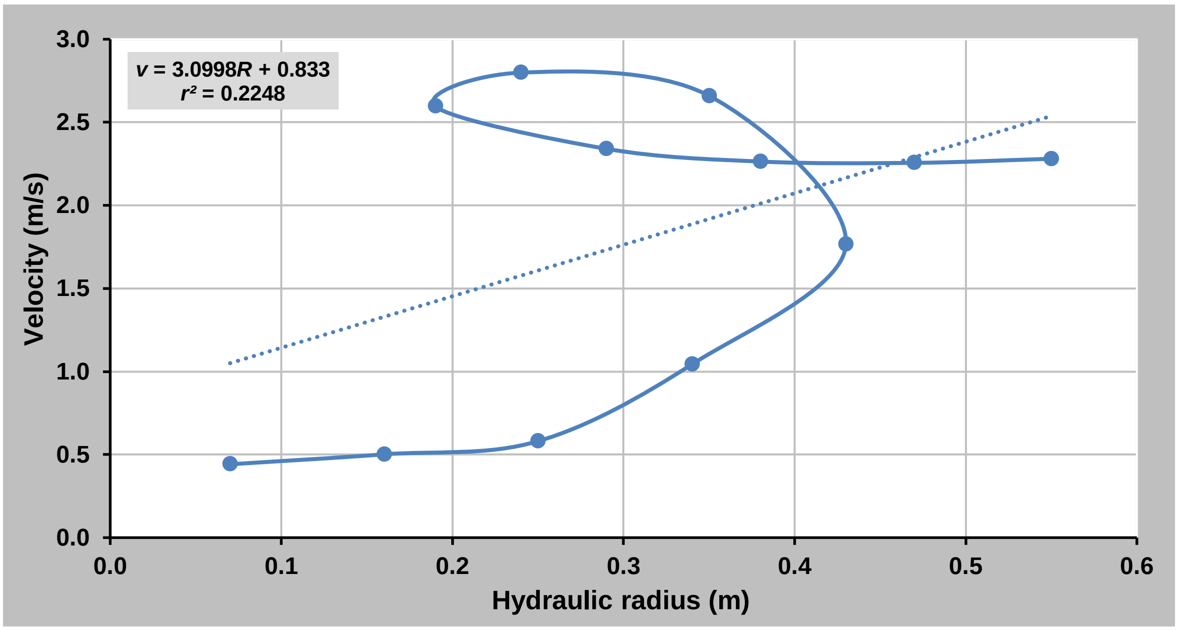

Figure B.39: Velocity vs. hydraulic radius at flow-gauging site V1H026 (VE-HRA)

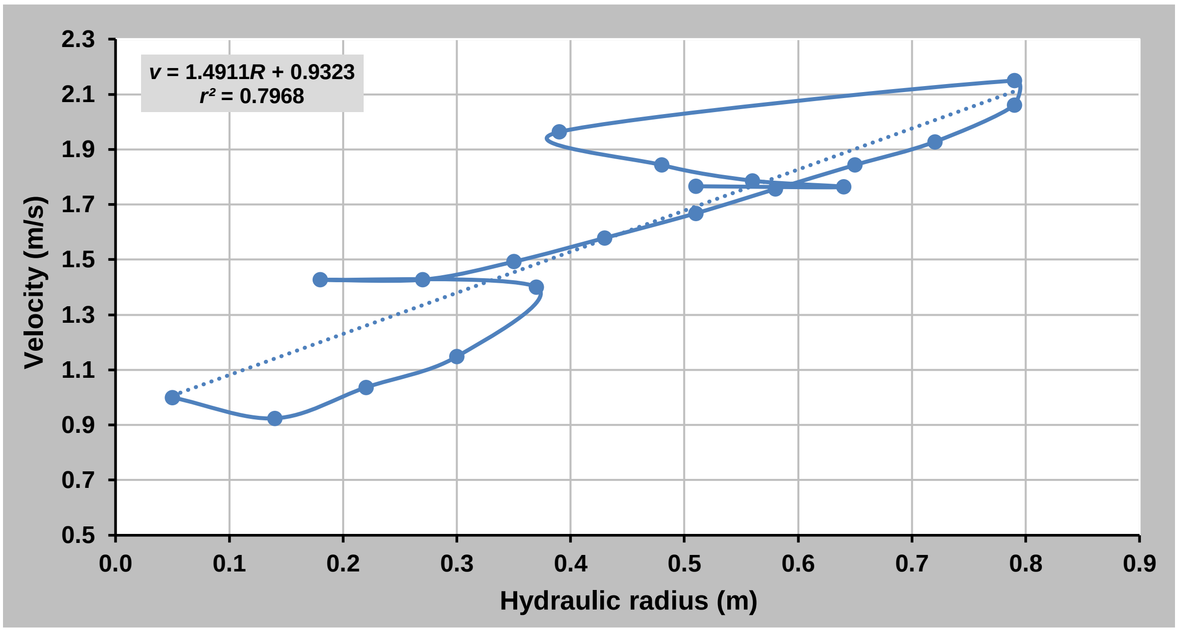

Figure B.40: Velocity vs. hydraulic radius at flow-gauging site X3H008 (VE-HRA)

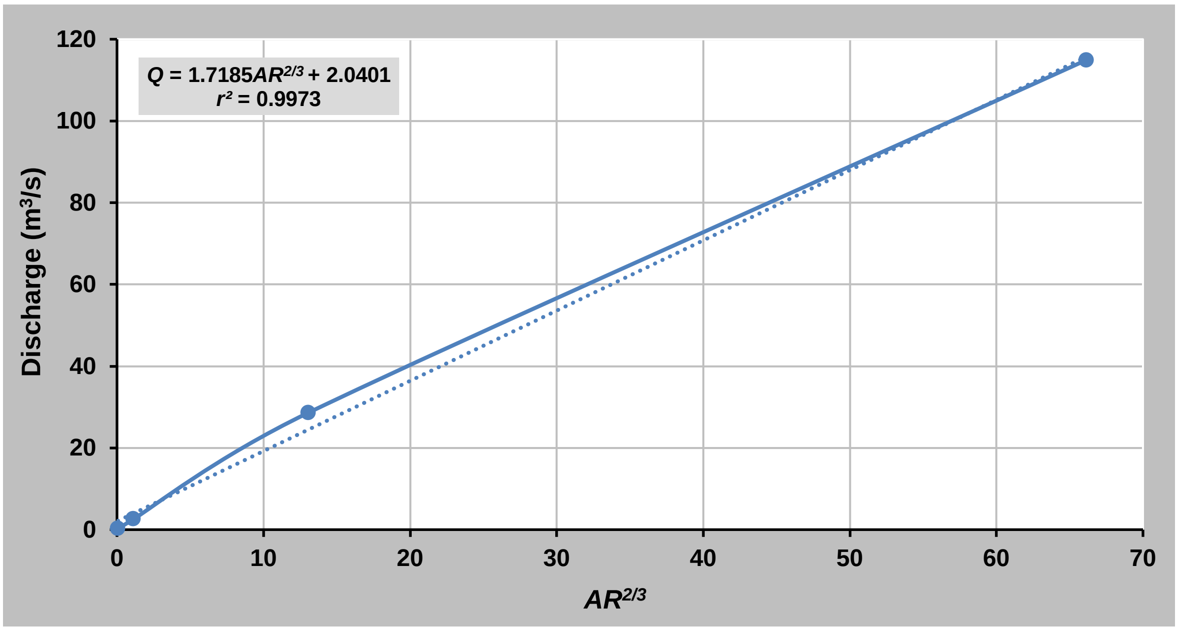

Figure B.41: Discharge vs. $AR^{2/3}$ at flow-gauging site A4H005 (VE-MA)

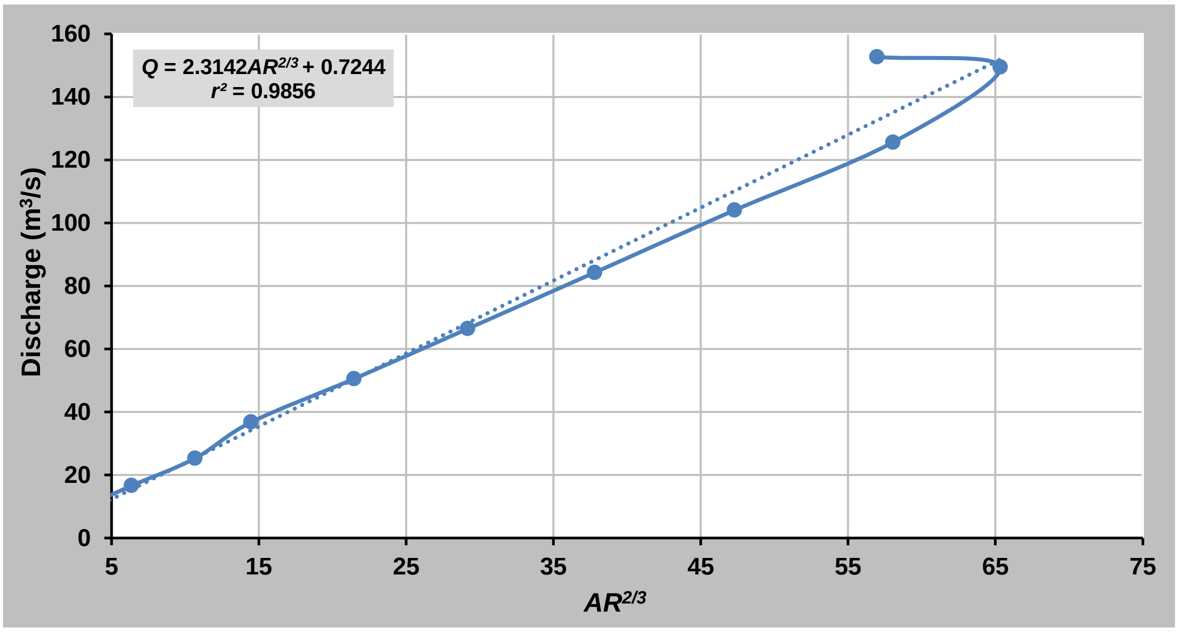

Figure B.42: Discharge vs. $AR^{2/3}$ at flow-gauging site A6H035 (VE-MA)

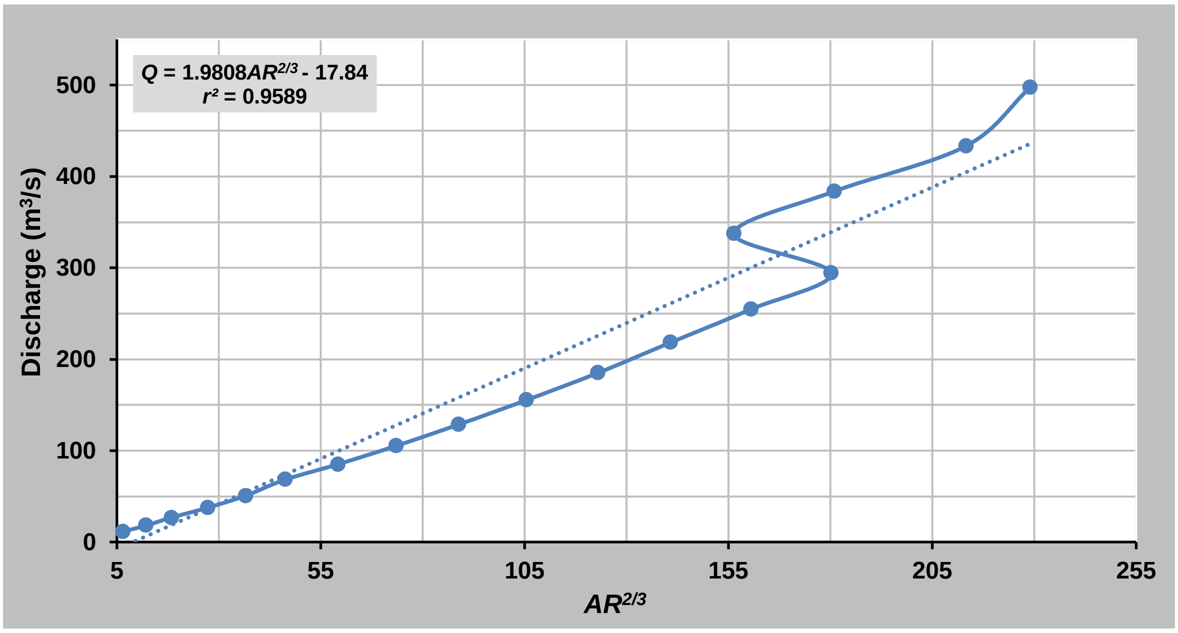

Figure B.43: Discharge vs. $AR^{2/3}$ at flow-gauging site C2H003/130 (VE-MA)

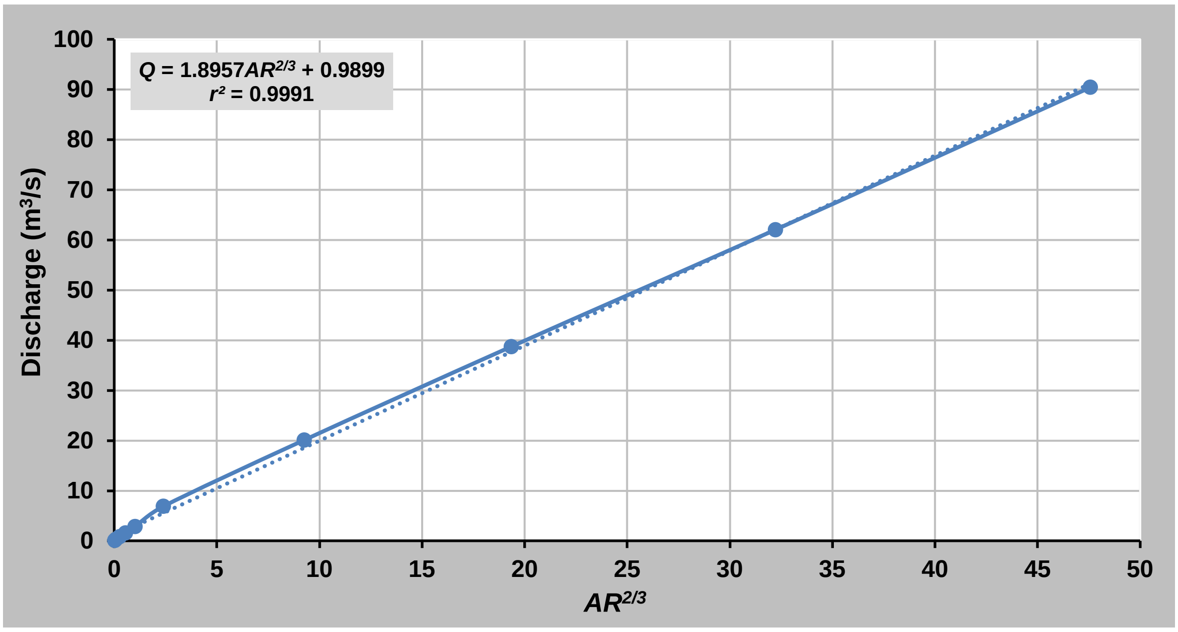

Figure B.44: Discharge vs. $AR^{2/3}$ at flow-gauging site C5H014 (VE-MA)

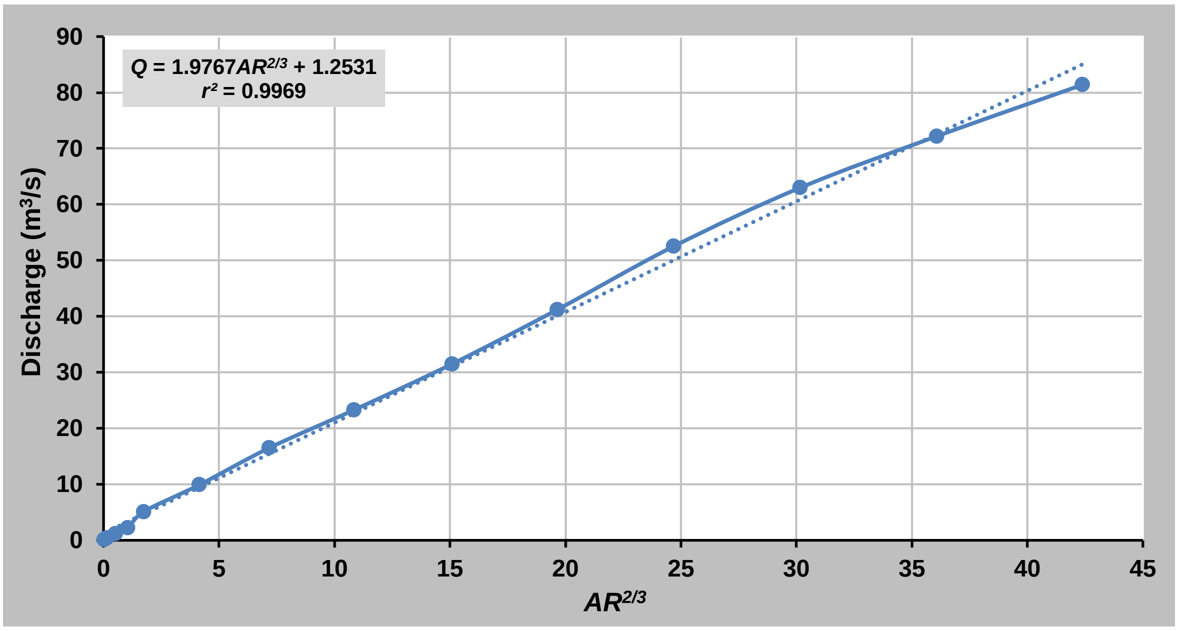

Figure B.45: Discharge vs. $AR^{2/3}$ at flow-gauging site H5H004 (VE-MA)

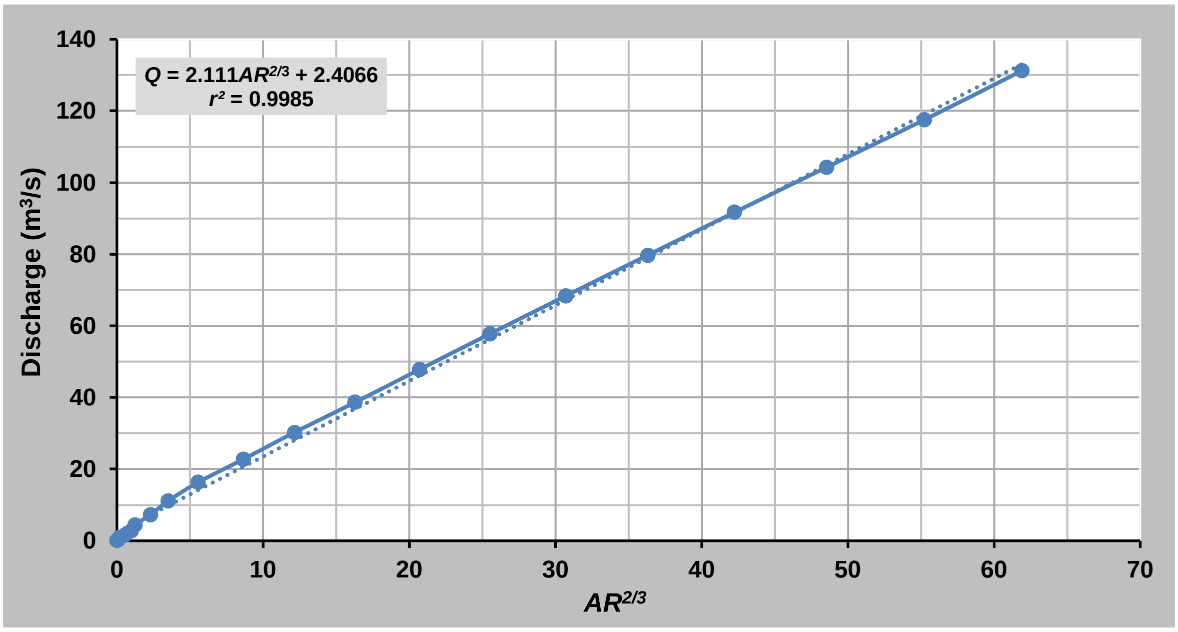

Figure B.46: Discharge vs. $AR^{2/3}$ at flow-gauging site J1H018 (VE-MA)

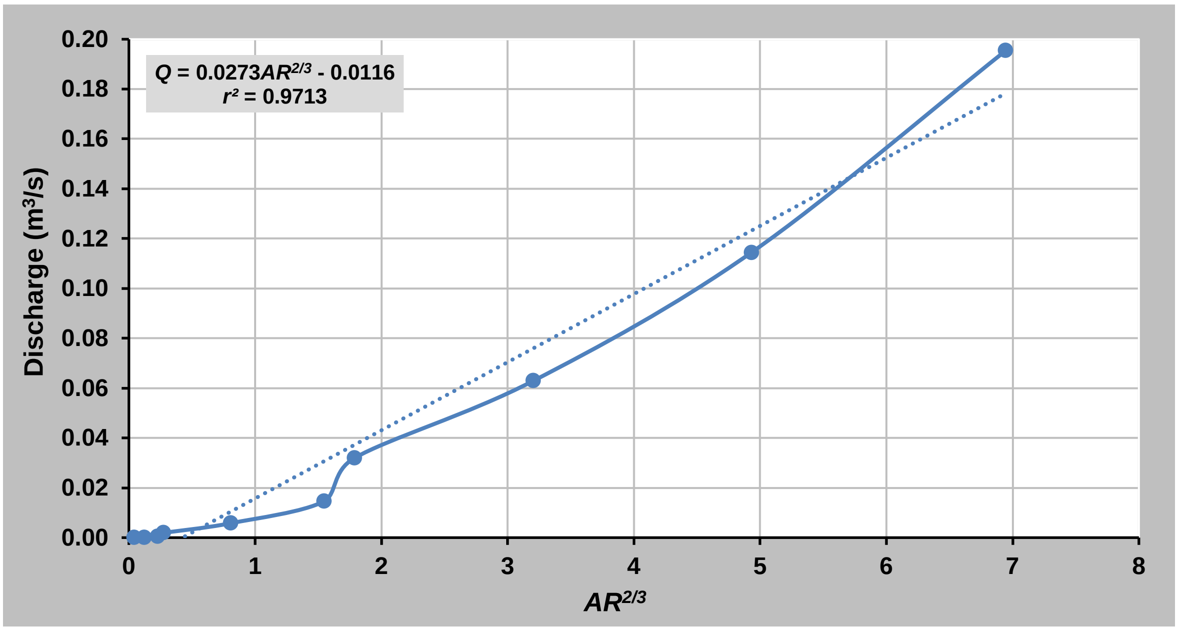

Figure B.47: Discharge vs. $AR^{2/3}$ at flow-gauging site J4H002 (VE-MA)

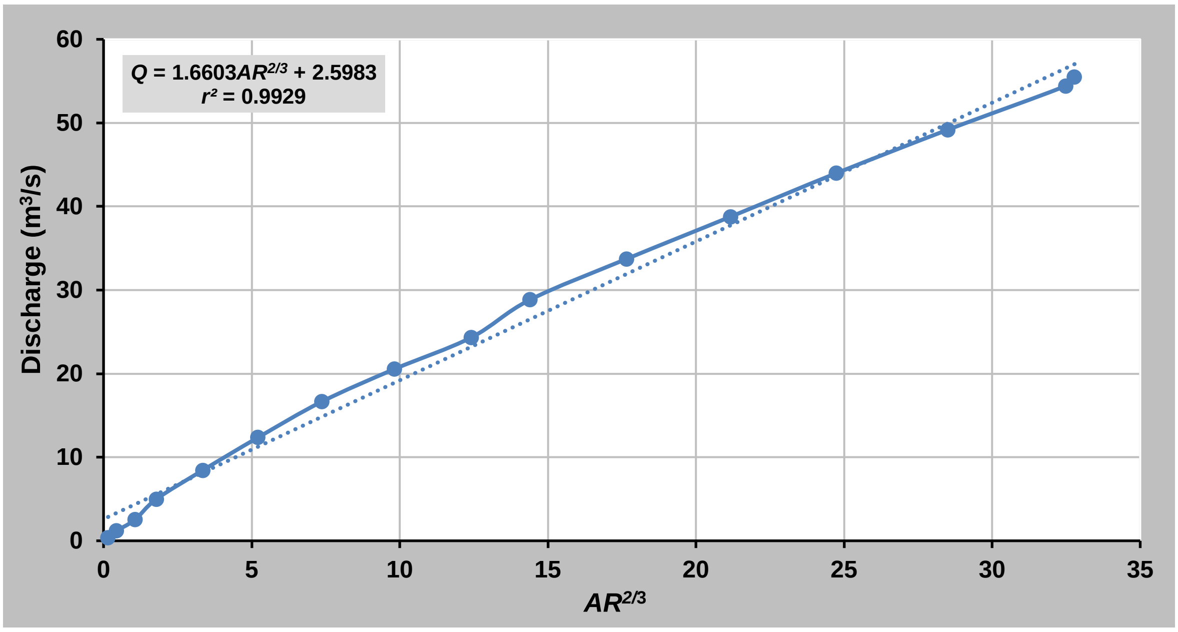

Figure B.48: Discharge vs. $AR^{2/3}$ at flow-gauging site K2H002 (VE-MA)

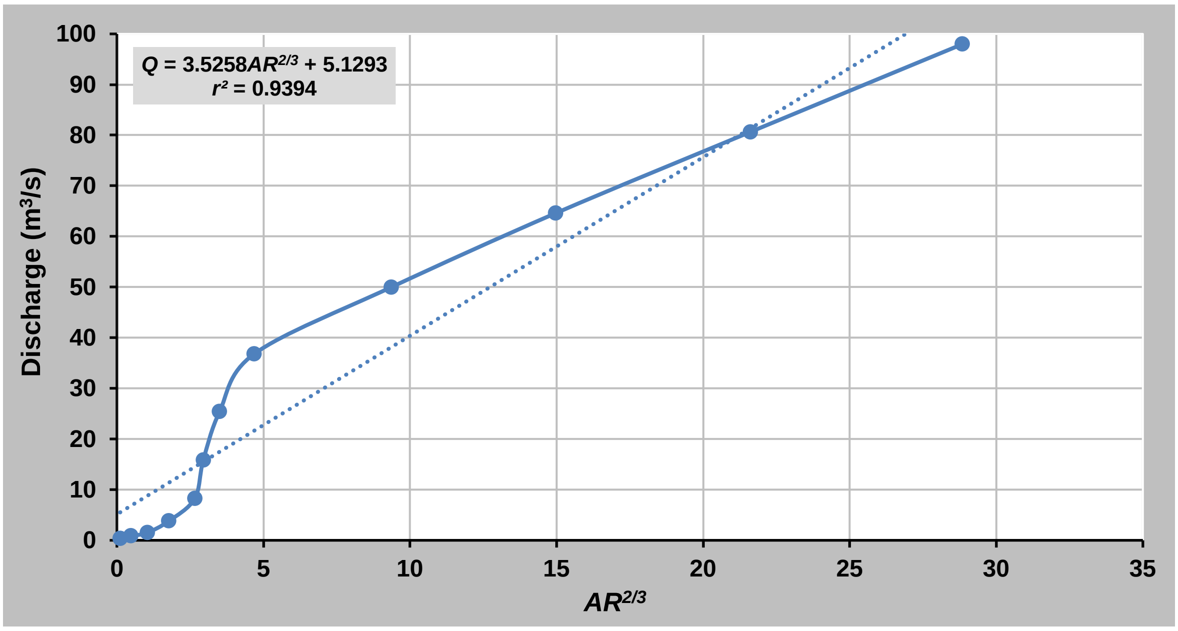

Figure B.49: Discharge vs. $AR^{2/3}$ at flow-gauging site V1H026 (VE-MA)

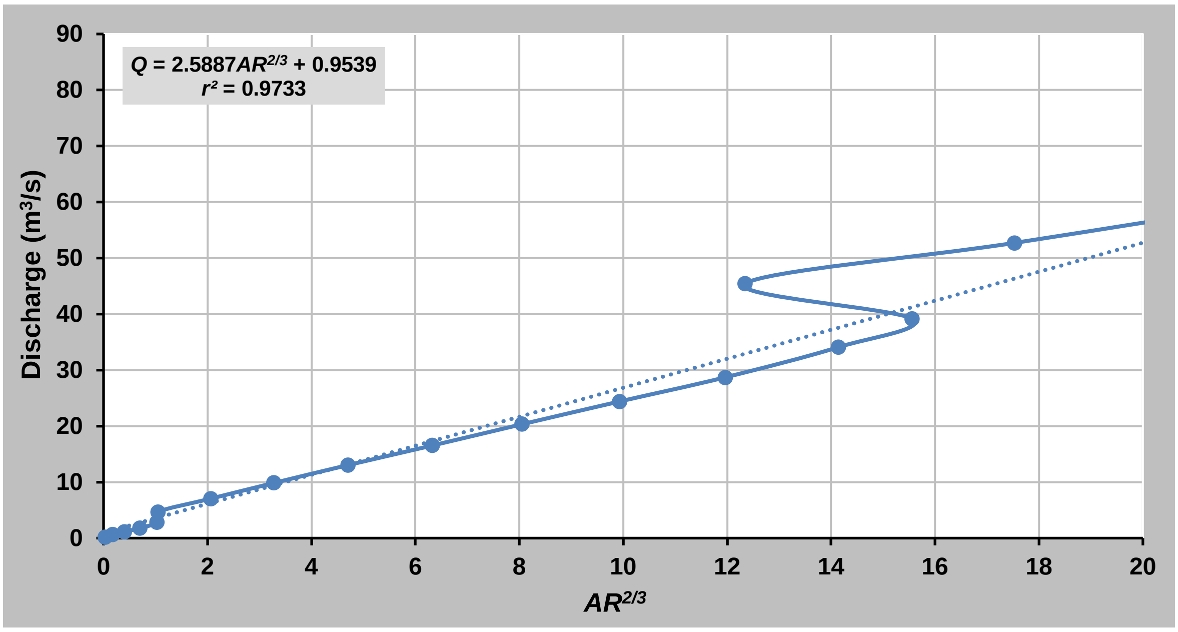

Figure B.50: Discharge vs. $AR^{2/3}$ at flow-gauging site X3H008 (VE-MA)

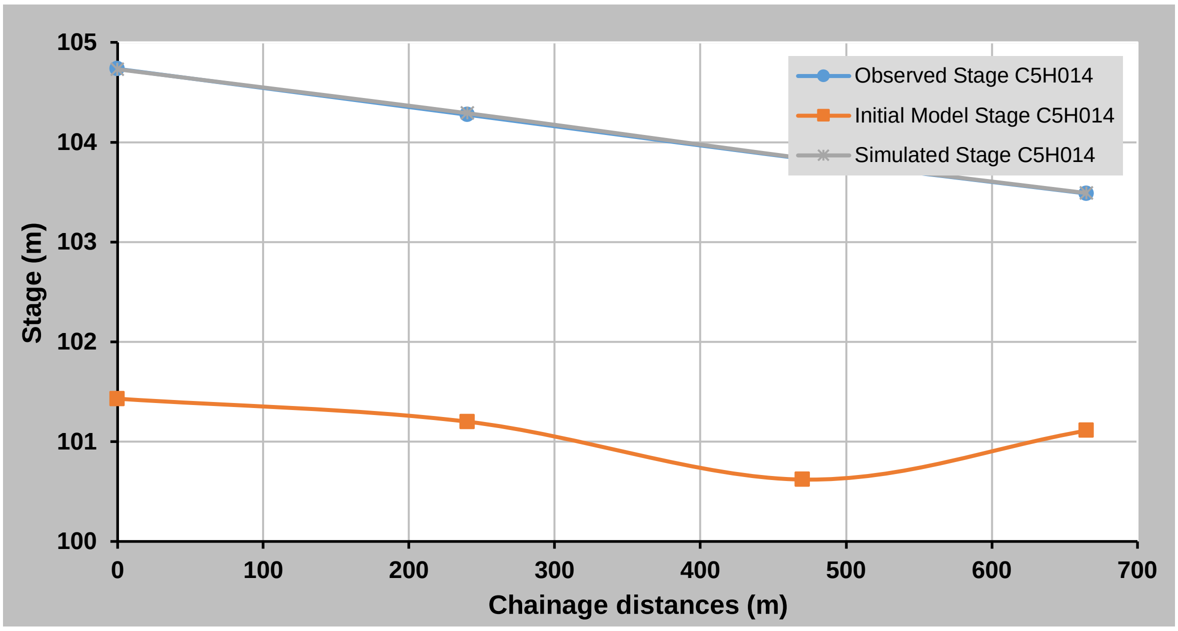

Figure B.51: Observed vs. simulated water surface profile (HEC-RAS) at C5H014

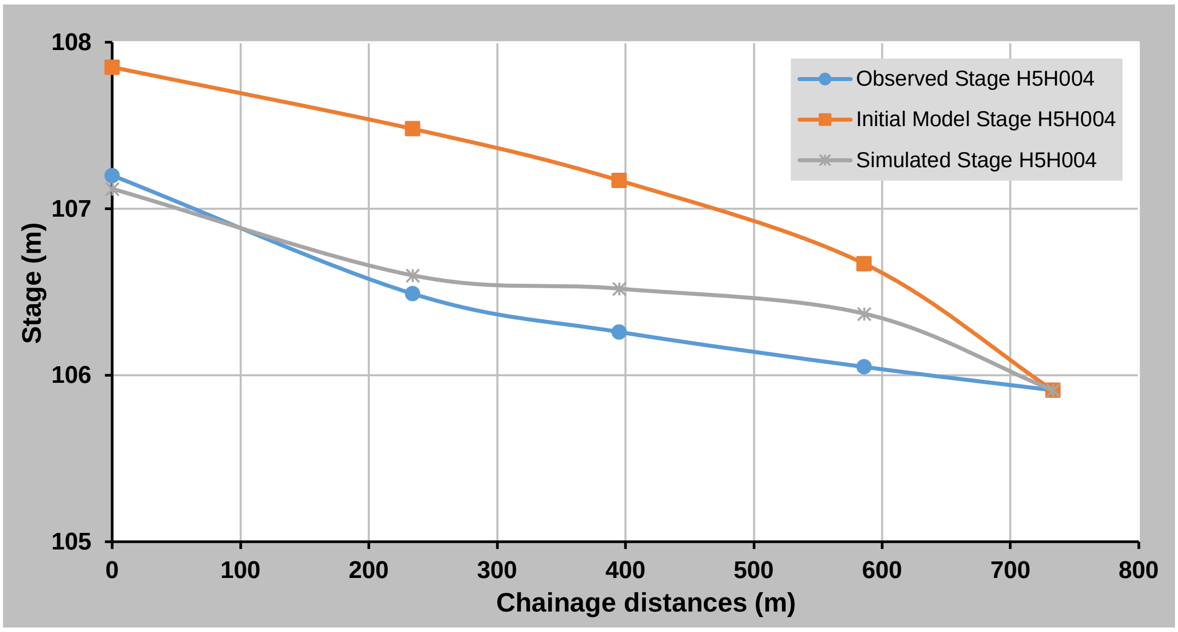

Figure B.52: Observed vs. simulated water surface profile (HEC-RAS) at H5H004

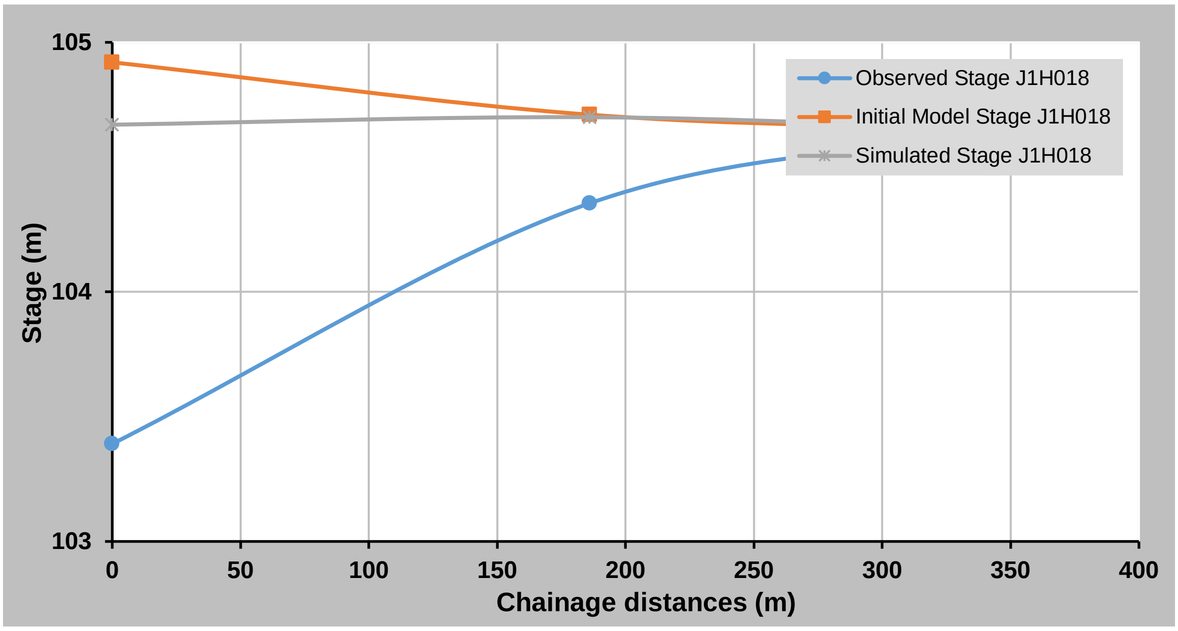

Figure B.53: Observed vs. simulated water surface profile (HEC-RAS) at J1H018

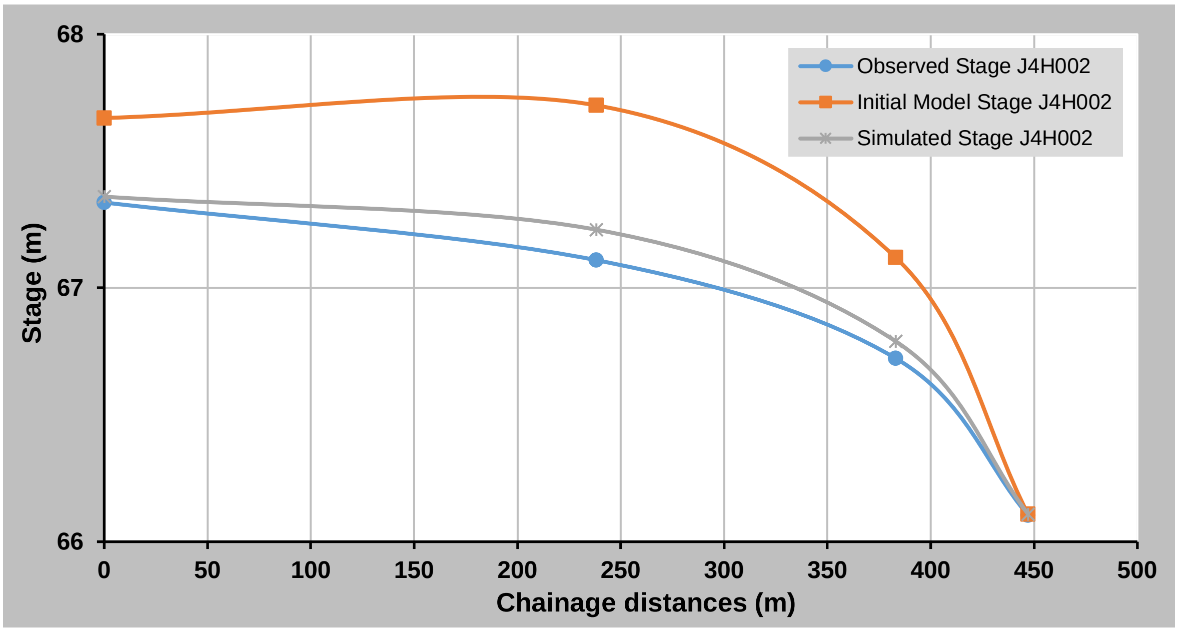

Figure B.54: Observed vs. simulated water surface profile (HEC-RAS) at J4H002

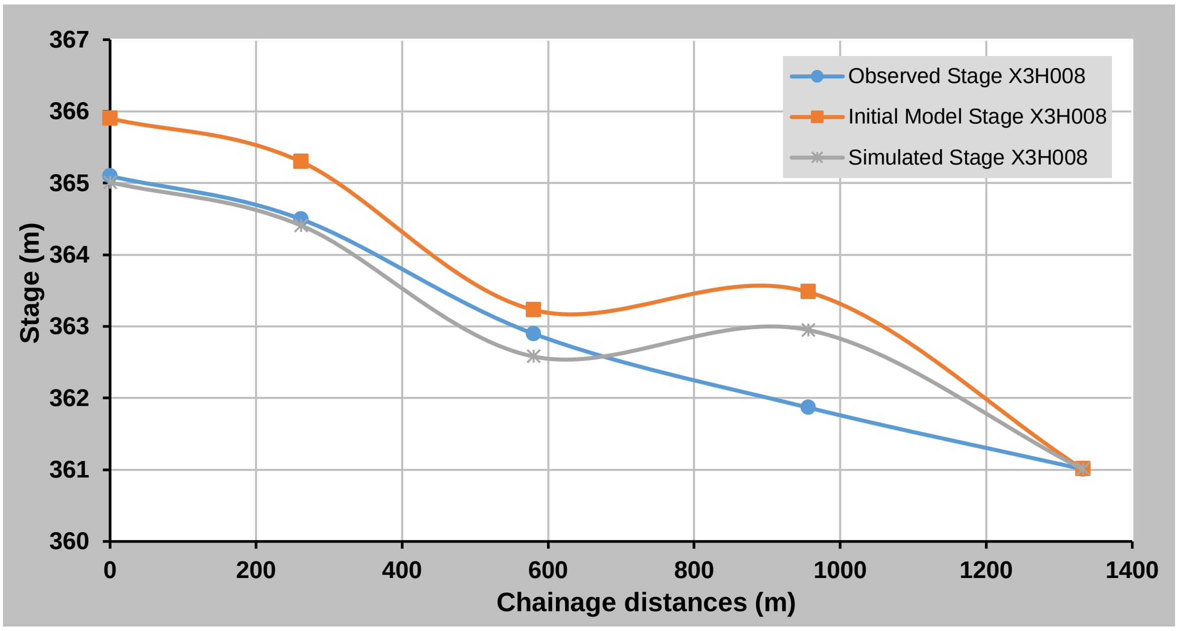

Figure B.55: Observed vs. simulated water surface profile (HEC-RAS) at X3H008